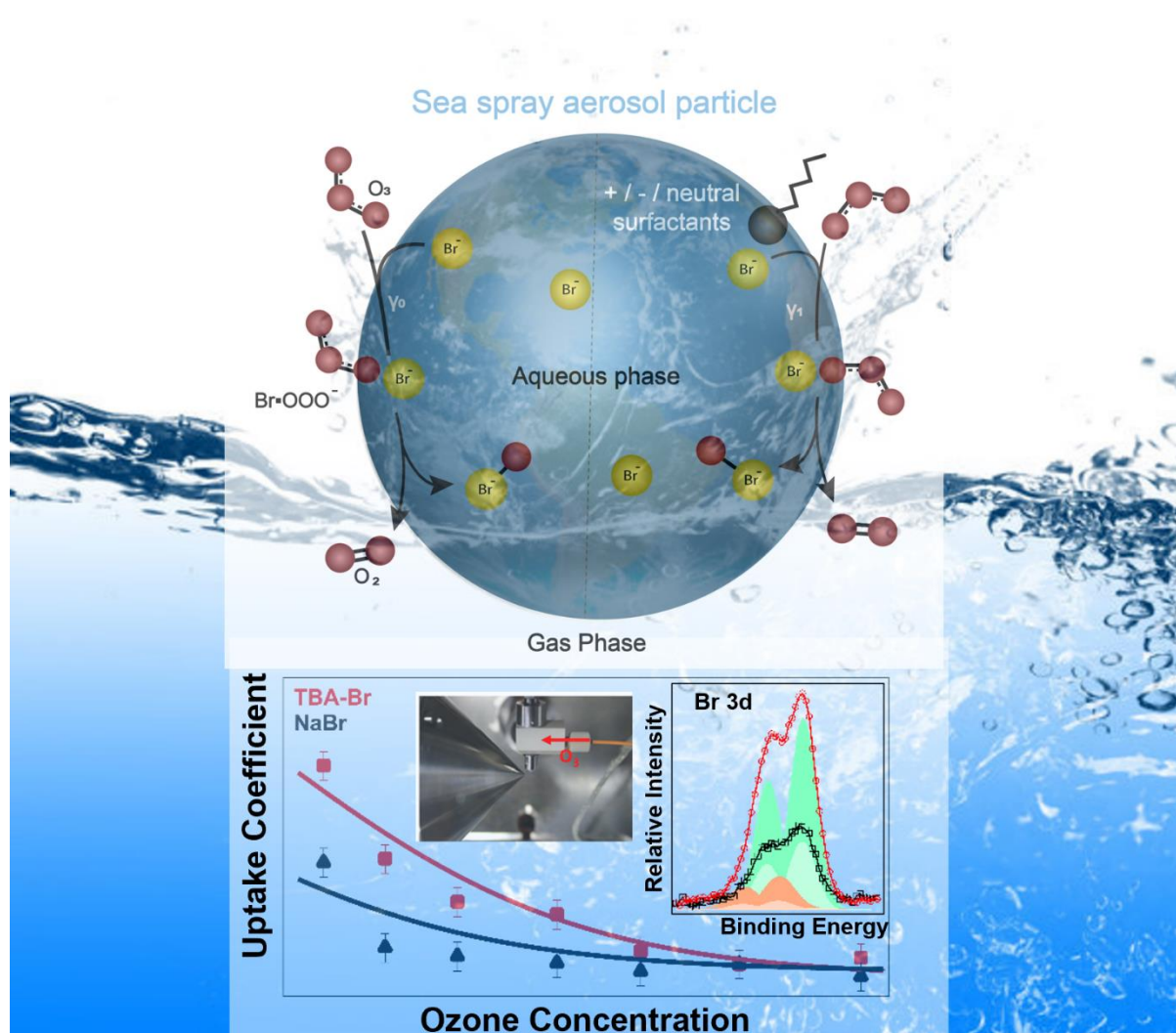


**SHUZHEN CHEN**

**MULTIPHASE KINETICS AND CHEMISTRY  
AT HALIDE SOLUTION-AIR INTERFACES**



DISS. ETH NO.28325



DISS. ETH NO. 28325

**MULTIPHASE KINETICS AND CHEMISTRY AT HALIDE SOLUTION-  
AIR INTERFACES**

A thesis submitted to attain the degree of  
DOCTOR OF SCIENCES of ETH ZURICH  
(Dr. sc. ETH Zurich)

presented by  
*SHUZHEN CHEN*

*MSc., Chemical Engineering and Technology,  
Central South University, China*

born on *16.04.1990*  
citizen of China

accepted on the recommendation of  
*Prof. Dr. Markus Ammann, examiner*  
*Prof. Dr. Thomas Peter, co-examiner*  
*Prof. Dr. Björneholm Olle, co-examiner*

2022



To my husband Xing, kids Ruisi and Ruixian



## List of Papers

This thesis is based on the following papers, which are referred to in the text.

### **1 Impact of tetrabutylammonium on the oxidation of bromide by ozone at the liquid-vapor interface**

Chen, S., Artiglia, L., Orlando, F., Edebeli, J., Kong, X., Yang, H., Boucly, A., Corral Arroyo, P., Prisle, N. and Ammann, M., *ACS Earth Space Chem.* 2021, 5, 11, 3008–3021.

### **2 Surface propensity of aqueous atmospheric bromine at the liquid–gas Interface**

Gladich, I., Chen, S., Vazdar, M., Boucly, A., Yang, H., Ammann, M. and Artiglia, L., *The Journal of Physical Chemistry Letters*, 2020, 11, 9, 3422-3429.

### **3 A surface-stabilized ozonide triggers bromide oxidation at the aqueous solution-vapor interface**

Artiglia, L., Edebeli, J., Orlando, F., Chen, S., Lee, M., Corral Arroyo, P., Gilgen, A., Bartels–Rausch, T., Kleibert, A., Vazdar, M., Carignano, M. A., Francisco, J. S., Shepson, P. B., Gladich, I. & Ammann, M., *Nature Communication*, 2017, 700, 1-8.

### **4 Influence of surfactants with differently charged headgroups on the surface propensity of bromide**

Chen, S., Artiglia, L., Yang, H., Boucly, A., Lezzi L., and Ammann, M., *Manuscript in preparation*.

The following is a list of publications to which I have contributed but which are not covered in this thesis.

**1 The Liquid–Gas Interface of Iron Aqueous Solutions and Fenton Reagents**

Gladich, I., Chen, S., Yang, H., Boucly, A., Winter, B., van Bokhoven, J., Ammann, M., Artiglia, L., *The Journal of Physical Chemistry Letters*, under review.

**2 Disordered adsorbed water layers on TiO<sub>2</sub> nanoparticles under subsaturated humidity conditions at 235 K**

Orlando, F., Artiglia, L., Yang, H., Kong, X., Roy, K., Waldner, A., Chen, S., Bartels-Rausch, T., and Ammann, M., *The Journal of Physical Chemistry Letters*, 2019, 10, 23, 7433-7438.

**3 Chemical composition and properties of the liquid–vapor interface of aqueous C1 to C4 monofunctional acid and alcohol solutions**

Lee, M., Orlando, F., Artiglia, L., Chen, S., and Ammann, M., *The Journal of Physical Chemistry A*, 2016, 120(49), 9749-9758.



---

# Contents

---

## Contents

<b>Chapter 1</b> .....	<b>1</b>
<b>1.1 Ozone and halogen chemistry</b> .....	<b>1</b>
<b>1.2 Multiphase kinetics of oxidation of bromide</b> .....	<b>3</b>
<b>1.3 The halide solution in presence of organics</b> .....	<b>4</b>
<b>1.4 Analytical methods to characterize the liquid-vapor interface</b> .....	<b>7</b>
<b>1.5 Thesis mission</b> .....	<b>9</b>
<b>1.6 Thesis outline</b> .....	<b>10</b>
<b>Chapter 2</b> .....	<b>15</b>
<b>2.1 Liquid microjet X-ray photoelectron spectroscopy</b> .....	<b>15</b>
<b>2.2 Flow reactor used in ozone uptake measurements</b> .....	<b>18</b>
<b>Chapter 3</b> .....	<b>21</b>
<b>3.1 The surface propensity of aqueous atmospheric bromine at the liquid-gas interface.</b> <b>21</b>	
3.1.1 Abstract.....	21
3.1.2 Introduction .....	22
3.1.3 Experimental Methods.....	24
3.1.4 Results and discussion .....	25
3.1.5 Conclusion.....	30
<b>3.2 Supplementary information</b> .....	<b>31</b>
<b>Chapter 4</b> .....	<b>37</b>
<b>4.1 A surface-stabilized ozonide triggers bromide oxidation at the aqueous solution-vapor interface</b> .....	<b>37</b>
4.1.1 Abstract.....	37
4.1.2 Introduction .....	38
4.1.3 Experimental method .....	40

4.1.4 Results and discussion .....	40
4.1.5 Conclusion.....	47
<b>4.2 Supplementary information .....</b>	<b>48</b>
<b>Chapter 5 .....</b>	<b>58</b>
<b>5.1 Influence of surfactants with differently charged headgroups on the surface propensity of bromide .....</b>	<b>58</b>
5.1.1 Abstract.....	58
5.1.2 Introduction .....	59
5.1.3 Experimental method .....	60
5.1.4 Results and discussion .....	61
5.1.5 Conclusion.....	66
<b>5.2 Supplementary Information .....</b>	<b>67</b>
<b>Chapter 6 .....</b>	<b>75</b>
<b>6.1 Impact of Tetrabutylammonium on the Oxidation of Bromide by Ozone.....</b>	<b>75</b>
6.1.1 Abstract.....	75
6.1.2 Introduction .....	76
6.1.3 Experimental method .....	78
6.1.4 Results and discussion .....	81
6.1.5 Conclusion.....	93
<b>6.2 Supplementary information .....</b>	<b>94</b>
<b>Chapter 7 .....</b>	<b>109</b>
<b>7.1 Summary .....</b>	<b>109</b>
<b>7.2 Outlook .....</b>	<b>111</b>

---

## ABSTRACT

---

Oxidation of halides at the aqueous solution – air interface initiates the release of gas-phase halogen compounds, representing 50% of the chemical sink of ozone in the global troposphere. Halide solution-air interfaces are ubiquitously present because about 71% of the Earth's surface is covered by seawater that contains large amounts of chloride and bromide. In addition, halides are emitted to the atmosphere in the form of sea spray aerosol and are therefore also transported over long distances over the continents. Since recently, with the development of differentially pumped electrostatic lens systems, liquid-jet X-ray photoelectron spectroscopy (XPS) allows us directly probing the aqueous solution – air interface at the molecular level in the presence of trace gases. In this project, we use liquid-jet XPS at the Swiss Light Source in conjunction with kinetic experiments to study the molecular level details of the surface reaction of aqueous bromide with  $O_3$  in the absence and presence of organic compounds. The aim is to support assessments of the impact of halogen chemistry on atmospheric oxidation capacity and climate.

The affinity of halide ions in aqueous solution for the liquid-gas interface, which may influence their reactivity with gaseous species, has been debated. We use liquid-jet XPS to investigate the interfacial depth profile of bromide, hypobromite, hypobromous acid and bromate. We compare solutions with different concentrations of bromide, mixtures of bromide and chloride, as well as the series of bromide, chloride and fluoride. Bromide ions, with and without chloride, tend to be not enhanced at the solution surface. In the halogen series, the surface propensity follows the series  $Br > Cl > F$ , which agrees with recent theory, classical surface tension measurements and recent spectroscopic experiments, suggesting the lightest halide ions being most depleted from the surface. Among the bromine species, hypobromous acid, a key species in the multiphase cycling of bromine, is the only species showing substantial surface propensity, which suggests a more critical role of the interface for this species in multiphase bromine chemistry than thought before.

In the aqueous bulk, oxidation of bromide by ozone involves a  $[Br\bullet OOO^-]$  complex as intermediate. Here, we report liquid jet XPS measurements that provide direct experimental evidence for the ozonide and establish its propensity for the solution-vapor interface. In experiments at low pH, the signal of the  $[Br\bullet OOO^-]$  intermediate was small and just at the detection limit, which may be due to the faster decay into products, thus release of molecular oxygen and formation of  $OBr^-$ . At neutral pH, the surface concentration of the  $[Br\bullet OOO^-]$

## ABSTRACT

---

intermediate increased almost linearly with the bromide concentration. This behavior was tightly correlated with that of the the loss rate of ozone determined in kinetic experiments over the same bromide concentration range.

Studying the impact of surface-active organics on the interfacial abundance of halide ions is important due to the ubiquitous presence of organic compounds in sea water in biologically active oceans. Here, we use liquid-jet XPS to assess the impact of a monofunctional surfactant with a positive headgroup (hexylammonium) and one with a negative headgroup (propylsulfate) on the abundance of bromide ions at the interface. We use a photoelectron attenuation model to retrieve the interfacial concentrations of bromide and sodium in the presence of those surfactants. The results show that even in basic solution, where only a small fraction of hexylamine is protonated, its surface activity leads to an enhanced interfacial concentration of bromide. This suggests that non-protonated hexylamine is already attracting bromide to the interface. In turn, the negatively charged sulfate group of propylsulfate does not affect the interfacial concentration of the bromide, but leads to an increased presence of the sodium cations. The present work demonstrates the vital role of electrostatic interactions at the interface. This concept can be applied to qualitatively assess other halide or alkaline cations, or even other inorganic ions, such as  $\text{SO}_4^{2-}$ ,  $\text{NO}_3^-$ ,  $\text{NH}_4^+$  that exist in atmospheric particles.

The oxidation of bromide by ozone is enhanced at aqueous interfaces, driven by the surface active bromide ozonide intermediate. In extension to the role that ionic surfactants have on the abundance of bromide at interface, the question arises how surfactants affect the reactivity of  $\text{O}_3$  with bromide. Here, we assess the surface propensity of cationic tetrabutylammonium (TBA) at the aqueous liquid-vapor interface by liquid-jet XPS and the effect of this surfactant on ozone uptake to aqueous bromide solutions. The results indicate that the positively charged nitrogen group in TBA, along with its surface activity, leads to an enhanced interfacial concentration of both bromide and the bromide ozonide reaction intermediate. In parallel, off-line kinetic experiments for the same system demonstrate a strongly enhanced ozone loss rate in the presence of TBA, which is attributed to an enhanced surface reaction rate. Again supported by a model of attenuation of photoelectrons by the carbon-rich layer established by the TBA surfactant, we found that the interfacial density of bromide is increased by an order of magnitude in solutions with TBA. The salting-out of TBA in the presence of additional 0.55 M sodium chloride is apparent. The increased interfacial bromide density can be rationalized by the association constants for bromide (and chloride) to form ion-pairs with TBA. The steady-state concentration of the bromide ozonide intermediate increases by a smaller degree, and the lifetime of the intermediate is one order of magnitude longer in the presence of TBA. Thus, the influence of cationic surfactants on the reactivity of bromide depends on the details of the complex environment at the interface.

---

## Zusammenfassung

---

Die Oxidation von Halogeniden an der Grenzfläche zwischen wässriger Lösung und Luft initiiert die Freisetzung von Halogenverbindungen in der Gasphase, die 50% der chemischen Ozonsenke in der globalen Troposphäre ausmachen. Halogenid-Lösung-Luft-Grenzflächen sind allgegenwärtig, da etwa 71% der Erdoberfläche von Meerwasser bedeckt sind, das große Mengen an Chlorid und Bromid enthält. Darüber hinaus werden diese in Form von Meersalz-Aerosolen in die Atmosphäre abgegeben und somit auch über weite Strecken über die Kontinente transportiert. Seit kurzem, mit der Entwicklung von differentiell gepumpten elektrostatischen Linsensystemen, ermöglicht uns die Flüssigkeitsstrahl-Röntgenphotoelektronenspektroskopie (XPS), die Grenzfläche zwischen wässriger Lösung und Luft auf molekularer Ebene direkt und in Anwesenheit von Spurengasen zu untersuchen. In diesem Projekt verwenden wir Flüssigstrahl-XPS an der Swiss Light Source in Verbindung mit kinetischen Experimenten, um Folgendes zu untersuchen: die molekularen Details der Oberflächenreaktion von wässrigem Bromid mit  $O_3$  in An- und Abwesenheit organischer Verbindungen. Ziel wird es sein, zukünftige Bewertungen der Halogenchemie hinsichtlich der atmosphärischen Oxidationskapazität und des Klimas zu unterstützen.

Die Affinität von Halogenidionen in wässriger Lösung für die Flüssig-Gas-Grenzfläche, die ihre Reaktivität mit gasförmigen Spezies beeinflussen kann, wird schon länger diskutiert. In-situ- XPS, an einem Flüssigkeitsstrahl durchgeführt, wurde verwendet, um das Grenzflächen-Tiefenprofil von Bromid, Hypobromit, unterbromiger Säure und Bromat zu untersuchen. Darüber hinaus wird über Spektren berichtet, die Lösungen mit niedrigen und hohen Konzentrationen von Bromid, Mischungen von Bromid und Chlorid sowie separat Bromid mit Chlorid und Fluorid vergleichen, um weiter zum Verständnis der Oberflächenaffinität von Halogenidionen beizutragen. Bromidionen neigen auch in Gegenwart von Chlorid dazu, sich eher nicht an der Lösungsoberfläche anzureichern. In der Halogenreihe folgt die Oberflächenaffinität der Reihe  $Br > Cl > F$ , und dies stimmt mit neueren Theorien und Experimenten überein, die zeigen, dass die leichtesten Halogenidionen am stärksten an der Oberfläche abgereichert sind. Unter den Bromspezies ist hypobromige Säure, eine Schlüsselspezies im Multiphasen-Kreislauf von Brom, die einzige Spezies, die eine beträchtliche Oberflächenaktivität zeigt, was darauf hindeutet, dass die Grenzfläche für diese Spezies in der Multiphasen-Bromchemie eine wichtigere Rolle spielt als bisher angenommen.

In der wässrigen Phase wird bei der Oxidation von Bromid durch Ozon ein  $[Br\cdot OOO^-]$ -Komplex als Zwischenstufe involviert. Hier berichten wir über Flüssigkeitsstrahl-XPS-Messungen, die direkte experimentelle Beweise für dieses Ozonid liefern und seine Affinität zur Lösung-Gas-Grenzfläche nachweisen. In weiteren Experimenten bei niedrigem pH-Wert war das Signal des Zwischenprodukts  $[Br\cdot OOO^-]$  klein und gerade an der Nachweisgrenze, was auf eine schnellere Bildung der Produkte, also Freisetzung von molekularem Sauerstoff und Bildung von Hypobromit, zurückzuführen sein könnte. Die Oberflächenkonzentration des  $[Br\cdot OOO^-]$ -Zwischenprodukts stieg fast linear mit der Bromidkonzentration

## ZUSAMMENFASSUNG

---

an. Dieses Verhalten war eng mit demjenigen der Verlustrate von Ozon korreliert, die in kinetischen Experimenten über denselben Konzentrationsbereich von Bromid gemessen wurde.

Das allgegenwärtige Vorkommen von organischen Verbindungen im Meerwasser von biologisch aktiven Ozeanen erfordert die Bewertung der Auswirkungen von oft oberflächenaktiven organischen Stoffen auf die Grenzflächenaffinität von Halogenidionen. Hier verwenden wir Flüssigkeitsstrahl-XPS an der Synchrotron Lichtquelle Schweiz, um den Unterschied zwischen einem monofunktionellen Tensid mit einer positiven Kopfgruppe (Hexylammonium) und einem mit einer negativen Kopfgruppe (Propylsulfat) in Bezug auf die Anreicherung von Bromidionen an der Grenzfläche zu beurteilen. Wir verwenden auch ein Modell für die Attenuierung von Photoelektronen, um die Grenzflächenkonzentration von Bromid und Natrium in Gegenwart der verschiedenen Tenside zu bestimmen. Die Ergebnisse zeigen, dass selbst in basischer Lösung, in der nur ein kleiner Teil des Hexylamins tatsächlich protoniert wird, seine Oberflächenaktivität zu einer erhöhten Bromidkonzentration an der Grenzfläche führt. Dies deutet darauf hin, dass wahrscheinlich nicht nur protoniertes Hexylamin Bromid an die Grenzfläche zieht. Die negativ geladene Sulfatgruppe von Propylsulfat wiederum beeinflusst nicht die Grenzflächenkonzentration von Bromid, führt jedoch zu einer erhöhten Anwesenheit von Natriumkationen. Die vorliegende Arbeit demonstriert die wichtige Rolle elektrostatischer Wechselwirkungen an der Grenzfläche. Dieses Konzept kann auch angewendet werden, um andere Halogenidanionen- oder Alkalikationen oder sogar Ionen anderer anorganischer Ionen wie  $\text{SO}_4^{2-}$ ,  $\text{NO}_3^-$ ,  $\text{NH}_4^+$  etc., die in atmosphärischen Partikeln vorkommen, in ihrer Wechselwirkung mit geladenen Tensiden vorauszusagen.

Die Oxidation von Bromid durch Ozon wird an wässrigen Grenzflächen verstärkt, getrieben durch das Bromid-Ozonid als Zwischenstufe. In Anbetracht des Einflusses von Tensiden auf die Anreicherung von Bromid an der Grenzfläche, stellt sich die Frage nach dem Einfluss auf die Reaktivität von Bromid mit Ozon. Hier bewerten wir die Oberflächenaffinität von kationischem Tetrabutylammonium (TBA) an der wässrigen Flüssigkeits-Dampf-Grenzfläche durch Flüssigkeitsstrahl-XPS und die Wirkung dieses Tensids auf die Ozonaufnahme in wässrige Bromidlösungen. Die Ergebnisse zeigen, dass die positiv geladene Stickstoffgruppe in TBA zusammen mit ihrer Oberflächenaktivität zu einer erhöhten Grenzflächenkonzentration von sowohl Bromid als auch der Bromid-Ozonid-Zwischenstufe führt. Parallel zeigen kinetische Experimente für dasselbe System eine stark erhöhte Ozonverlustrate in Gegenwart von TBA, was einer erhöhten Oberflächenreaktionsrate zugeschrieben wird. Wiederum wurde ein Modell verwendet, um die Attenuierung von Photoelektronen durch die kohlenstoffreiche Schicht zu berücksichtigen, die durch das TBA-Tensid gebildet wird. Daraus können wir schliessen, dass die Grenzflächendichte von Bromid in Lösungen mit TBA um eine Größenordnung erhöht ist. Das Aussalzen von TBA in Gegenwart von 0.55 M Natriumchlorid ist offensichtlich. Die erhöhte Bromiddichte an der Grenzfläche kann durch die Assoziationskonstanten von Bromid (und Chlorid) für die Bildung von Ionenpaaren mit TBA erklärt werden. Die Steady-State-Konzentration des Bromid-Ozonid-Zwischenprodukts nimmt in geringerem Maße zu, und die Lebensdauer des Zwischenprodukts ist in Gegenwart von TBA um eine Größenordnung länger. Somit hängt der Einfluss kationischer Tenside auf die Reaktivität von Bromid von den Details der komplexen Umgebung an der Grenzfläche ab.

#### 1.1 Ozone and halogen chemistry

The atmosphere of the Earth is predominantly made up of molecular nitrogen and oxygen. Ozone is a gas that is naturally present in small amounts in our atmosphere. Each ozone molecule contains three oxygen atoms and has the chemical formula  $O_3$ . In the mid-1800s, ozone was discovered in the laboratory. Later, ozone was identified using chemical and optical measurement methods. Ozone has a pungent odor that can be detected even if present in very low amounts. About 90% of atmospheric ozone is found in the stratosphere, which begins about 10-16 kilometers above the Earth's surface and extends up to about 50 kilometers altitude [Hegglin *et al.*, 2015]. This region is commonly known as the "ozone layer", which protects us from biologically harmful ultraviolet radiation from the sun. Stratospheric ozone is considered "good" ozone because of its beneficial role. Most of the remaining ozone, about 10%, is found in the troposphere, which is the lowest region of the atmosphere, between Earth's surface and the stratosphere [Hegglin *et al.*, 2015]. Tropospheric ozone above natural levels is considered as "bad" ozone, which is harmful to humans, plants, and other living systems as it reacts strongly to destroy or alter many biological molecules [Hegglin *et al.*, 2015]. "Bad" ozone is formed by reactions involving human-made pollutant gases. In the mid-1970s, it was discovered that gases containing chlorine and bromine atoms released by human activities could cause stratospheric ozone depletion [Steinfeld, 1998]. These gases, referred to as halogen source gases and as ozone-depleting substances, chemically release their chlorine and bromine atoms after they reach the stratosphere. Ozone depletion increases surface UV-B radiation above naturally occurring doses.

Interfacial chemistry is playing a crucial role in atmospheric sciences, like the chemistry of halogen compounds [Finlayson-Pitts, 2003], cycling of nitrogen oxides [Pöschl and Shiraiwa, 2015], cloud droplet activation [Ruehl et al., 2016], and ice nucleation [Knopf et al., 2018]. Halogens are species containing fluoride, chloride, bromide or iodide. Halide solution-air interfaces are ubiquitously present because about 71% of the Earth's surface is covered by seawater that contains large amounts of chloride and bromide. In the gas phase, they represent a sink for ozone through catalytic reactions involving halogen atoms. It has been estimated that halogen chemistry contributes 50% of the chemical sink for tropospheric ozone globally [Simpson et al., 2015; Wang et al., 2015]. This impacts the ozone concentration, which is relevant for the oxidation capacity and the radiative budget and thus climate [Sherwen et al., 2017]. Halogens are furthermore emitted to the atmosphere in the form of sea spray aerosol and are therefore also transported over long distances over the continents. Halogens may also be transported to the stratosphere and influence stratospheric O<sub>3</sub> levels [Wang et al., 2015; Lopez et al., 2004].

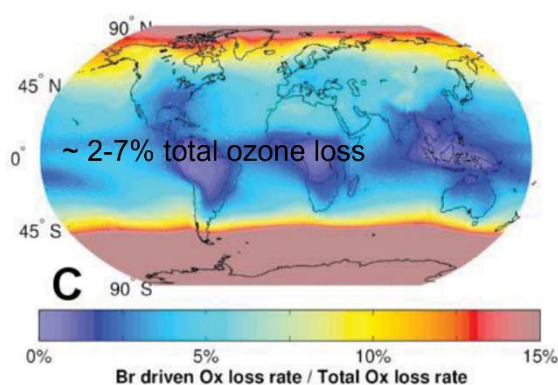


**Figure 1:** Tropospheric column integral of ozone change with bromine chemistry. The figure is adapted from [Wang et al., 2015].

Halogen chemistry has been studied for decades for its role in O<sub>3</sub> depletion in the stratosphere. However, the role halogens (e.g. Br atoms or BrO) play in the troposphere is not well understood yet. Read et al. found that the absence of halogens in their box model results in underestimating the total O<sub>3</sub> loss by half and the O<sub>3</sub> concentrations by 12% (annual averages) [Read et al., 2008]. Wang et al. [Wang et al., 2015] also found that bromine contributes to around 2-7% of the tropospheric column integral of ozone, which is shown in Figure 1. Interestingly, the observed levels of bromine oxidize mercury up to 3.5 times faster than models predict. Such effects have not been sufficiently elucidated. In order for bromine (and the other halogens) to participate in gas phase O<sub>3</sub> depleting reaction cycles, it has to be oxidized from the bromide present in the aqueous phase, and released to the gas phase. Therefore, an important and not well understood processes of halogen chemistry are those at aqueous solution – air interfaces. In part, our poor understanding is related to the lack of experimental methods and approaches to selectively probe the interfacial region and processes thereon.



The so-called O<sub>3</sub> depletion events, which were caused by reactive halogen species, in particular, the halogen oxides BrO and IO, happen in the troposphere through auto-catalytic reactions, destroying O<sub>3</sub> [Simpson *et al.*, 2007]. A specific sequence, which is called the “bromine explosion”, is thought to be the main series of reactive processes by which halogens enter the O<sub>3</sub> depleting cycles during O<sub>3</sub> depletion events [Jones *et al.*, 2009; Simpson *et al.*, 2007]. Figure 2 shows a simplified representation of bromine explosion reactions [Haag and Hoigné, 1984]. The Major halogen-related reactions in the gas and aqueous phase are: The liquid brine solution degassing of bromide (Br<sup>-</sup>) in the form of Br<sub>2</sub> (or BrCl) into the gas phase through multiphase reactions. Then the gas phase bromine forms two reactive bromine atoms by photolysis, which can further react with ozone. On the one hand, it can make a small cycle to decrease the ozone, and on the other hand, via hypobromous acid (HOBr), it initiates reaction with more of the condensed phase bromide leading to more release of Br<sub>2</sub> to the gas phase. Light is needed for the production of HO<sub>2</sub> radicals through gas phase photochemistry to allow the formation of HOBr. Therefore, without light, when photochemically produced radicals and oxidants are not abundant, the multiphase reaction of O<sub>3</sub> with bromide in the condensed phase is believed to be one of the significant dark oxidants for bromide to lead to the release sources of molecular bromine.

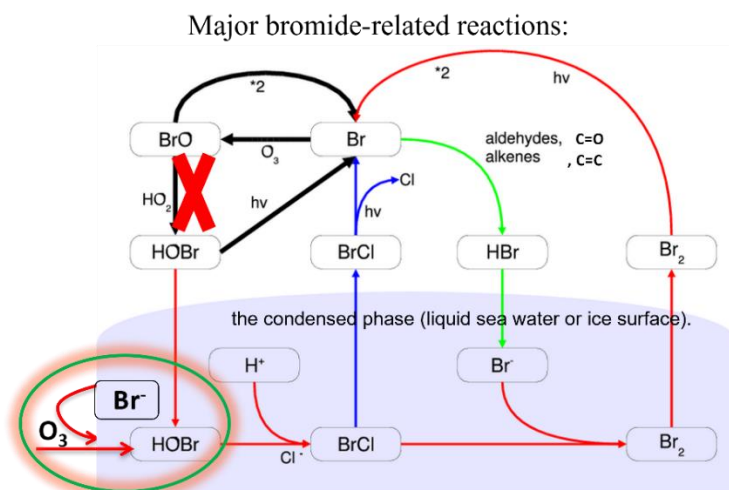


**Figure 2:** A simplified representation of bromine explosion reactions. The figure is adapted from [Simpson *et al.*, 2007; Haag and Hoigné, 1984].

## 1.2 Multiphase kinetics of oxidation of bromide

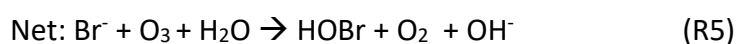
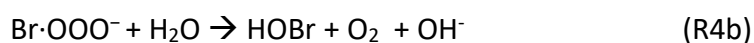
Multiphase reactions between gas-phase species and halides in seawater are centrally important because halogen cycles exert a powerful influence on the chemical composition of the troposphere, thus may affect the global oxidation capacity and the fate of pollutants, tropospheric ozone (and thus its radiative impact) and the production of particles [Carpenter *et al.*, 2013; Wang *et al.*, 2015]. The reaction of O<sub>3</sub> with Br<sup>-</sup> ions is believed to be one of the significant dark sources of gas-phase halogen compounds to produce HOBr when photochemically produced radicals and oxidants are not abundant. These initial halide oxidation processes are the starting point of the multiphase cycling reaction mechanisms that lead to

the release of bromine, chlorine, and iodine compounds also referred to as halogen activation.

The net aqueous phase reaction of gaseous O<sub>3</sub> with Br<sup>-</sup> is as follows [Lee *et al.*, 2015; Oldridge and Abbatt, 2011]:



The pKa of HOBr is 8.65. Liu *et al.* [Liu *et al.*, 2001] suggests that R1 occurs through an acid-catalyzed mechanism, where O<sub>3</sub> reacts with Br<sup>-</sup> to form the steady-state intermediate Br·OOO<sup>-</sup>. This intermediate would subsequently react with H<sup>+</sup> or H<sub>2</sub>O to give HOBr and O<sub>2</sub> (reactions R3 and R4a, R4b):



On the other hand, Haag *et al.* [Haag and Hoigne, 1983] proposed the following mechanism for recycling of OBr<sup>-</sup> (formed from the reaction R1) by H<sub>2</sub>O<sub>2</sub> back to Br<sup>-</sup>:



Halogen peroxides (BrOO<sup>-</sup>) are formed by the reaction R6 of H<sub>2</sub>O<sub>2</sub> with OBr<sup>-</sup> and decompose rapidly to O<sub>2</sub> and Br<sup>-</sup> as in reaction R7. Therefore, the ubiquitously present H<sub>2</sub>O<sub>2</sub> could limit the extent of bromide oxidation.

With a rate coefficient of 163 M<sup>-1</sup> s<sup>-1</sup> at room temperature in the bulk aqueous phase, R1 is of limited relevance to explain field observations of halogen activation. Several reports have suggested that R1 may occur at enhanced rates at the aqueous solution – air interface [Clifford and Donaldson, 2007; Oldridge and Abbatt, 2011; Oum *et al.*, 1998]; however, this has not been understood in detail. Furthermore, it has also remained unclear how such a surface reaction would be affected by organic compounds [Carpenter and Nightingale, 2015]. The ocean surface water and sea spray aerosol derived therefrom contain a complex mixture of not only inorganic salts but also organic compounds deriving from marine biota [Bernard *et al.*, 2016; Donaldson and George, 2012; O'Dowd *et al.*, 2004]. Organics may have a significant effect on the way halide ions are distributed at the interface [Stemmler *et al.*, 2008], and on the mass transfer across the interface [Morris, 2013; Vignati *et al.*, 2010].

### 1.3 The halide solution in the presence of organics

The seawater contains a complex mixture of not only inorganic salts but also organic compounds deriving from marine biotas, like proteins, carbohydrates, fatty acids [O'Dowd *et*

al., 2004; Kanakidou et al., 2005; Vignati et al., 2010; Donaldson and George, 2012]. For example, Figure 3 shows the chemical composition of submicrometre marine aerosols measured over the North Atlantic Ocean during (a) the winter, with low biological activity, and (b) during the plankton blooms progressing from spring through to autumn, with high biological activity, respectively [O'Dowd et al., 2004]. They found during bloom periods, the organic fraction dominates and contributes 63% to the submicrometre aerosol mass (about 45% is water-insoluble and about 18% water-soluble). In winter, when biological activity is at its lowest, the organic fraction decreases to 15%. The organic fraction dominates aerosol mass at small diameter size, while the inorganic fraction dominates at large diameter size, which may have similar compositions as seawater. The model simulations indicate that organic matter can enhance the cloud droplet concentration by 15% to more than 100% and is, therefore, an important component of the aerosol–cloud–climate feedback system involving marine biota.

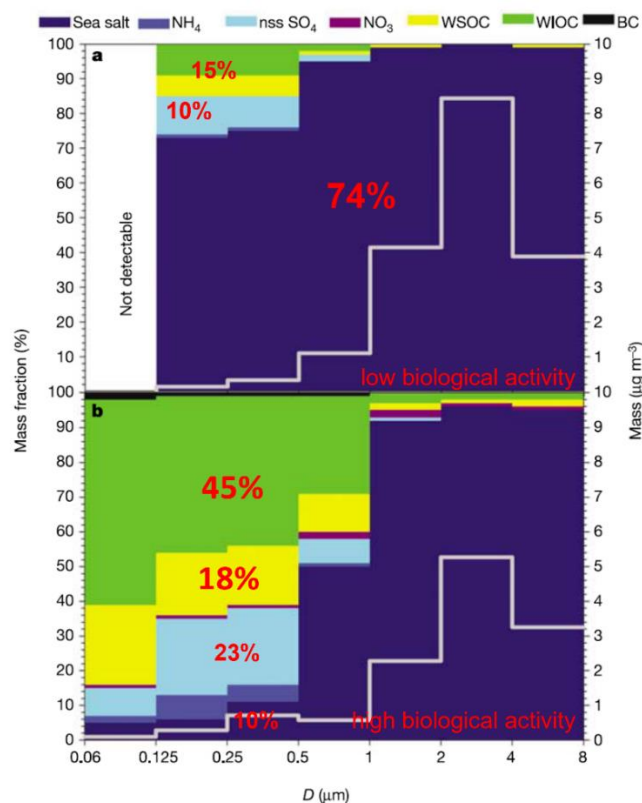


**Figure 3:** Chemical composition of marine aerosols. Shown are average size-segregated chemical compositions and absolute mass concentrations for North Atlantic marine aerosols sampled with a Berner Impactor for (a) low biological activity and (b) high biological activity periods. The concentrations of water-soluble organic compounds (WSOC), water-insoluble organic compounds (WIOC), and black carbon (BC) are reported as mass of organic matter. The graphs is adapted from [O'Dowd et al., 2004].

The ubiquitous presence of organic material at the ocean surface calls for an assessment of the impact of surface-active organic compounds on the interfacial density of halide ions ([Krisch et al., 2007], which may hinder the mass transfer between the gas and particle phases [Rouviere and Ammann, 2010] or even promote it [Faust et al., 2013; Morris, 2013]. Figure 4

shows the examples of surface-active solutes affecting the surface propensity of bromide at the aqueous solution-air interface from our previous work. Six years ago, we studied the reaction of ozone with NaBr in the presence of citric acid. It showed that the bromide ion becomes depleted by 30%, even though the reactivity was enhanced [Lee *et al.*, 2015]. This was attributed to the effect of acidity that was overriding the reduction in surface concentration. Two years ago, our liquid jet XPS measurements provided direct experimental evidence for the  $[\text{Br}\cdot\text{OOO}^-]$  intermediate, which was found to exhibit preference for the surface and is the reason why the reaction of NaBr with  $\text{O}_3$  is enhanced at the surface [Artiglia *et al.*, 2017]. In addition, our group observed that 1-butanol increases the interfacial density of bromide by 25%, while butyric acid reduces it by 40%. They may change the arrangement of bromide at the interface for reaction [Lee *et al.*, 2019].

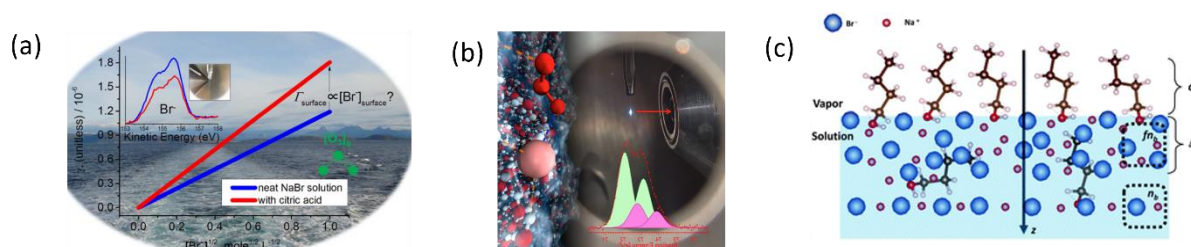


**Figure 4:** Examples of surface-active solutes affect the surface propensity of bromide at the aqueous solution-air interface. The graphs are adapted from [Lee *et al.*, 2015; Artiglia *et al.*, 2017; Lee *et al.*, 2019].

Thus, the interaction between bromide ions and surface-active solutes could affect the abundance and the local environment of bromide at the aqueous solution-air interface. For instance, surface-active organic carboxylic acids with neutral functional headgroups could on one hand compete with bromide for space at the interface, or on the other hand accelerate the reaction with  $\text{O}_3$  via acid catalysis.

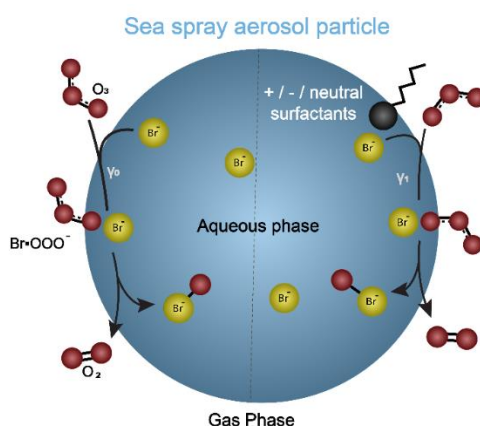


**Figure 5:** The schematic shows the multiphase reaction between gas-phase ozone and condensed phase bromine aqueous solution, with a certain overall ozone uptake coefficient ( $Y_0$ ), involving the formation of the bromide ozonide intermediate  $[\text{Br}\cdot\text{OOO}^-]$ ; Besides, the surface-active organic compounds with different functional groups such as  $-\text{COOH}$  (neutral),  $-\text{SO}_4$  (negative),  $-\text{NH}_4$  (positive), may play an additional role, to influence the ozone uptake coefficient ( $Y_1$ ).

In a different way, organosulfates with a negative functional headgroup may affect the bromide aqueous solution surface through electrostatic effects, as they may push away the

bromide ions from the surface and thereby decrease the reaction rate at the surface. In turn, alkylamines with a positive functional headgroup, which are present everywhere in the atmosphere, may pull the bromide closer to the surface. Furthermore, such surface-active solutes may also influence the bromide ozonide intermediate species, eventually enhancing the reaction rate. In Figure 5, the schematic shows the multiphase reaction between gas-phase ozone and condensed phase bromine aqueous solution, with a certain overall ozone uptake coefficient ( $Y_0$ ), and involving the steady-state bromide ozonide intermediate [ $\text{Br}\cdot\text{OOO}^-$ ], and how these interact with different functional groups such as  $-\text{COOH}$  (neutral),  $-\text{SO}_4$  (negative),  $-\text{NH}_4$  (positive).

## 1.4 Analytical methods to characterize the liquid-vapor interface

The liquid-vapor interfacial region is an experimental challenge because many surface-selective experimental techniques require high or ultra-high vacuum for use and cannot be easily applied to liquids with reasonable vapor pressures. There are numerous outstanding analytical techniques capable of investigating the liquid-vapor interface. Among these, there are some notable examples: surface tension [*Leroy et al.*, 2010], which gives a macroscopic picture of the composition of the interface; sum-frequency generation spectroscopy [*Jubb et al.*, 2012; *Götte et al.*, 2017], which provides detailed information on the structure and orientation of water within the non-centrosymmetric region at the interface; and liquid-based X-ray photoelectron spectroscopy (XPS) [*Winter et al.*, 2004; *Ghosal et al.*, 2005; *Krisch et al.*, 2007; *Oldridge and Abbatt*, 2011; *Brown et al.*, 2013; *Björneholm et al.*, 2014; *Lee et al.*, 2015], which provides information about the electronic structure, chemical composition, orientation, co-solutes and other interface properties.

The traditional approach to studying the chemical composition at the aqueous solution – air interface through the contribution of constituents to the surface free energy and experimentally accessed via recording the surface tension as a function of solute concentration is not straightforward for complex solutions [*Donaldson and Anderson*, 1999]. Both chemical composition and processes at interfaces can be characterized by XPS which provides chemical selectivity and surface sensitivity straightforwardly. It is based on the excitation of core electrons by X-rays and detection of the photoelectron kinetic energy (KE) spectrum. The surface sensitivity results from the short, KE-dependent, inelastic mean free path (IMFP,  $\lambda$ ) of electrons in condensed matter in the range from just below one to a few nanometers.

However, traditional XPS is limited to solid samples held in a vacuum, which may exhibit dramatic differences to the same material in real environments, where atmospheric processes occur. Over the past decade, near ambient pressure photoemission (NAPP) was developed, which allows investigating aqueous solution surfaces by XPS in the form of a liquid jet up to pressures equivalent to the equilibrium vapor pressure of water at ambient temperatures [*Brown et al.*, 2013]. Liquid jet XPS directly provides the composition of inorganic and organic compounds at the aqueous solution-vapor interface, thus, within the

top-most molecular layers of the liquid. The liquid jet is typically running at high enough velocity to avoid radical chemistry initiated by X-rays affecting the measured composition and avoid an impact of evaporation on the water activity of the solution [Winter and Faubel, 2006]. In turn, the speed is slow enough to allow equilibration of solutes by diffusion between the bulk aqueous phase and the surface [Lee et al., 2015; Winter and Faubel, 2006]. Liquid jet XPS operated at variable pressure allows studying the liquid-vapor interface for environmentally relevant cases.

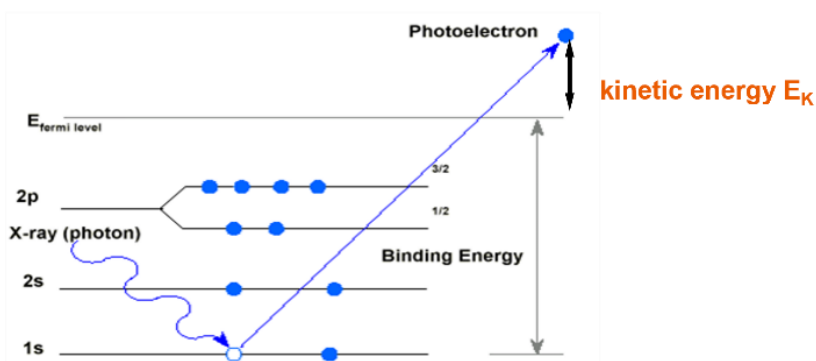


**Figure 6:** Scheme of X-ray photoelectron spectroscopy principle.

The photoemission spectroscopy technique is based on the photoelectric effect. The basic principle of XPS is shown in Figure 6: A photon with energy  $h\nu$  excites an atom by transferring its energy to a core level electron. If  $h\nu >$  the binding energy of the electron, it will be emitted as a photoelectron with kinetic energy  $E_K$  equal to the excess energy.

$$KE = h\nu - BE - \phi$$

where  $h$  is the Planck constant,  $\nu$  is the frequency of the radiation;  $BE$  is the binding energy, and  $\phi$  is the specific work function of the material, which represents the additional energy barrier related to passing across the surface.

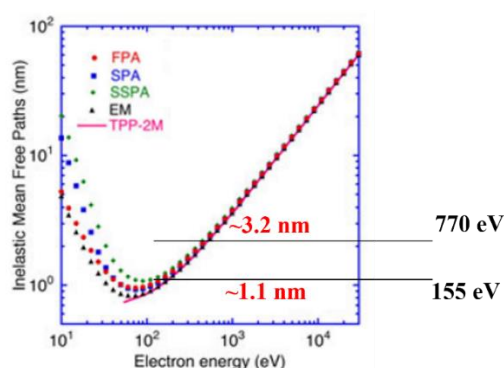


**Figure 7:** Inelastic mean free paths. Graphs are adapted from [Shinotsuka et al., 2017].

One of the essential properties of photoelectron spectroscopy, namely, surface sensitivity, is related to the inelastic mean free path (IMFP) of electrons in solids or liquids. The photoelectrons can only escape without loss of energy (inelastic scattering) from a few nm, as Figure 7 shows in the form of the relationship between the IMFP and the kinetic energy for water [Shinotsuka et al., 2017]. Hence, for a homogeneous sample, the contribution of an

atom to the measured photoemission signal exponentially drops with the distance from the surface, establishing the probe depth. 80% of the photoemission signal originates from the depth equivalent to two times the IMFP, and 98% of the signal is from three IMFPs. XPS quantitatively measures the amounts of molecules within the probe depth since the intensity of photoelectron signals is proportional to the atom density after all normalizations (like photon flux, cross-section, inelastic mean free path, and transmission function of the analyzer). Starting from 100 eV, the inelastic mean free path (IMFP or  $\lambda$ ) increases with kinetic energy, which can be used to obtain a cumulative depth profile. In this thesis, we will use the photoelectron kinetic energy range from 270 eV to 770 eV, which means the inelastic mean free paths are from around 1.1 nm to 3.2 nm.

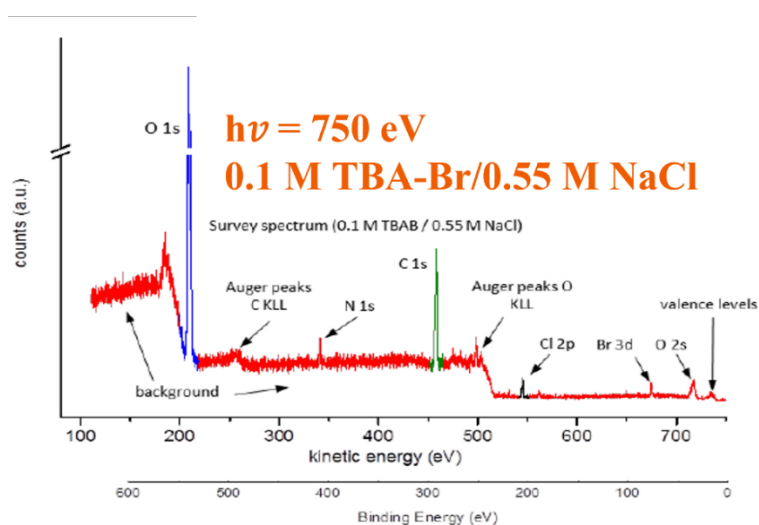


**Figure 8:** Survey spectrum of photoelectrons emitted from an aqueous solution containing 0.1 M tetrabutylammonium bromide and 0.55 M NaCl, excited by 750 eV photons, with characteristic photoemission and Auger peaks.

Figure 8 shows a survey spectrum of photoelectrons emitted from an aqueous solution containing 0.1 M tetrabutylammonium bromide and 0.55 M NaCl, excited by 750 eV photons, with characteristic photoemission and Auger peaks. We can collect different elemental signals at different kinetic energy.

## 1.5 Thesis mission

The mission of this thesis is to combine standard kinetic experiments with the liquid jet XPS method to unravel kinetic and mechanistic aspects down to the molecular level for the oxidation of bromide at the halide solution – air interface. Working on this thesis driven by the above mission, XPS is used on the one hand to characterize the interplay of anions and cations near the aqueous solution – air interface in the presence and absence of organic compounds. On the other hand, XPS will also be used to directly probe the interface in the presence of O<sub>3</sub> in the gas phase to obtain in situ spectroscopic evidence for a reaction intermediate during oxidation of bromide that we suspect to mediate efficient oxidation on the surface. Finally, the classical flow tube method will be used to obtain a more detailed picture of the kinetics in terms of chloride and pH and the organic surfactants with different

charged headgroup compounds. Since we suspect that the charge of the head group of the surfactants has a crucial influence on the ion distribution at the interface, we focus on this aspect for our planned experiments.

Oxidation of bromide by  $O_3$  in aqueous solution involves a  $[Br\bullet OOO^-]$  intermediate [Liu et al., 2001; Gladich et al., 2015], that may be stabilized at the interface and thereby open a route for faster bromide oxidation that has been suspected earlier [Oum et al., 1998; Clifford and Donaldson, 2007; Oldridge and Abbatt, 2011]. Identifying  $[Br\bullet OOO^-]$  at the interface will be a significant step forward in understanding the multiphase oxidation of bromide. As a next step, we will study the impact of different bromide concentrations, pH and the effect of other halide ions ( $Cl^-$ ) on the  $O_3$  –bromide reaction system using liquid jet XPS to observe the behavior of the intermediate *in situ* and with kinetic experiments to study the overall kinetics and establish the contribution of the surface reaction for various environmental conditions.

On the other hand, we will investigate the kinetics of oxidation of  $Br^-$  with  $O_3$  (and of  $Br^-$  mixed with 0.55 M NaCl corresponding to actual sea water) in the presence of amphiphilic organic compounds with differently charged headgroups using both liquid jet XPS and the flow tube method. This will provide us with information about: 1) the distribution of the surfactant headgroup, bromide and chloride anions and sodium cations with depth at and below the interface; 2) the abundance of the reaction intermediate at the surface; 3) the extent to which the surface reaction dominates overall reaction kinetics. These experiments will be performed for: 1) a neutral carboxylic acid; 2) organic sulfate compounds with an anionic head group at the surface; 3) alkylamines with a positively charged head group. Organic sulfate compounds, e.g., alkyl sulfates, form in the atmosphere from secondary chemistry in a sulfate-containing aerosol. Alkylamines derive from the degradation of marine or atmospheric biological material. We expect cationic and anionic surfactant headgroups to interact differently with  $Br^-$  and thus also expect an impact on the reaction rates and especially on the contribution of the surface reaction.

## 1.6 Thesis outline

The PhD work includes analysis of the surface propensity of bromide and its oxidation products hypobromide and bromate, and of organic surfactants with differently charged headgroups, both individually and in combination with bromide, using liquid jet XPS. Finally, the impacts of surfactants on oxidation kinetics are assessed in laboratory-based flow tube experiments. Below, I present a summary of the following chapters, highlighting the outcomes.

Chapter 2 presents the liquid jet XPS methods and technical aspects. Also, the experimental setup for experiments addressing the multiphase kinetics of ozone using a flow reactor is shown.

Chapter 3 summarizes the liquid jet XPS experiments of different bromine-based compounds involved in bromine activation and cycling. Our results have shown that a similar absence of



enhancement is observed for bromide as well as for hypobromite and bromate. Similarly, to other undissociated, neutral forms of acids, hypobromous acid shows a propensity for the liquid-gas interface.

Chapter 4 reports liquid jet XPS measurements that provide direct experimental evidence for the bromide ozonide and its preference for the liquid-vapor interface. In addition, we focus on the surface propensity of bromide ozonide at low pH and as a function of bromide concentration and compare the corresponding interfacial density of bromide ozonide with the ozone uptake coefficient.

Chapter 5 presents the impact of a monofunctional surfactant with a positive headgroup (hexylammonium) and a negative headgroup (propylsulfate) on the abundance of bromide and sodium ions at the liquid-vapor interface. A photoelectron attenuation model is used to retrieve the interfacial concentration of bromide and sodium in the presence of the different surfactants.

Chapter 6 presents the impact of tetrabutylammonium (TBA) on the abundance of bromide and the bromide ozonide at the aqueous solution – air interface and compares the spectroscopic information with the results of O<sub>3</sub> uptake kinetic experiments performed in parallel. Again, a model is used to account for the attenuation of photoelectrons by the carbon-rich layer established by the TBA surfactant. The results demonstrate a strong enhancement of O<sub>3</sub> loss in presence of TBA.

Chapter 7 summarizes the experimental achievements, with an outlook on future experiments.

---

## Bibliography

---

- Artiglia, L., et al. (2017), A surface-stabilized ozonide triggers bromide oxidation at the aqueous solution-vapour interface, *Nature Communications*, 8(1), 700, doi:10.1038/s41467-017-00823-x.
- Bernard, F., R. Ciuraru, A. Boréave, and C. George (2016), Photosensitized Formation of Secondary Organic Aerosols above the Air/Water Interface, *Environmental Science & Technology*, 50(16), 8678-8686, doi:10.1021/acs.est.6b03520.
- Björneholm, O., J. Werner, N. Ottosson, G. Öhrwall, V. Ekholm, B. Winter, I. Unger, and J. Söderström (2014), Deeper Insight into Depth-Profiling of Aqueous Solutions Using Photoelectron Spectroscopy, *The Journal of Physical Chemistry C*, 118(50), 29333-29339, doi:10.1021/jp505569c.
- Brown, M. A., et al. (2013), A new endstation at the Swiss Light Source for ultraviolet photoelectron spectroscopy, X-ray photoelectron spectroscopy, and X-ray absorption spectroscopy measurements of liquid solutions, *Review of Scientific Instruments*, 84(7), 073904, doi:10.1063/1.4812786.
- Carpenter, L. J., S. M. MacDonald, M. D. Shaw, R. Kumar, R. W. Saunders, R. Parthipan, J. Wilson, and J. M. Plane (2013), Atmospheric iodine levels influenced by sea surface emissions of inorganic iodine, *Nature Geoscience*, 6(2), 108-111.
- Carpenter, L. J., and P. D. Nightingale (2015), Chemistry and Release of Gases from the Surface Ocean, *Chemical Reviews*, 115(10), 4015-4034, doi:10.1021/cr5007123.
- Chen, S., L. Artiglia, F. Orlando, J. Edebeli, X. Kong, H. Yang, A. Boucly, P. Corral Arroyo, N. Prisle, and M. Ammann (2021), Impact of Tetrabutylammonium on the Oxidation of Bromide by Ozone, *ACS Earth and Space Chemistry*, 5(11), 3008-3021, doi:10.1021/acsearthspacechem.1c00233.
- Clifford, D., and D. J. Donaldson (2007), Direct Experimental Evidence for a Heterogeneous Reaction of Ozone with Bromide at the Air–Aqueous Interface, *The Journal of Physical Chemistry A*, 111(39), 9809-9814, doi:10.1021/jp074315d.
- Donaldson, D., and D. Anderson (1999), Does molecular HNO<sub>3</sub> adsorb onto sulfuric acid droplet surfaces?, *Geophysical research letters*, 26(24), 3625-3628.
- Donaldson, D. J., and C. George (2012), Sea-Surface Chemistry and Its Impact on the Marine Boundary Layer, *Environmental Science & Technology*, 46(19), 10385-10389, doi:10.1021/es301651m.
- Faust, J. A., L. P. Dempsey, and G. M. Nathanson (2013), Surfactant-Promoted Reactions of Cl<sub>2</sub> and Br<sub>2</sub> with Br<sup>-</sup> in Glycerol, *The Journal of Physical Chemistry B*, 117(41), 12602-12612, doi:10.1021/jp4079037.
- Finlayson-Pitts, B. J. (2003), The Tropospheric Chemistry of Sea Salt: A Molecular-Level View of the Chemistry of NaCl and NaBr, *Chemical Reviews*, 103(12), 4801-4822, doi:10.1021/cr020653t.
- Ghosal, S., J. C. Hemminger, H. Bluhm, B. S. Mun, E. L. D. Hebenstreit, G. Ketteler, D. F. Ogletree, F. G. Requejo, and M. Salmeron (2005), Electron Spectroscopy of Aqueous Solution Interfaces Reveals Surface Enhancement of Halides, *Science*, 307(5709), 563-566, doi:10.1126/science.1106525.
- Gladich, I., J. S. Francisco, R. J. Buszek, M. Vazdar, M. A. Carignano, and P. B. Shepson (2015), Ab Initio Study of the Reaction of Ozone with Bromide Ion, *The Journal of Physical Chemistry A*, 119(19), 4482-4488.
- Götte, L., K. M. Parry, W. Hua, D. Verreault, H. C. Allen, and D. J. Tobias (2017), Solvent-Shared Ion Pairs at the Air–Solution Interface of Magnesium Chloride and Sulfate Solutions Revealed by Sum Frequency Spectroscopy and Molecular Dynamics Simulations, *The Journal of Physical Chemistry A*, 121(34), 6450-6459, doi:10.1021/acs.jpca.7b05600.
- Haag, W. R., and J. Hoigne (1983), Ozonation of bromide-containing waters: kinetics of formation of hypobromous acid and bromate, *Environmental Science & Technology*, 17(5), 261-267.
- Haag, W. R., and J. Hoigné (1984), Kinetics and products of the Reactions of Ozone with Various forms of Chlorine and Bromine in Water, *Ozone: Science & Engineering*, 6(2), 103-114, doi:10.1080/01919518408551009.
- Hegglin, M. I., D. W. Fahey, M. McFarland, S. A. Montzka, and E. R. Nash (2015), *Twenty Questions and Answers About the Ozone Layer: 2014 Update-Scientific Assessment of Ozone Depletion: 2014*.

- 
- Herrmann, H., T. Schaefer, A. Tilgner, S. A. Styler, C. Weller, M. Teich, and T. Otto (2015), Tropospheric aqueous-phase chemistry: kinetics, mechanisms, and its coupling to a changing gas phase, *Chemical reviews*, 115(10), 4259-4334.
- Jones, A. E., P. S. Anderson, M. Begoin, N. Brough, M. A. Hutterli, G. J. Marshall, A. Richter, H. K. Roscoe, and E. W. Wolff (2009), BrO, blizzards, and drivers of polar tropospheric ozone depletion events, *Atmos. Chem. Phys.*, 9(14), 4639-4652, doi:10.5194/acp-9-4639-2009.
- Jubb, A. M., W. Hua, and H. C. Allen (2012), Organization of Water and Atmospherically Relevant Ions and Solutes: Vibrational Sum Frequency Spectroscopy at the Vapor/Liquid and Liquid/Solid Interfaces, *Accounts of Chemical Research*, 45(1), 110-119, doi:10.1021/ar200152v.
- Kanakidou, M., et al. (2005), Organic aerosol and global climate modelling: a review, *Atmos. Chem. Phys.*, 5(4), 1053-1123, doi:10.5194/acp-5-1053-2005.
- Knopf, D. A., P. A. Alpert, and B. Wang (2018), The Role of Organic Aerosol in Atmospheric Ice Nucleation: A Review, *ACS Earth and Space Chemistry*, 2(3), 168-202, doi:10.1021/acsearthspacechem.7b00120.
- Krisch, M. J., R. D'Auria, M. A. Brown, D. J. Tobias, C. Hemminger, M. Ammann, D. E. Starr, and H. Bluhm (2007), The Effect of an Organic Surfactant on the Liquid-Vapor Interface of an Electrolyte Solution, *The Journal of Physical Chemistry C*, 111(36), 13497-13509, doi:10.1021/jp073078b.
- Lee, M.-T., M. A. Brown, S. Kato, A. Kleibert, A. Türler, and M. Ammann (2015), Competition between Organics and Bromide at the Aqueous Solution-Air Interface as Seen from Ozone Uptake Kinetics and X-ray Photoelectron Spectroscopy, *The Journal of Physical Chemistry A*, 119(19), 4600-4608, doi:10.1021/jp510707s.
- Lee, M.-T., F. Orlando, M. Khabiri, M. Roeselová, M. A. Brown, and M. Ammann (2019), The opposing effect of butanol and butyric acid on the abundance of bromide and iodide at the aqueous solution-air interface, *Physical Chemistry Chemical Physics*, 21(16), 8418-8427, doi:10.1039/C8CP07448H.
- Leroy, P., A. Lassin, M. Azaroual, and L. André (2010), Predicting the surface tension of aqueous 1:1 electrolyte solutions at high salinity, *Geochimica et Cosmochimica Acta*, 74(19), 5427-5442, doi:10.1016/j.gca.2010.06.012.
- Liu, Q., L. M. Schurter, C. E. Muller, S. Aloisio, J. S. Francisco, and D. W. Margerum (2001), Kinetics and Mechanisms of Aqueous Ozone Reactions with Bromide, Sulfite, Hydrogen Sulfite, Iodide, and Nitrite Ions, *Inorganic Chemistry*, 40(17), 4436-4442, doi:10.1021/ic000919j.
- Morris, J. R. (2013), Developing a Molecular-Level Understanding of Organic Chemistry and Physics at the Gas-Surface Interface, *The Journal of Physical Chemistry Letters*, 4(23), 4055-4057.
- O'Dowd, C. D., M. C. Facchini, F. Cavalli, D. Ceburnis, M. Mircea, S. Decesari, S. Fuzzi, Y. J. Yoon, and J.-P. Putaud (2004), Biogenically driven organic contribution to marine aerosol, *Nature*, 431(7009), 676-680.
- Oldridge, N. W., and J. P. D. Abbatt (2011), Formation of Gas-Phase Bromine from Interaction of Ozone with Frozen and Liquid NaCl/NaBr Solutions: Quantitative Separation of Surficial Chemistry from Bulk-Phase Reaction, *The Journal of Physical Chemistry A*, 115(12), 2590-2598, doi:10.1021/jp200074u.
- Oum, K. W., M. J. Lakin, D. O. DeHaan, T. Brauers, and B. J. Finlayson-Pitts (1998), Formation of Molecular Chlorine from the Photolysis of Ozone and Aqueous Sea-Salt Particles, *Science*, 279(5347), 74-76, doi:10.1126/science.279.5347.74.
- Pöschl, U., and M. Shiraiwa (2015), Multiphase Chemistry at the Atmosphere-Biosphere Interface Influencing Climate and Public Health in the Anthropocene, *Chemical Reviews*, 115(10), 4440-4475, doi:10.1021/cr500487s.
- Read, K. A., et al. (2008), Extensive halogen-mediated ozone destruction over the tropical Atlantic Ocean, *Nature*, 453(7199), 1232-1235, doi:10.1038/nature07035.
- Rouviere, A., and M. Ammann (2010), The effect of fatty acid surfactants on the uptake of ozone to aqueous halogenide particles, *Atmospheric Chemistry and Physics*, 10(23), 11489-11500, doi:10.5194/acp-10-11489-2010.
- Rouvière, A., Y. Sosedova, and M. Ammann (2010), Uptake of Ozone to Deliquesced KI and Mixed KI/NaCl Aerosol Particles, *The Journal of Physical Chemistry A*, 114(26), 7085-7093, doi:10.1021/jp103257d.
- Ruehl, C. R., J. F. Davies, and K. R. Wilson (2016), An interfacial mechanism for cloud droplet formation on organic aerosols, *Science*, 351(6280), 1447-1450, doi:10.1126/science.aad4889.
- Saiz-Lopez, A., J. M. C. Plane, and J. A. Shillito (2004), Bromine oxide in the mid-latitude marine boundary layer, *Geophysical Research Letters*, 31(3), doi:10.1029/2003GL018956.
- Sherwen, T., M. J. Evans, L. J. Carpenter, J. A. Schmidt, and L. J. Mickley (2017), Halogen chemistry reduces tropospheric O<sub>3</sub> radiative forcing, *Atmos. Chem. Phys.*, 17(2), 1557-1569, doi:10.5194/acp-17-1557-2017.
- Shinotsuka, H., B. Da, S. Tanuma, H. Yoshikawa, C. J. Powell, and D. R. Penn (2017), Calculations of electron inelastic mean free paths. XI. Data for liquid water for energies from 50 eV to 30 keV, *Surface and Interface Analysis*, 49(4), 238-252, doi:10.1002/sia.6123.
- Simpson, W. R., S. S. Brown, A. Saiz-Lopez, J. A. Thornton, and R. v. Glasow (2015), Tropospheric Halogen Chemistry: Sources, Cycling, and Impacts, *Chemical Reviews*, 115(10), 4035-4062, doi:10.1021/cr5006638.

- 
- Simpson, W. R., et al. (2007), Halogens and their role in polar boundary-layer ozone depletion, *Atmos. Chem. Phys.*, 7(16), 4375-4418, doi:10.5194/acp-7-4375-2007.
- Steinfeld, J. I. (1998), Atmospheric Chemistry and Physics: From Air Pollution to Climate Change, *Environment: Science and Policy for Sustainable Development*, 40(7), 26-26, doi:10.1080/00139157.1999.10544295.
- Stemmler, K., A. Vlasenko, C. Guimbaud, and M. Ammann (2008), The effect of fatty acid surfactants on the uptake of nitric acid to deliquesced NaCl aerosol, *Atmos. Chem. Phys.*, 8(17), 5127-5141, doi:10.5194/acp-8-5127-2008.
- Vignati, E., M. C. Facchini, M. Rinaldi, C. Scannell, D. Ceburnis, J. Sciare, M. Kanakidou, S. Myriokefalitakis, F. Dentener, and C. D. O'Dowd (2010), Global scale emission and distribution of sea-spray aerosol: Sea-salt and organic enrichment, *Atmospheric Environment*, 44(5), 670-677, doi:10.1016/j.atmosenv.2009.11.013.
- Wang, S., et al. (2015), Active and widespread halogen chemistry in the tropical and subtropical free troposphere, *Proceedings of the National Academy of Sciences*, 112(30), 9281-9286, doi:10.1073/pnas.1505142112.
- Winter, B., and M. Faubel (2006), Photoemission from liquid aqueous solutions, *Chemical reviews*, 106(4), 1176-1211.
- Winter, B., R. Weber, P. M. Schmidt, I. V. Hertel, M. Faubel, L. Vrbka, and P. Jungwirth (2004), Molecular Structure of Surface-Active Salt Solutions: Photoelectron Spectroscopy and Molecular Dynamics Simulations of Aqueous Tetrabutylammonium Iodide, *The Journal of Physical Chemistry B*, 108(38), 14558-14564, doi:10.1021/jp0493531.

## 2.1 Liquid microjet X-ray photoelectron spectroscopy

We will make use of the NAPP endstation with the liquid microjet setup [Brown *et al.*, 2013] at the ‘Surfaces/Interfaces: Microscopy’ (SIM) beamline for X-ray energies between 150 eV and 7000 eV provided by the Swiss Light Source (SLS) at Paul Scherrer Institute (PSI). The experimental setup is shown in Figure 1.

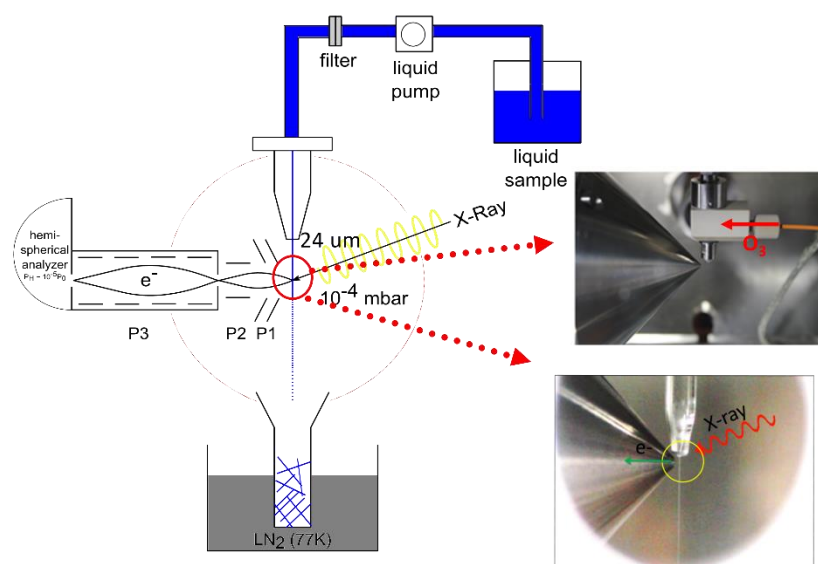


**Figure 1:** Schematic illustration of the experimental setup for photoemission studies using a liquid jet. P1, P2 and P3 denote sections of the differentially pumped electrostatic lens system to sample photoelectrons from the sample into the electron analyzer. Graphs are adapted from Lee *et al.* [Lee *et al.*, 2015].

## Chapter 2 Methods

---

The liquid microjet endstation is connected to the beamline using a series of differential pumping stages separated by small apertures that allow for both windowless operations and operation with a window (e.g., silicon nitride) at higher pressures. The electron analyzer uses a three-stage differentially pumped electrostatic lens system and a hemispheric analyzer to collect photoelectrons from samples in chamber pressures up to a few mbar. For the present experiments, a quartz nozzle, forming a liquid microjet with a diameter of 22-26  $\mu\text{m}$ , is used to deliver a liquid sample into the vacuum chamber. The liquid is cooled to 279 K immediately before entry into the ionization chamber, and a flow rate of 0.35-0.6 mL/min is used, leading to downward velocities of around 100  $\text{m s}^{-1}$ . For experiments related to monitoring the reaction of  $\text{O}_3$  with bromide in situ, a gas dosing system consisting of a second concentric nozzle around the quartz nozzle for the liquid will be used to allow for efficient exposure of the liquid surface to  $\text{O}_3$ . The chamber pressure with the jet running is around  $10^{-3}$  mbar for experiments related to solution characterization and about 0.1 mbar for experiments in the presence of  $\text{O}_2$  and  $\text{O}_3$ . The photoelectrons from the liquid surface enter the analyzer through an orifice (skimmer) with a diameter of 500  $\mu\text{m}$ . The working distance between the liquid jet and the detector orifice is 500  $\mu\text{m}$ .

For each beamtime at the Swiss Light Source, we have started the experiment with alignment procedures. We usually use a gold wire as a fake “jet” to get enough counts and find a suitable position. Besides, the setup of the liquid jet frame is cleaned right after the beamtime experiment.

After each beamtime, the setup needs to be cleaned on time to avoid corrosion. The cleaned liquid jet setup parts will be stored until the next beamtime.

Right before each beamtime, the liquid jet setup will be built and prepared for use.

As shown below, we assemble the liquid jet setup step by step.

First, we will fix the bottom DN-200 flange of the liquid jet set up on the table with three screws. Second, fix the liquid jet tube entrance into the microjet flange. Third, assembling the ice cutter and fixing it into the microjet flange, as shown in Figure 2.

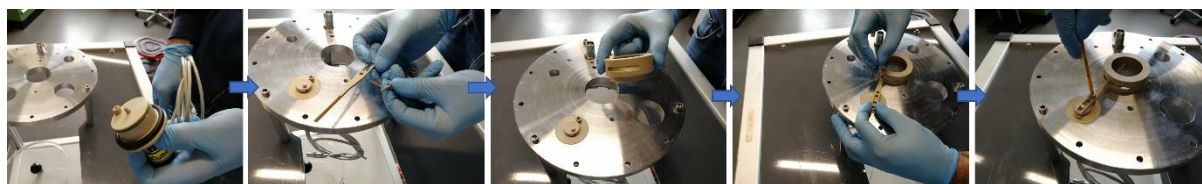


**Figure 2:** assembling the ice cutter and fixing it into the microjet flange

Four, setting the spring-loaded mu-metal liner into the microjet flange, as shown in Figure 3.



**Figure 3:** fixing the spring loaded mu-metal liner into the microjet flange

## Chapter 2 Methods

---

Five, set the motor mount into the microjet flange, as shown in figure 4.

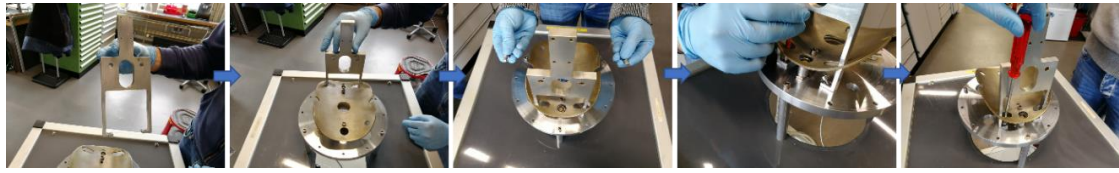


**Figure 4:** fixing the motor mount into the microjet flange

Six, assembling the smarACT in vacuum piezo motors and fixing them into the motor mount, as shown in figure 5.

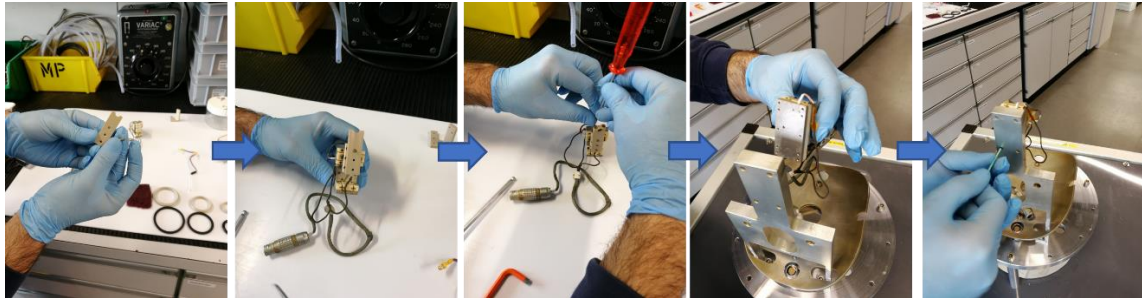


**Figure 5:** assembling the smarACT in vacuum piezo motors and fixing them into the motor mount

Seven, connecting the motors connector, as shown in figure 6.

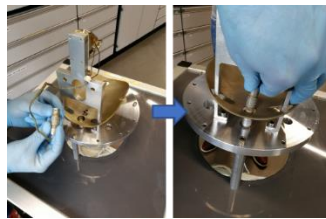


**Figure 6:** connecting the motors connector

Eight, fix the light into the motor mount and assemble it to the microjet flange, as shown in figure 7.

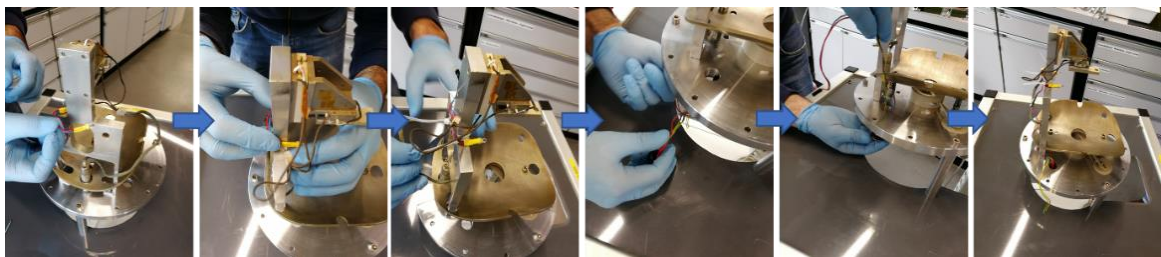


**Figure 7:** fixed the light into the motor mount and assembled it to the microjet flange

Nine, close the spare hole in the microjet flange.

Ten, assembling the aluminum liquid catcher into the microjet flange, as shown in figure 8.



**Figure 8:** assembling the aluminum liquid catcher into the microjet flange

Finally, connect the ice cutter to the controller. Figure 9 shows the assembly of the liquid jet setup in the lab.

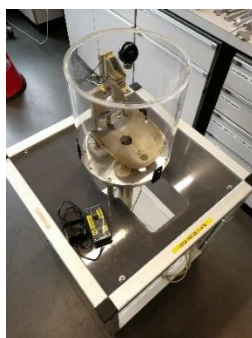


**Figure 9:** Assembled liquid jet setup

## 2.2 Flow reactor used in ozone uptake measurements

Multiphase kinetics experiments employing various flow tube methods remain an invaluable tool to support impact assessment [Ammann *et al.*, 2013; Crowley *et al.*, 2010]. Gas-condensed phase interactions are usually described by the uptake coefficient,  $\gamma$ , defined as the ratio of the net flux of molecules from the gas phase to the condensed phase divided by the gas-kinetic collision flux of the molecules to the surface of the condensed phase [Knipping *et al.*, 2000].

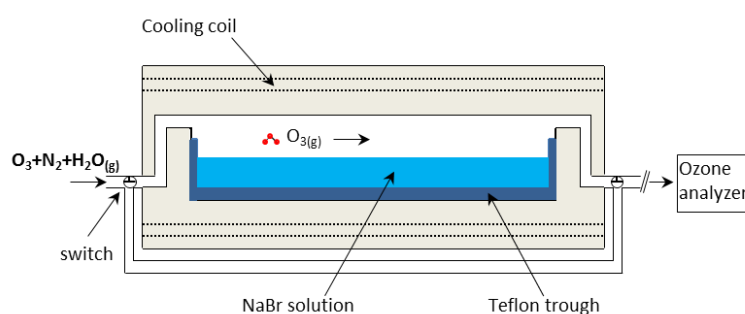


**Figure 17:** A Schematic diagram [Lee *et al.*, 2015] of the flow reactor used in  $O_3$  uptake measurements to solutions filled into a Teflon trough.

A schematic diagram of the flow reactor with a Teflon trough is shown in Figure 17. After about one hour of stabilizing the background  $O_3$  concentration, the bypass is switched to experimental mode (solid arrow), which leads to exposure of the film to  $O_3$ , allowing the multiphase reactions to occur. Finally, the concentration after the reactor is measured in bypass mode again to confirm that the background has not changed during the experiment. The



## Chapter 2 Methods

---

uptake coefficient of  $O_3$  is then derived from the observed loss of  $O_3$  above the trough [Lee *et al.*, 2015]. For the fairly slow reaction studied in this thesis, with uptake coefficients in the range of  $3 \times 10^{-7}$  to  $2 \times 10^{-6}$ , the analysis is straightforward, because diffusion neither in the gas phase nor in the aqueous phase affects the uptake.

The uptake coefficient can be measured as a function of the concentration of the reactive solute and as a function of the partial pressure of  $O_3$  in the gas phase. This allows disentangling the contributions of bulk aqueous phase reaction and surface reaction [Lee *et al.*, 2015; Oldridge and Abbatt, 2011].

---

## Bibliography

---

- Ammann, M., R. Cox, J. Crowley, M. Jenkin, A. Mellouki, M. Rossi, J. Troe, and T. Wallington (2013), Evaluated kinetic and photochemical data for atmospheric chemistry: Volume VI–heterogeneous reactions with liquid substrates, *Atmospheric Chemistry and Physics*, 13(16), 8045-8228.
- Brown, M. A., I. Jordan, A. B. Redondo, A. Kleibert, H. J. Wörner, and J. A. van Bokhoven (2013), In situ photoelectron spectroscopy at the liquid/nanoparticle interface, *Surface Science*, 610, 1-6.
- Crowley, J., M. Ammann, R. Cox, R. Hynes, M. E. Jenkin, A. Mellouki, M. Rossi, J. Troe, and T. Wallington (2010), Evaluated kinetic and photochemical data for atmospheric chemistry: Volume V–heterogeneous reactions on solid substrates, *Atmospheric Chemistry and Physics*, 10(18), 9059-9223.
- Knipping, E., M. Lakin, K. Foster, P. Jungwirth, D. Tobias, R. Gerber, D. Dabdub, and B. Finlayson-Pitts (2000), Experiments and simulations of ion-enhanced interfacial chemistry on aqueous NaCl aerosols, *Science*, 288(5464), 301-306.
- Lee, M.-T., M. A. Brown, S. Kato, A. Kleibert, A. Türler, and M. Ammann (2015), Competition between organics and bromide at the aqueous solution–air interface as seen from ozone uptake kinetics and X-ray photoelectron spectroscopy, *The Journal of Physical Chemistry A*, 119(19), 4600-4608.
- Oldridge, N., and J. Abbatt (2011), Formation of gas-phase bromine from interaction of ozone with frozen and liquid NaCl/NaBr solutions: Quantitative separation of surficial chemistry from bulk-phase reaction, *The Journal of Physical Chemistry A*, 115(12), 2590-2598.

---

# Aqueous atmospheric bromine species at the liquid-gas interface

---

Parts of this chapter are adapted from the publication: Gladich, I., Chen, S., Vazdar, M., Boucly, A., Yang, H., Ammann, M. and Artiglia, L., 2020. The surface propensity of aqueous atmospheric bromine at the liquid-gas interface. *The Journal of Physical Chemistry Letters*, 11(9), pp.3422-3429. My contribution to this publication was to participate in the synchrotron beamtimes, process the XPS data, to get Figure 1, and 2, and Figure S1.

In addition, I contributed to the design. I joined the liquid jet XPS experiment of comparing solutions of low and high concentrations of bromide, mixtures of bromide and chloride, and comparisons with chloride and fluoride. I processed and analyzed the XPS data and drafted the rest of the chapter. I prepared figures 3 and 4, and figure S2-S5 in the chapter.

### **3.1 The surface propensity of aqueous atmospheric bromine at the liquid-gas interface**

#### **3.1.1 Abstract**

Multiphase reactions of halide ions in aqueous solutions exposed to the atmosphere initiate the formation of molecular halogen compounds in the gas phase. Their photolysis leads to halogen atoms, which are catalytic sinks for ozone, making these processes relevant for the regional and global tropospheric ozone budget. The affinity of halide ions in aqueous solution for the liquid-gas interface, which may influence their reactivity with gaseous species, has been debated. Our study focuses on the surface properties of the bromide ion and its oxidation products. In situ x-ray photoelectron spectroscopy carried out on a liquid jet was

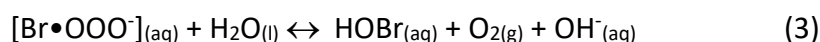
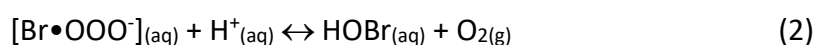
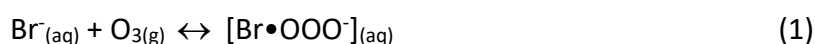
## Chapter 3 Aqueous atmospheric bromine related species at the liquid-gas interface

---

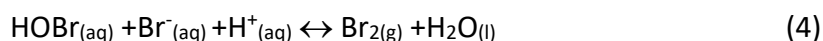
used to investigate the interfacial depth profile of bromide, hypobromite, hypobromous acid and bromate. In addition, spectra comparing solutions of low and high concentrations of bromide, mixtures of bromide and chloride, and comparisons with chloride and fluoride are reported to further contribute to the understanding of the surface propensity of halide ions. Bromide ions, also in the presence of chloride, tend to be not enhanced at the solution surface. In the halogen series, the surface propensity follows the series  $\text{Br} > \text{Cl} > \text{F}$ , and this is in agreement with recent theory and experiments, suggesting the lightest halide ions are most depleted from the surface. Among the bromine species, hypobromous acid, a key species in the multiphase cycling of bromine, is the only species showing substantial surface propensity, which suggests a more important role of the interface for this species in multiphase bromine chemistry than thought so far.

### 3.1.2 Introduction

Discovered in the 80's, ozone depletion events in the lower levels of the polar atmosphere have been shown to correlate with a notable increment of bromine species contained in both gas and particle phases [Barrie *et al.*, 1988]. Photolysis of molecular bromine and, more generally, halogen compounds lead to the corresponding halogen atoms, which are a catalytic sink for ozone. While dramatic in extent in the shallow polar marine boundary layer [Domine and Shepson, 2002], it has meanwhile been recognized that processes leading to activation of halogens from their reservoirs, mostly halide ions in marine environments at all latitudes, have regional and global impacts on the oxidation capacity of the troposphere [Abbatt *et al.*, 2012; Pratt *et al.*, 2013; Schmidt *et al.*, 2016; Sherwen *et al.*, 2017; Sherwen *et al.*, 2016; Simpson *et al.*, 2015; Simpson *et al.*, 2007]. Bromine activation is the result of a complex and multiphase (i.e., in the gas and/or at the interface and in the bulk of condensed water) reaction cycles. Oxidation of bromide may occur through various routes involving photolytically generated radicals, excited chromophoric organic matter [Arroyo *et al.*, 2019] or ozone. In the latter case, acid-catalyzed oxidation of bromide leads to the formation of hypobromous acid (HOBr) [Liu *et al.*, 2001; Simpson *et al.*, 2007]:



HOBr is also formed in the gas phase by the reaction of BrO radicals with HO<sub>2</sub> radicals. Wherever it has been generated, HOBr reacts with bromide in the aqueous phase, again in an acid catalyzed reaction, which yields molecular Br<sub>2</sub>.



The overall efficiency of these complex multiphase reactions and cycles to affect the oxidation capacity depends a lot on the properties of the aqueous phases (pH, other solutes) in sea water, salt pans, sea spray aerosol, sea ice or snow and also on the oxidant levels in the gas and aqueous phases [Wren and Donaldson, 2012]. The oxidation of bromide by ozone involves the formation of a precomplex, [Br•OOO<sup>-</sup>], also referred to as "ozonide", whose existence was postulated based on kinetics measurements [Liu *et al.*, 2001] and which has been recently detected in situ at the liquid-gas interface by means of x-ray photoelectron spectroscopy

## Chapter 3 Aqueous atmospheric bromine related species at the liquid-gas interface

---

(XPS) [Artiglia *et al.*, 2017]. This ozonide is likely at the origin of the surface enhanced bromide oxidation rates observed in many multiphase kinetic experiments [Artiglia *et al.*, 2017; Oldridge and Abbatt, 2011]. For the other bromide oxidation pathways and the reaction of HOBr with bromide, such surface enhancements have been discussed but not proven experimentally [Ammann *et al.*, 2013; Peterson *et al.*, 2017; Simpson *et al.*, 2015; Wang *et al.*, 2019].

Surface enhanced reactions were previously thought to be driven by a surface propensity of the halide ions, which was also supported by theoretical arguments that large polarizable anions preferentially accommodate at the surface of the water [Jungwirth and Tobias, 2001; 2002; Tobias *et al.*, 2013]. Starting from the year 2000, the group of J.C. Hemminger has focused on the investigation, by means of ex-situ and in situ XPS, of the deliquescence of halide salt crystals [Ghosal *et al.*, 2008; Ghosal *et al.*, 2005; Ghosal *et al.*, 2000]. The in situ XPS study of concentrated aqueous solutions generated from the controlled deliquescence of binary salts suggested the surface propensity of bromide ions [Ghosal *et al.*, 2005]. Other studies have suggested such behavior by means of surface sensitive experimental techniques like sum frequency generation spectroscopy and metastable impact electron spectroscopy [Höfft *et al.*, 2006; Schnitzer *et al.*, 2000] in spite of the known increase in surface tension with halide salt concentration. In turn, Winter *et al.* characterized aqueous solutions containing iodide ions by means of in situ XPS on a liquid microjet [Weber *et al.*, 2004]. Although no depth profile analysis was shown, the data suggested that iodide shows a neutral behavior, i.e., neither surface enrichment nor surface depletion. The reasons for the contrast to the earlier static saturated solution drop experiments is not entirely clear, but may be related to contaminations, beam damage (not an issue when using liquid jets) or the thermodynamic conditions. In 2009 the Winter group analyzed the surface properties of mixtures of chlorine species [Ottosson *et al.*, 2009]. Combining XPS with molecular dynamics (MD) calculations, they demonstrated that  $\text{ClO}_n^-$  ions having higher  $n$  (from 2 to 4) are more surface active, whereas hypochlorite shows a slight surface depletion [Ottosson *et al.*, 2009].

Computer simulations have been called to support the experimental efforts, but the literature is still sparse due to the difficulties in treating highly polarizable species [Gladich *et al.*, 2015; Rayne and Forest, 2014; Trogolo *et al.*, 2019] with the different spin state between reactants and products [Gladich *et al.*, 2015]. Electronic structure calculations have been performed in the gas phase to address the thermodynamics and kinetics of the reaction of bromide ions with ozone [Gladich *et al.*, 2015; Rayne and Forest, 2014; Trogolo *et al.*, 2019] reporting the reaction pathway for both spin surfaces. Lately, *first principle* MD in combination with in situ XPS measurements has proven the stability of an ozonide complex at the water-gas interface [Artiglia *et al.*, 2017]. Classical molecular dynamics (MD) simulations have shown bromide enhancement at the liquid interface [Jungwirth and Tobias, 2002; Tobias *et al.*, 2013] and in mixtures of different sodium salts [Gladich *et al.*, 2011]. Other MD and laboratory studies report surface segregation of halide ions on a growing ice crystal, populating the quasi-liquid layer in the ice-gas interface [Carignano *et al.*, 2007; Cho *et al.*, 2002]. This would suggest, in agreement with ref. [Ghosal *et al.*, 2008; Ghosal *et al.*, 2000], that the surface of seawater or sea ice is a possible source of bromine to fuel ozone depletion events [Hunt *et al.*, 2004]. However, recent liquid jet XPS and theory results, as mentioned above, indicate a less pronounced surface enrichment of halide ions in aqueous solutions [Baer and Mundy, 2011; Horinek *et al.*, 2009; Olivieri *et al.*, 2018; Olivieri *et al.*, 2016] questioning the amount of

## Chapter 3 Aqueous atmospheric bromine related species at the liquid-gas interface

---

interfacial bromide to be immediately available for reactions with ozone or HOBr molecules colliding from the gas phase. Moreover, the acidity of the liquid-gas and ice-gas interfaces is still highly debated [Agmon *et al.*, 2016; Beattie *et al.*, 2009; Buch *et al.*, 2007; Tse *et al.*, 2015] and the interfacial stability of some species, such as hypobromous acid, is unknown. Since ozone is poorly soluble in water [Chameides and Davis, 1982], reaction (1) may proceed faster at the interface between the gas and condensed aqueous phase. If any of the follow-up species is surface active as well, reactions (2) to (4) may occur via a surface specific route as well.

In this work, we investigate the interfacial solvation of different bromine-based compounds involved in bromine activation and cycling at the liquid-gas interface using liquid jet XPS. XPS is a powerful method to assess the structure of the liquid interface with high element selectivity and depth information limited to the first interfacial layers [Roy *et al.*, 2018; Seidel *et al.*, 2011; Winter and Faubel, 2006]. Our results have shown a molecular picture of the solvation of bromide in the aqueous solution that differs from the one suggested by polarizable MD [Jungwirth and Tobias, 2002; Tobias *et al.*, 2013; Gladich *et al.*, 2020] or XPS experiments on static deliquesced crystals [Ghosal *et al.*, 2000]: similar absence of enhancement is observed for bromide as well as for hypobromite and bromate. Similar to other undissociated, neutral forms of acids [Baer *et al.*, 2014], hypobromous acid shows a propensity for the liquid-gas interface.

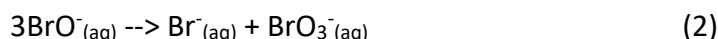
### 3.1.3 Experimental Methods

#### Preparation of the solutions

The disproportionation of bromine in an alkaline environment (0.5 M NaOH aqueous solution, pH>13) was used to synthesize hypobromite, following the recipe reported by Farkas and Lewin [Farkas and Lewin, 1947]:



Such a reaction produces bromide and hypobromite starting from liquid bromine. Because it is a powerful oxidant, hypobromite has been used as titrant mostly for easily oxidized species. However, it is thermodynamically unstable with respect to disproportionation:



For this reason, we prepared the solution right before injecting it and kept it in an ice bath for the whole duration of the experiment. Thanks to these precautions, there was no evidence of hypobromite disproportionation (i.e. formation of bromate) in the investigated solutions.

In order to synthesize the conjugate acid of hypobromite (hypobromous acid), a new solution was synthesized using reaction (1), but the pH value was adjusted to 9.0 to move the equilibrium toward the undissociated acid. The pKa of hypobromous acid is 8.65, thus a pH of 9.0 should favor the partial protonation of hypobromite to its conjugate acid.

#### In situ photoelectron spectroscopy

In situ photoemission spectra were collected with a Scienta R4000 HiPP-2 electron analyzer equipped with the liquid-jet chamber setup described before [Brown *et al.*, 2013] The endstation was connected to the Surfaces/Interfaces: Microscopy (SIM) beamline of the Swiss Light Source (SLS) synchrotron at the Paul Scherrer Institute (PSI). For the present

## Chapter 3 Aqueous atmospheric bromine related species at the liquid-gas interface

---

experiments, quartz nozzles with diameters ranging from 20 to 25  $\mu\text{m}$  were used to deliver the aqueous solutions into the chamber at a flow rate of 0.35 ml/min. The liquids were pre-cooled to 277 K in a coil located immediately before entry into the experimental chamber. During the experiment, we made use of linearly polarized light at  $0^\circ$ , and set the photon energy for the detection of Br 3d to 230, 350, 450, 650, 850 and 980 eV, resulting in photoelectron kinetic energies of approximately 150, 270, 370, 570, 770 and 900 eV, respectively. Each kinetic energy corresponds to a specific value of the inelastic mean free path (IMFP) in liquid water, which we took from Shinotsuka et al. [Shinotsuka et al., 2017]. The solid angle between the incoming photon beam and the analyzer is  $90^\circ$ . In order to take into account such geometry and assuming that the liquid filament has a cylindrical shape, the IMFP was normalized as follows to obtain the mean escape depth (MED) of photoelectrons [Winter and Faubel, 2006]:

$$\text{MED} = (2/\pi) \text{IMFP} \quad (3)$$

The binding energy scale of the spectra was calibrated using the valence spectra, setting the BE value of the  $1b_1$  molecular orbital of water to 11.3 eV [Kurahashi et al., 2014]. The error bars in Figure 2 were evaluated based on the standard deviation calculated from the fittings of a statistical sample of spectra corresponding to the same solution. The standard deviation values were propagated to get the error of the signal intensity ratios. This does not take into account either small movements of the liquid filament in front of the aperture of the analyzer or uncertainty in the measurement of the photon flux.

Thanks to the two elliptical twin undulators UE56, the SIM beamline delivers a high photon flux. Because the liquid filament used in this work flows in front of the electron analyzer, where it is hit by the photon beam at the focal distance, the liquid interface is continuously renewed and beam-induced effects are minimized. The high photon flux and energy resolution available in the 200-1000 eV photon energy range allowed us to carry out depth profiles starting from surface-sensitive conditions (kinetic energy = 150 eV, corresponding to approximately 0.7 nm information depth) and reaching more bulk sensitive ones (kinetic energy = 770 eV, corresponding to about 2.0 nm information depth).

### 3.1.4 Results and discussion

Figure 1a shows the Br 3d photoemission spectra of four aqueous solutions investigated in this study: 100 mM bromide, 100 mM bromate and 80 mM hypobromite at pH 13.7 and at pH 9.0. The Br 3d spectrum of the 100 mM bromide solution shows a peak that can be nicely fitted using a doublet due to spin-orbit splitting. The peak positions (binding energy -BE- of the Br  $3d_{5/2}$ =72.1 eV) and the fitting parameters used are reported in Table 1 and are in good agreement with the photoemission data shown in ref. [Artiglia et al., 2017]. The Br 3d spectrum of the 80 mM hypobromite solution at pH=13.7 shows two peaks separated by approximately 2.1 eV, which can be fitted using two doublets whose  $3d_{5/2}$  peaks are found at 72.1 and at 74.25 eV, respectively. The former corresponds to bromide ions, whereas the latter to hypobromite ions (the preparation of the solutions is described in the experimental part). The Br 3d spectrum of the hypobromite solution at pH=9 shows a complex line shape, with two main features at approximately 72 and 76 eV. A deconvolution procedure demonstrates that two doublets, centered at 72.1 and 76.2 eV, are not enough to correlate well with the raw experimental data. Thus, a third doublet component, centered at 74.25 is added. While the 72.1 eV and the 74.25 eV components are assigned to bromide and

## Chapter 3 Aqueous atmospheric bromine related species at the liquid-gas interface

hypobromite ions, respectively, the 76.2 eV peak can be assigned to hypobromous acid formed at pH=9. The last solution, 100 mM bromate, shows a doublet whose  $3d_{5/2}$  peak centroid is at 79.1 eV. The BEs of the Br  $3d_{5/2}$  peaks of different species in Figure 1a are plotted as a function of the oxidation state of bromine in Figure 1b. The bromide, hypobromite and bromate ions show a good linear correlation, which means that the positive chemical shift measured is proportional to the screening effects caused by the increase of the oxidation state from -1 to +5. Interestingly, the dot corresponding to hypobromous acid lays outside. Because the oxidation state of bromine in hypobromite and in hypobromous acid is the same, the electronic state of bromine, and thus the CEBE, in the latter is influenced by the different protonation state.

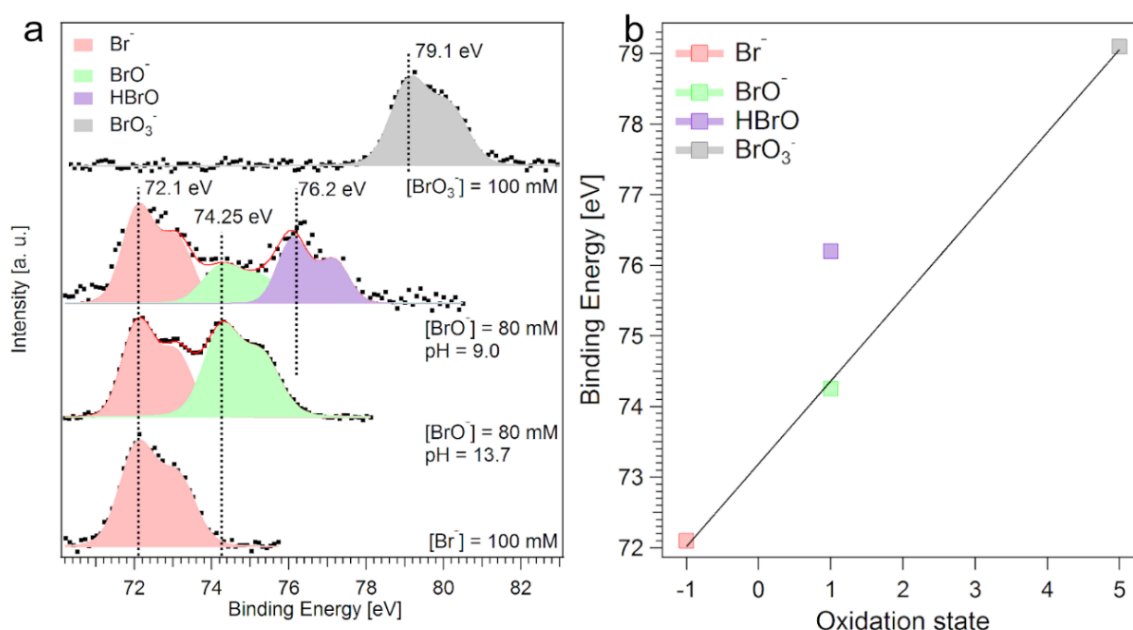


**Figure 1:** (a) XPS of the Br 3d ( $h\nu=350$  eV, corresponding to a kinetic energy of the Br 3d of approximately 270 eV) core level peaks of 4 different bromine species. The plot also shows the deconvolution of the peaks and their assignments. (b) A plot of the binding energy shift was observed experimentally with the corresponding oxidation state of bromine.

Figure 2a shows the results of a depth profile of the Br 3d photoemission signal of 100 mM solutions of bromide and bromate. The corresponding Br 3d photoemission spectra with increasing KE are shown in Figure S2a and S 2b, where the Br 3d signal was acquired at increasing excitation energies. Changing the KE allows tuning the information depth of the analysis so that different thicknesses of the liquid filament (top axis of the graph) are probed. The areas of the Br 3d spectra were normalized to the total cross-section, to the photon flux and to the mean escape depth (MED, see Equation 3) of the photoelectrons calculated at each KE. Such a procedure allowed us to consider the effect of the anisotropy parameter at the measurement geometry used during the experiments, which can affect the interpretation of the measured electron signal [Lewis *et al.*, 2019]. In the case of surface propensity (depletion) of a species, an increase (decrease) of the normalized area towards low kinetic energy is expected. Although the signals oscillate around an average value of the area, our data do not show a clear trend. A more detailed investigation with careful analysis of the O 1s spectra to account for small movements of the liquid jet and an assessment of higher-order light



## Chapter 3 Aqueous atmospheric bromine related species at the liquid-gas interface

contributions to the photon flux would be necessary to address the surface propensity in more detail.

**Table 1:** Fitting parameters (binding energy, spin-orbit splitting – S.O.S. – and full width at half maximum – FWHM –) were used for the deconvolutions of the Br 3d spectra.

	BE Br 3d <sub>5/2</sub> [eV]	S.O.S. [eV]	FWHM [eV]
<b>Br<sup>-</sup></b>	72.1	1.00	0.96
<b>BrO<sup>-</sup></b>	74.25	1.05	1.15
<b>HBrO</b>	76.2	1.05	0.92
<b>BrO<sub>3</sub><sup>-</sup></b>	79.1	1.05	1.13

The series of Br 3d spectra obtained from 80 mM hypobromite solutions at pH = 13.7 and at pH = 9.0, acquired in the 150 eV - 770 eV KE range, are shown in Figure S1a and S1b, respectively. The peaks were deconvoluted using the parameters shown in Table 1. We focused the analysis on the hypobromite solution at pH=9.0 (Figure S1.b), because it contains hypobromous acid, which is relevant in the multiphase bromine chemistry. The areas of the species are displayed in Figure 2b. As already shown in Figure 2a, the area of the bromide component does not indicate a specific behavior, i.e. neither surface propensity nor surface depletion. The behavior of the hypobromite component resembles that of bromide, whereas hypobromous acid shows a gradual decrease moving toward higher KEs. Because the bromide ions show a neutral behavior and given the uncertainties, we divided the areas of hypobromite and hypobromous acid by the area of bromide, which removes uncertainties related to the photon flux. The results, normalized to the maximum, are displayed in Figure 2c. Hypobromous acid shows a 50% decrease at the highest KE, and such a trend suggests a surface propensity. The hypobromite component also indicates a reduction of approximately 25%. Because hypobromite is the least intense component in the Br 3d spectra acquired at pH=9.0 (Figure S1b), whereas its intensity is high at pH=13.7, the BrO<sup>-</sup>/Br<sup>-</sup> ratio was recalculated for the latter solution. The results are shown in Figure 2c (empty squares) and display a neutral behavior, thus comparable to the one of bromide. In addition, the line shapes of the Br 3d spectra of the pH=9 solution acquired at low KEs (150-370 eV, Figure S1b) suggest the surface propensity of hypobromous acid. At a pH of 9, being the pK<sub>a</sub> of hypobromous acid 8.65, the expected HBrO/BrO<sup>-</sup> ratio should be around 1. In contrast, the intensity of the hypobromite component is much lower than that of hypobromous acid. At higher KEs (550-770 eV), where the technique is more sensitive to the bulk, the ratio converges to 1. Such behavior suggests the segregation of hypobromous acid in the first liquid layers.

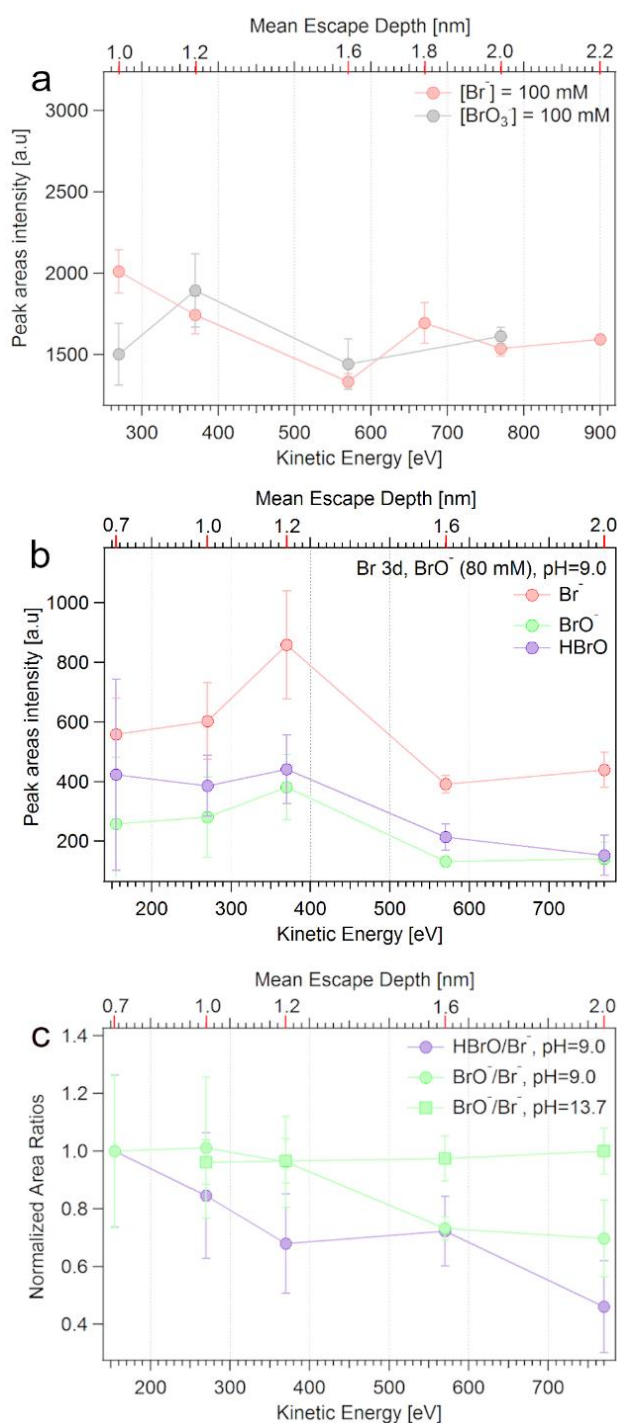


**Figure 2:** Normalized areas of the Br 3d photoemission peaks acquired at increasing KE (a) of 100 mM bromide and 100 mM bromate aqueous solutions (b) of an 80 mM hypobromite aqueous solution. (c) Areas of the Br 3d peaks of hypobromite and of hypobromous acid normalized to the area of bromide in 80 mM hypobromite aqueous solutions at pH=9.0 and 13.7.

As mentioned above, the depth profile for bromide remains a bit uncertain given the uncertainty resulting from jet instabilities. In view of the debate on the extent of the surface propensity of bromide over the past 20 years, we have acquired depth profiles from a few more solutions to investigate the effect of bromide concentration, of the mixture with chloride, and to see the comparison with the other halides. Using the same strategy of

## Chapter 3 Aqueous atmospheric bromine related species at the liquid-gas interface

normalizing the depth profiles to that of the 0.1 M NaBr solution as in Figure 2c, Figure 3 compares 0.1 M and 2 M NaBr aqueous solutions, respectively, with the 2 M solution data being divided by a factor of 20. The series of the corresponding raw Br 3d spectra are shown in Figure S2a and S3a, respectively. Obviously, the interfacial properties of bromide at 2M are similar to that at 0.1 M. The areas of the Br 3d photoemission peaks acquired at increasing KE are shown in Figure S4a. The relative Br intensity of 2 M NaBr shown in Figure S8 is 20 times that of the 0.1 M NaBr aqueous solutions for the whole KE range.

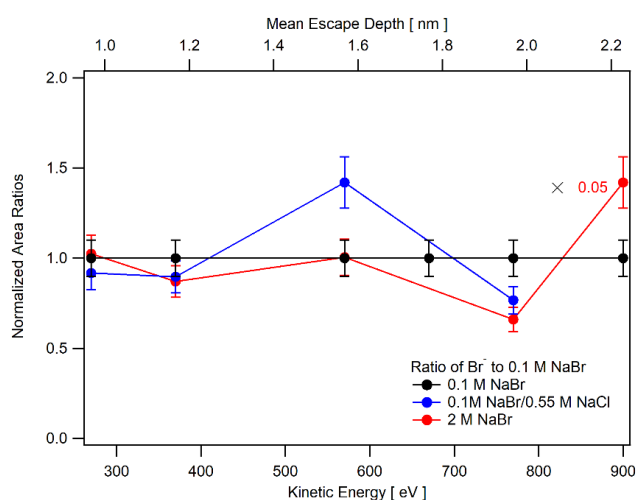


**Figure 3:** Areas of the Br 3d photoemission peaks were acquired with increasing KE of 0.1 M NaBr, 2 M NaBr and mixed 0.1 M NaBr/0.55 M NaCl aqueous solutions normalized to the area of bromide in 0.1 M NaBr aqueous solutions.

Figure 3 also shows the corresponding results for the mixed 0.1 M NaBr / 0.55 M NaCl aqueous solutions, indicating no significant impact of 0.5 M NaCl on the depth profile of bromide. The series of Br 3d spectra obtained for 0.1 M and mixed 0.1 M NaBr / 0.55 M NaCl aqueous solutions with increasing KE are shown in Figure S2a and S3b, respectively. The corresponding Br 3d photoemission peak areas are shown in Figure S4b. Thus, the surface propensity of bromide under sea water conditions (0.55M NaCl) is not different from that of pure NaBr solutions.

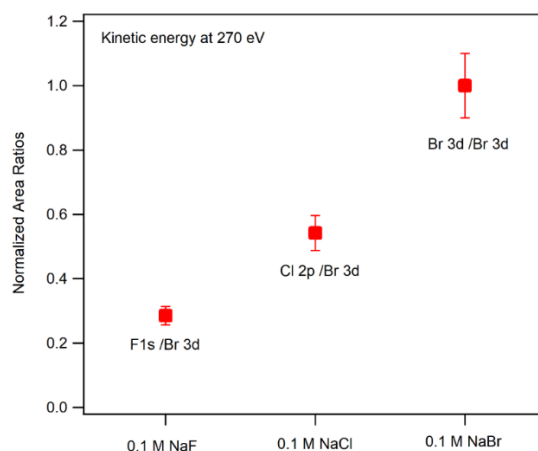


**Figure 4:** Photoemission intensity of F 1s and Cl 2p relative to that of Br 3d, all normalized to cross-section and photon flux, at 270 eV KE for 0.1 M NaF, 0.1 M NaCl and 0.1 M NaBr aqueous solutions.

## Chapter 3 Aqueous atmospheric bromine related species at the liquid-gas interface

---

Figure 4 compares the different 0.1 M halide solutions at one KE, 270 eV. The F 1s, Cl 2p and Br 3d photoemission signals have all been normalized to cross-section and photon flux for the photon energy at which they have been measured (959 eV, 475 eV and 350 eV, respectively). In line with the analysis above, the data are shown relative to the intensity for Br 3d. Measurements at 370 eV and 570 eV show similar behavior. The series of individual Br 3d, F 1s and Cl 2p spectra are shown in Figure S2a, S5a and S5b, respectively. This comparison clearly indicates that at the same bulk concentration, the degree of depletion increases from bromide to chloride to fluoride, in agreement with both MD simulations [Hantal *et al.*, 2020] and surface tension results [Hantal *et al.*, 2020; Shah *et al.*, 2013]. Thus, depletion is more pronounced the smaller the anion is. Thus for the small anions, the electrostatic repulsion from the interface dominates, while for the larger anions, this is partially compensated by the effect of polarizability.

### 3.1.5 Conclusion

To summarize, we determined the solvation environment of different bromine species at the liquid-gas interface by combining depth profile measurements from liquid jet XPS. Our results show that bromide does not display a net surface preference, in good agreement with in situ XPS performed on a liquid filament containing iodide ions [Weber *et al.*, 2004b] and recent MD simulations [Horinek *et al.*, 2009]. Parallel to that, chloride and fluoride are more strongly depleted than bromide, as expected from their smaller size. As mentioned in the introduction, previous literature reports demonstrated the surface propensity of bromide ions in deliquesced salt surfaces [Ghosal *et al.*, 2005a; Höfft *et al.*, 2006; Schnitzer *et al.*, 2000]. However, such measurements were performed on a deliquesced salt, thus in static conditions allowing more pronounced beam damage effects. Such effects are limited in a liquid jet experiment because the purity and concentration of the solutions can be controlled and because beam-induced effects are negligible due to the permanently renewed liquid surface. Similar to bromide, also hypobromite and bromate do not display a net interfacial/bulk surface preference. Our results suggest that hypobromous acid shows an apparent surface propensity as proven by the BE shift compared to the conjugate base and by the depth profile measurements.

Our results have important implications for the multiphase chemistry of bromine species, including reactions (1)-(4), in the atmosphere. Moreover, the findings of this work also clarify the solvation environment of chemical players involved in multiphase bromine chemistry, which are also relevant in the debromination chemistry of wastewater [Michèle B. Heeb *et al.*, 2014]. Our recent work has demonstrated that the ozonide formed in reaction (1), the [Br•OOO<sup>-</sup>] pre-complex, has a high propensity for the liquid-gas interface [Artiglia *et al.*, 2017], which is the main reason for the oxidation of bromide by ozone proceeding more efficiently at the surface than in the bulk liquid and not any enhancement of bromide itself at the interface suggested early on [Ghosal *et al.*, 2005]. This is now confirmed by the present study demonstrating the absence of enhancement for bromide. Secondly, HOBr (hypobromous acid), either formed by reactions (2) and (3) or photochemical cycles in the gas phase, exhibits significant surface enrichment. This opens up the possibility of a surface-specific reaction route for reaction (4). Kinetic experiments available so far are not conclusive in that regard [Ammann *et al.*, 2013; Clifford and Donaldson, 2007; Hunt *et al.*, 2004; Moreno and Baeza-Romero, 2019; Oldridge and Abbatt, 2011] and require future efforts.

### 3.2 Supplementary information

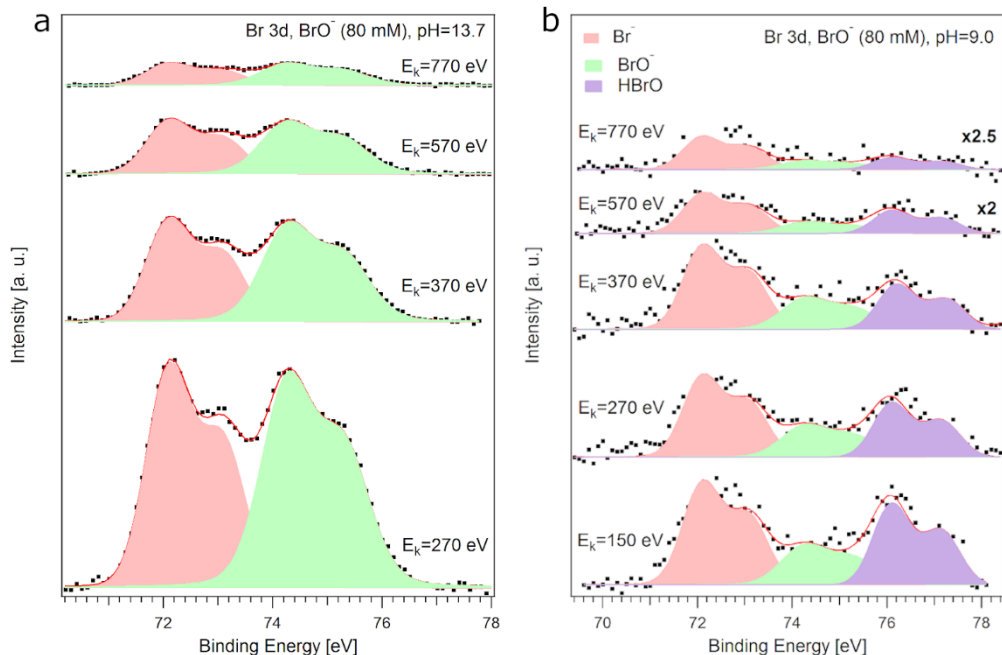


**Figure S1:** Br 3d photoemission spectra acquired at increasing KE. (a) 80 mM hypobromite solution at pH=13.7. (b) 80 mM solution at pH=9.0. As mentioned in the main manuscript, the pH of the latter solution is close to the  $pK_a$  of hypobromous acid. This is the reason why only the bromide and the hypobromite components are present in Figure S1a, whereas a third component, centered at 76.2 eV, is present in Figure S1b. It can be associated with hypobromous acid.

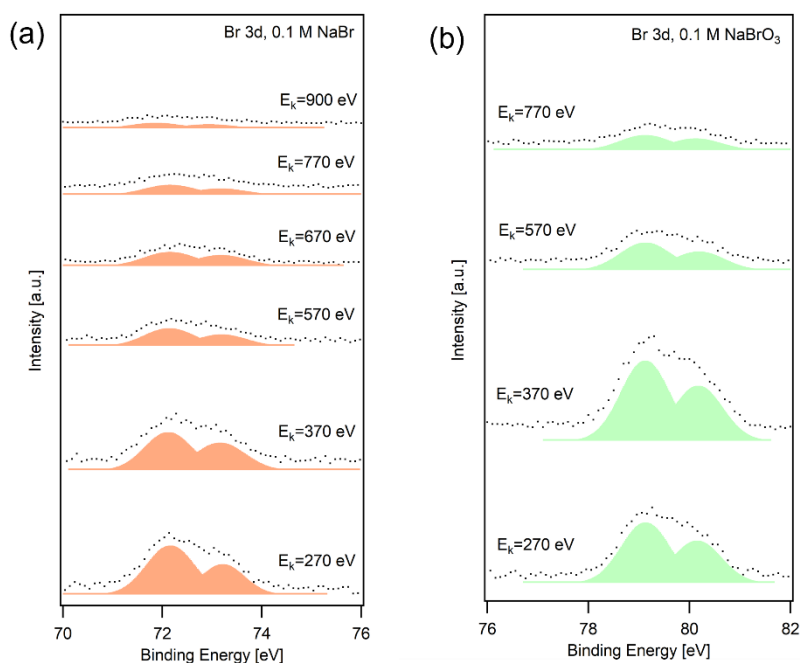


**Figure S2:** Br 3d photoemission spectra of (a) 0.1 M NaBr and (b) 0.1 M NaBrO<sub>3</sub> solution acquired at increasing KE.

## Chapter 3 Aqueous atmospheric bromine related species at the liquid-gas interface

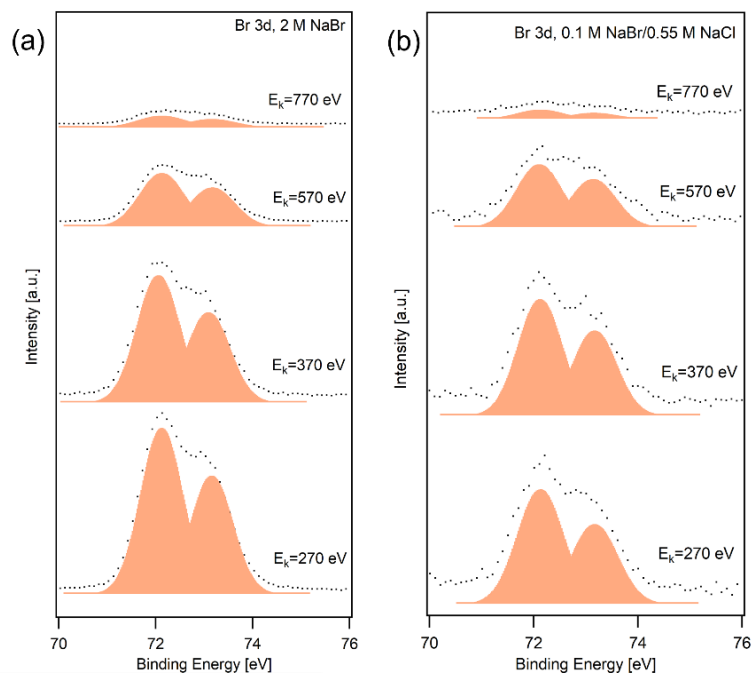


**Figure S3:** Br 3d photoemission spectra of (a) 2 M NaBr and (b) 0.1 M NaBr/0.55 M NaCl solution acquired at increasing KE.

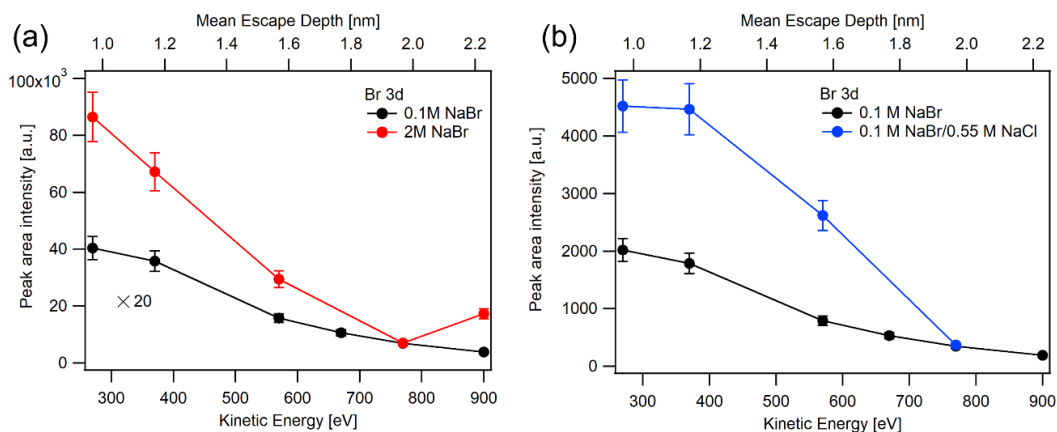


**Figure S4:** Areas of the raw Br 3d photoemission peaks acquired at increasing KE of (a) 0.1 M NaBr and 2 M NaBr aqueous solutions, and (b) 0.1 M NaBr and 0.1 M NaBr/0.55 M NaCl, without normalization to photon flux, cross-section, or mean escape depth.

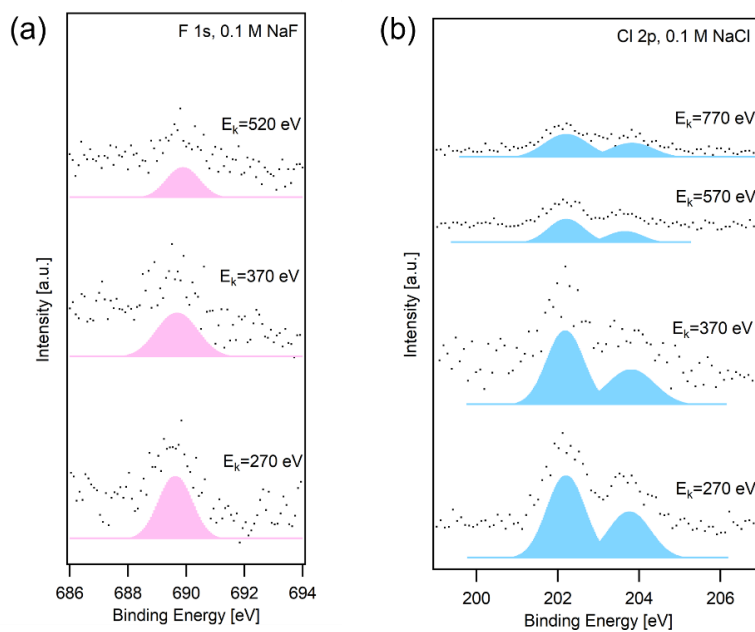


**Figure S5:** (a) F 1s photoemission spectra of 0.1 M NaF and (b) Cl 2p photoemission spectra of 0.1 M NaCl solution acquired at increasing KE.

---

## Bibliography

---

- Abbatt, J. P. D., J. L. Thomas, K. Abrahamsson, C. Boxe, A. Granfors, A. E. Jones, M. D. King, A. Saiz-Lopez, P. B. Shepson, J. Sodeau, D. W. Toohey, C. Toubin, R. von Glasow, S. N. Wren and X. Yang (2012). "Halogen activation via interactions with environmental ice and snow in the polar lower troposphere and other regions." *Atmos. Chem. Phys.* 12(14): 6237-6271.
- Agmon, N., H. J. Bakker, R. K. Campen, R. H. Henchman, P. Pohl, S. Roke, M. Thämer and A. Hassanali (2016). "Protons and Hydroxide Ions in Aqueous Systems." *Chemical Reviews* 116(13): 7642-7672.
- Ammann, M., R. A. Cox, J. N. Crowley, M. E. Jenkin, A. Mellouki, M. J. Rossi, J. Troe and T. J. Wallington (2013). "Evaluated kinetic and photochemical data for atmospheric chemistry: Volume VI – heterogeneous reactions with liquid substrates." *Atmos. Chem. Phys.* 13(16): 8045-8228.
- Artiglia, L., J. Edebeli, F. Orlando, S. Chen, M.-T. Lee, P. Corral Arroyo, A. Gilgen, T. Bartels-Rausch, A. Kleibert, M. Vazdar, M. Andres Carignano, J. S. Francisco, P. B. Shepson, I. Gladich and M. Ammann (2017). "A surface-stabilized ozonide triggers bromide oxidation at the aqueous solution-vapour interface." *Nature Communications* 8(1): 700.
- Baer, M. D. and C. J. Mundy (2011). "Toward an understanding of the specific ion effect using density functional theory." *The Journal of Physical Chemistry Letters*: 1088-1093.
- Baer, M. D., D. J. Tobias and C. J. Mundy (2014). "Investigation of Interfacial and Bulk Dissociation of HBr, HCl, and HNO<sub>3</sub> Using Density Functional Theory-Based Molecular Dynamics Simulations." *The Journal of Physical Chemistry C* 118(50): 29412-29420.
- Barrie, L. A., J. W. Bottenheim, R. C. Schnell, P. J. Crutzen and R. A. Rasmussen (1988). "Ozone destruction and photochemical reactions at polar sunrise in the lower Arctic atmosphere." *Nature* 334(6178): 138-141.
- Beattie, J. K., A. M. Djerdjev and G. G. Warr (2009). "The surface of neat water is basic." *Faraday Discussions* 141(0): 31-39.
- Brown, M. A., A. B. Redondo, I. Jordan, N. Duyckaerts, M.-T. Lee, M. Ammann, F. Nolting, A. Kleibert, T. Huthwelker, J.-P. Mächler, M. Birrer, J. Honegger, R. Wetter, H. J. Wörner and J. A. van Bokhoven (2013). "A new endstation at the Swiss Light Source for ultraviolet photoelectron spectroscopy, X-ray photoelectron spectroscopy, and X-ray absorption spectroscopy measurements of liquid solutions." *Review of Scientific Instruments* 84(7): 073904.
- Buch, V., A. Milet, R. Vácha, P. Jungwirth and J. P. Devlin (2007). "Water surface is acidic." *Proceedings of the National Academy of Sciences* 104(18): 7342.
- Carignano, M. A., P. B. Shepson and I. Szleifer (2007). "Ions at the ice/vapor interface." *Chemical Physics Letters* 436(1-3): 99-103.
- Chameides, W. L. and D. D. Davis (1982). "The free radical chemistry of cloud droplets and its impact upon the composition of rain." *Journal of Geophysical Research: Oceans* 87(C7): 4863-4877.
- Cho, H., P. B. Shepson, L. A. Barrie, J. P. Cowin and R. Zaveri (2002). "NMR investigation of the quasi-brine layer in ice/brine mixtures." *Journal of Physical Chemistry B* 106(43): 11226-11232.
- Clifford, D. and D. J. Donaldson (2007). "Direct Experimental Evidence for a Heterogeneous Reaction of Ozone with Bromide at the Air–Aqueous Interface." *The Journal of Physical Chemistry A* 111(39): 9809-9814.
- Corral Arroyo, P., R. Aellig, P. A. Alpert, R. Volkamer and M. Ammann (2019). "Halogen activation and radical cycling initiated by imidazole-2-carboxaldehyde photochemistry." *Atmos. Chem. Phys.* 19(16): 10817-10828.
- Domine, F. and P. B. Shepson (2002). "Air-snow interactions and atmospheric chemistry." *Science* 297(5586): 1506-1510.
- Farkas, L. and M. Lewin (1947). "Analysis of Hypochlorite-Hypobromite Solutions." *Analytical Chemistry* 19(9): 662-664.
- Ghosal, S., M. A. Brown, H. Bluhm, M. J. Krisch, M. Salmeron, P. Jungwirth and J. C. Hemminger (2008). "Ion Partitioning at the Liquid/Vapor Interface of a Multicomponent Alkali Halide Solution: A Model for Aqueous Sea Salt Aerosols." *The Journal of Physical Chemistry A* 112(48): 12378-12384.



## Bibliography

---

- Ghosal, S., J. C. Hemminger, H. Bluhm, B. S. Mun, E. L. D. Hebenstreit, G. Ketteler, D. F. Ogletree, F. G. Requejo and M. Salmeron (2005). "Electron Spectroscopy of Aqueous Solution Interfaces Reveals Surface Enhancement of Halides." *Science* 307(5709): 563.
- Ghosal, S., A. Shbeeb and J. C. Hemminger (2000). "Surface segregation of bromine in bromide doped NaCl: Implications for the seasonal variations in Arctic ozone." *Geophysical Research Letters* 27(13): 1879-1882.
- Gladich, I., J. S. Francisco, R. J. Buszek, M. Vazdar, M. a. Carignano and P. B. Shepson (2015). "Ab Initio Study of the Reaction of Ozone with Bromide Ion." *The Journal of Physical Chemistry A*: 150210155932002.
- Gladich, I., P. B. Shepson, M. A. Carignano and I. Szleifer (2011). "Halide Affinity for the Water–Air Interface in Aqueous Solutions of Mixtures of Sodium Salts." *The Journal of Physical Chemistry A* 115(23): 5895-5899.
- Hantal, G., R. A. Horváth, J. Kolafa, M. Sega and P. Jedlovsky (2020). "Surface Affinity of Alkali and Halide Ions in Their Aqueous Solution: Insight from Intrinsic Density Analysis." *The Journal of Physical Chemistry B* 124(44): 9884-9897.
- Heeb, M. B., J. Criquet, S. G. Zimmermann-Steffens and U. von Gunten (2014). "Oxidative treatment of bromide-containing waters: Formation of bromine and its reactions with inorganic and organic compounds — A critical review." *Water Research* 48: 15-42.
- Höfft, O., A. Borodin, U. Kahnert, V. Kempter, L. X. Dang and P. Jungwirth (2006). "Surface Segregation of Dissolved Salt Ions." *The Journal of Physical Chemistry B* 110(24): 11971-11976.
- Horinek, D., A. Herz, L. Vrbka, F. Sedlmeier, S. I. Mamatkulov and R. R. Netz (2009). "Specific ion adsorption at the air/water interface: The role of hydrophobic solvation." *Chemical Physics Letters* 479(4): 173-183.
- Hunt, S. W., M. Roeselová, W. Wang, L. M. Wingen, E. M. Knipping, D. J. Tobias, D. Dabdub and B. J. Finlayson-Pitts (2004). "Formation of Molecular Bromine from the Reaction of Ozone with Deliquesced NaBr Aerosol: Evidence for Interface Chemistry." *The Journal of Physical Chemistry A* 108(52): 11559-11572.
- Jungwirth, P. and D. J. Tobias (2001). "Molecular structure of salt solutions: A new view of the interface with implications for heterogeneous atmospheric chemistry." *Journal of Physical Chemistry B* 105(43): 10468-10472.
- Jungwirth, P. and D. J. Tobias (2002). "Ions at the air/water interface." *Journal of Physical Chemistry B* 106(25): 6361-6373.
- Kurahashi, N., S. Karashima, Y. Tang, T. Horio, B. Abulimiti, Y.-I. Suzuki, Y. Ogi, M. Oura and T. Suzuki (2014). "Photoelectron spectroscopy of aqueous solutions: Streaming potentials of NaX (X = Cl, Br, and I) solutions and electron binding energies of liquid water and X-." *The Journal of Chemical Physics* 140(17): 174506.
- Lewis, T., B. Winter, S. Thürmer, R. Seidel, A. B. Stephansen, J. A. Freites, D. J. Tobias and J. C. Hemminger (2019). "Molecular Arrangement of a Mixture of Organosulfur Surfactants at the Aqueous Solution–Vapor Interface Studied by Photoelectron Intensity and Angular Distribution Measurements and Molecular Dynamics Simulations." *The Journal of Physical Chemistry C* 123(13): 8160-8170.
- Liu, Q., L. M. Schurter, C. E. Muller, S. Aloisio, J. S. Francisco and D. W. Margerum (2001). "Kinetics and Mechanisms of Aqueous Ozone Reactions with Bromide, Sulfite, Hydrogen Sulfite, Iodide, and Nitrite Ions." *Inorganic Chemistry* 40(17): 4436-4442.
- Moreno, C. and M. T. Baeza-Romero (2019). "A kinetic model for ozone uptake by solutions and aqueous particles containing I<sup>-</sup> and Br<sup>-</sup>, including seawater and sea-salt aerosol." *Physical Chemistry Chemical Physics* 21(36): 19835-19856.
- Oldridge, N. W. and J. P. D. Abbatt (2011). "Formation of Gas-Phase Bromine from Interaction of Ozone with Frozen and Liquid NaCl/NaBr Solutions: Quantitative Separation of Surficial Chemistry from Bulk-Phase Reaction." *The Journal of Physical Chemistry A* 115(12): 2590-2598.
- Olivieri, G., K. M. Parry, R. D'Auria, D. J. Tobias and M. A. Brown (2018). "Specific Anion Effects on Na<sup>+</sup> Adsorption at the Aqueous Solution–Air Interface: MD Simulations, SESSA Calculations, and Photoelectron Spectroscopy Experiments." *The Journal of Physical Chemistry B* 122(2): 910-918.
- Olivieri, G., K. M. Parry, C. J. Powell, D. J. Tobias and M. A. Brown (2016). "Quantitative interpretation of molecular dynamics simulations for X-ray photoelectron spectroscopy of aqueous solutions." *The Journal of chemical physics* 144(15): 154704-154704.
- Ottosson, N., R. Vácha, E. F. Aziz, W. Pokapanich, W. Eberhardt, S. Svensson, G. Öhrwall, P. Jungwirth, O. Björneholm and B. Winter (2009). "Large variations in the propensity of aqueous oxychlorine anions for the solution/vapor interface." *The Journal of Chemical Physics* 131(12): 124706.
- Peterson, P. K., D. Pöhler, H. Sihler, J. Zielcke, S. General, U. Frieß, U. Platt, W. R. Simpson, S. V. Nghiem, P. B. Shepson, B. H. Stirm, S. Dhaniyala, T. Wagner, D. R. Caulton, J. D. Fuentes and K. A. Pratt (2017). "Observations of bromine monoxide transport in the Arctic sustained on aerosol particles." *Atmos. Chem. Phys.* 17(12): 7567-7579.

## Bibliography

---

- Pratt, K. A., K. D. Custard, P. B. Shepson, T. A. Douglas, D. Pöhler, S. General, J. Zielcke, W. R. Simpson, U. Platt, D. J. Tanner, L. Gregory Huey, M. Carlsen and B. H. Stirm (2013). "Photochemical production of molecular bromine in Arctic surface snowpacks." *Nature Geoscience* 6(5): 351-356.
- Rayne, S. and K. Forest (2014). "A G4MP2 and G4 theoretical study on reactions occurring during the ozonation of bromide containing waters." *Computational and Theoretical Chemistry* 1031: 22-33.
- Roy, K., L. Artiglia and J. A. van Bokhoven (2018). "Ambient Pressure Photoelectron Spectroscopy: Opportunities in Catalysis from Solids to Liquids and Introducing Time Resolution." *ChemCatChem* 10(4): 666-682.
- Schmidt, J. A., D. J. Jacob, H. M. Horowitz, L. Hu, T. Sherwen, M. J. Evans, Q. Liang, R. M. Suleiman, D. E. Oram, M. Le Breton, C. J. Percival, S. Wang, B. Dix and R. Volkamer (2016). "Modeling the observed tropospheric BrO background: Importance of multiphase chemistry and implications for ozone, OH, and mercury." *Journal of Geophysical Research: Atmospheres* 121(19): 11,819-811,835.
- Schnitzer, C., S. Baldelli and M. J. Shultz (2000). "Sum Frequency Generation of Water on NaCl, NaNO<sub>3</sub>, KHSO<sub>4</sub>, HCl, HNO<sub>3</sub>, and H<sub>2</sub>SO<sub>4</sub> Aqueous Solutions." *The Journal of Physical Chemistry B* 104(3): 585-590.
- Seidel, R., S. Thürmer and B. Winter (2011). "Photoelectron Spectroscopy Meets Aqueous Solution: Studies from a Vacuum Liquid Microjet." *The Journal of Physical Chemistry Letters* 2(6): 633-641.
- Shah, A.-u.-H. A., K. Ali and S. Bilal (2013). "Surface tension, surface excess concentration, enthalpy and entropy of surface formation of aqueous salt solutions." *Colloids and Surfaces A: Physicochemical and Engineering Aspects* 417: 183-190.
- Sherwen, T., M. J. Evans, L. J. Carpenter, J. A. Schmidt and L. J. Mickley (2017). "Halogen chemistry reduces tropospheric O<sub>3</sub> radiative forcing." *Atmos. Chem. Phys.* 17(2): 1557-1569.
- Sherwen, T., J. A. Schmidt, M. J. Evans, L. J. Carpenter, K. Großmann, S. D. Eastham, D. J. Jacob, B. Dix, T. K. Koenig, R. Sinreich, I. Ortega, R. Volkamer, A. Saiz-Lopez, C. Prados-Roman, A. S. Mahajan and C. Ordóñez (2016). "Global impacts of tropospheric halogens (Cl, Br, I) on oxidants and composition in GEOS-Chem." *Atmos. Chem. Phys.* 16(18): 12239-12271.
- Shinotsuka, H., B. Da, S. Tanuma, H. Yoshikawa, C. J. Powell and D. R. Penn (2017). "Calculations of electron inelastic mean free paths. XI. Data for liquid water for energies from 50 eV to 30 keV." *Surface and Interface Analysis* 49(4): 238-252.
- Simpson, W. R., S. S. Brown, A. Saiz-Lopez, J. A. Thornton and R. von Glasow (2015). "Tropospheric Halogen Chemistry: Sources, Cycling, and Impacts." *Chemical Reviews* 115(10): 4035-4062.
- Simpson, W. R., R. von Glasow, K. Riedel, P. Anderson, P. Ariya, J. Bottenheim, J. Burrows, L. J. Carpenter, U. Frieß, M. E. Goodsite, D. Heard, M. Hutterli, H. W. Jacobi, L. Kaleschke, B. Neff, J. Plane, U. Platt, A. Richter, H. Roscoe, R. Sander, P. Shepson, J. Sodeau, A. Steffen, T. Wagner and E. Wolff (2007). "Halogens and their role in polar boundary-layer ozone depletion." *Atmos. Chem. Phys.* 7(16): 4375-4418.
- Tobias, D. J., A. C. Stern, M. D. Baer, Y. Levin and C. J. Mundy (2013). "Simulation and Theory of Ions at Atmospherically Relevant Aqueous Liquid-Air Interfaces." *Annual Review of Physical Chemistry* 64(1): 339-359.
- Trogolo, D., J. S. Arey and P. R. Tentscher (2019). "Gas-Phase Ozone Reactions with a Structurally Diverse Set of Molecules: Barrier Heights and Reaction Energies Evaluated by Coupled Cluster and Density Functional Theory Calculations." *The Journal of Physical Chemistry A* 123(2): 517-536.
- Tse, Y.-L. S., C. Chen, G. E. Lindberg, R. Kumar and G. A. Voth (2015). "Propensity of Hydrated Excess Protons and Hydroxide Anions for the Air–Water Interface." *Journal of the American Chemical Society* 137(39): 12610-12616.
- Wang, S., S. M. McNamara, C. W. Moore, D. Obrist, A. Steffen, P. B. Shepson, R. M. Staebler, A. R. W. Raso and K. A. Pratt (2019). "Direct detection of atmospheric atomic bromine leading to mercury and ozone depletion." *Proceedings of the National Academy of Sciences* 116(29): 14479.
- Weber, R., B. Winter, P. M. Schmidt, W. Widdra, I. V. Hertel, M. Dittmar and M. Faubel (2004). "Photoemission from Aqueous Alkali-Metal–Iodide Salt Solutions Using EUV Synchrotron Radiation." *The Journal of Physical Chemistry B* 108(15): 4729-4736.
- Winter, B. and M. Faubel (2006). "Photoemission from Liquid Aqueous Solutions." *Chemical Reviews* 106(4): 1176-1211.
- Wren, S. N. and D. J. Donaldson (2012). "How does deposition of gas phase species affect pH at frozen salty interfaces?" *Atmos. Chem. Phys.* 12(21): 10065-10073.

---

# The surface propensity of the $[\text{Br}\cdot\text{OOO}^-]$ intermediate at the liquid-vapor interface

---

Parts of this chapter are adopted from the publication: Artiglia, L., Edebeli, J., Orlando, F., Chen, S., Lee, M., Corral Arroyo, P., Gilgen, A., Bartels–Rausch, T., Kleibert, A., Vazdar, M., Carignano, M. A., Francisco, J. S., Shepson, P. B., Gladich, I. & Ammann, M. A surface–stabilized ozonide triggers bromide oxidation at the aqueous solution–vapor interface. *Nat. Commun.*, **8**, 700, 1–8, 2017. My contribution to this publication was to participate in the synchrotron beamtimes, process the XPS data to get the Figure 1, 2, and Figure S1, S2.

In addition, I contributed to the design and joined the liquid jet XPS experiment related to the surface propensity of the  $[\text{Br}\cdot\text{OOO}^-]$  intermediate at low pH and to the dependence of bromide concentration. I processed and analyzed the XPS data and drafted the rest of the chapter. I prepared figures 3-6, and figure S3-S7 in the chapter.

### **4.1 A surface-stabilized ozonide triggers bromide oxidation at the aqueous solution-vapor interface**

#### **4.1.1 Abstract**

Oxidation of bromide in aqueous environments initiates the formation of molecular halogen compounds, which is essential for the global tropospheric ozone budget. In the aqueous bulk, oxidation of bromide by ozone involves a  $[\text{Br}\cdot\text{OOO}^-]$  complex as intermediate. Here, we report liquid jet X-ray photoelectron spectroscopy measurements that provide direct experimental evidence for the ozonide and establish its propensity for the solution-vapor interface. Theoretical calculations [Artiglia *et al.*, 2017] support these findings, showing that water

## Chapter 4 Surface propensity of [Br•OOO<sup>-</sup>] intermediate at the liquid-vapor interface

---

stabilizes the ozonide and lowers the energy of the transition state at neutral pH. In further experiments at low pH, the signal of the [Br•OOO<sup>-</sup>] intermediate was small and just at the detection limit. The low steady-state concentration of the [Br•OOO<sup>-</sup>] intermediate under acidic conditions may be due to the faster release of molecular oxygen. The surface concentration of the [Br•OOO<sup>-</sup>] intermediate increased almost linearly with the bromide concentration; the trend towards a smaller [Br•OOO<sup>-</sup>] to bromide ratio at high concentration could be a sign of saturation driven by a maximum coverage. The [Br•OOO<sup>-</sup>] intermediate concentration at the interface turned out to be tightly correlated with the uptake coefficient of ozone (the loss rate of ozone normalized to the gas kinetic collision rate) over the same bromide concentration range. The surface-enhanced bromide oxidation is of substantial interest in basic and applied chemistry and engineering.

### 4.1.2 Introduction

In atmospheric chemistry, halogen atoms resulting from photolysis of both organic and inorganic halogen compounds [De Haan *et al.*, 1999; Oum *et al.*, 1998] are essential catalysts for ozone depletion both in the stratosphere and in the troposphere, with varying relative roles of chlorine, bromine and iodine in these compartments [Raso *et al.*, 2017]. Halogen atoms are also oxidants themselves towards organic compounds and are implicated in mercury deposition [Parrella *et al.*, 2012; Schmidt *et al.*, 2016]. Furthermore, halogen atoms are intermediates in waste water treatment, where halogenated organic secondary products are concerned [Heeb *et al.*, 2014].

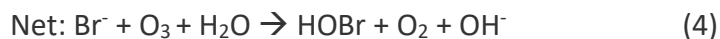
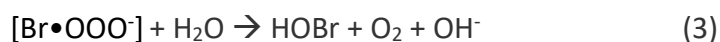
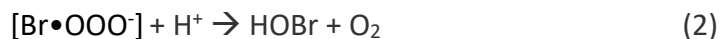
For tropospheric chemistry, the main inorganic route of halogen activation is initiated by the oxidation of aqueous phase bromide to either bromine atom or hypobromous acid (HOBr), which combine with other halide ions to form molecular halogen compounds that are released to the gas phase. Bromide is abundant and sometimes enriched [Sander *et al.*, 2003] in sea water and thus at the ocean surface, in sea spray particles, in brines associated with sea ice, frost flowers or snow, in artificial or natural salt pans, and in volcanic emissions.

Many radical oxidants such as ·OH or excited triplets of organic chromophores require UV or near UV light to drive bromide oxidation. Therefore, both in the (dark) polar marine boundary layer and the upper troposphere, ozone (O<sub>3</sub>) is one of the most critical oxidants [Cao *et al.*, 2016; Schmidt *et al.*, 2016]. The product HOBr (pK<sub>a</sub>=8.65) reacts further in an acid-catalyzed mechanism with chloride, bromide or iodide to form bromine (Br<sub>2</sub>), BrCl or BrI. The initial formation of HOBr limits the release of halogens to the gas phase. In contrast, a complex suite of gas-phase and multiphase processes controls the halogen chemistry and the O<sub>3</sub> budget later on.

The bulk aqueous phase, acid-catalyzed oxidation of bromide by O<sub>3</sub> to HOBr, has been studied for a long time due to its relevance in debromination of waste water [Haruta and Takeyama, 1981; Haag and Hoigne, 1983; Haag *et al.*, 1984; Liu *et al.*, 2001; Gunten, 2003; Heeb *et al.*, 2014; Gladich *et al.*, 2015].

## Chapter 4 Surface propensity of [Br•OOO<sup>-</sup>] intermediate at the liquid-vapor interface

---



Liu et al. proposed that there must be an ozone adduct (a steady-state intermediate formed in (1)) with the nucleophile, bromide, prior to oxygen atom transfer with the release of molecular oxygen [Liu et al., 2001] (2,3). The structure of the [Br•OOO<sup>-</sup>] adduct (which we refer to as an “ozonide”), involves a weak bond between the bromide and the oxygen of ozone [Liu et al., 2001]. The aqueous solvation sphere has a large effect on the stability and reactivity of [Br•OOO<sup>-</sup>]. The kinetic data indicated the formation of [Br•OOO<sup>-</sup>] as a steady-state intermediate with an acid-assisted step to form HOBr and molecular oxygen [Liu et al., 2001]. Further calculations, performed for the gas phase, confirmed the stability of the [Br•OOO<sup>-</sup>] intermediate, showing intricate details of its reactivity during the oxygen atom transfer process [Gladich et al., 2015].

So far, it has been assumed that [Br•OOO<sup>-</sup>] is stabilized by solvation and that the reaction occurs in the bulk. Further, the rate coefficient for the overall reaction [Liu et al., 2001] and the low solubility of ozone (0.025 M atm<sup>-1</sup> at 273 K) [Chameides and Davis, 1982] suggest that the formation of HOBr through the bulk aqueous phase route is rather inefficient and would not seem important as a source of gas-phase bromine in the environment. In turn, heterogeneous oxidation experiments have consistently shown that oxidation at the aqueous solution-air interface may dominate in environments with a high aqueous surface to volume ratio [Oum et al., 1998; Hunt et al., 2004; Clifford and Donaldson, 2007; Abbatt et al., 2010; Wren et al., 2010; Oldridge and Abbatt, 2011; Nissenon et al., 2014; Lee et al., 2015]. Oldridge and Abbatt [Oldridge and Abbatt, 2011] used the inverse ozone concentration dependence of the uptake coefficient to suggest a Langmuir-Hinshelwood type process occurring on the surface in parallel to the bulk aqueous phase oxidation [Oldridge and Abbatt, 2011]. The uptake coefficient is the oxidation rate normalized by the gas collision rate of ozone with the surface.

Linked to a single composition and temperature, the nature of the surface reaction, the identity of the potential precursor, and its preference for the surface have never been tracked down. Similar behavior of other heterogeneous oxidation processes suggests a general type of ozone intermediate formed on electron-rich surfaces of widely differing chemical composition and phase [McCabe and Abbatt, 2009; Shiraiwa et al., 2011; Lampimaki et al., 2013; Berkemeier et al., 2016].

Finally, the idea of efficient surface oxidation of bromide had initially been related to the preference of the larger, more polarizable halide ions for the aqueous solution – vapor interface, as observed in molecular dynamics (MD) simulations [Jungwirth and Tobias, 2001; Hofft et al., 2006] and X-ray photoelectron spectroscopy (XPS) experiments on static

## Chapter 4 Surface propensity of [Br•OOO<sup>-</sup>] intermediate at the liquid-vapor interface

---

deliquesced crystals [Ghosal *et al.*, 2000]. Recent MD simulations predicting the photoemission signal intensity using photoelectron scattering calculations and liquid jet XPS data indicate a less pronounced surface enhancement, which is in better agreement with the overall positive surface tension change (and thus negative surface excess) of bromide solutions [Weber *et al.*, 2004; Olivieri *et al.*, 2016]. Therefore, the surface precursor limited bromide oxidation is likely unrelated to the amount of bromide ions directly at the interface of a neat salt solution.

In this work, we use liquid jet XPS, a powerful tool to directly assess the structure of the interfacial region with high chemical selectivity and high selectivity for the interface due to the probe (or information) depth of just a few nanometers [Winter and Faubel, 2006]. The continuously renewed surface of the flowing liquid jet avoids radiation damage effects but still allows probing a surface that is locally in equilibrium with the first few tens of nanometer of bulk aqueous phase [Thurmer *et al.*, 2013; Slavicek *et al.*, 2016] (as explained further in Supplementary Note 1.) The results provide strong evidence for the [Br•OOO<sup>-</sup>] intermediate, its preference for the liquid-vapor interface, the effect of water on its stabilization, and the reaction path to products. In addition, we studied the surface propensity of [Br•OOO<sup>-</sup>] intermediate at low pH and as a function of bromide concentration and compared the corresponding interfacial density of the [Br•OOO<sup>-</sup>] intermediate with the ozone uptake coefficient.

### 4.1.3 Experimental method

In-situ XPS was acquired at the near-ambient pressure photoemission endstation (NAPP), equipped with the liquid microjet setup. Measurements were performed at the Surfaces/Interfaces: Microscopy (SIM) beamline of the Swiss Light Source (SLS) at the Paul Scherrer Institute (PSI). The electron analyzer uses a three-stage differentially pumped electrostatic lens system and a hemispheric analyzer to collect photoelectrons from samples in chamber pressures up to the mbar range [Brown *et al.*, 2013]. For the present experiments, a quartz nozzle, forming a liquid microjet with a diameter of 24  $\mu\text{m}$ , was used to deliver a 0.125 M aqueous solution of Br<sup>-</sup> into the chamber at a flow rate of 0.35 mL/min. The liquid was cooled to 277 K in a pre-cooling coil located immediately before entry into the experimental chamber. Based on these parameters, and considering the working distance of the quartz nozzle with respect to the detection point, a 100  $\mu\text{s}$  time can be estimated between the injection of the liquid and the detection point. Further technical details about the procedures adopted during the experiments can be found in the Supplementary Note 1.

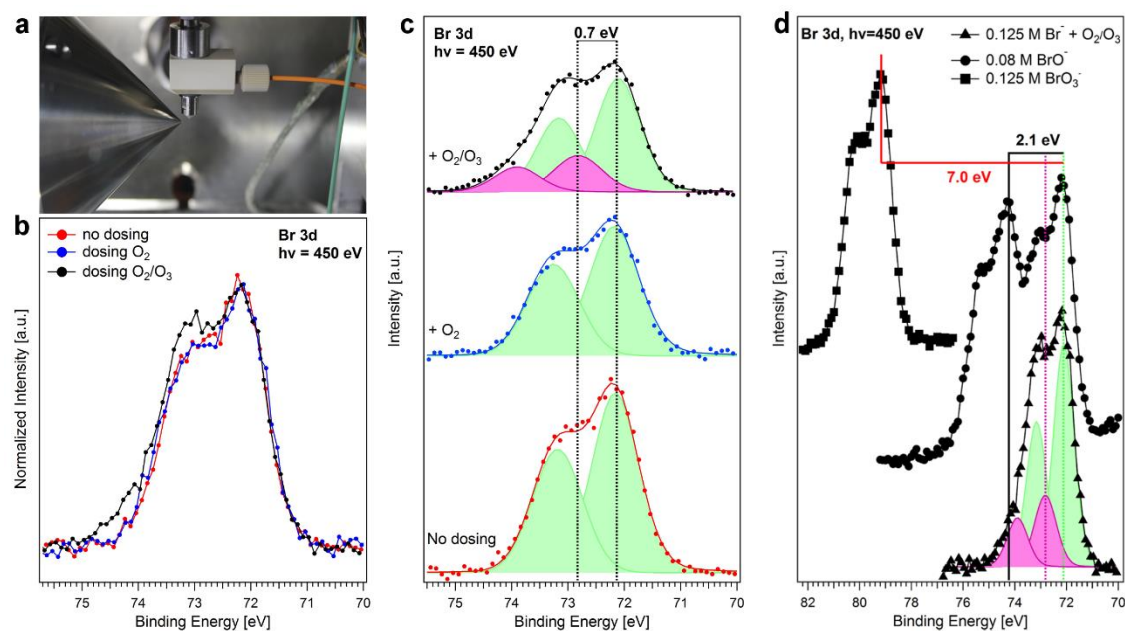
### 4.1.4 Results and discussion

Figure 1 shows the photoemission signal of the Br 3d core level region, a double-peak structure due to the spin-orbit splitting. After normalization to the maximum, the spectra acquired before and during in-situ dosing of oxygen at a pressure of 0.25 mbar are identical. The signal collected while dosing a mixture of oxygen and ozone (approx. 1.0 % ozone, same

## Chapter 4 Surface propensity of $[\text{Br}\bullet\text{OOO}^-]$ intermediate at the liquid-vapor interface

pressure) displays apparent changes both in the  $3d_{5/2}$  and  $3d_{3/2}$  regions. This suggests the presence of a second doublet, which is highlighted in purple in Fig. 1c, positively shifted by 0.7 eV with respect to the main peaks assigned to bromide (72.10 and 73.15 eV). The corresponding O 1s spectra of 0.125 M NaBr with and without dosing are shown in Figure S3.

To identify the new spectral feature, we acquired the Br 3d spectra of two reference aqueous solutions of possible oxidation products, i.e. 0.08 M hypobromite and 0.125 M bromate (Figure. 1d). As expected, the higher the oxidation state of bromine, the larger the positive shift of the binding energy. A chemical shift of +2.1 eV is observed for hypobromite, and of +7.0 eV for bromate. None of them corresponds to that of the new doublet. It is well known that x-rays can induce the radiolysis of water [George *et al.*, 2012], leading to the production of reactive hydroxyl radicals that may react with bromide ions. All the Br 3d spectra were recorded under the same experimental conditions (excitation energy, photon flux), and the high speed of the liquid filament ensures that the concentration of photo-generated hydroxyl radicals remains below  $1.0 \cdot 10^{-6}$  mol/L. Therefore beam damage can be excluded. In summary, the combination of in-situ XPS and theoretical calculations [Artiglia *et al.*, 2017] provides solid indications for forming an ozonide complex.



**Figure 1:** Photoemission spectra of the Br 3d peak acquired in-situ. a, Picture of the liquid microjet assembly, equipped with the gas dosing system, during operation; b, Superimposition of the Br 3d photoemission spectra, normalized to the maximum, acquired before dosing (red), while dosing oxygen (blue), and while dosing a mixture of 1% ozone in oxygen; c, deconvolution of the raw spectra in plot b, performed using Gaussian peaks after subtraction of a Shirley background; d, comparison of the Br 3d photoemission spectra acquired while dosing a mixture of 1% ozone in oxygen with two reference spectra of hypobromite and bromate.

First-principle MD simulations, which are a particularly suitable tool to study the dynamics and stability of non-standard compounds, were used to address the bulk vs. surface propensity of the different reaction intermediates [Marx and Hutter, 2009], as explained in

## Chapter 4 Surface propensity of $[\text{Br}\bullet\text{OOO}^-]$ intermediate at the liquid-vapor interface

full detail by Artiglia et al. [Artiglia et al., 2017]. Figure 2a shows a snapshot (corresponding to 8.5 ps) of the MD trajectory of the pre-complex on the surface of a water slab at 300 K. The inset shows the distance between bromine and each of the oxygen atoms of  $^1[\text{Br}\bullet\text{OOO}^-]$  along the MD trajectory. This distance fluctuates around the average value of 2.7 Å, which is consistent with that obtained for the optimized geometries by electronic structure calculations [Artiglia et al., 2017]. This further supports the scenario of a pre-complex stabilized on the surface of liquid water. Moreover, Figure 2b shows the density profile of the Br and OOO groups in the  $^1[\text{Br}\bullet\text{OOO}^-]$  intermediate position along the coordinate perpendicular to the water interface, confirming that  $^1[\text{Br}\bullet\text{OOO}^-]$  remains at the interface during the whole trajectory, with the Br group close to the OOO group.

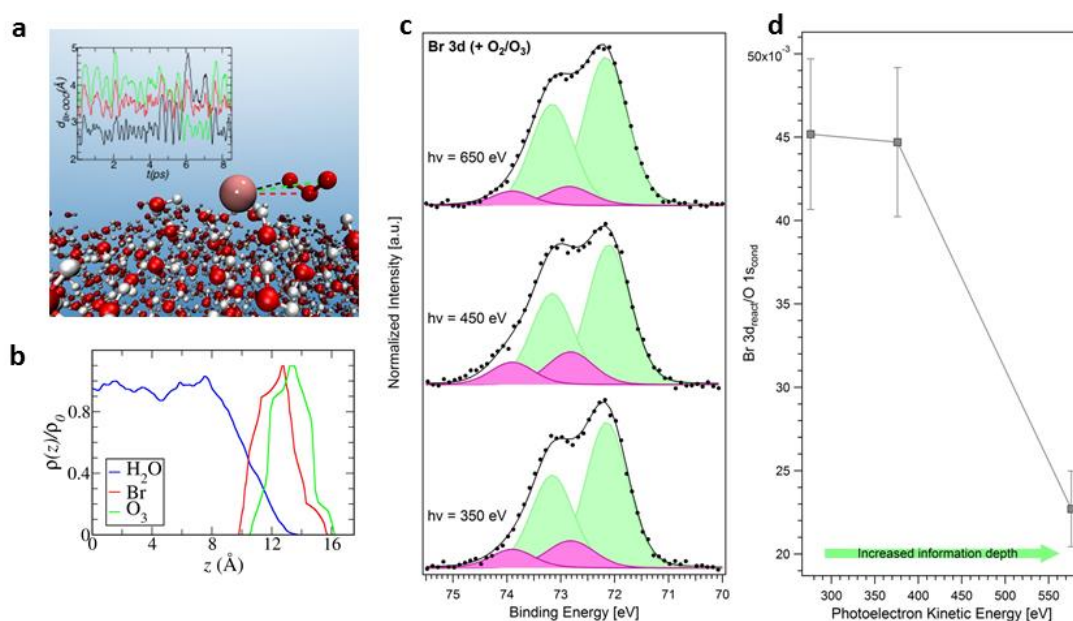


**Figure 2:** The surface propensity of  $[\text{Br}\bullet\text{OOO}^-]$ : experiment and theory a) Snapshot from the first-principal MD trajectory demonstrating the stability of  $[\text{Br}\bullet\text{OOO}^-]$  on the surface of liquid water. The inset shows the distances between the bromine and each of the oxygen atoms in the ozone molecule recorded during the 8.5 ps MD trajectory. b) From the same trajectory, the bromide and ozone density profile shows the position of the center of mass of these two groups along the coordinate perpendicular to the interface. In blue, the water profile is a reference in arbitrary units. c) deconvolution of the Br 3d photoemission spectra (performed using Gaussian peaks after subtraction of a Shirley background), normalized to the area, acquired at  $h\nu=350, 450,$  and  $650 \text{ eV}$ , and corresponding to photoelectron kinetic energies of 276, 376 and 575 eV (Br 3d region centroid). d) Plot of the intensity of the Br 3d peaks associated to the  $[\text{Br}\bullet\text{OOO}^-]$  complex normalized to the O 1s (peak acquired with second-order light) from the condensed phase (see Supplementary Note), as a function of the photoelectron kinetic energy. The error bars were calculated by propagating the errors associated with each peak area of three independent measurements.

In parallel to the MD simulations [Artiglia et al., 2017], we acquired the Br 3d photoemission peak at increasing excitation energies, hence, at increasing photoelectron kinetic energy or information depth, as shown in Fig. 2c. A decrease of the relative intensity of the peaks associated with the  $[\text{Br}\bullet\text{OOO}^-]$  complex is observed at the highest excitation energy. We



## Chapter 4 Surface propensity of $[\text{Br}\bullet\text{OOO}^-]$ intermediate at the liquid-vapor interface

acquired the O 1s signal at the same photoelectron kinetic energies (Supplementary Figure S1a) and used the area of the peak corresponding to the condensed phase to normalize the area of the  $[\text{Br}\bullet\text{OOO}^-]$  doublet. Figure 2d shows that this ratio, normalized to the cross-sections of the elements, decreases considerably at a kinetic energy of 576 eV, i.e. with greater depth sampled. This indicates that the  $[\text{Br}\bullet\text{OOO}^-]$  complex has a propensity for the surface, in good agreement with the theoretical calculations discussed above. The photoemission intensity ratio between the complex and the bromide in the bulk ( $I_{\text{BrOOO}^-}/I_{\text{Br}^-}$ ) shows a similar behavior as a function of the photoelectron kinetic energy (Supplementary Figure S2). An estimate of the surface coverage of the  $[\text{Br}\bullet\text{OOO}^-]$  complex at the ozone concentration used in this study ( $2.5 \cdot 10^{-8} \text{ mol L}^{-1}$ ), obtained employing different models, yields approx.  $2.0 \cdot 10^{12} \text{ complexes cm}^{-2}$  (see Supplementary Note and Supplementary Figure S2 for more details). In conclusion, both MD results [Artiglia *et al.*, 2017] and XPS data confirm that  $[\text{Br}\bullet\text{OOO}^-]$  resides at the interface, where it is stabilized by interfacial water molecules.

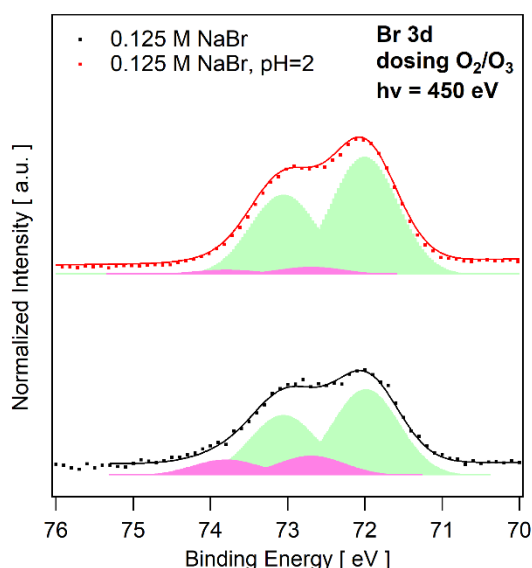


**Figure 3:** Deconvolution of the Br 3d photoemission spectra (performed using Gaussian peaks after subtraction of a Shirley background), normalized to the area, acquired at  $h\nu=450 \text{ eV}$ , and corresponding to photoelectron kinetic energies of 376 eV of a 0.125 M NaBr aqueous solution at neutral and low pH conditions.

The Br 3d and O 1s spectra of 0.125 M NaBr at low pH (pH=2) with and without dosing are shown in Figure S4. Figure 3 shows the Br 3d photoemission peak of 0.125 M NaBr at neutral and low pH. The corresponding O 1s spectra are shown in Figure S5. The O 1s spectra were made of two components, one on the high binding energy side for gas phase water and one on the low binding energy side for condensed phase water. Here we normalized the Br spectra to the area of the condensed phase O 1s. The relative intensity of Br is higher for the solutions at low pH than in neutral solutions, eventually driven by different surface propensity of bromide. While for neutral pH, the fit shows clearly the presence of the intermediate, for low pH condition, we may fit the  $[\text{Br}\bullet\text{OOO}^-]$  intermediate and  $\text{Br}^-$  with the latter fit as a constraint. The ratio of  $[\text{Br}\bullet\text{OOO}^-]$  intermediate to  $\text{Br}^-$  is very small, which is around 0.06:1, which is at or

## Chapter 4 Surface propensity of $[\text{Br}\bullet\text{OOO}^-]$ intermediate at the liquid-vapor interface

below the detection limit, as apparent from the figure. The Br 3d peak could well be fitted with one single component. The uptake coefficient of ozone at 0.125 M NaBr aqueous solutions with low pH is much higher compared with neutral pH [Artiglia *et al.*, 2017], which indicates that the overall reaction rate is much faster, leading to depletion of the intermediate concentration at the surface, likely due to the faster release of molecular oxygen from the  $[\text{Br}\bullet\text{OOO}^-]$  intermediate.

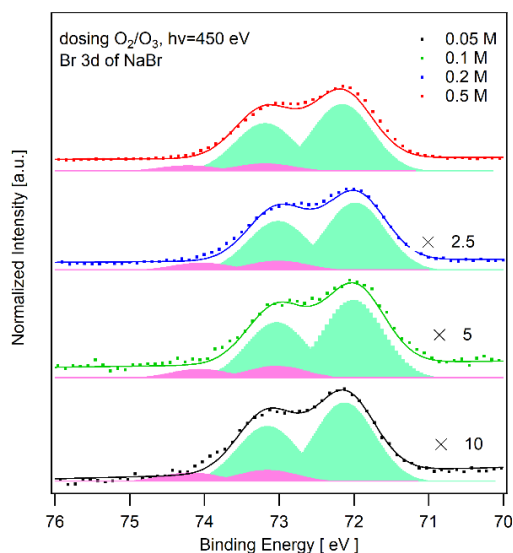


**Figure 4:** Fitting of the Br 3d spectra of NaBr aqueous solutions in the presence of ozone as a function of bromide concentration in the condensed phase, along with the fits (solid lines) components of bromide (green) and the bromide ozonide (pink) shown as shadings.

The Br 3d and O 1s spectra of NaBr as a function of bromide concentration with and without dosing are shown in Figures S6 and S7. Figure 4 shows the Br 3d photoemission peak deconvolutions for the different NaBr aqueous solution concentrations. The O 1s spectrum in Figure S10 was made of four contributions, two at low binding energy for gas-phase water and condensed phase water, the other two at high binding energy for gas phase oxygen. In Figure 4, the Br photoelectron peak acquired while dosing a mixture of oxygen and ozone clearly displays the two doublets as already shown in Figure 1, one main doublet assigned to bromide (72.10 and 73.15 eV), and the other doublet positively shifted by 0.7 eV assigned to the  $[\text{Br}\bullet\text{OOO}^-]$  intermediate.

Figure 5 shows the  $\text{Br}^-$  (black) and  $[\text{Br}\bullet\text{OOO}^-]$  (red) components of the Br 3d photoemission intensity, normalized to the condensed phase O 1s intensity, photon flux and cross-section of NaBr aqueous solutions as a function of concentration. The interfacial bromide concentration (black) is linearly correlated with the bromide concentration, which agrees with the negative surface excess derived from surface tension results [Shah *et al.*, 2013]. Thus no saturation is expected. The interfacial  $[\text{Br}\bullet\text{OOO}^-]$  concentration (red) also increases with bromide concentration. The ratio of  $[\text{Br}\bullet\text{OOO}^-]$  to  $\text{Br}^-$  (blue) appears to decrease somewhat from 0.15 at 0.05 M NaBr to 0.12 at 0.5 M. This could be indicative of a saturation effect and consistent

## Chapter 4 Surface propensity of $[\text{Br}\bullet\text{OOO}^-]$ intermediate at the liquid-vapor interface

with the assumption that the  $[\text{Br}\bullet\text{OOO}^-]$  intermediate exhibits a maximum of surface coverage.

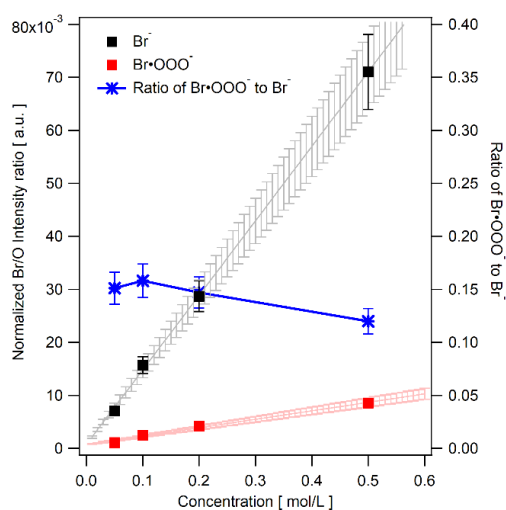


**Figure 5:**  $\text{Br}^-$  (black) and  $[\text{Br}\bullet\text{OOO}^-]$  (red) component photoemission intensity, as well as their ratio (blue), for NaBr aqueous solutions exposed to  $\text{O}_3$  as a function of bromide concentration, after normalization to the condensed phase O 1s intensity, photon flux and cross-section. The corresponding linear fit is shown with grey and pink line (10% error bar), respectively.

The uptake coefficient is the loss rate of gas-phase ozone to the aqueous solution normalized to the gas kinetic collision rate with the aqueous solution surface. In Figure 6, data from experiments published by [Artiglia *et al.*, 2017] performed at 274 K (pH=7, dashed red line) and pH 1 (dashed black line) are shown as a function of the bromide concentration in the aqueous phase for low ozone mixing ratios in the gas phase (70 ppb). This data set confirms that the *uptake coefficient* increases with increasing bromide concentration. Reactivity in the bulk aqueous phase depends on the solubility of ozone, ionic strength of the solution, and diffusivity of ozone. It exhibits a square root dependence of the bromide concentration. At low ozone mixing ratios, however, the reaction rate scales linearly with the intermediate concentration at the surface [Artiglia *et al.*, 2017]. This is directly demonstrated in Figure 6 by the close correlation of the measured ozone uptake coefficients at neutral pH (dashed red line) with the  $[\text{Br}\bullet\text{OOO}^-]$  intermediate concentration at the surface (red symbols), expressed by the photoemission intensity ratio of the Br 3d component of the intermediate to that of the condensed phase O 1s component (thus water). As already seen in Figure 5, the latter is linearly related to the bromide concentration. Even though the measured ozone uptake coefficients under acidic conditions (pH=1, dash black line) is much larger compared to neutral conditions, as discussed above, we could not reliably quantify the  $[\text{Br}\bullet\text{OOO}^-]$  intermediate component in the photoemission spectra. As mentioned before, this indicates that the  $[\text{Br}\bullet\text{OOO}^-]$  intermediate is less stable under acidic conditions, with a larger rate of reactions (2) and (3). The uptake coefficient at pH=1 seems to saturate at high bromide concentration which may be due to the maximum intermediate coverage at the liquid-vapor interface.

## Chapter 4 Surface propensity of $[\text{Br}\bullet\text{OOO}^-]$ intermediate at the liquid-vapor interface

As previously mentioned, the reaction of ozone with bromide in the bulk aqueous phase is relatively slow, with a rate coefficient of around  $163 \text{ M}^{-1} \text{ s}^{-1}$  at 293 K and neutral pH [Haruta and Takeyama, 1981], and  $38 \text{ M}^{-1} \text{ s}^{-1}$  at 273 K and neutral pH [Liu et al., 2001]. Therefore, when ozone is dosed, we would not expect the formation of HOBr or hypobromite within the  $\sim 100 \mu\text{s}$  exposure between the gas dosing system and the detection point of XPS. In turn, the actual collision rate of ozone molecules with the surface at about  $6.0 \cdot 10^{17} \text{ molecules cm}^{-2} \text{ s}^{-1}$  is sufficient to build up a high surface coverage of the complex with bromide, if the association kinetics is fast (see Supplementary Note 1). This of course also requires that the availability of bromide at the surface is sufficient. In the absence of any pre-existing enhanced concentration on the surface, formation of an even maximum conceivable complex surface coverage of around  $10^{12} \text{ molecules cm}^{-2}$  (as estimated from the XPS data) would deplete roughly the topmost few nanometers of a 0.1 M solution. Replenishing this by diffusion from the deeper bulk requires a few microseconds (see Supplementary Note 1) [Winter and Faubel, 2006; Lee et al., 2015], fast enough to ensure equilibration between the surface and the bulk under the present experimental conditions. Due to the substantial transition state barrier towards products, the steady state surface coverage establishes quickly and is determined by the rapid association and dissociation of ozone and bromide.

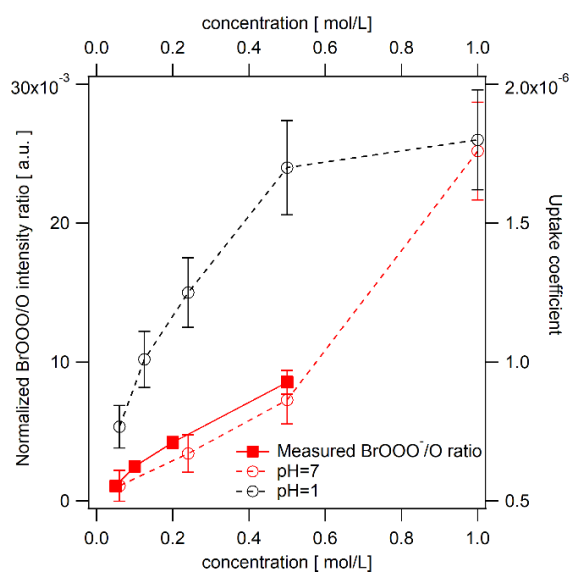


**Figure 6:** Measured [Artiglia et al., 2017] ozone uptake coefficients at 274 K (pH=7, open red circles and dashed red line) and pH 1 (open black circles and dashed black line) as a function of the bromide concentration in the aqueous phase for low ozone mixing ratios in the gas phase (70 ppb). Error bars represent standard deviations of measured values. The interfacial concentration of  $[\text{Br}\bullet\text{OOO}^-]$  (filled red squares and solid red line) as a function of the bromide concentration in the aqueous phase is expressed by the Br 3d of  $[\text{Br}\bullet\text{OOO}^-]$  to condensed phase O 1s photoemission intensity ratio.

The kinetic data shown in Figure 6 and reported in more detail by Artiglia et al. [Artiglia et al., 2017] are consistent with those of Oldridge and Abbatt [Oldridge and Abbatt, 2011] within less than a factor of two, both with respect to the absolute value of the uptake coefficient and the concentration range where the surface reaction dominates. The  $[\text{Br}\bullet\text{OOO}^-]$  complex

## Chapter 4 Surface propensity of [Br•OOO<sup>-</sup>] intermediate at the liquid-vapor interface

---

is in fast equilibrium with gas-phase ozone. Its surface coverage is saturated above  $10^{11}$  molecule  $\text{cm}^{-3}$ , thus both at the lowest ozone concentration of the present study and at all atmospheric levels, and depends very weakly on the temperature. The extent of the surface reaction, manifesting itself in the positive deviation from the bulk phase reactivity with decreasing gas phase concentration, gets relatively larger at lower bromide concentration. This is nicely reproduced by the surface reaction model constructed in Artiglia et al. [Artiglia et al., 2017] and used in chapter 6 of this thesis. The measured kinetic data do not allow constraining the magnitude of the saturating surface coverage (to compare with that derived from XPS), since no data are available at low enough ozone concentrations to escape the saturating regime. For the present data, the rate of the surface reaction is only constrained by the product of the coverage and the surface reaction rate coefficient. The first-order rate coefficient for the decomposition of the complex into hypobromite on the surface as derived from the kinetic data is about  $10^{-3} \text{ s}^{-1}$ .

Since the global distribution of BrO responds notably to the oxidation of bromide by ozone [Schmidt et al., 2016], and since our new results provide a significantly larger contribution by the surface reaction than the previously recommended parameterization [Ammann et al., 2013], we expect notable changes to the relative importance of this reaction among the multiphase halogen chemical cycling reactions.

### 4.1.5 Conclusion

In summary, the XPS results provide clear spectroscopic evidence of the bromide ozonide intermediate, the [Br•OOO<sup>-</sup>] pre-complex. Furthermore, a rough estimate of the surface coverage from the photoemission spectra of the Br 3d at increasing information depths shows that the new species prefers the interface, in good agreement with first-principle MD simulations [Artiglia et al., 2017]. We further studied the formation of the intermediate at low pH, indicating a much lower surface concentration under acidic conditions, possibly due to faster release of molecular oxygen, which is in agreement with the larger ozone uptake coefficients [Artiglia et al., 2017]. The surface concentration of the [Br•OOO<sup>-</sup>] intermediate increased almost linearly with the bromide concentration; the trend towards a smaller [Br•OOO<sup>-</sup>] to bromide ratio at high concentration could be a sign of saturation driven by a maximum coverage. The [Br•OOO<sup>-</sup>] intermediate concentration at the interface turned out to be tightly correlated with the uptake coefficient of ozone over the same bromide concentration range. This work clearly shows the preference of the intermediate for the liquid-gas interface and sheds light on mechanical and structural aspects of the reaction. The results provide evidence for a stronger contribution of the surface oxidation of bromide than previously thought, which will require re-assessment of the impacts on the global ozone budget and mercury deposition [Schmidt et al., 2016]. In turn, the formation of ozonides on surfaces may be a widespread phenomenon and a key step of critical oxidation processes relevant not only for atmospheric chemistry but also for the effects of atmospheric particles on human health [Shiraiwa et al., 2011; Berkemeier et al., 2016; Lakey et al., 2016].

### 4.2 Supplementary information

#### Supplementary Note 1. Liquid-jet x-ray photoelectron spectroscopy

##### Technical and experimental details

A gas dosing system, developed by Microliquids GmbH, was connected to the liquid jet assembly. A second nozzle, made of titanium, was screwed concentrically to the quartz nozzle delivering the liquid (see Figure 1a). The outer nozzle has a 500  $\mu\text{m}$  orifice, which is placed 1.0 mm far from the aperture of the quartz nozzle. The gas (either pure oxygen or a mixture of 1% ozone in oxygen, generated in situ by means of a commercial ozone generator (502, Fischer Technology), whose flow was adjusted using a variable leak valve connected to the nozzle via a 1/16" PEEK tube, reached the nozzle and was interacting efficiently with the liquid wire in the area before injection into the experimental chamber. The efficiency of O<sub>2</sub> to O<sub>3</sub> conversion in the ozone generator was checked in separate experiments utilizing the same ozone analyzer as described in the context of the kinetic experiments above. The purity of the gas was checked through a quadrupole mass spectrometer installed in the second differential pumping stage of the electron analyzer. During the experiment, we used two cold traps (liquid nitrogen) and a 27 m<sup>3</sup> h<sup>-1</sup> root pump. Before dosing the gas, the pressure in the experimental chamber was 3·10<sup>-2</sup> mbar. While dosing the gas, we set the pressure to 0.25 mbar. The advantage of using a gas delivery nozzle is that we can expect a higher local pressure in the area between the orifice of the quartz nozzle and that of the titanium one. The diffusion of the gas into the liquid is fast enough that gas–liquid equilibrium over the probe depth of the XPS experiments is established within 1  $\mu\text{s}$ . Because the solubility of ozone is low, the net flux into the liquid is low, and no gradients will limit this flux in the gas phase. The residence time of the liquid filament within the dosing system is approx. 100  $\mu\text{s}$  and between the dosing system and the point at which it hits the X-ray is 100  $\mu\text{s}$ . Therefore, the gas – surface and gas–liquid equilibria follow the changing pressure in the gas phase. A preliminary experiment carried out without the gas dosing system showed a similar evolution of the Br 3d spectrum while dosing ozone (0.1-0.2 mbar background pressure). However, the effect was less pronounced than after employing the gas dosing system, indicating that loss of ozone to the chamber walls has a significant impact on the gas exposure on the liquid.

Concerning the diffusion of bromide ions in the solution, the evolution of the surface concentration of an initially free surface by diffusion from the bulk with time is given by equation 12:

$$c_s = 2 \left( \frac{D}{\pi} \right)^{1/2} c t^{1/2} \quad (1)$$

where  $c$  is the bulk concentration of the bromide solution ( $7.53 \cdot 10^{19}$  molecules cm<sup>-3</sup>),  $c_s$  is the surface concentration of [Br•OOO<sup>-</sup>] (estimated as  $2 \cdot 10^{12}$  molecules cm<sup>-2</sup>), and  $D$  is the diffusion coefficient ( $2.41 \cdot 10^{-10}$  cm<sup>2</sup>s<sup>-1</sup>), evaluated through the Stokes-Einstein equation. The

## Chapter 4 Surface propensity of [Br•OOO<sup>-</sup>] intermediate at the liquid-vapor interface

---

time needed to re-establish the equilibrium concentration is approx. 2  $\mu\text{s}$ , much lower than the time between the injection of the liquid filament and the detection point (100  $\mu\text{s}$ ).

The Swiss light source synchrotron operates in top-up mode thus the photon flux did not change during measurements. It is well known from the literature that X-rays can induce the radiolysis of water, leading to the formation of highly reactive hydroxyl radicals [George *et al.*, 2012], which could affect the measurements. Thanks to the high speed of the injected liquid filament, the liquid microjet technique limits the beam damage. The concentration of radicals does not reach  $1 \cdot 10^{-6}$  mol/L under the experimental conditions adopted in this study.

The 0.125 mol L<sup>-1</sup> solutions of bromide and bromate were prepared by adding sodium bromide (NaBr,  $\geq 99.0\%$ , Sigma-Aldrich) and sodium bromate (NaBrO<sub>3</sub>,  $\geq 99.5\%$ , Sigma-Aldrich), respectively, to Milli-Q water (Millipore, 18.2 M $\Omega$  cm<sup>-1</sup> at 25 °C). The 0.08 mol L<sup>-1</sup> hypobromite solution was prepared by disproportionating Br<sub>2</sub> in a 0.5 mol L<sup>-1</sup> solution of NaOH [Polak *et al.*, 1966]. Hypobromite and bromide were generated based on the reaction:

$$\text{Br}_2 + 2 \text{OH}^- \rightarrow \text{Br}^- + \text{BrO}^- + \text{H}_2\text{O}.$$

Hypobromite is thermodynamically unstable and disproportionates to bromide and bromate. To slower this reaction, we cooled the solution to 0°C both during the preparation and the experiment. According to our spectra (Figure 1c), bromate was not formed for the whole duration of the experiment.

The photoemission spectra were fitted using Shirley background subtraction and Gaussian line shapes [Lee *et al.*, 2015]. For Br 3d, the spin-orbit split was fixed at 1.03 eV. The Full width at half maximum (FWHM) of the peaks was constrained for the whole set of processed data (1.05 eV). A single doublet allowed getting a good deconvolution of the Br 3d signals acquired without dosing and while dosing oxygen. In the presence of ozone, a second doublet had to be added to reach the same correlation. The second doublet is made of Gaussian peaks having a spin-orbit split fixed at 1.09 eV and FWHM of 1.10 eV. The best correlation was obtained by applying a chemical shift of +0.7 eV to the binding energy of the second doublet.

### Evolution of the O 1s spectrum as a function of the excitation energy

The spectra reported in Figure S1a show the O 1s spectra (excited by second-order photon light) acquired at increasing excitation energy, which corresponds to the increasing kinetic energy of the photoelectrons. The three kinetic energies are the same as those of the Br 3d spectra plotted in Figure 2c. The spectra were separated into two components: one at high binding energy (centered at 539.9 eV), associated with the gas phase of water, and another, centered at 537.9 eV, associated with the condensed phase of water. The latter was used to normalize the area of the Br 3d signal of the [Br•OOO<sup>-</sup>] complex (Figure 2d). Water being the solvent, it can be considered as a reference during the measurements. Figure S1b shows the ratio between the area of the peak of the oxygen gas phase and that of the condensed phase. The ratio decreases as the kinetic energy of the photoelectrons increases. Indeed, an increase of the kinetic energy of the photoelectrons corresponds to an increase of the probed depth.

## Chapter 4 Surface propensity of $[\text{Br}\bullet\text{OOO}^-]$ intermediate at the liquid-vapor interface

As long as the energy is increased, a larger thickness of the liquid wire is probed, while the contribution of the gas phase remains constant, apart from changes due to changes in photon flux and cross-section (the pressure in the experimental chamber was constant during the whole duration of the experiment).

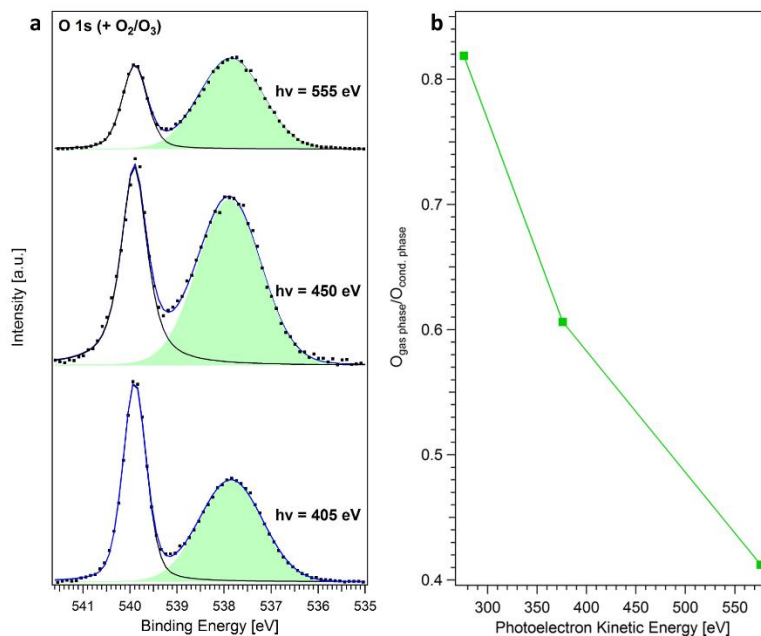


**Figure S1:** Signal of the O 1s acquired at different excitation energies,  $h\nu=405$ , 450, and 555 eV (corresponding to the second-order excitation energies  $h\nu=810$ , 900, and 1110 eV), corresponding to the kinetic energies (peak centroid) of 276, 376 and 575 eV, respectively.

### Evaluation of the $[\text{Br}\bullet\text{OOO}^-]$ surface coverage

Figure S2 shows a rough estimate of the surface coverage of  $[\text{Br}\bullet\text{OOO}^-]$  complex based on the XPS data acquired at increasing photoelectron kinetic energy (276, 376, and 576 eV). We employed two models to fit the behavior of the ratio between the intensity of the peaks related to the complex ( $I_{\text{BrOOO}^-}$ ) and that of the peaks related to the bulk  $0.125 \text{ mol L}^{-1}$  solution of  $\text{Br}^-$  ( $I_{\text{Br}^-}$ ) (see Figure 2c). Passing from 276 to 376 eV there is not a significant decrease of the  $I_{\text{BrOOO}^-}/I_{\text{Br}^-}$  ratio, reflecting the quality of the fitting (the experimental point corresponding to 376 eV is out of the confidence interval). A possible reason is that the difference in the excitation energy (100 eV) is not enough to vary the information depth considerably.

The first model (Supplementary Figure S2 a and b) does not take into account the attenuation of the photoemission signal from the bulk by the overlayer ( $[\text{Br}\bullet\text{OOO}^-]$  complex). The formula adopted is the following:

$$\frac{I_{[\text{Br}\bullet\text{OOO}^-]}}{I_{\text{Br}^-}} = \frac{n([\text{Br}\bullet\text{OOO}^-], \text{surface})}{n(\text{Br}^-, \text{bulk}) \cdot \text{MED}} \quad (2)$$

where  $n([\text{Br}\bullet\text{OOO}^-], \text{surface})$  is the surface coverage of the  $[\text{Br}\bullet\text{OOO}^-]$  complex (complexes/ $\text{cm}^2$ ),  $n(\text{Br}^-, \text{bulk})$  is the ion density of bromide ions in the solution (ions/ $\text{cm}^3$ ), and MED is the mean escape depth of the photoelectrons emitted from the ions (defined as



## Chapter 4 Surface propensity of $[\text{Br}\bullet\text{OO}\cdot]$ intermediate at the liquid-vapor interface

$\langle \text{MED} \rangle_{\text{avg}} = 2/\pi \cdot \text{IMFP}$ , where  $\text{IMFP}$  is the inelastic mean free path of the photoelectrons at each kinetic energy) [Winter and Faubel, 2006]. We estimated the surface coverage is employing two sets of IMFPs. In 2010, Ottosson et al. obtained an experimental curve of the electron attenuation length (EAL) in the 70-900 eV range for water [Ottosson et al., 2010]. Recently, Shinotsuka et al. calculated the electron inelastic mean free path for liquid water from its optical energy-loss function [Shinotsuka et al., 2016]. The values are different from each other. Thus, we calculated the surface coverage using Shinotsuka's IMFPs in Supplementary Figure S2a, and Ottosson's EALs in Supplementary Figure S2b. The surface coverages are  $1.9$  and  $2.9 \cdot 10^{12}$  complexes  $\text{cm}^{-2}$ , respectively.

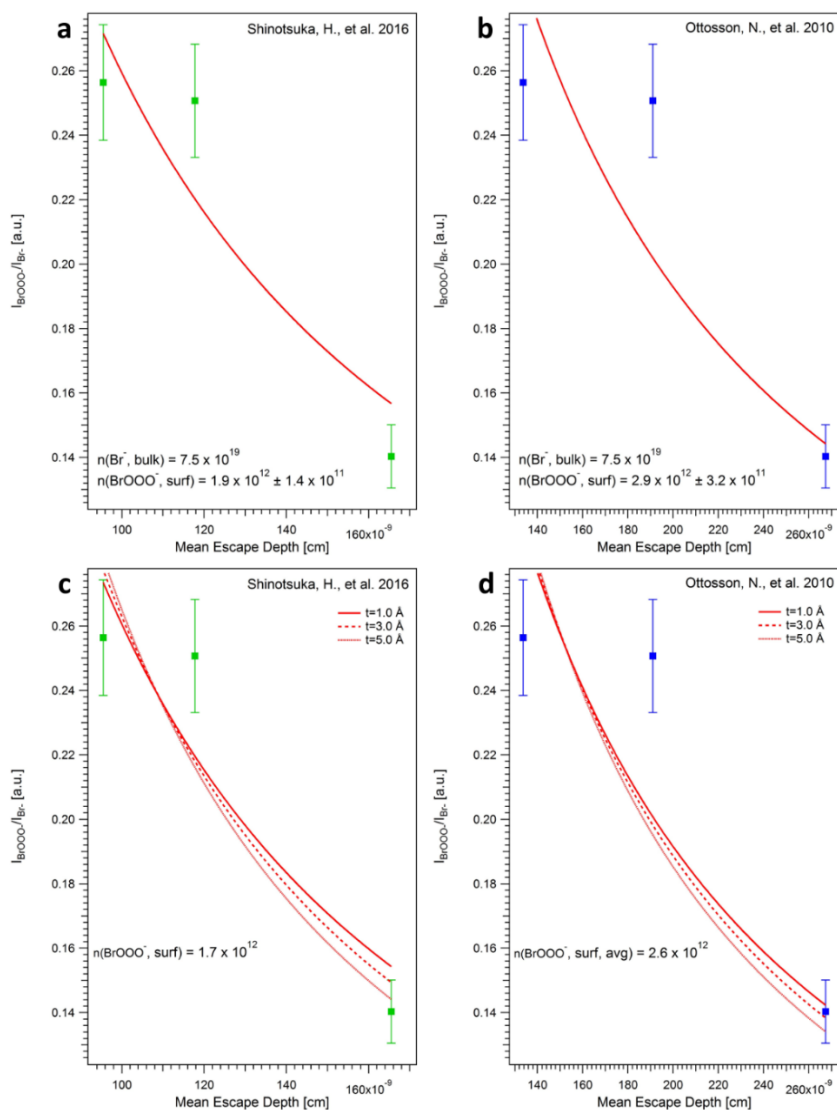


**Figure S2:** Evaluation of the surface coverage of the  $[\text{Br}\bullet\text{OO}\cdot]$  complex (a)-(b) Simple approximation, without considering the surface attenuation due to the  $[\text{Br}\bullet\text{OO}\cdot]$  complex; (c)-(d) considering the attenuation of the signal from the bulk ( $0.125 \text{ mol L}^{-1}$  aqueous solution of  $\text{Br}\cdot$ ) by a surface layer containing the  $[\text{Br}\bullet\text{OO}\cdot]$  complex. The error bars were calculated, propagating the errors associated with the peak areas of three different measurements.

## Chapter 4 Surface propensity of $[\text{Br}\bullet\text{OOO}^-]$ intermediate at the liquid-vapor interface

We adopted a second model to fit the experimental data available, which considers the attenuation of the signal from the bulk aqueous solution by a thin surface layer of  $[\text{Br}\bullet\text{OOO}^-]$  complex. The simplified equation, inspired by the literature [Cimino *et al.*, 1999; Fadley, 1978], is the following:

$$\frac{I_{[\text{Br}\bullet\text{OOO}^-]}}{I_{\text{Br}^-}} = \frac{\rho_{[\text{Br}\bullet\text{OOO}^-]}}{n_{(\text{Br}^-, \text{bulk})}} \cdot \left[ 1 - \exp\left(-\frac{t}{\text{MED}}\right) \right] \cdot \exp\left(\frac{t}{\text{MED}}\right) \quad (3)$$

where  $\rho_{[\text{Br}\bullet\text{OOO}^-]}$  is the ion density of the  $[\text{Br}\bullet\text{OOO}^-]$  complex (complexes  $\text{cm}^{-3}$ ), and  $t$  is the thickness of the surface layer ( $[\text{Br}\bullet\text{OOO}^-]$  complex). Supplementary Figures S 2c and d show the results attained using the MED from Shinotsuka and Ottosson, respectively. Three fitting functions, obtained employing three pre-set values of  $t$  (in the 1.0 to 5.0 Å range) are shown. The best correlation is found using the lower values, i.e. 1.0 and 3.0 Å, proving that the complex does not diffuse toward the bulk. The surface coverages (average value between the three thicknesses, obtained multiplying  $\rho_{[\text{Br}\bullet\text{OOO}^-]}$  by  $t$ ) are in good agreement with the results shown in Figures S2a and S2b. The values,  $1.7$  and  $2.6 \cdot 10^{12}$  complexes  $\text{cm}^{-2}$ , decrease by ca. 10% compared to those obtained with the first model because of the attenuation.

### Supplementary spectra 2

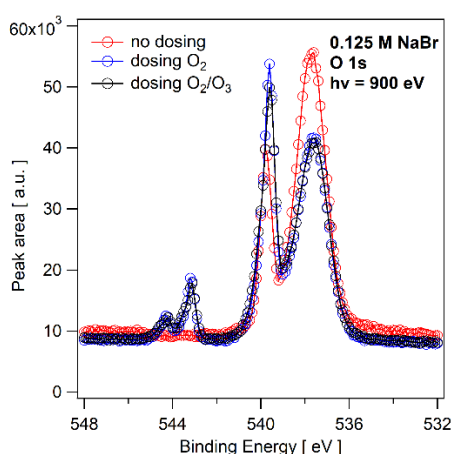


Figure S3: O 1s spectra of 0.125 M NaBr with and without gas dosing

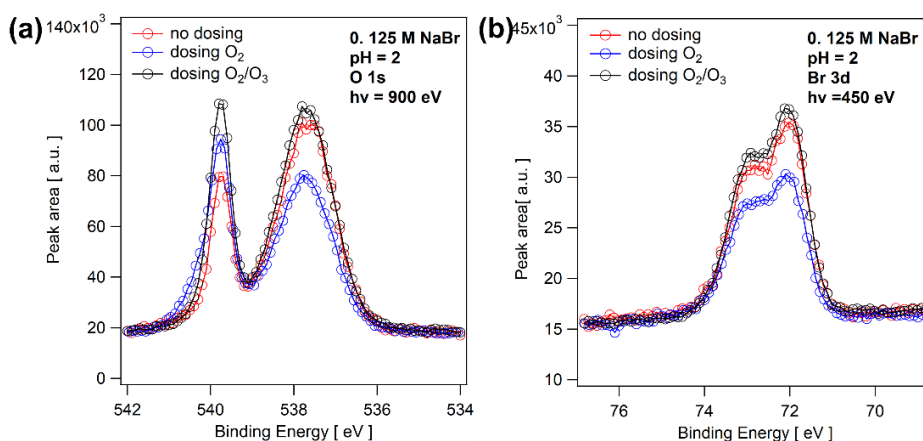


Figure S4: O 1s and Br 3d spectra of 0.125 M NaBr at pH=2, with and without gas dosing

# Chapter 4 Surface propensity of $[\text{Br}\cdot\text{OOO}^-]$ intermediate at the liquid-vapor interface

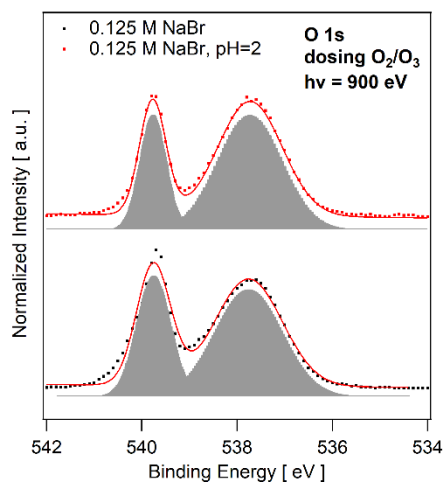


Figure S5: Fitting for O 1s spectra of 0.125 M NaBr at pH = 7 and pH = 2, both in presence of  $\text{O}_2/\text{O}_3$ .

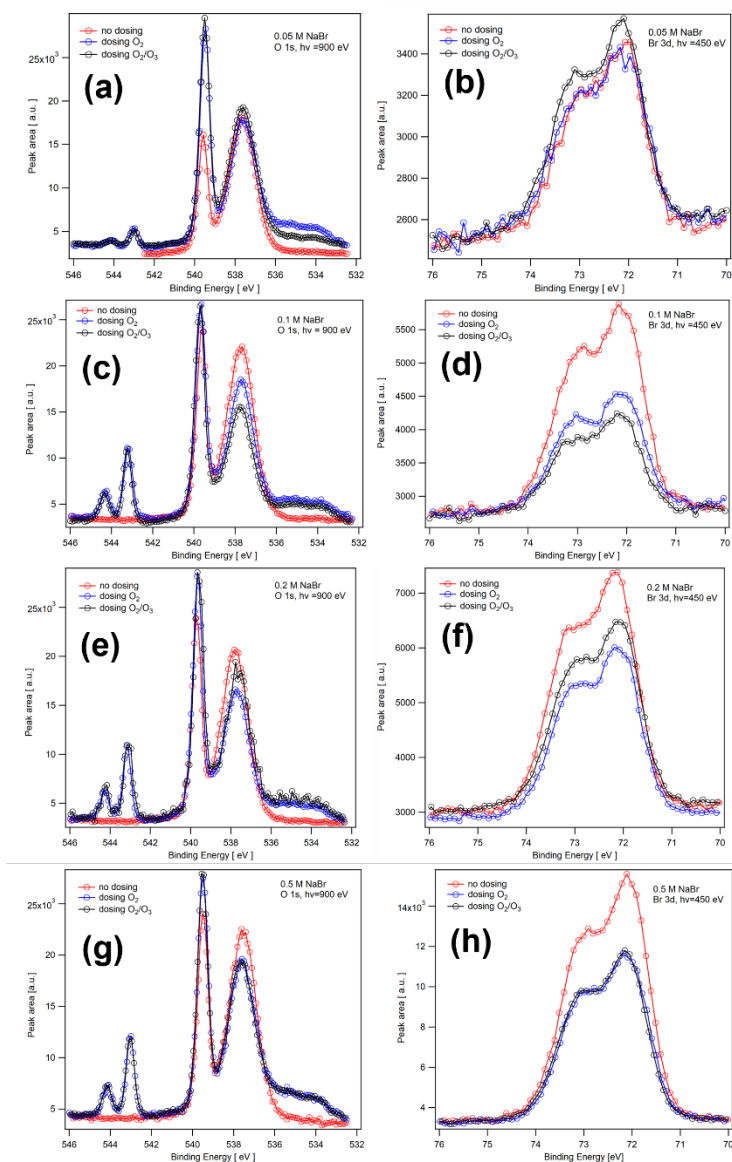
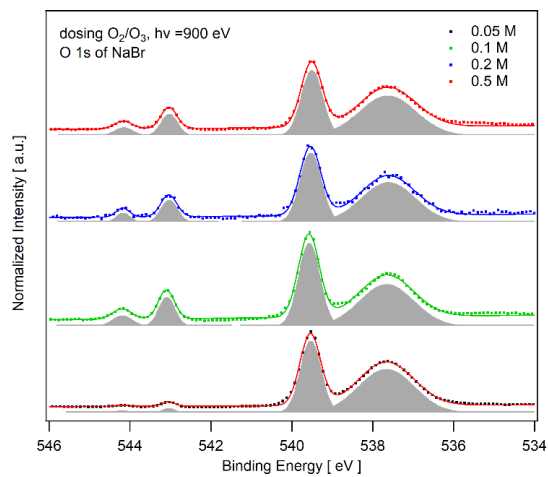


Figure S6: O 1s and Br 3d spectra of 0.05, 0.1, 0.2, 0.5 M NaBr, with and without gas dosing

## Chapter 4 Surface propensity of $[\text{Br}\bullet\text{OOO}^-]$ intermediate at the liquid-vapor interface

---



**Figure S7:** The graphs fit O 1s spectra of NaBr solutions with varying NaBr concentration.

---

## Bibliography

---

- Abbatt, J., N. Oldridge, A. Symington, V. Chukalovskiy, R. D. McWhinney, S. Sjostedt, and R. A. Cox (2010), Release of Gas-Phase Halogens by Photolytic Generation of OH in Frozen Halide-Nitrate Solutions: An Active Halogen Formation Mechanism?, *J. Phys. Chem. A*, 114(23), 6527-6533, doi:10.1021/jp102072t.
- Artiglia, L., et al. (2017), A surface-stabilized ozonide triggers bromide oxidation at the aqueous solution-vapour interface, *Nature Communications*, 8(1), 700, doi:10.1038/s41467-017-00823-x.
- Ammann, M., Cox, R.A., Crowley, J.N., Jenkin, M.E., Mellouki, A., Rossi, M.J., Troe, J. and Wallington, T.J., 2013. Evaluated kinetic and photochemical data for atmospheric chemistry: Volume VI—heterogeneous reactions with liquid substrates. *Atmospheric Chemistry and Physics*, 13(16), pp.8045-8228.
- Berkemeier, T., S. S. Steimer, U. K. Krieger, T. Peter, U. Poschl, M. Ammann, and M. Shiraiwa (2016), Ozone uptake on glassy, semi-solid and liquid organic matter and the role of reactive oxygen intermediates in atmospheric aerosol chemistry, *PCCP*, 18(18), 12662-12674, doi:10.1039/c6cp00634e.
- Brown, M. A., et al. (2013), A new endstation at the Swiss Light Source for ultraviolet photoelectron spectroscopy, X-ray photoelectron spectroscopy, and X-ray absorption spectroscopy measurements of liquid solutions, *Rev. Sci. Instrum.*, 84(7), doi:10.1063/1.4812786.
- Cao, L., C. G. Wang, M. Mao, H. Grosshans, and N. W. Cao (2016), Derivation of the reduced reaction mechanisms of ozone depletion events in the Arctic spring by using concentration sensitivity analysis and principal component analysis, *Atmos Chem Phys*, 16(23), 14853-14873, doi:10.5194/acp-16-14853-2016.
- Chameides, W. L., and D. D. Davis (1982), The Free-Radical Chemistry of Cloud Droplets and Its Impact Upon the Composition of Rain, *J Geophys Res-Oc Atm*, 87(Nc7), 4863-4877, doi:DOI 10.1029/JC087iC07p04863.
- Cimino, A., D. Gazzoli, and M. Valigi (1999), XPS quantitative analysis and models of supported oxide catalysts, *J. Electron. Spectrosc. Relat. Phenom.*, 104(1-3), 1-29, doi:Doi 10.1016/S0368-2048(98)00300-4.
- Clifford, D., and D. J. Donaldson (2007), Direct experimental evidence for a heterogeneous reaction of ozone with bromide at the air-aqueous interface, *J. Phys. Chem. A*, 111(39), 9809-9814, doi:10.1021/jp074315d.
- De Haan, D. O., T. Brauers, K. Oum, J. Stutz, T. Nordmeyer, and B. J. Finlayson-Pitts (1999), Heterogeneous chemistry in the troposphere: experimental approaches and applications to the chemistry of sea salt particles, *Int. Rev. Phys. Chem.*, 18(3), 343-385, doi:Doi 10.1080/014423599229910.
- Fadley, C. S., Brundle, C. R., Baker, A. D. (1978), *Electron Spectroscopy: Theory, Techniques and Applications*, Academic Press, New York.
- George, G. N., et al. (2012), X-ray-induced photo-chemistry and X-ray absorption spectroscopy of biological samples, *J Synchrotron Radiat*, 19, 875-886, doi:10.1107/S090904951203943x.
- Ghosal, S., A. Shbeeb, and J. C. Hemminger (2000), Surface segregation of bromine in bromide doped NaCl: Implications for the seasonal variations in Arctic ozone, *Geophys. Res. Lett.*, 27(13), 1879-1882, doi:Doi 10.1029/2000gl011381.
- Gladich, I., J. S. Francisco, R. J. Buszek, M. Vazdar, M. A. Carignano, and P. B. Shepson (2015), Ab Initio Study of the Reaction of Ozone with Bromide Ion, *J. Phys. Chem. A*, 119(19), 4482-4488, doi:10.1021/jp5101279.
- Gunten, U. v. (2003), Ozonation of drinking water: Part II. Disinfection and by-product formation in presence of bromide, iodide or chlorine, *Water Res.*, 37(7).
- Haag, W. R., and J. Hoigne (1983), Ozonation of Bromide-Containing Waters - Kinetics of Formation of Hypobromous Acid and Bromate, *Environ. Sci. Technol.*, 17(5), 261-267, doi:DOI 10.1021/es00111a004.
- Haag, W. R., J. Hoigne, and H. Bader (1984), Improved Ammonia Oxidation by Ozone in the Presence of Bromide Ion during Water-Treatment, *Water Res.*, 18(9), 1125-1128, doi:Doi 10.1016/0043-1354(84)90227-6.
- Haruta, K., and T. Takeyama (1981), Kinetics of Oxidation of Aqueous Bromide Ion by Ozone, *J. Phys. Chem.*, 85(16), 2383-2388, doi:DOI 10.1021/j150616a018.

## Bibliography

---

- Heeb, M. B., J. Criquet, S. G. Zimmermann-Steffens, and U. von Gunten (2014), Oxidative treatment of bromide-containing waters: Formation of bromine and its reactions with inorganic and organic compounds - A critical review, *Water Res.*, 48, 15-42, doi:10.1016/j.watres.2013.08.030.
- Hofft, O., A. Borodin, U. Kahnert, V. Kempter, L. X. Dang, and P. Jungwirth (2006), Surface segregation of dissolved salt ions, *J. Phys. Chem. B*, 110(24), 11971-11976, doi:10.1021/jp061437h.
- Hunt, S. W., M. Roeselova, W. Wang, L. M. Wingen, E. M. Knipping, D. J. Tobias, D. Dabdub, and B. J. Finlayson-Pitts (2004), Formation of molecular bromine from the reaction of ozone with deliquesced NaBr aerosol: Evidence for interface chemistry, *J. Phys. Chem. A*, 108(52), 11559-11572, doi:10.1021/jp0467346.
- Jungwirth, P., and D. J. Tobias (2001), Molecular structure of salt solutions: A new view of the interface with implications for heterogeneous atmospheric chemistry, *J. Phys. Chem. B*, 105(43), 10468-10472, doi:DOI 10.1021/jp012750g.
- Kurahashi, N., S. Karashima, Y. Tang, T. Horio, B. Abulimiti, Y. I. Suzuki, Y. Ogi, M. Oura, and T. Suzuki (2014), Photoelectron spectroscopy of aqueous solutions: Streaming potentials of NaX (X = Cl, Br, and I) solutions and electron binding energies of liquid water and X-, *J. Chem. Phys.*, 140(17), doi:10.1063/1.4871877.
- Lakey, P. S. J., T. Berkemeier, H. J. Tong, A. M. Arangio, K. Lucas, U. Poschl, and M. Shiraiwa (2016), Chemical exposure-response relationship between air pollutants and reactive oxygen species in the human respiratory tract, *Sci Rep-Uk*, 6, doi:10.1038/srep32916.
- Lampimaki, M., V. Zelenay, A. Krepelova, Z. Liu, R. Chang, H. Bluhm, and M. Ammann (2013), Ozone-Induced Band Bending on Metal-Oxide Surfaces Studied under Environmental Conditions, *Chemphyschem*, 14(11), 2419-2425, doi:10.1002/cphc.201300418.
- Lee, M. T., M. A. Brown, S. Kato, A. Kleibert, A. Turler, and M. Ammann (2015), Competition between Organics and Bromide at the Aqueous Solution-Air Interface as Seen from Ozone Uptake Kinetics and X-ray Photoelectron Spectroscopy, *J. Phys. Chem. A*, 119(19), 4600-4608, doi:10.1021/jp510707s.
- Liu, Q., L. M. Schurter, C. E. Muller, S. Aloisio, J. S. Francisco, and D. W. Margerum (2001), Kinetics and mechanisms of aqueous ozone reactions with bromide, sulfite, hydrogen sulfite, iodide, and nitrite ions, *Inorg. Chem.*, 40(17), 4436-4442, doi:10.1021/ic000919j.
- Marx, D., and J. Hutter (2009), *Ab initio molecular dynamics*, edited, Cambridge University Press.
- McCabe, J., and J. P. D. Abbatt (2009), Heterogeneous Loss of Gas-Phase Ozone on n-Hexane Soot Surfaces: Similar Kinetics to Loss on Other Chemically Unsaturated Solid Surfaces, *J Phys Chem C*, 113(6), 2120-2127, doi:10.1021/jp806771q.
- Nissenson, P., L. M. Wingen, S. W. Hunt, B. J. Finlayson-Pitts, and D. Dabdub (2014), Rapid formation of molecular bromine from deliquesced NaBr aerosol in the presence of ozone and UV light, *Atmos. Environ.*, 89, 491-506, doi:10.1016/j.atmosenv.2014.02.056.
- Oldridge, N. W., and J. P. D. Abbatt (2011), Formation of Gas-Phase Bromine from Interaction of Ozone with Frozen and Liquid NaCl/NaBr Solutions: Quantitative Separation of Surficial Chemistry from Bulk-Phase Reaction, *J. Phys. Chem. A*, 115(12), 2590-2598, doi:10.1021/jp200074u.
- Olivieri, G., K. M. Parry, C. J. Powell, D. J. Tobias, and M. A. Brown (2016), Quantitative interpretation of molecular dynamics simulations for X-ray photoelectron spectroscopy of aqueous solutions, *J. Chem. Phys.*, 144(15), doi:10.1063/1.4947027.
- Ottosson, N., M. Faubel, S. E. Bradforth, P. Jungwirth, and B. Winter (2010), Photoelectron spectroscopy of liquid water and aqueous solution: Electron effective attenuation lengths and emission-angle anisotropy, *J. Electron. Spectrosc. Relat. Phenom.*, 177(2-3), 60-70, doi:10.1016/j.elspec.2009.08.007.
- Oum, K. W., M. J. Lakin, and B. J. Finlayson-Pitts (1998), Bromine activation in the troposphere by the dark reaction of O<sub>3</sub> with seawater ice, *Geophys. Res. Lett.*, 25(21), 3923-3926, doi:Doi 10.1029/1998gl900078.
- Parrella, J. P., et al. (2012), Tropospheric bromine chemistry: implications for present and pre-industrial ozone and mercury, *Atmos Chem Phys*, 12(15), 6723-6740, doi:10.5194/acp-12-6723-2012.
- Polak, H. L., G. Fennstra, and J. Slagman (1966), Stability of Hypobromite Solutions, *Talanta*, 13(5), 715-&, doi:Doi 10.1016/0039-9140(66)80006-1.
- Raso, A. R. W., et al. (2017), Active Molecular Iodine Snowpack Photochemistry in the Arctic, *PNAS*, under review.
- Sander, R., et al. (2003), Inorganic bromine in the marine boundary layer: a critical review, *Atmos Chem Phys*, 3, 1301-1336.
- Schmidt, J. A., et al. (2016), Modeling the observed tropospheric BrO background: Importance of multiphase chemistry and implications for ozone, OH, and mercury, *J Geophys Res-Atmos*, 121(19), 11819-11835, doi:10.1002/2015jd024229.
- Shah, A.-u.-H. A., K. Ali, and S. Bilal (2013), Surface tension, surface excess concentration, enthalpy and entropy of surface formation of aqueous salt solutions, *Colloids and Surfaces A: Physicochemical and Engineering Aspects*, 417, 183-190, doi:10.1016/j.colsurfa.2012.10.054.

## Bibliography

---

- Shinotsuka, H., B. Da, S. Tanuma, H. Yoshikawa, C. J. Powell, and D. R. Penn (2016), Calculations of electron inelastic mean free paths. XI. Data for liquid water for energies from 50eV to 30keV, *Surf. Interface Anal.*, doi:10.1002/sia.6123.
- Shiraiwa, M., Y. Sosedova, A. Rouviere, H. Yang, Y. Y. Zhang, J. P. D. Abbatt, M. Ammann, and U. Poschl (2011), The role of long-lived reactive oxygen intermediates in the reaction of ozone with aerosol particles, *Nat Chem*, 3(4), 291-295, doi:10.1038/Nchem.988.
- Slavicek, P., N. V. Kryzhevoi, E. F. Aziz, and B. Winter (2016), Relaxation Processes in Aqueous Systems upon X-ray Ionization: Entanglement of Electronic and Nuclear Dynamics, *J Phys Chem Lett*, 7(2), 234-243, doi:10.1021/acs.jpcclett.5b02665.
- Thurmer, S., M. Oncak, N. Ottosson, R. Seidel, U. Hergenbahn, S. E. Bradforth, P. Slavicek, and B. Winter (2013), On the nature and origin of dicationic, charge-separated species formed in liquid water on X-ray irradiation, *Nat Chem*, 5(7), 590-596, doi:10.1038/Nchem.1680.
- Weber, R., B. Winter, P. M. Schmidt, W. Widdra, I. V. Hertel, M. Dittmar, and M. Faubel (2004), Photoemission from aqueous alkali-metal-iodide salt solutions using EUV synchrotron radiation, *J. Phys. Chem. B*, 108(15), 4729-4736, doi:10.1021/jp030776x.
- Winter, B., E. F. Aziz, U. Hergenbahn, M. Faubel, and I. V. Hertel (2007), Hydrogen bonds in liquid water studied by photoelectron spectroscopy, *J. Chem. Phys.*, 126(12), 124504, doi:10.1063/1.2710792.
- Winter, B., and M. Faubel (2006), Photoemission from liquid aqueous solutions, *Chem. Rev.*, 106(4), 1176-1211, doi:10.1021/cr040381p.
- Wren, S. N., T. F. Kahan, K. B. Jumaa, and D. J. Donaldson (2010), Spectroscopic studies of the heterogeneous reaction between O<sub>3</sub>(g) and halides at the surface of frozen salt solutions, *J Geophys Res-Atmos*, 115, doi:10.1029/2010jd013929.

---

# Influence of surfactants with differently charged headgroups on the surface propensity of bromide

---

This chapter is in preparation for publication as: Chen, S., Artiglia, L., Yang, H., Boucly, A., Lezzi L., and Ammann, M. Influence of surfactants with differently charged headgroups on the surface propensity of bromide, 2022. Additional supporting molecular dynamics simulation are currently underway at the University of Lille (group of C. Toubin) and will be included in the publication.

## **5.1 Influence of surfactants with differently charged headgroups on the surface propensity of bromide**

### **5.1.1 Abstract**

Halide ions in oceans and sea spray aerosol particles are an important source of reactive halogen species in the atmosphere that impact the ozone budget and radiative balance. The multiphase cycling of halogen species is linked to the abundance of halide ions at the aqueous solution–air interfaces. The ubiquitous presence of organic compounds deriving from marine biota at the ocean surface calls for an assessment of the impact of often surface-active organics on the interfacial abundance of halide ions. Here, we use liquid jet X-ray photoelectron spectroscopy (XPS) to assess the impact of a monofunctional surfactant with a positive headgroup (hexylammonium) and one with a negative headgroup (propylsulfate) on the abundance of bromide ions at the interface. Core level spectra of Br 3d, Na 2s, and O 1s with kinetic energy varied from 155 eV to 770 eV are compared for solutions with both hexylammonium and propylsulfate containing solutions. We also use a photoelectron attenuation model to retrieve the interfacial concentration of bromide and sodium in the



presence of the different surfactants. The results clearly show that even in basic solution, where only a small fraction of hexylamine is actually protonated, its surface activity leads to an enhanced interfacial concentration of bromide, indicating that likely non-protonated hexylamine is already attracting bromide to the interface. In turn, the negatively charged sulfate group of propylsulfate does not affect the interfacial concentration of bromide, but leads to an increased presence of sodium anions. The present work demonstrates the important role of electrostatic interactions at the interface. This concept can be applied to qualitatively assess other halide or alkaline cations, or even other inorganic group ions, such as  $\text{SO}_4^{2-}$ ,  $\text{NO}_3^-$ ,  $\text{NH}_4^+$  that exist in atmospheric particles.

### 5.1.2 Introduction

Bromide ions in oceans and sea-spray aerosol (SSA) are the most critical sources of bromine to the atmosphere [Hegglin *et al.*, 2015, Wang *et al.*, 2015]. Oxidation of bromide leads to reactive bromine species that, together with iodine and chlorine, initiate multiphase chemical and photochemical cycles that affect the ozone budget [Wang *et al.*, 2015]. The multiphase cycling of bromine species is affected by the abundance of bromide and other bromine species at the aqueous solution – air interface. [Ghosal *et al.*, 2005; Gladich *et al.*, 2020] While bromide in neat NaBr solutions is depleted from the interface, the reaction intermediate with ozone, a bromide ozonide, is surface-active [Artiglia *et al.*, 2017] (Chapter 4). Also, the follow-up product, hypobromous acid, HOBr, shows some surface propensity [Ivan Gladich *et al.*, 2020] (chapter 3), which is an essential intermediate in the formation of the molecular halogen compounds  $\text{Br}_2$  and  $\text{BrCl}$ . In mixed solutions, e.g., in the presence of NaCl, bromide experiences higher abundance at the surface than in pure NaBr solutions [Ghosal *et al.*, 2008]. In the presence of organic co-solutes, such as citric acid [Lee *et al.*, 2015], butanol and butyric acid [Lee *et al.*, 2019], both attraction or repulsion of bromide have been observed, indicating subtle effects governing the presence of bromide at the interface. Here we consider the impact of differently charged ionic surfactants to obtain a more comprehensive understanding of the abundance of bromide ions at the aqueous solution – air interface at the ocean surface or in sea-spray aerosol (SSA) particles. Such ionic organic surfactants ubiquitously occur in presence of marine biota and may get strongly enriched in SSA particles [O'Dowd *et al.*, 2004; Prather *et al.*, 2013; Pinxteren *et al.*, 2020]. In view of 71% of the Earth's surface being covered by oceans and in view of the large contribution of SSA to the global aerosol burden, an assessment of the impact of often surface-active organics on the interfacial abundance of bromide ions is important for understanding multiphase cycling of bromine. Alkylamines, such as hexylamine used as a proxy for cationic surfactants in this work also occur more widely from other natural and anthropogenic sources [Ge *et al.*, 2011; Pinxteren *et al.*, 2020]. Similarly also for the negatively charged surfactants, organosulfate compounds are significantly contributing to atmospheric particulate organic matter, resulting mostly from multiphase processing of secondary organic compounds in presence of  $\text{SO}_2$  [Munger *et al.*, 1986; Herrmann *et al.*, 2015; McNeill, 2015]. Organosulfates, both through their hygroscopicity and surface activity, are also relevant as cloud condensation nuclei

[Hansen *et al.*, 2015]. The interplay of organosulfates with inorganic ions at the interface is therefore relevant also in that context.

X-ray photoelectron spectroscopy (XPS) provides chemically selective molecular level information from solid and liquid surfaces. With a tunable synchrotron X-ray source, the probe depth of the method can be adjusted from around one nanometer to a few nanometers by varying the kinetic energy of photoelectrons from a given core level via changing the exciting photon energy. Our recent work using liquid jet XPS demonstrated the power of this technique to assess the composition in terms of halide ions, organic solutes and their mixtures at the aqueous solution – air interface [Pruyne *et al.*, 2014; Lee *et al.*, 2015; Lee *et al.*, 2016]. The photoemission signal provides a direct spectroscopic signature from the surface and carries further information about acid dissociation, molecular orientation and electronic structure.

Here, we use liquid jet X-ray photoelectron spectroscopy (XPS) at the Swiss Light Source (SLS) [Matthew A. Brown *et al.*, 2013] to assess the difference between a monofunctional surfactant with a positive headgroup (hexylammonium) and a negative headgroup (propylsulfate) on the abundance of bromide and sodium ions at the interface.

### 5.1.3 Experimental method

#### Materials

This study was conducted using sodium bromide (NaBr, Sigma Aldrich, > 99.0%), sodium chloride (NaCl, Sigma Aldrich, > 99.0%), hexylamine (CH<sub>3</sub>(CH<sub>2</sub>)<sub>4</sub>CH<sub>2</sub>NH<sub>2</sub>, Sigma Aldrich, > 99.0%), and sodium propylsulfate (C<sub>3</sub>H<sub>7</sub>SO<sub>4</sub>Na, Sigma Aldrich, > 98.0%). The solutions were prepared by adding stock solutions to Milli-Q water (Millipore, 18.2 MΩ cm at 25 °C) and degassing with Ar gas. 0.1 M NaBr, 0.1 M NaBr /0.1 M hexylamine, 0.1 M NaBr/0.1 M hexylamine/0.55 M NaCl, 0.1 M NaBr/0.1 M propylsulfate, and 0.1 M NaBr/0.1 M propylsulfate/0.55 M NaCl aqueous solutions was prepared for liquid jet XPS experiment. The pH of the 0.1 M NaBr/0.1 M hexylamine at T=21.1°C is pH= 12.15 and the PH of the 0.1 M NaBr/0.1 M hexylamine/0.55 M NaCl at T=20.7 °C is pH= 12.46.

#### Liquid microjet XPS

XPS experiments with a Scienta R4000 electron analyzer and a HiPP-2 pre lens using a liquid micro-jet were conducted at the Surfaces/Interfaces: Microscopy (SIM) beamline of the Swiss Light Source using the near ambient pressure photoemission (NAPP) endstation [Brown *et al.*, 2013]. For the present experiments, a quartz nozzle (MicroLiquids), forming a liquid microjet with a diameter of from 23 to 25 μm, was used to deliver the liquid sample into the vacuum chamber. The liquid jet was operated at a flow rate of 0.5 ml/min, and the capillary transporting the liquid was immersed in a cooling bath set to 277 K upstream of the feedthrough into the chamber. The electron analyzer was operated at 20 eV pass energy (photoelectron kinetic energy at 155 eV) and 50 eV pass energy (photoelectron kinetic energy at 370 eV to 770 eV) with a 0.1 eV step size. The photoelectron kinetic energy was varied from 155 eV to 770 eV for obtaining core level spectra of Br 3d, N 1s, C 1s, Cl 2p, S 2p and O 1s to

allow variation of the information depth. Each kinetic energy corresponds to a specific value of the inelastic mean free path (IMFP) in liquid water [Shinotsuka *et al.*, 2017]. To take into account 90° detection angle and the cylindrical liquid filament geometry, the mean escape depth (MED) of photoelectrons was obtained as: [Winter and Faubel, 2006]  $MED = (2/\pi) IMFP$ .

Reported binding energies are relative to the vacuum level and calibrated to the 1b1 orbital of liquid water at 11.3 eV [Kurahashi *et al.*, 2014]. The spectral region was fit using pure Gaussian functions following standard linear background subtraction. The error bars of reported spectra were evaluated based on the standard deviation calculated from the fits of a statistical sample of spectra corresponding to the same solution. The standard deviation values were propagated to get the error of the signal intensity ratios. This does not take into account either small movements of the liquid filament in front of the aperture of the analyzer or uncertainty in the measurement of the photon flux.

### 5.1.4 Results and discussion

Figure 1 shows combined a) Br 3d, Na 2s and b) O 1s photoelectron spectra of mixed 0.1 M NaBr/0.1 M hexylamine/0.55 M NaCl (pink), mixed 0.1 M NaBr/0.1 M hexylamine (red), 0.1 M NaBr (black), mixed 0.1 M NaBr/0.1 M sodium propylsulfate (light-blue) and mixed 0.1 M NaBr/0.1 M sodium propylsulfate/0.55 M NaCl (dark-blue) aqueous solutions, which were measured at photon energies of 229 eV for Br 3d, Na 2s, and 696 eV for O 1s to obtain the same kinetic energy of around 155 eV. The reference case, a neat (organic-free) NaBr solution, is shown in black in the middle of the figure. The higher binding energy portion of the spectra in Figure 1a shows the spin-orbit split Br 3d<sub>5/2</sub> and 3d<sub>3/2</sub> peaks, while the lower binding energy portion features the Na 2s peak at 67.9 eV of Na<sup>+</sup> ions in the solutions. Upon adding 0.1 M hexylamine or 0.1 M hexylamine/0.55 M NaCl, shown on top of Figure 1, the Br 3d peak area increases apparently compared to pure NaBr solutions. As discussed further below, this is either due to hexylamine itself or due to a small fraction of positively charged hexylammonium. In contrast, upon adding 0.1 M propylsulfate or 0.1 M propylsulfate/0.55 M NaCl, the bromine photoemission intensity decreases (bottom of Figure 1a). Compared with pure NaBr, in the presence of 0.1 M hexylamine, the sodium intensity is barely detectable (top of Figure 1a), possibly due to the presence of positively charged headgroups. Note that the increased sodium intensity for solutions in the presence of 0.1 M hexylamine/0.55 M NaCl is due to the 5 fold increase of the bulk concentration of sodium. Upon adding propylsulfate, we observed a strong increase of the sodium intensity, likely due to the negatively charged headgroup attracting Na<sup>+</sup> towards the interface. The difference in this increase between 0.1 M Na-propylsulfate and 0.1 M Na-propylsulfate/0.55 M NaCl is again due to the much higher bulk concentration of sodium from the addition of 0.55 M NaCl. Note that the changes in photoemission intensity among the different solutions is not only due to the different abundances of Br<sup>-</sup> and Na<sup>+</sup> at the interface but also due to attenuation of photoelectrons by the aliphatic carbon chains accumulating at the interface.

The O 1s spectra in Figure 1b are fitted by two components that are assigned to gas-phase oxygen of H<sub>2</sub>O at higher binding energy and condensed phase oxygen of liquid H<sub>2</sub>O at lower binding energy. The binding energy differences between O1s liquid and gas are different for the different solutions, likely due to differences in surface potentials, as observed in previous studies [Lee *et al.*, 2019; Winter *et al.*, 2004]. The condensed phase O 1s intensities were found to decrease in the presence of the added organics, due to electron attenuation by the additional density of mostly carbon atoms at the interface. Therefore, for further analysis, we take into account this attenuation to assess the impact of hexylamine and propylsulfate on the changes in bromine and sodium intensities more quantitatively.

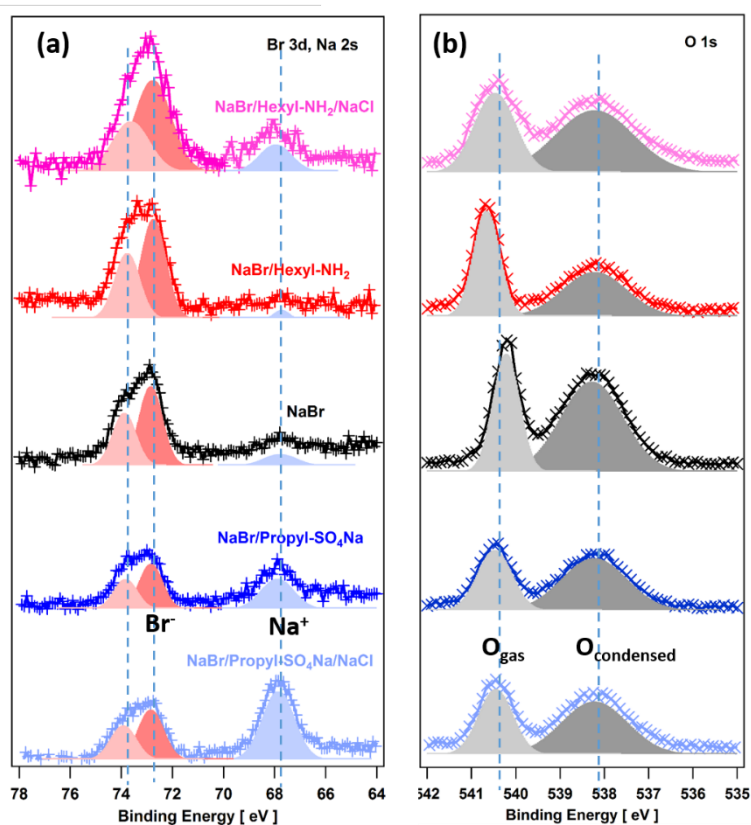


**Figure 1:** a) Br 3d, Na 2s and b) O 1s spectra of mixed 0.1 M NaBr/0.1 M hexylamine/0.55 M NaCl, mixed 0.1 M NaBr/0.1 M hexylamine, 0.1 M NaBr, mixed 0.1 M NaBr/0.1 M sodium propylsulfate and mixed 0.1 M NaBr/0.1 M sodium propylsulfate/0.55 M NaCl aqueous solutions at kinetic energy at 155 eV.

C 1s, N 1s, S 2p and Cl 2p spectra are shown in the supporting material (Figure S1). The C 1s (Figure S1a) exhibits two features representing aliphatic chain carbon (-C<sub>5</sub>H<sub>11</sub>) and the ammonium coupled carbon (-CH<sub>2</sub>-N) at a binding energy of 289.7 and 290.5 eV, for solutions in the presence of hexyl-NH<sub>2</sub>. Correspondingly, the two features represent aliphatic chain carbon (-C<sub>2</sub>H<sub>5</sub>) and the sulfate coupled carbon (-CH<sub>2</sub>-SO<sub>4</sub>) at a binding energy of 289.7 and 291.3 eV for solutions in the presence of propyl-SO<sub>4</sub>Na, respectively. Note that the C 1s spectra in Figure S1a are enlarged by a factor of 5. The lower C 1s intensity for the propylsulfate is due to the lower surface activity of this solute and the shorter aliphatic carbon chain. Upon adding NaCl, the C 1s intensity signal of NaBr/hexylamine/NaCl is much smaller

than the NaBr/hexylamine solutions. In contrast, the C 1s intensity signal of NaBr/ sodium propylsulfate/NaCl is much smaller than the NaBr/ sodium propylsulfate solutions.

The N 1s region in Figure S1b is fitted by three components that are assigned to protonated hexyl-NH<sub>3</sub><sup>+</sup> (which is labeled with R-NH<sub>3</sub><sup>+</sup> in the graphs) at binding energy at 407.1 eV, gas phase hexyl-NH<sub>2</sub> (which labeled with R-NH<sub>2,gas</sub> in the graphs) at binding energy at 405.6 eV, and condensed phase neutral hexyl-NH<sub>2</sub> (which labeled with R-NH<sub>2,liquid</sub> in the graphs) at binding energy at 404.4 eV, respectively [Brown *et al.*, 2013; Ekholm *et al.*, 2018]. As we can see from Figure S1a, both NaBr/hexylamine and NaBr/hexylamine/NaCl solutions is dominated by condensed phase hexyl-NH<sub>2</sub>, and the hexyl-NH<sub>3</sub><sup>+</sup> is only a small fraction. Note that the pKa of hexylamine is 10.64 [Perrin, 1965]. Since the pH of the hexylamine solutions was around 12, only a few percent were in the form of protonated hexylammonium ions in the aqueous solutions. We also caution that the signal to background ratio of the N1s spectra as a function of kinetic energy, shown in Figure S2, was not ideal, especially at higher kinetic energies. Due to the higher photon energies used, the background increases substantially due to C and O KLL Auger electrons. Therefore, whether the sole appearance of hexyl-NH<sub>3</sub><sup>+</sup> at the lowest kinetic energy would suggest that protonated form of hexylamine is accumulated at the interface cannot be conclusively answered.

The S 2p spectra (Figure S1c) exhibit a double-peak structure due to spin-orbit splitting into 2p<sub>3/2</sub> and 2p<sub>1/2</sub>. The addition of NaCl to NaBr/ hexyl-NH<sub>2</sub> aqueous solutions led to slightly increasing S intensity, likely due to salting-out by the additional ions in the solutions, which we will discuss in detail below.

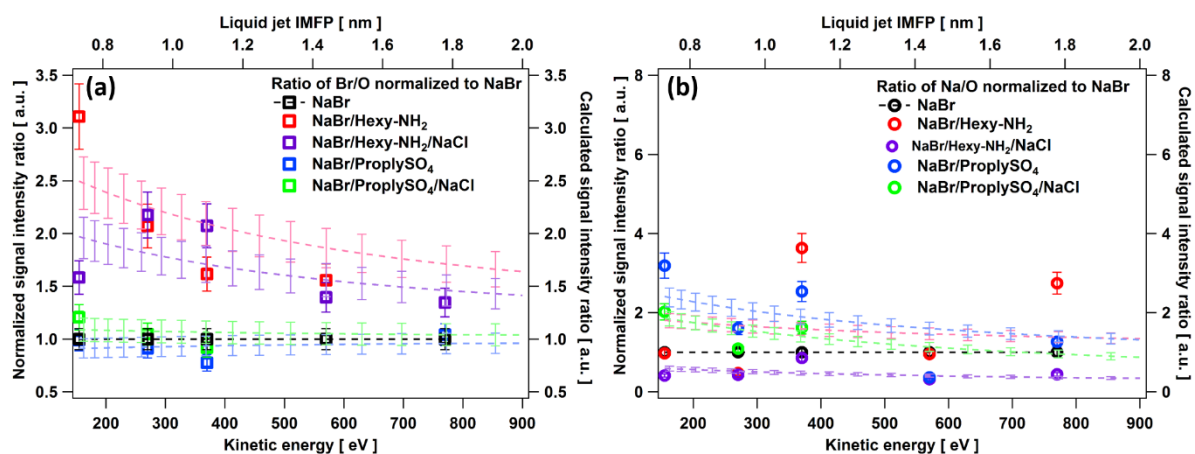


**Figure 2:** Relative intensity ratio of a) Br/O and b) Na/O of 0.1 M NaBr, mixed 0.1 M NaBr/0.1 M hexylamine, mixed 0.1 M NaBr/0.1 M hexylamine/0.55 M NaCl, mixed 0.1 M NaBr/0.1 M sodium propylsulfate and mixed 0.1 M NaBr/0.1 M sodium propylsulfate/0.55 M NaCl aqueous solutions as a function of electron kinetic energy, after normalized to the intensity ratio of 0.1 M NaBr, the photon flux, cross-section, and the total Na bulk concentration, respectively.

The Cl 2p spectra (Figure S1d) show a double-peak structure due to spin-orbit splitting into 2p<sub>3/2</sub> and 2p<sub>1/2</sub>. The chloride intensity is slightly higher in NaBr/propyl sulfate/NaCl compared with NaBr/hexyl-NH<sub>2</sub>/NaCl solutions, which is likely due to the higher bulk concentration of

Na<sup>+</sup>, as the propylsulfate was added as a sodium salt. Thus, the additional Na<sup>+</sup> attracts more Cl<sup>-</sup> into the interface.

For further interpretation of the analysis, we also applied a simple attenuation model developed previously [Lee *et al.*, 2019, Chen *et al.*, 2021] to fit calculated ratios to the measured ones. For the neat NaBr solution, this model features a layer near the surface of thickness  $\Delta$ , which exhibits a bromide (or sodium) concentration,  $n_{\text{Br},\Delta}$ , enhanced or reduced from that in bulk,  $n_{\text{Br},b}$ , by a factor  $f = f_0$ , such that  $n_{\text{Br},\Delta} = f_0 n_{\text{Br},b}$ , see Figure S3. This concentration can be related to the surface excess of bromide, as shown in Supporting Materials, Equation S1. Choosing  $\Delta = 1$  nm and  $f_0 = 0.55$  is equivalent to a negative surface excess of bromide of  $-2.6 \times 10^{12}$  cm<sup>-2</sup> consistent with measured surface tension. [Shah *et al.*, 2013] See also Supporting Materials, section III, and Table S1. This means that within this surface layer, the average concentration of bromide is about 50% of its bulk value, thus 0.05 M, or an effective surface concentration of  $3.3 \times 10^{12}$  ions cm<sup>-2</sup> (see Table S1). The depleted character at the surface of halide solutions is also in agreement with surface tension data, other liquid jet photoemission studies and also molecular dynamics simulations with revised force fields [Gladich *et al.*, 2020]. Using these parameters, the photoemission signal intensity for Br 3d can be calculated using Equation (S4). In turn, the density profile of H<sub>2</sub>O(l) is assumed to be constant up to the surface, with the O 1s signal intensity given by Equation S3. Taking the ratio of intensities (Equation S5) removes kinetic energy dependent measurement parameters.

In the presence of surfactants, this model is extended by a layer on top of the aqueous phase that contains the aliphatic portion of propylsulfate or hexylamine. In this work, we refrain from quantifying the effective thickness of this layer and relate it to the surface excess of these two surfactants as done in Lee *et al.* [Lee *et al.*, 2019] and Chen *et al.* [Chen *et al.*, 2021]. Instead, we assume that H<sub>2</sub>O(l), as well as Na<sup>+</sup> and Br<sup>-</sup> are residing below this layer. Therefore, Br 3d, Na 2s and O 1s photoelectrons are all attenuated by the same factor, and thus, the resulting Br/O, Na/O ratios are not depending on the thickness of this layer. Hence, in Equation (S7), the factor  $f$ , describing the enrichment or depletion of bromide (or sodium) just underneath the surfactant, now different from  $f_0$ , is the only variable for the fit to the experimental data. As mentioned above, to avoid further photon energy dependent calibrations, we report the Br/O and Na/O ratios for the surfactant containing solutions as a ratio to those for the neat NaBr solution. Equation (S8) was thus fitted to measured data in Figure 3 by varying  $f$ . The resulting values for  $f$  and the corresponding local concentrations of Br<sup>-</sup> and Na<sup>+</sup> within the depth  $\Delta$  below the surface are reported in Table S1.

In NaBr/hexylamine and NaBr/hexylamine/NaCl solutions, relative to pure NaBr, the Br signal intensity is enhanced (normalized ratio > 1) at all kinetic energies, and this enhancement decreases with kinetic energy from 155 eV to 770 eV. This indicates that the bromide interfacial intensity is enhanced at the liquid-vapor interface of the solutions in the presence of hexylamine. The interfacial concentration of Br<sup>-</sup> calculated from the Br/O photoemission intensity ratio is 0.19 M, which is a factor of 3 higher than in the case of the pure NaBr solution

(Table S1). This may be related to the electrostatic attraction between cation and anion for hexylammonium and bromide. However, as mentioned above, the protonated hexyl-NH<sub>3</sub><sup>+</sup> was only a minor fraction of hexylamine due to the absence of a neutralizing cation. Therefore, either the total abundance of hexylamine at the interface is large enough so that a small fraction of it being protonated is sufficient to cause the observed enhancement of bromide at the interface, or the hexylamine itself also has an attractive effect on the abundance of bromide.

When 0.55 M NaCl (representing roughly ocean water chloride concentration), is present together with 0.1 M NaBr and 0.1 M hexylamine, the interfacial concentration of Br<sup>-</sup> calculated from Br/O photoemission intensity ratio is 0.14 M, which is a factor of 2.5 higher compared with the pure NaBr Br intensity. This is the result of several effects coming together. Apart from the salting out of bromide in the presence of an excess of chloride, which has been reported before [Ghosal *et al.*, 2008] hexylamine seems to be less abundant at the interface in the presence of NaCl (see C 1s spectra in Figure S1). Finally, chloride may compete with bromide for ion-pairing with hexyl-NH<sub>3</sub><sup>+</sup> at the interface and explain the reduced bromide concentration compared to when just hexylamine is present.

In the presence of sodium propylsulfate, the Br intensity is exhibiting a marginal depletion over the whole range of kinetic energy compared with pure NaBr. The fits indicate an about 15% depletion of the interfacial bromide concentration. This shows that the negatively charged headgroup of propylsulfate has only a small impact on the depletion of bromide from the interface further than is already the case in the neat NaBr solution. In the presence of an additional 0.55 M NaCl, this small effect is even turned around, as then the interfacial bromide concentration is 15% higher. Again, as in the case of hexylamine the combination of salting out of bromide and the lower abundance of propylsulfate may explain this.

Figure 3b shows the kinetic energy dependence of the observed (symbols) and fitted (dashed lines) relative intensity ratio of Na/O of the same solutions and normalized in the same way. The only difference to the case of bromide in Figure 3a is that the data, in addition, was normalized to the total bulk concentration of Na<sup>+</sup>, since that was not the same in all solutions. The interfacial Na<sup>+</sup> concentrations were obtained from fits to the Na/O ratios equivalent to those of Br<sup>-</sup> and also listed in Table S1.

As apparent from Figure 1, the signal-to-noise ratio for the Na 2s peak is relatively poor, also at other kinetic energies, due to the low cross-section for this core level. Therefore, the data for the propyl sulfate solutions scatter substantially. Consequently, we remain very cautious with the results of the fitting procedure. On average, the interfacial Na<sup>+</sup> concentration tended about a factor of 2 higher based on the fit (Table S1) in the presence of hexylamine and about 40% lower when in addition 0.55 M NaCl was present. If hexylamine, as a neutral species, would be responsible for the attraction of part of the bromide anions to the interface, some Na<sup>+</sup> cations may follow them, thus explaining such an enhancement. In the presence of the 5 times higher NaCl concentration, the overall depletion of Na<sup>+</sup> from the interface would still dominate. In the presence of propylsulfate, the Na/O intensity ratio is clearly and significantly

higher than 1. The interfacial concentration of  $\text{Na}^+$  is around 3 times higher compared with pure NaBr, which indicates that the negatively charged propylsulfate attracts the positively charged  $\text{Na}^+$  into the interface due to electrostatic interactions. When 0.55 M NaCl is present together with NaBr and propylsulfate, the interfacial concentration of  $\text{Na}^+$  was around 2 times higher than in pure NaBr. The smaller enhancement, in this case, is likely related to the smaller amount of propylsulfate at the interface (Figure S1).

In extension and comparison to our previous study with tetrabutylammonium (TBA) (chapter 6), where Br 3d spectra are only reported at one fixed kinetic energy, we also performed additional measurements with TBA bromide solutions at the same kinetic energies as with hexylamine and propylsulfate discussed above. We also performed the same analysis and applied the attenuation model in the same way as for the other solutions of this work. The results are shown in the Supporting Materials, Table S1 and Figure S4. The TBA bromide solutions, with all TBA fully protonated, attracts more Br into the interface, leading to a 46 fold enhanced interfacial bromide concentration. Qualitatively, this also indicates that the enhancement of bromide for the hexylamine solutions observed here can not only be due to the small fraction of hexylammonium, but likely also due to hexylamine itself.

### 5.1.5 Conclusion

In this study, we use liquid jet X-ray photoelectron spectroscopy to assess the difference between a monofunctional surfactant with a positive headgroup (hexylammonium) and a negative headgroup (propylsulfate) on the abundance of bromide and sodium ions at the interface within the probe depth of XPS. The spectroscopic data were analyzed with the support of an attenuation model to obtain quantitative information about the enhancement or depletion of cations and anions at the interface. The positively charged nitrogen group (even only a few percent at the liquid-vapor interface) in hexylamine, along with its surface activity, is leading to the enhanced interfacial concentration of bromide, while the negatively charged sulfate group in propylsulfate is having only a small effect on the interfacial concentration of bromide. In turn, sodium cations showed a corresponding enhancement in the presence of propylsulfate and only minor changes in the presence of hexylamine. In the presence of additional sodium chloride, salting effects and competition for ion-pairing with the ionic surfactant in combination determine the abundance of bromide anions and sodium cations. In the presence of soluble surface-active organics, the charge of the headgroup has a substantial impact on the abundance of inorganic ions at the liquid-vapor interface. Thus, to some degree, this conceptual picture allows us to more generally predict how ionic surfactants are affecting the interfacial abundance of the prominent halide,  $\text{SO}_4^{2-}$ ,  $\text{NO}_3^-$ , anions and  $\text{NH}_4^+$  and other cations as a function of pH. However, other effects, such as ion-pairing and molecular interactions among the surfactants, complicate this picture.



## 5.2 Supplementary Information

### Section I. C 1s, N 1s, S 2p, and Cl 2p spectra taken at KE=155 eV

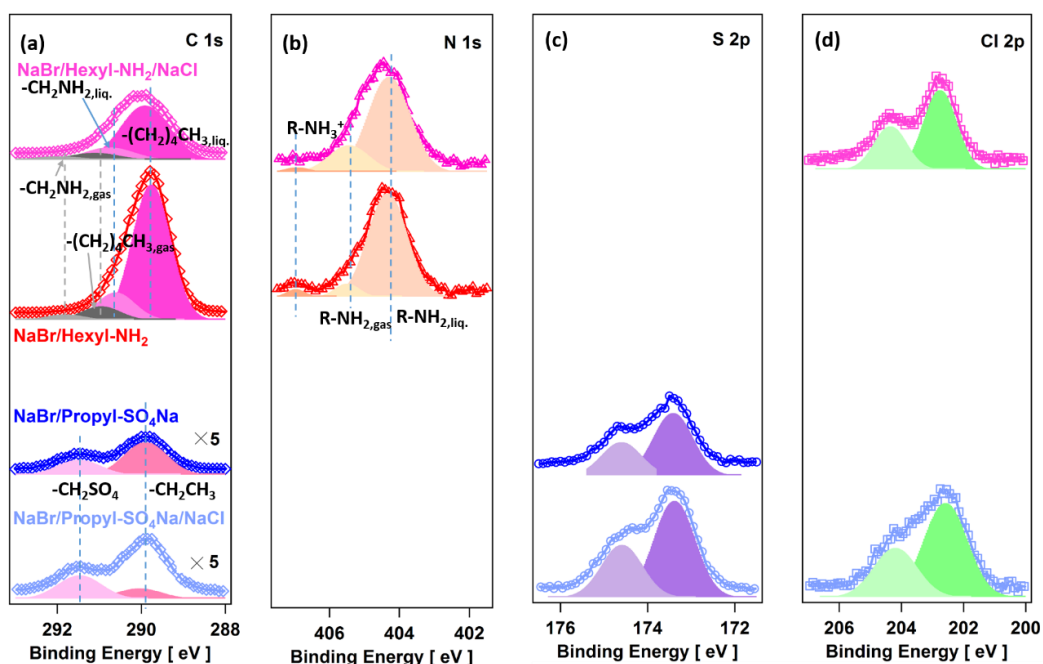


**Figure S1:** a) C 1s, b) N 1s, c) S 2p, and d) Cl 2p spectra of mixed 0.1 M NaBr/0.1 M hexylamine, mixed 0.1 M NaBr/0.1 M hexylamine/0.55 M NaCl, mixed 0.1 M NaBr/0.1 M sodium propylsulfate and mixed 0.1 M NaBr/0.1 M sodium propylsulfate/0.55 M NaCl aqueous solutions at kinetic energy at 155 eV.

Figure S1 shows the photoemission spectra of the C 1s (a), N 1s (b), S 2p (c) and Cl 2p (d) core level regions for mixed 0.1 M NaBr/0.1 M hexylamine (red), mixed 0.1 M NaBr/0.1 M hexylamine/0.55 M NaCl (pink), mixed 0.1 M NaBr/0.1 M sodium propylsulfate (light-blue) and mixed 0.1 M NaBr/0.1 M sodium propylsulfate/0.55 M NaCl (dark-blue) aqueous solutions, which were measured at photon energies of 448 eV for C 1s, 560 eV for N 1s, 330 eV for S 2p and 360 eV for Cl 2p to obtain the same kinetic energy of around 155 eV.

### Section II. N 1s spectra at different kinetic energies

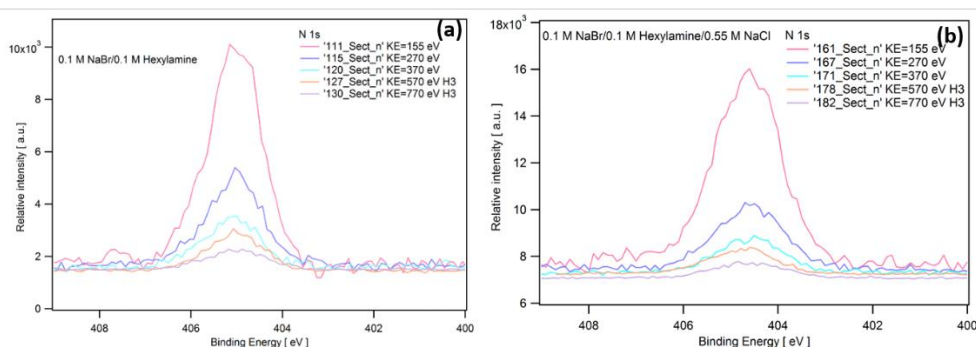


**Figure S2:** N 1s spectra of mixed 0.1 M NaBr/0.1 M hexylamine, mixed 0.1 M NaBr/0.1 M hexylamine/0.55 M NaCl aqueous solutions at kinetic energy from 155 eV to 770 eV.

### Section III. Calculation of photoemission signal intensity ratios based on the attenuation model

Its setup is represented by Figure S3 assumes that the interfacial region contains the organic surfactant, the concentration of which is constrained by surface tension measurements. In more detail, we assume that the aliphatic carbon chains reside above the side of the interface, within a layer of thickness  $d_1$ , and that the headgroup ( $-\text{NH}_2$  or  $-\text{SO}_4$ ) is residing just at the interface. We do not explicitly resolve that these headgroups, being likely hydrated, reside slightly below the water surface. We further consider a region of thickness  $\Delta$  within which the bromide concentration differs from that in the bulk aqueous phase, as in Lee et al. [Lee et al., 2019].

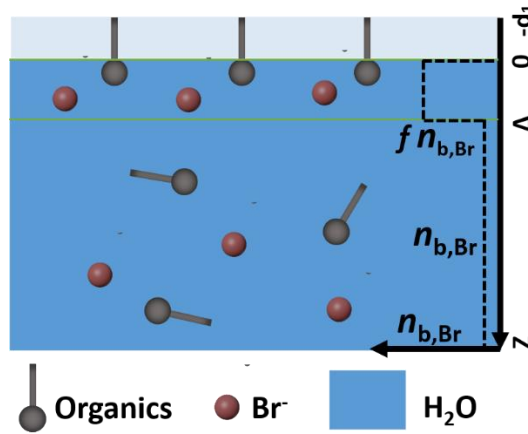


**Figure S3:** Scheme of the organic compounds covered interface used for the attenuation model. The reference level 0 for the depth scale ( $z$ ) is where the water density drops (assuming a rectangular profile). The top layer  $-d_1 < z < 0$  represents the layer containing the aliphatic carbon chain, while the layer following next, with thickness  $\Delta$ , represents the layer in which the concentration of bromide is deviating from its bulk value,  $n_{b,Br}$ , by the factor  $f$ . The bromide density profile is schematically depicted as the dashed line. Red and light grey spheres denote bromide ions and headgroup (in our case,  $-\text{NH}_2$  or  $-\text{SO}_4$ ) of organic compounds, respectively.

We simplify the task by assuming the aliphatic carbon atoms are assembled as in a liquid layer with the properties of a liquid alkane and that electron attenuation in that layer is equal to that in liquid water.  $\lambda_0$  is the inelastic mean free path for electrons in water [Shinotsuka et al., 2017]. We used  $\lambda = 2/\pi * \lambda_0$  to account for the liquid jet measurement configuration [Winter and Faubel, 2006].

We introduced an additional layer of thickness  $\Delta$ , just below the aliphatic carbon layer, starting at depth  $z = 0$ , within the aqueous solution. In this layer, the Br atom density is set different from that of the bulk density by a factor,  $f$ , i.e.,  $f n_{b,Br}$ , while the density of the organic is equal to that in the bulk.  $f$  is a function of the surface excess of the surfactant,  $\Gamma_{\text{hex}}$  or  $\Gamma_{\text{org}}$ . In the simple terms of this model and in the absence of organic  $f = f_0$  is related to the surface excess of the bromide ions,  $\Gamma_{\text{Br-}}$ , via:

$$\Gamma_{\text{Br-}} = n_{b,Br} \Delta (f_0 - 1) \quad f_0 = \frac{\Gamma_{\text{Br-}} - n_{b,Br} \Delta}{-n_{b,Br} \Delta} = \frac{\Gamma_{\text{Br-}}}{n_{b,Br} \Delta} + 1 \quad (\text{S1})$$

We calculate the photoemission signal contribution of O atoms, assumed to be homogeneously distributed over the bulk up to below the aliphatic carbon layer, which is not containing oxygen, completely analogously to C in the bulk:

$$I_{O1s, \text{bulk}} = A e^{-d1/\lambda} \int_0^{\infty} n_{b,O} e^{-(z)/\lambda} dz = A n_{b,O} \lambda e^{-d1/\lambda} \quad (S2)$$

If there is no organic surfactant on the solutions, d1 will be 0, then

$$I_{O1s, \text{bulk}} = A \int_0^{\infty} n_{b,O} e^{-(z)/\lambda} dz = A n_{b,O} \lambda \quad (S3)$$

And the Br photoemission signal intensity is then obtained as follows:

$$\begin{aligned} I_{Br-} &= B \left( \int_0^{\Delta} \left( \frac{\Gamma}{\Delta} + n_{b,Br-} \right) e^{-\frac{(z)}{\lambda}} dz + e^{-\frac{\Delta}{\lambda}} \int_{\Delta}^{\infty} n_{b,Br-} e^{-\frac{(z-\Delta)}{\lambda}} dz \right) \\ &= B \lambda \left( \frac{\Gamma}{\Delta} + n_{b,Br-} \right) \left( 1 - e^{-\frac{(z)}{\lambda}} \right) + B \lambda n_{b,Br-} e^{-\frac{\Delta}{\lambda}} \end{aligned} \quad (S4)$$

For 0.1 M NaBr and 0.1 M NaBr/0.55 M NaCl solutions, the Br 3d to O 1s signal intensity ratio is:

$$\frac{I_{Br-}}{I_{O1s}} = \frac{B \lambda \left( \frac{\Gamma}{\Delta} + n_{b,Br-} \right) \left( 1 - e^{-\frac{(z)}{\lambda}} \right) + B \lambda n_{b,Br-} e^{-\frac{\Delta}{\lambda}}}{A n_{b,O} \lambda} = \frac{B \left( \frac{\Gamma}{\Delta} + n_{b,Br-} \right) \left( 1 - e^{-\frac{(z)}{\lambda}} \right) + n_{b,Br-} e^{-\frac{\Delta}{\lambda}}}{A n_{b,O}} \quad (S5)$$

For pure 0.1 M NaBr solutions, the surface excess is  $-2.7 \times 10^{12}$  molecules per  $\text{cm}^{-2}$ , which was derived from surface tension data [Shah *et al.*, 2013]. We assume  $\Delta=1$  nm and calculate  $\frac{B}{A}$  value from the measured Br 3d to O 1s signal ratios of pure 0.1 M NaBr solutions, based on equation (S5), which we will get  $\frac{B}{A}$  equals to 12.027. Then we get the calculated Br/O intensity ratio as a basis for the normalized data shown in Figure 2.

If the organic surfactant is present in the solutions, the Br photoemission signal intensity is then obtained from the following integration:

$$\begin{aligned} I_{Br, \text{bulk}} &= B e^{-\frac{d1}{\lambda}} \left[ \int_0^{\Delta} f n_{b,Br} e^{-(z)/\lambda} dz + e^{-\frac{\Delta}{\lambda}} \int_{\Delta}^{\infty} n_{b,Br} e^{-(z-\Delta)/\lambda} dz \right] = \\ I_{Br, \text{bulk}} &= B e^{-\frac{d1}{\lambda}} \left[ f n_{b,Br} \lambda - f n_{b,Br} \lambda e^{-\Delta/\lambda} + n_{b,Br} \lambda e^{-\frac{\Delta}{\lambda}} \right] \\ I_{Br, \text{bulk}} &= B e^{-d1/\lambda} n_{b,Br} \lambda [f + e^{-\Delta/\lambda} (1 - f)] \end{aligned} \quad (S6)$$

Then, the Br 3d to O 1s signal intensity ratio is based on the ratio between equation S2 and equation S6:

$$\frac{I_{Br-}}{I_{O1s}} = \frac{B e^{-d1/\lambda} n_{b,Br} \lambda [f + e^{-\Delta/\lambda} (1 - f)]}{A n_{b,O} \lambda e^{-d1/\lambda}} = \frac{B n_{b,Br} [f + e^{-\Delta/\lambda} (1 - f)]}{A n_{b,O}} \quad (S7)$$

For pure NaBr solutions, we use equation S1 and assume  $\Delta=1$  nm, surface excess of  $-2.7 \times 10^{12}$  molecules per  $\text{cm}^{-2}$  for a 0.1 M NaBr solution, which is consistent with surface

tension data, [Shah *et al.*, 2013] we get  $f_0=0.55$ . Then we apply it to the Br 3d to O 1s signal intensity ratio normalized to 0.1 M NaBr solution:

$$\frac{\frac{I_{Br-,solutions}}{I_{O1s}}}{\frac{I_{Br-,NaBr}}{I_{O1s}}} = \frac{\frac{Bn_{b,Br}[f+e^{-\Delta/\lambda}(1-f)]}{An_{b,O}}}{\frac{Bn_{b,Br}[f_0+e^{-\Delta/\lambda}(1-f_0)]}{An_{b,O}}} = \frac{[f+e^{-\Delta/\lambda}(1-f)]}{f_0+e^{-\Delta/\lambda}(1-f_0)} \quad (S8)$$

We then calculate  $f$  from the measured Br 3d to O 1s signal ratios for the solutions, based on equation (S8), which is shown in table S1 below.

On the other hand, since the sodium concentration is also influenced by the top carbon layer of organic surfactant in the solutions, for the Na/O intensity ratio, we can use the same equation (equation S8) to then calculate  $f$  from the measured Na 2s to O 1s signal ratios for the solutions, for which the results are shown in Table S1 below.

Based on the  $f$  factor we get, we can have the relation between the measured and the calculated Br/O and Na/O intensity ratio for solutions varies with depth profile, shown in Figure 3 for different charged headgroup organic compounds and in Figure S5 for solutions in the presence of TBA-Br.

**Table S1:** Calculated interfacial concentrations of bromide and the driving parameters were obtained for different solutions for Br/O and Na/O cases. The error associated with the individual photoemission signal intensities is estimated at around  $\pm 10\%$ , which considers uncertainties due to the variability of the liquid-jet XPS experiment, the solution preparation, spectral fitting. Propagation leads to around 15% for elemental ratios and around 20% for the concentrations given. This does not include systematic errors related to the choice of the value for  $\Delta$  or other inherent assumptions of the attenuation model.

Solutions	$n_{\text{Br,b}}$ [M]	f value for Br/O	Standard error bar for f value	$n_{\text{Br},\Delta}$ [M]	$n_{\text{Br},\Delta\Delta}$ [ $10^{13}$ $\text{cm}^{-2}$ ]	$n_{\text{Na,b}}$ [M]	f value for Na/O	Standard error bar for f value	$n_{\text{Na},\Delta}$ [M]	$n_{\text{Na},\Delta\Delta}$ [ $10^{13}$ $\text{cm}^{-2}$ ]
0.1 M NaBr	0.1	0.55	/	0.055	0.33	0.1	0.55	/	0.055	0.33
0.1 M NaBr/0.1 M Hexylamine	0.1	1.89	0.27	0.189	1.14	0.1	1.27	0.78	0.127	0.76
0.1 M NaBr/0.1 M Hexylamine/0.55 M NaCl	0.1	1.42	0.20	0.142	0.85	0.65	3.10	0.81	0.310	1.86
0.1 M NaBr/0.1 M Propylsulfate	0.1	0.47	0.07	0.047	0.28	0.2	3.96	0.94	0.396	2.38
0.1 M NaBr/0.1 M Propylsulfate/0.55 M NaCl	0.1	0.63	0.08	0.063	0.38	0.75	12.20	1.82	1.22	7.32
0.1 M TBA-Br	0.1	25.44	1.74	2.54	15.24	/	/		/	/
0.1 M TBA-Br/0.55 M NaCl	0.1	12.46	0.42	1.25	7.50	/	/		/	/

#### Section IV. Ratio of Br/O normalized to NaBr of TBA-Br solutions

To better understand the influence of positively charged organic compounds, we also measured the Br 3d and O 1s spectra of the solutions in the presence of tetrabutylammonium (TBA) bromide. Figure S4 shows the observed (dot) and calculated (dash line) relative intensity ratio of Br/O of 0.1 M TBA-Br, mixed 0.1 M TBA-Br/0.55 M NaCl and 0.1 M NaBr aqueous solutions as a function of electron kinetic energy, after normalization to the Br/O intensity ratio of 0.1 M NaBr, the photon flux and cross-section, respectively. The Br/O intensity ratio is set to 1 for the whole range of kinetic energy.

Using  $f$ , we obtained the interfacial bromide concentration, which is enhanced by a factor of 46 compared to the pure NaBr solution. This takes into account the attenuation by TBA on

the surface. As mentioned above and suggested in earlier studies based on photoemission studies with TBA iodide, this enhancement is likely due to electrostatic interactions between bromide and the positively charged TBA, including the formation of ion pairs.

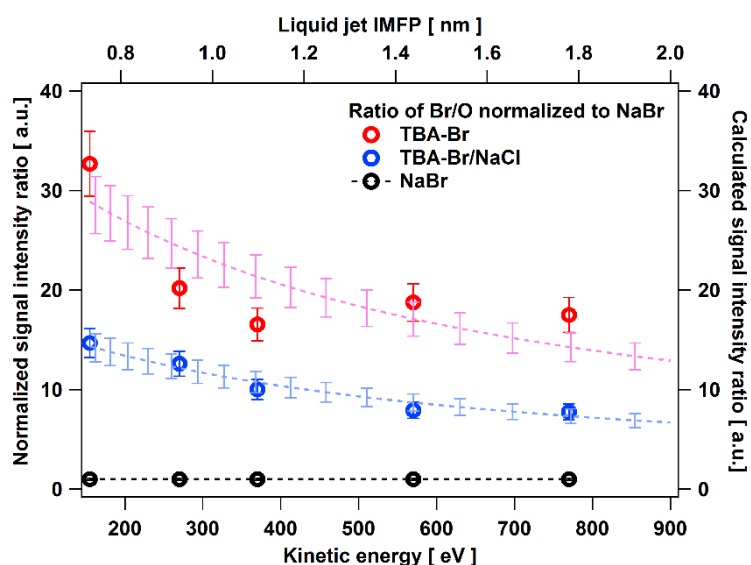


**Figure S4:** Relative intensity ratio of Br/O of 0.1 M TBA-Br, mixed 0.1 M TBA-Br/0.1 M NaBr, mixed 0.1 M TBA-Br/0.1 M NaBr/0.55 M NaCl, mixed 0.1 M TBA-Br/0.55 M NaCl, 0.1 M NaBr and mixed 0.1 M NaBr/0.55 M NaCl aqueous solutions as a function of electron kinetic energy, after normalization to the Br/O intensity ratio of 0.1 M NaBr, the photon flux and cross section, respectively.

When 0.55 M NaCl (representing roughly ocean water chloride concentration), is present together with 0.1 M NaBr, but in the absence of TBA, the interfacial concentration of  $\text{Br}^-$  is a factor of 22 higher than in the case of the pure NaBr solution. This apparent salting out of bromide in the presence of an excess of chloride has been reported before [Ghosal *et al.*, 2008], and it has not been the scope of the present study to explore this further. There are several effects that come together. Apart from the higher surface propensity of bromide due to chloride, TBA contributes salting out too. Besides, the chloride may also have a competition with bromide with TBA for ion-pairing at the interface.

---

## Bibliography

---

- Artiglia, L., J. Edebeli, F. Orlando, S. Chen, M.-T. Lee, P. Corral Arroyo, A. Gilgen, T. Bartels-Rausch, A. Kleibert, M. Vazdar, M. Andres Carignano, J. S. Francisco, P. B. Shepson, I. Gladich and M. Ammann (2017). "A surface-stabilized ozonide triggers bromide oxidation at the aqueous solution-vapour interface." *Nature Communications* 8(1): 700.
- Brown, M. A., I. Jordan, A. Beloqui Redondo, A. Kleibert, H. J. Wörner and J. A. van Bokhoven (2013). "In situ photoelectron spectroscopy at the liquid/nanoparticle interface." *Surface Science* 610: 1-6.
- Brown, M. A., A. B. Redondo, I. Jordan, N. Duyckaerts, M.-T. Lee, M. Ammann, F. Nolting, A. Kleibert, T. Huthwelker, J.-P. Mächler, M. Birrer, J. Honegger, R. Wetter, H. J. Wörner and J. A. van Bokhoven (2013). "A new endstation at the Swiss Light Source for ultraviolet photoelectron spectroscopy, X-ray photoelectron spectroscopy, and X-ray absorption spectroscopy measurements of liquid solutions." *Review of Scientific Instruments* 84(7): 073904.
- Chen, S., L. Artiglia, F. Orlando, J. Edebeli, X. Kong, H. Yang, A. Boucly, P. Corral Arroyo, N. Prisle, and M. Ammann (2021), Impact of Tetrabutylammonium on the Oxidation of Bromide by Ozone, *ACS Earth and Space Chemistry*, 5(11), 3008-3021, doi:10.1021/acsearthspacechem.1c00233.
- Ekholm, V., C. Coleman, N. Bjärnhall Prytz, M.-M. Walz, J. Werner, G. Öhrwall, J.-E. Rubensson and O. Björneholm (2018). "Strong enrichment of atmospherically relevant organic ions at the aqueous interface: the role of ion pairing and cooperative effects." *Physical Chemistry Chemical Physics* 20(42): 27185-27191.
- Ge, X., A. S. Wexler and S. L. Clegg (2011). "Atmospheric amines – Part I. A review." *Atmospheric Environment* 45(3): 524-546.
- Ghosal, S., M. A. Brown, H. Bluhm, M. J. Krisch, M. Salmeron, P. Jungwirth and J. C. Hemminger (2008). "Ion Partitioning at the Liquid/Vapor Interface of a Multicomponent Alkali Halide Solution: A Model for Aqueous Sea Salt Aerosols." *The Journal of Physical Chemistry A* 112(48): 12378-12384.
- Ghosal, S., J. C. Hemminger, H. Bluhm, B. S. Mun, E. L. D. Hebenstreit, G. Ketteler, D. F. Ogletree, F. G. Requejo and M. Salmeron (2005). "Electron Spectroscopy of Aqueous Solution Interfaces Reveals Surface Enhancement of Halides." *Science* 307(5709): 563-566.
- Gladich, I., S. Chen, M. Vazdar, A. Boucly, H. Yang, M. Ammann and L. Artiglia (2020). "Surface Propensity of Aqueous Atmospheric Bromine at the Liquid–Gas Interface." *The Journal of Physical Chemistry Letters* 11(9): 3422-3429.
- Hansen, A. M. K., J. Hong, T. Raatikainen, K. Kristensen, A. Ylisirniö, A. Virtanen, T. Petäjä, M. Glasius and N. L. Prisle (2015). "Hygroscopic properties and cloud condensation nuclei activation of limonene-derived organosulfates and their mixtures with ammonium sulfate." *Atmos. Chem. Phys.* 15(24): 14071-14089.
- Herrmann, H., T. Schaefer, A. Tilgner, S. A. Styler, C. Weller, M. Teich and T. Otto (2015). "Tropospheric Aqueous-Phase Chemistry: Kinetics, Mechanisms, and Its Coupling to a Changing Gas Phase." *Chemical Reviews* 115(10): 4259-4334.
- Hegglin, M. I., D. W. Fahey, M. McFarland, S. A. Montzka, and E. R. Nash (2015), Twenty Questions and Answers About the Ozone Layer: 2014 Update-Scientific Assessment of Ozone Depletion: 2014.
- Kurahashi, N., S. Karashima, Y. Tang, T. Horio, B. Abulimiti, Y.-I. Suzuki, Y. Ogi, M. Oura and T. Suzuki (2014). "Photoelectron spectroscopy of aqueous solutions: Streaming potentials of NaX (X = Cl, Br, and I) solutions and electron binding energies of liquid water and X<sup>-</sup>." *The Journal of Chemical Physics* 140(17): 174506.
- Lee, M.-T., M. A. Brown, S. Kato, A. Kleibert, A. Türlér and M. Ammann (2015). "Competition between Organics and Bromide at the Aqueous Solution–Air Interface as Seen from Ozone Uptake Kinetics and X-ray Photoelectron Spectroscopy." *The Journal of Physical Chemistry A* 119(19): 4600-4608.
- Lee, M.-T., F. Orlando, L. Artiglia, S. Chen and M. Ammann (2016). "Chemical Composition and Properties of the Liquid–Vapor Interface of Aqueous C1 to C4 Monofunctional Acid and Alcohol Solutions." *The Journal of Physical Chemistry A* 120(49): 9749-9758.

- Lee, M.-T., F. Orlando, M. Khabiri, M. Roeselová, M. A. Brown and M. Ammann (2019). "The opposing effect of butanol and butyric acid on the abundance of bromide and iodide at the aqueous solution–air interface." *Physical Chemistry Chemical Physics* 21(16): 8418-8427.
- McNeill, V. F. (2015). "Aqueous Organic Chemistry in the Atmosphere: Sources and Chemical Processing of Organic Aerosols." *Environmental Science & Technology* 49(3): 1237-1244.
- MUNGER, J. W., C. TILLER and M. R. HOFFMANN (1986). "Identification of Hydroxymethanesulfonate in Fog Water." *Science* 231(4735): 247-249.
- O'Dowd, C. D., M. C. Facchini, F. Cavalli, D. Ceburnis, M. Mircea, S. Decesari, S. Fuzzi, Y. J. Yoon and J.-P. Putaud (2004). "Biogenically driven organic contribution to marine aerosol." *Nature* 431(7009): 676-680.
- Perrin, D. D. (1965). *Dissociation constants of organic bases in aqueous solution*. London, Butterworths.
- Prather, K. A., T. H. Bertram, V. H. Grassian, G. B. Deane, M. D. Stokes, P. J. DeMott, L. I. Aluwihare, B. P. Palenik, F. Azam, J. H. Seinfeld, R. C. Moffet, M. J. Molina, C. D. Cappa, F. M. Geiger, G. C. Roberts, L. M. Russell, A. P. Ault, J. Baltrusaitis, D. B. Collins, C. E. Corrigan, L. A. Cuadra-Rodriguez, C. J. Ebben, S. D. Forestieri, T. L. Guasco, S. P. Hersey, M. J. Kim, W. F. Lambert, R. L. Modini, W. Mui, B. E. Pedler, M. J. Ruppel, O. S. Ryder, N. G. Schoepp, R. C. Sullivan and D. Zhao (2013). "Bringing the ocean into the laboratory to probe the chemical complexity of sea spray aerosol." *Proceedings of the National Academy of Sciences* 110(19): 7550-7555.
- Pruyne, J. G., M.-T. Lee, C. Fábri, A. Beloqui Redondo, A. Kleibert, M. Ammann, M. A. Brown and M. J. Krisch (2014). "Liquid–Vapor Interface of Formic Acid Solutions in Salt Water: A Comparison of Macroscopic Surface Tension and Microscopic in Situ X-ray Photoelectron Spectroscopy Measurements." *The Journal of Physical Chemistry C* 118(50): 29350-29360.
- Shah, A.-u.-H. A., K. Ali and S. Bilal (2013). "Surface tension, surface excess concentration, enthalpy and entropy of surface formation of aqueous salt solutions." *Colloids and Surfaces A: Physicochemical and Engineering Aspects* 417: 183-190.
- Shinotsuka, H., B. Da, S. Tanuma, H. Yoshikawa, C. J. Powell and D. R. Penn (2017). "Calculations of electron inelastic mean free paths. XI. Data for liquid water for energies from 50 eV to 30 keV." *Surface and Interface Analysis* 49(4): 238-252.
- van Pinxteren, M., K. W. Fomba, N. Triesch, C. Stolle, O. Wurl, E. Bahlmann, X. Gong, J. Voigtländer, H. Wex, T. B. Robinson, S. Barthel, S. Zeppenfeld, E. H. Hoffmann, M. Roveretto, C. Li, B. Grosselin, V. Daële, F. Senf, D. van Pinxteren, M. Manzi, N. Zabalegui, S. Frka, B. Gašparović, R. Pereira, T. Li, L. Wen, J. Li, C. Zhu, H. Chen, J. Chen, B. Fiedler, W. von Tümpling, K. A. Read, S. Punjabi, A. C. Lewis, J. R. Hopkins, L. J. Carpenter, I. Peeken, T. Rixen, D. Schulz-Bull, M. E. Monge, A. Mellouki, C. George, F. Stratmann and H. Herrmann (2020). "Marine organic matter in the remote environment of the Cape Verde islands – an introduction and overview to the MarParCloud campaign." *Atmos. Chem. Phys.* 20(11): 6921-6951.
- Wang, S., J. A. Schmidt, S. Baidar, S. Coburn, B. Dix, T. K. Koenig, E. Apel, D. Bowdalo, T. L. Campos, E. Eloranta, M. J. Evans, J. P. DiGangi, M. A. Zondlo, R.-S. Gao, J. A. Haggerty, S. R. Hall, R. S. Hornbrook, D. Jacob, B. Morley, B. Pierce, M. Reeves, P. Romashkin, A. ter Schure and R. Volkamer (2015). "Active and widespread halogen chemistry in the tropical and subtropical free troposphere." *Proceedings of the National Academy of Sciences* 112(30): 9281-9286.
- Winter, B. and M. Faubel (2006). "Photoemission from liquid aqueous solutions." *Chemical reviews* 106(4): 1176-1211.
- Winter, B., R. Weber, P. M. Schmidt, I. V. Hertel, M. Faubel, L. Vrbka and P. Jungwirth (2004). "Molecular Structure of Surface-Active Salt Solutions: Photoelectron Spectroscopy and Molecular Dynamics Simulations of Aqueous Tetrabutylammonium Iodide." *The Journal of Physical Chemistry B* 108(38): 14558-14564.



---

# Impact of Tetrabutylammonium on the Oxidation of Bromide by Ozone

---

Published as: Chen, S., Artiglia, L., Orlando, F., Edebeli, J., Kong, X., Yang, H., Boucly, A., Corral Arroyo, P., Prisle, N. and Ammann, M. Impact of Tetrabutylammonium on the Oxidation of Bromide by Ozone. *ACS Earth and Space Chemistry*, 5(11), pp.3008-3021, 2021.

## 6.1 Impact of Tetrabutylammonium on the Oxidation of Bromide by Ozone

### 6.1.1 Abstract

The reaction of ozone with sea-salt derived bromide is relevant for marine boundary layer atmospheric chemistry. The oxidation of bromide by ozone is enhanced at aqueous interfaces. Ocean surface water and sea spray aerosol are enriched in organic compounds, which may also have a significant effect on this reaction at the interface. Here we assess the surface propensity of cationic tetrabutylammonium at the aqueous liquid-vapor interface by liquid micro-jet X-ray photoelectron spectroscopy (XPS) and the effect of this surfactant on ozone uptake to aqueous bromide solutions. The results clearly indicate that the positively charged nitrogen group in TBA, along with its surface activity, is leading to an enhanced interfacial concentration of both bromide and the bromide ozonide reaction intermediate. In parallel, off-line kinetic experiments for the same system demonstrate a strongly enhanced ozone loss rate in the presence of TBA, which is attributed to an enhanced surface reaction rate. We used liquid jet XPS to obtain detailed chemical composition information from the aqueous solution-vapor interface of mixed aqueous solutions containing bromide or bromide and chloride with and without TBA surfactant. Core level spectra of Br 3d, C 1s, N 1s and O 1s

were used for this comparison. A model was developed to account for the attenuation of photoelectrons by the carbon-rich layer established by the TBA surfactant. We observed that the interfacial density of bromide is increased by an order of magnitude in solutions with TBA. The salting-out of TBA in the presence of 0.55 M sodium chloride is apparent. The increased interfacial bromide density can be rationalized by the association constants for bromide and chloride to form ion-pairs with TBA. Still, the interfacial reactivity is not increasing simply proportionally with the increasing interfacial bromide concentration in response to the presence of TBA. The steady-state concentration of the bromide ozonide intermediate increases by a smaller degree, and the lifetime of the intermediate is one order of magnitude longer in the presence of TBA. Thus, the influence of cationic surfactants on the reactivity of bromide depends on the details of the complex environment at the interface.

### 6.1.2 Introduction

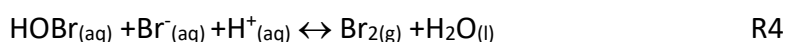
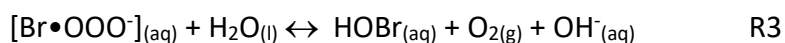
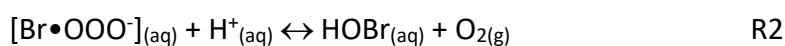
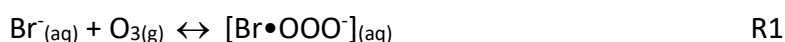
In atmospheric science, halogen chemistry and its impact on the ozone budget remains a hot topic [Abbatt *et al.*, 2012; Simpson *et al.*, 2015b; Sherwen *et al.*, 2017]. The halide solution-air interfaces associated with seawater and sea spray aerosol are especially important, because about 71% of the Earth's surface is covered by seawater that represents a substantial reservoir for chloride, bromide, and iodide. Multiphase reactions between gas-phase species and halides in seawater are centrally important because they lead to the activation of halogen species to the gas phase [Carpenter *et al.*, 2013; Wang *et al.*, 2015]. Cycling of these halogen species exerts a powerful influence on the chemical composition of the troposphere. It has been estimated that halogen chemistry contributes 50% of the chemical sink for tropospheric ozone globally [William R. Simpson *et al.*, 2015a]. It may affect the global oxidation capacity and the fate of pollutants, tropospheric ozone (including its radiative impact) and the production of particles [Carpenter *et al.*, 2013; Wang *et al.*, 2015]. Particle phase halogen species also contribute to ozone loss in the stratosphere [Koenig *et al.*, 2020].

The multiphase oxidation of bromide ( $\text{Br}^-$ ) by  $\text{O}_3$  is a significant dark source of hypobromic acid (HOBr) when shorter-lived photochemically produced radicals and oxidants are not abundant [Abbatt and Waschewsky, 1998; Simpson *et al.*, 2015]. These initial bromide oxidation processes are the starting point of the multiphase cycling reactions that lead to the release of bromine, thus bromine activation. Under the special circumstances of the spring-time polar marine boundary layer, bromine activation is a strong component of local and episodic  $\text{O}_3$  depletion [Simpson *et al.*, 2007].

Ocean surface water and sea spray aerosol often contain complex mixtures of organics deriving from marine biota with variable surface affinity and functionalities, such as proteins, carbohydrates, phospholipids and fatty acids [O'Dowd *et al.*, 2004; Prather *et al.*, 2013; Pinxteren *et al.*, 2020]. Surface active organics may affect multiphase chemical reactions by changing the interfacial activity of the halide ions or of reaction intermediates [Mata *et al.*, 2004; Cochran *et al.*, 2017], or actively engage in chemistry and photochemistry [Ciuraru *et*

*al.*, 2015; *Alpert et al.*, 2017]. Such effects have not been sufficiently elucidated, mostly because of the lack of studies selectively probing the interfacial region and processes thereon.

The kinetics of multiphase reactions initiated by gas-phase oxidants are described by the uptake coefficient,  $\gamma$ , defined as the ratio of the net flux of molecules from the gas phase to the condensed phase divided by the gas-kinetic collision flux of the molecules to the surface of the condensed phase [*Ammann et al.*, 2013]. The multiphase reaction of O<sub>3</sub> with Br<sup>-</sup> ions to HOBr has been studied for two decades and suggested to be enhanced at the aqueous solution-air interface [*Artiglia et al.*, 2017; *Clifford and Donaldson*, 2007; *Edebeli et al.*, 2019; *Hunt et al.*, 2004b; *Jung et al.*, 2017; *Moreno and Baeza-Romero*, 2019; *Oldridge and Abbatt*, 2011; *Oum et al.*, 1998; *Sakamoto et al.*, 2018]. In aqueous solution, Liu et al. [*Liu et al.*, 2001] suggested that the mechanism involves a bromide ozonide as an intermediate (R1), which then decomposes into molecular oxygen (R2, R3) and HOBr in an acid assisted step. HOBr then reacts further with Br<sup>-</sup>, again in an acid-catalyzed reaction, to form Br<sub>2</sub> (R4). Nevertheless, the reason for the surface-enhanced reactivity had remained elusive.



The traditional approach to studying the chemical composition at the aqueous solution–air interface through the contribution of constituents to the surface free energy is via recording the surface tension as a function of solute concentration [*Donaldson and Anderson*, 1999]. However, this is not straightforward for complex solutions because the synergistic effects and their composition dependence make it extremely difficult to assign concentration dependent contributions to the surface tension for individual components in solution. Both chemical composition and processes at interfaces can be characterized by X-ray Photoelectron Spectroscopy (XPS), which provides both chemical selectivity and surface sensitivity. [*Ammann et al.*, 2018] Liquid jet XPS directly provides the composition of inorganic and organic compounds at the aqueous solution-vapor interface within the top-most molecular layers of the liquid [*Lee et al.*, 2015; *Lee et al.*, 2019; *Öhrwall et al.*, 2015; *Prisle et al.*, 2012]. Using this technique, supporting theoretical calculation and additional kinetic experiments, Artiglia et al. [*Artiglia et al.*, 2017] reported direct experimental evidence for the ozonide in R1 and found it to exhibit a high propensity for the liquid-vapor interface. This surface-active intermediate turned out to cause the surface-enhanced reaction rate rather than the debated abundance of bromide itself at the interface [*Gladich et al.*, 2020].

In an attempt to address the impact of organics on the oxidation of bromide by O<sub>3</sub>, Lee et al. [*Lee et al.*, 2015] recently studied the reaction of bromide with ozone in the presence and absence of citric acid, a proxy for highly functionalized organic compounds in the atmosphere, under ambient conditions. With citric acid, the uptake kinetics of O<sub>3</sub> was faster than that

predicted by bulk reaction-limited uptake and faster than expected based on an acid-catalyzed mechanism. Parallel liquid-jet XPS revealed that bromide became depleted by around 30% within the probe depth of the experiment of around one nm. In 2019, Lee et al. [Lee et al., 2019] found an opposite effect of butanol and butyric acid on the abundance of bromide and iodide at the liquid-vapor interface. In comparison to the pure aqueous halide solution, 1-butanol increased the interfacial density of bromide by 25%, while butyric acid reduced it by 40%, respectively, which is probably controlled by a subtle interplay of electrostatic, dipole and hydrogen bonding interactions. Therefore, looking at the effects of surfactant co-solutes with different properties is an important task for better constraining the interfacial reactivity of halides under environmental conditions.

Tetrabutylammonium (TBA) may be considered as a proxy for atmospherically relevant organic amines and other cationic surfactants deriving from oceanic biogenic material [Ge et al., 2011; Pinxteren et al., 2020]. Its amphiphilic character with aliphatic side chains makes it strongly surface-active in an aqueous solution. Based on surface tension measurements, TBA bromide is expected to exhibit a surface excess of  $\sim 3.0 \times 10^{14}$  molecules per  $\text{cm}^2$  at 0.1 M [Mata et al., 2004]. TBA also exhibits strong ion-pairing capacity, which makes TBA ions important in various areas of chemistry, e.g., in phase-transfer catalysis, where relatively hydrophobic cations are used for precipitating large anions [Ohtani et al., 2004]. Several studies have addressed the interfacial properties of TBA-containing iodide solutions (including mixtures with bromide) with VUV photoemission [Karashima and Suzuki, 2019; Watanabe et al., 1998; Winter et al., 2005; Winter et al., 2004]. Also, molecular beam scattering experiments of  $\text{N}_2\text{O}_5$  interacting with a liquid jet containing tetraalkylammonium surfactants indicated interactions between the positively charged surfactant and reactants or products, also depending on the solvent [Shaloski et al., 2017; Sobyra et al., 2019]. Therefore, the details of charged surfactant ions affect the halide ions, their reactivity and potentially reaction products have remained open.

In this work, we used liquid-jet XPS to directly assess the impact of TBA on the abundance of bromide and the bromide ozonide at the aqueous solution – air interface and to compare the spectroscopic information with the results of  $\text{O}_3$  uptake kinetic experiments performed in parallel.

### 6.1.3 Experimental method

#### Materials

This study was conducted using sodium bromide (NaBr, Sigma Aldrich, > 99.0%), sodium chloride (NaCl, Sigma Aldrich, > 99.0%), tetrabutylammonium bromide (TBA-Br, Sigma Aldrich, > 99.0%) without further purification. Sample solutions were prepared by adding stock solutions to Milli-Q water (Millipore, 18.2 M $\Omega$  cm at 25 °C). 0.1 M NaBr, 0.1 M NaBr /0.55 M NaCl, 0.1 M TBA-Br, 0.1 M TBA-Br/0.55 M NaCl, and 0.1 M TBA-Br/0.1 M NaBr/0.55 M NaCl aqueous solutions were prepared for liquid jet XPS and kinetic experiments.

## Liquid microjet X-ray photoelectron spectroscopy (XPS)

XPS experiments using a liquid micro-jet were conducted at the Surfaces/Interfaces: Microscopy (SIM) beamline of the Swiss Light Source (SLS) [Flechsigt et al., 2010] using the near ambient pressure photoemission (NAPP) endstation [Brown et al., 2013; Flechsigt et al., 2010]. The electron analyzer uses a three-stage differentially pumped electrostatic lens system (Scienta HiPP-2) and a hemispherical analyzer (Scienta R4000) to collect photoelectrons from samples in chamber pressures up to a few mbar. For the present experiments, a quartz nozzle (MicroLiquids), forming a liquid microjet with a diameter of 25  $\mu\text{m}$ , was used to deliver a liquid sample into the analysis chamber.

The liquid jet was operated with a flow rate of 0.5 ml/min. The capillary transporting the liquid was immersed in a cooling bath set to 277 K upstream of the feedthrough into the chamber. The characterization of aqueous solutions, without gas dosing, was performed in vacuum ( $1.0 \times 10^{-3}$  to  $1.0 \times 10^{-4}$  mbar). The diameter of the entrance orifice of the electron sampling aperture into the pre lens and the working distance to the liquid jet were both 500  $\mu\text{m}$ . The electron analyzer was operated at 20 eV pass energy (photoelectron kinetic energy at 155 eV) and 50 eV pass energy (photoelectron kinetic energy at 370 eV) with a 0.1 eV step size. The liquid filament position was adjusted to spatially overlap with the 100  $\mu\text{m}$  (vertical) by 60  $\mu\text{m}$  (horizontal) synchrotron light beam [Flechsigt et al., 2010]. Optimum alignment was achieved by monitoring the condensed phase O 1s at 900 eV photon energy.

For experiments, in which the liquid jet was exposed to gas phase  $\text{O}_3$ , we used a gas delivery system, which has been described in our previous work [Artiglia et al., 2017]. In brief, a second gas nozzle was fixed concentrically around the quartz nozzle delivering the liquid. The second gas nozzle reaches about 0.1 mm beyond the liquid jet nozzle. The gas starts to interact with the liquid wire from the end of the quartz nozzle delivering the liquid jet before expansion into the vacuum chamber at the end of the second nozzle. The admitted gas was either pure oxygen or a mixture of up to a few % of ozone in oxygen. Before dosing the gas, the pressure in the experimental chamber was raised to  $1 \times 10^{-3}$  mbar (with the turbo molecular pump stopped and a  $\text{SiN}_x$  window mounted between the X-ray beamline and the liquid jet chamber). While dosing the gas, the pressure was set to 0.25 mbar by means of a leak valve, connected to the gas nozzle via a 1/16" PEEK tube, leading to a gas flow rate of around 15 sccm/min. Ozone was generated online by means of a home-built corona discharge ozone generator. We varied the ozone concentration by changing the flow rate of  $\text{O}_2$  through the corona discharge unit in the range of 2 – 12 ml/min. The corresponding change in the dilution ratio (around 1:7000) was taken into account for the ozone concentration calibration. The mixing ratio of  $\text{O}_3$  in  $\text{O}_2$  in the gas admitted to the experimental chamber was in the range of 1% to 3%. The efficiency of  $\text{O}_2$  to  $\text{O}_3$  conversion in the ozone generator was checked in separate experiments by means of the same ozone analyzer as described further below for the kinetics experiments. The gas composition in the analysis chamber with respect to the major components  $\text{N}_2$ ,  $\text{O}_2$ ,  $\text{H}_2\text{O}$  and  $\text{CO}_2$  was checked by means of a quadrupole mass spectrometer installed in the second differential pumping stage of the electron analyzer.

Core level spectra of Br 3d, N 1s, C 1s, Cl 2p and O 1s were acquired at photon energies allowing photoelectron kinetic energies at 155 eV and 370 eV. Due to the high photon flux at the SIM beamline, using 1<sup>st</sup> order light to ionize the O 1s orbital of solutions would lead to potentially damaging count rates at the detector. We, therefore, made use of the around 10% of photon flux associated with 2<sup>nd</sup> order light, which simultaneously passes the monochromator, to ionize the O 1s orbital. Thus, the monochromator was set to 348 eV and 450 eV to obtain O 1s spectra with excitation energies of 696 eV and 900 eV for a KE of 155 eV and 370 eV, respectively.

Reported binding energies are relative to the vacuum level and calibrated to the O 1b<sub>1</sub> orbital of liquid water at 11.31 eV [Winter *et al.*, 2004]. Exemplary valence spectra are shown in the SI, Figure S1. The total photoionization cross-section ( $\sigma_{tot}$ ) was calculated by considering cross-sections ( $\sigma$ ) and asymmetry parameters ( $\beta$ ) as follows [Ottosson *et al.*, 2010; Yeh and Lindau, 1985]:

$$\sigma_{tot} = \frac{\sigma}{4\pi} (1 + \beta) \quad (1)$$

Core level spectra were fit using pure Gaussian functions following standard linear background subtraction, except for the Br 3d spectra related to the experiments with O<sub>3</sub>, where a Shirley background was subtracted. For C 1s, the full width at half maximum (FWHM) of the peaks was constrained to the same value for the peaks contributed by the carbon atoms attached to the ammonium ion and the butyl chain carbons. The spin-orbit split (SOS) for Br 3d was fixed at 1.03 eV for both bromide in pure NaBr solutions, and the bromide ozonide was also present when dosing O<sub>3</sub> [Artiglia *et al.*, 2017]. We forced the FWHM at the same value for the spin-orbit split peaks of Br 3d (3d<sub>3/2</sub>, 3d<sub>5/2</sub>) of bromide and Cl 2p (2p<sub>1/2</sub>, 2p<sub>3/2</sub>) of chloride, respectively, 1.03 eV. The FWHM of the Br 3d peaks of bromide ozonide was 1.05 eV. The chemical shift between bromide and bromide ozonide was +0.70 eV [Artiglia *et al.*, 2017].

#### **Flow reactor:**

Kinetic experiments were conducted in a flow reactor setup previously described by Lee *et al.* [Lee *et al.*, 2015] and Artiglia *et al.* [Artiglia *et al.*, 2017]. Briefly, the setup comprises of a temperature regulated Teflon trough (surface area = 102 cm<sup>2</sup>) on which 15 ml of the reactive solution is loaded uniformly. The trough was kept at 4°C for all experiments. Ozone was generated by 185 nm photolysis of O<sub>2</sub> at different light intensities in a quartz cell at a flow rate of 400 ml/min O<sub>2</sub>, then mixed with 2000 ml/min N<sub>2</sub> (all flow rates given for 1 atm and 0°C). Part of this gas flow (980 ml/min) was humidified to the saturation water vapour pressure at the temperature of the trough before admission to the trough. The gas flow was alternated between a bypass to measure the initial O<sub>3</sub> concentration and the trough to measure the O<sub>3</sub> concentration remaining after reactive uptake by the solution. The O<sub>3</sub> concentration was measured using a commercial ozone monitor (Teledyne API model 400).

After about 1 h of stabilizing the background O<sub>3</sub> concentration measured while the gas flow was bypassing the flow reactor, the gas flow was switched to the trough reactor (solid arrow), which led to the exposure of the film to O<sub>3</sub> allowing the multiphase reactions to take place. Finally, the concentration after the reactor was measured in by-pass mode again to confirm that the background did not change during the experiment. The uptake coefficient of O<sub>3</sub>,  $\gamma$ , is equal to the rate of O<sub>3</sub> loss to the aqueous phase divided by the gas kinetic collision rate (Equation 2). The fractional loss of O<sub>3</sub> was obtained from the average ozone concentration through the bypass ([O<sub>3</sub>]<sub>bypass</sub>) line measured before and after exposing the trough, and while the gas passed through the flow tube ([O<sub>3</sub>]<sub>flow tube</sub>) for each cycle [Lee *et al.*, 2015].

$$\gamma = \frac{4\varphi \times \left[ \ln \left( \frac{[\text{O}_3]_{\text{bypass}}}{[\text{O}_3]_{\text{flow tube}}} \right) \right]}{\omega_{\text{O}_3} \times SA} \quad (2)$$

$$\omega_{\text{O}_3} = \sqrt{\frac{8RT}{\pi M_{\text{O}_3}}} \quad (3)$$

Where  $\varphi$  is the flow rate of O<sub>3</sub> through the flow tube (980 ml/min);  $\omega_{\text{O}_3}$  is the mean thermal velocity of O<sub>3</sub> in the gaseous phase, cm/s; SA is the exposed internal surface area of the tube;  $M_{\text{O}_3}$  is the molecular weight of O<sub>3</sub>.

The average O<sub>3</sub> uptake coefficient of the three cycles between the bypass and the flow tube per replicate is taken as the mean uptake coefficient for the experiment. We note that for the low uptake rates observed in this work, gas phase diffusion was not limiting O<sub>3</sub> loss, and the observed  $\gamma$  was used without further correction. The uptake coefficient was measured as a function of the partial pressure of O<sub>3</sub> in the gas phase. This allows disentangling the contributions by the bulk aqueous phase reaction in the reacto-diffusive regime and the surface reaction [Lee *et al.*, 2015; Oldridge and Abbatt, 2011] as described in more detail in the SI.

#### 6.1.4 Results and discussion

Figures 1a and 1b show O 1s and Br 3d photoelectron spectra, respectively, of 0.1 M NaBr, and 0.1 M TBA-Br aqueous solutions at a photon energy of 900 eV (2<sup>nd</sup> order light) and 450 eV, respectively. The O 1s region in Figure 1a is fitted by two components that are assigned to gas phase water at ca. 541 eV binding energy and liquid water at ca. 539 eV binding energy. The chemical shift between O 1s of liquid and gas-phase water differs from NaBr and TBA-Br solutions. This is also apparent in the valence spectra shown in Figure S1, which were used to align the binding energy scale with the O 1b<sub>1</sub> level of liquid water. This shift may be due to different surface potentials, and a similar effect has been observed for different solutions in our previous work [Lee *et al.*, 2019]. The substantial photoemission intensity from gas-phase water is related to the beam width of 60  $\mu\text{m}$  is larger than the liquid filament diameter of 25  $\mu\text{m}$ , so that photoelectrons from excitations in the gas phase surrounding the liquid are also collected. The Br 3d spectrum (Figure 1b) exhibits a double-peak structure due to spin-orbit splitting into 3d<sub>5/2</sub> and 3d<sub>3/2</sub>. TBA-Br is expected to show a surface excess of  $\sim 3 \times 10^{14}$  molecule per cm<sup>2</sup> at 0.1 M [Mata *et al.*, 2004].

It becomes already apparent from the spectra shown in Figure 1b that the Br 3d signal intensity is much larger in TBA bromide solutions than in pure NaBr solutions. This is likely related to the positive surface excess of TBA and to either ion-pairing or longer range electrostatic interaction with the positively charged TBA. This way, more Br<sup>-</sup> ions are attracted into the liquid-vapor interface than in the neat NaBr solution with the same bromide bulk concentration. The surface activity of TBA, resulting in a carbon-rich layer at the interface, leads to attenuation of both Br 3d and O 1s photoemission signals, which is directly apparent for the O1s signal of liquid water and which will be quantitatively analyzed together with the C 1s spectra further below. The gas-phase signals in Figure 1a remained the same, and provided that the liquid jet position was stable, this indicates that the evaporation of H<sub>2</sub>O from the liquid was not strongly affected by the presence of TBA.

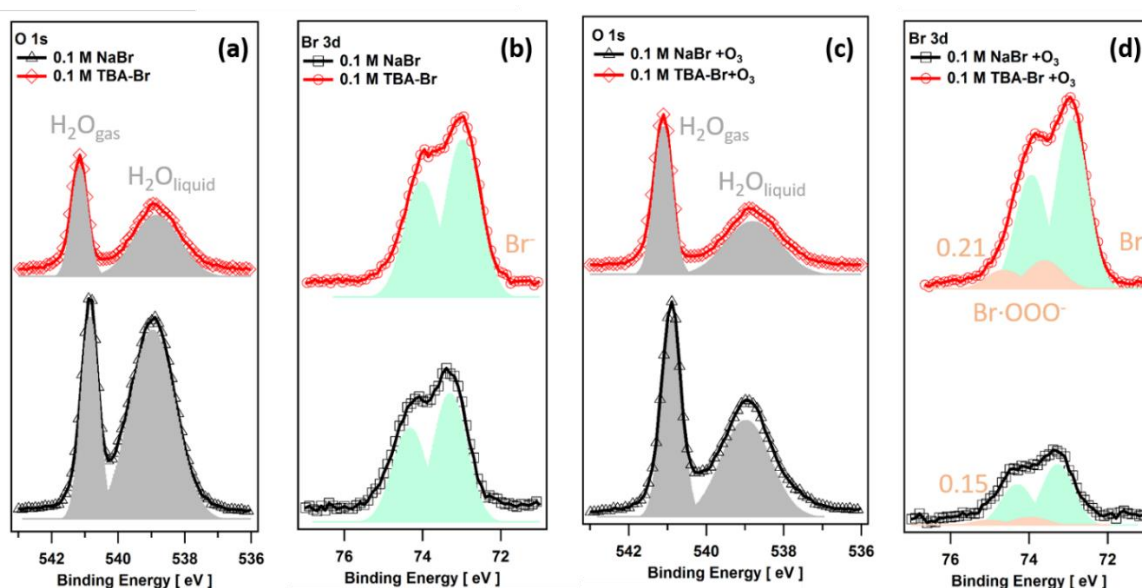


**Figure 1:** a) O 1s and b) Br 3d photoelectron spectra of 0.1 M TBA-Br and 0.1 M NaBr aqueous solutions at a photon energy of 900 eV and 450 eV, respectively; c) O 1s and d) Br 3d photoelectron spectrum of 0.1 M TBA-Br and 0.1 M NaBr aqueous solutions in the presence of O<sub>3</sub>, at a photon energy of 900 eV and 450 eV, respectively.

The same O 1s (Figure 1c) and Br 3d (Figure 1d) spectra were taken in presence of O<sub>3</sub> / O<sub>2</sub> to probe the bromide ozonide (intermediate in the reaction to hypobromite) at the same information depth. The relatively larger contribution of gas-phase water compared to the experiments without gas dosing is due to the presence of gas-phase oxygen (0.25 mbar), which leads to higher local water vapor concentration around the liquid filament due to diffusion limitation. The higher pressure also leads to more attenuation of the O 1s signal from condensed phase water. Note that the O 1s peak related to gas-phase oxygen is at a binding energy of about 7 eV higher than that of gas-phase water (see Figure S2), thus outside the binding energy range shown in Figure 1c.

In Figure 1d, both Br species show two spin-orbit split doublets, which are assigned to Br<sup>-</sup> and the [Br·OOO]<sup>-</sup> intermediate. The doublet assigned to the [Br·OOO]<sup>-</sup> intermediate is positively shifted by 0.7 eV with respect to Br<sup>-</sup>, in line with the previous study by Artiglia et al. [Artiglia et al., 2017]. In a vacuum, the Br 3d signal intensity was larger in TBA bromide



containing solutions than in pure NaBr solutions. In the presence of  $O_2/O_3$ , the ratio between the two is even larger. Note that even though the ratio of the signal intensity contributed by the  $[Br\cdot OOO]^-$  intermediate to that contributed by the  $Br^-$  species is somewhat similar in presence and absence of TBA-Br,  $0.21\pm 0.04$  and  $0.15\pm 0.03$ , respectively, concentration and stability of the intermediate are different in the presence of TBA, as discussed in detail in the second part.

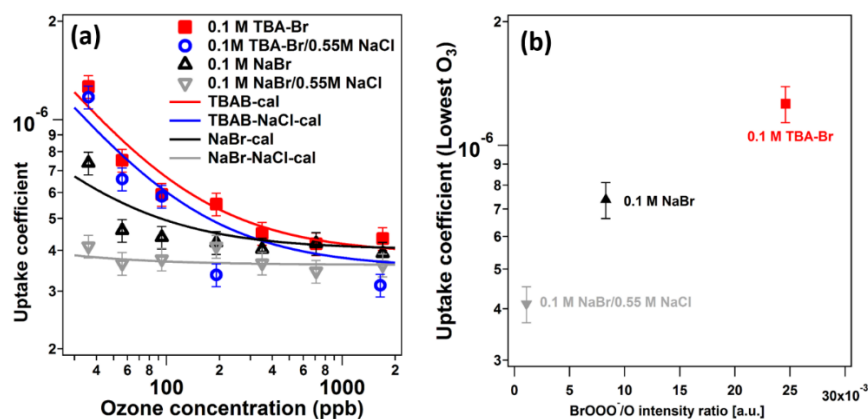


**Figure 2:** Measured and parameterized uptake coefficients of  $O_3$  as a function of gas phase  $O_3$  concentration for 0.1 M NaBr (black), 0.1 M NaBr/0.55 M NaCl (grey), 0.1 M TBA-Br (red), 0.1 M TBA-Br/0.55 M NaCl (dark-blue) in the aqueous solutions; b) uptake coefficient of  $O_3$  at 36 ppb compared with measured  $[Br\cdot OOO]^-/O$  intensity ratio for three different aqueous solutions.

Figure 2a) shows the measured and parameterized uptake coefficients of  $O_3$  as a function of gas phase  $O_3$  concentration for aqueous solutions containing 0.1 M NaBr (black), 0.1 M NaBr/0.55 M NaCl (grey), 0.1 M TBA-Br (red), 0.1 M TBA-Br/0.55 M NaCl (dark-blue), which directly demonstrate the obvious enhancement of reactivity for the TBA containing solutions at low  $O_3$  mixing ratios. Lines fit with a kinetic model consisting of a combination of a Langmuir-Hinshelwood type surface reaction and a reaction-diffusion mechanism in the bulk phase based on our previous study [Artiglia *et al.*, 2017] as described in the Supporting Materials, Section VIII. At high ozone concentrations (above 200 ppb), uptake coefficients are constant, whereas uptake coefficients increase towards the lower atmospherically relevant ozone mixing ratios (between 100 and 30 ppb). In previous studies [Artiglia *et al.*, 2017; Oldridge and Abbatt, 2011], this behavior has been attributed to a surface reaction dominating low ozone concentration. It results from the fact that the surface coverage of  $O_3$  is saturating at a higher concentration, which leads to the surface reaction rate saturating with higher ozone concentration, as described by Equation S21 in the SI.

In contrast, the bulk phase concentration of  $O_3$  scales linearly with the gas phase partial pressure (Henry's law) in the relevant concentration range, which leads to the bulk reaction rate remaining independent of the ozone concentration in the gas phase (Equation S22 in the SI). In a recent study with a similar reactor of comparable geometry, it has been suggested that liquid phase diffusion may limit the uptake coefficient [Schneider *et al.*, 2020]. As also explained in the SI, bulk diffusion limitation of bromide can be excluded under the present conditions. The measured ozone uptake coefficients in the absence of TBA are consistent with

previous studies from our group [Artiglia *et al.*, 2017] and the work by Oldridge and Abbatt. [Oldridge and Abbatt, 2011]. The slight difference between the pure NaBr and the mixed NaBr/NaCl solutions at high ozone concentration is explained by the 10% lower solubility of  $O_3$  due to salting out by the 0.55 M NaCl and the slight difference in diffusivity caused by a small change in viscosity. Both are included in the parameterization for the uptake coefficient (see Supporting Materials, section VIII). In the presence of TBA, the ozone uptake coefficient is higher than on the pure NaBr and NaBr/NaCl mixed solutions at low ozone concentration, whereas they tend to be similar to the systems without TBA at higher ozone concentrations, indicating the surface reaction contribution is more strongly affected by the presence of TBA than the bulk reaction. The relatively small difference between ozone uptake in solutions with and without TBA at high ozone concentration could be explained by 11.5% larger viscosity and 1.5% larger solubility of  $O_3$  in TBA-Br solutions compared with pure NaBr. In presence of TBA, the effect of 0.55 M NaCl is also seen, especially at high ozone concentration, which is due to both the higher viscosity (11.5% higher) and the lower solubility of  $O_3$  (7.8% lower) compared with pure NaBr. For the bulk reaction, the parameterization for the uptake coefficient is based solely on known parameters (solubility, rate coefficient, diffusivity) without any additional adjustable parameters. For the loss rate on the surface, as described in the Supporting Materials (section VIII), the essential parameters are the equilibrium constant for the formation of the intermediate ( $K_{Lang}$  in Equation S21), the maximum surface coverage of the intermediate ( $N_{max}$ ) and the first-order decay rate coefficient ( $k_s$ ) for the formation of the product  $BrO^-$ . Whereas the value for  $K_{Lang}$  was taken from Artiglia *et al.* [Artiglia *et al.*, 2017], which was also consistent with Oldridge and Abbatt [Oldridge and Abbatt, 2011], the maximum surface coverage was constrained by the XPS data (as described further below), and the rate coefficient was the only adjustable parameter used to fit the data, leading to very good fits for each solution, as shown in Figure 2a.

The strikingly parallel behavior of the enhancement of the surface contribution of the uptake coefficient in the presence of TBA and that of the increased presence of both bromide and the reaction intermediate, as determined by XPS, supports the hypothesis that the positively charged ammonium group in TBA helps to attract  $Br^-$  ions to the interface and establishes an enhanced surface concentration of the  $[Br\cdot OOO]^-$  intermediate limiting the reaction rate. Sobyra *et al.* [Sobyra *et al.*, 2019] have studied the production of  $Br_2$  from the reaction of  $N_2O_5$  with  $Br^-$  in TBA-Br solutions. They found a reduction of  $Br_2$  formation in the presence of TBA and attributed that to ion-pairing of  $TBA^+$  with  $Br_3^-$  at the liquid-vapor interface. Since our experiments are not sensitive to the products, neither in the kinetics nor in the spectroscopy experiment, we cannot assess the fate of  $BrO^-$  in our case. Similarly, a possibly enhanced loss rate of  $N_2O_5$  to an enriched bromide interface would have remained undetected in the experiments by Sobyra *et al.* To make the rate-limiting role of the  $[Br\cdot OOO]^-$  intermediate directly apparent, figure 2b shows the linear correlation between the uptake coefficient of  $O_3$  at 36 ppb and the measured ratio of the Br 3d photoemission intensity from the  $[Br\cdot OOO]^-$  intermediate to the O 1s intensity of liquid water for three different aqueous solutions. Note that it was not possible to reliably fit the Br 3d spectrum in terms of the

intermediate in the case of the mixed solution of 0.1 M TBA-Br and 0.55 M NaCl. Note that in the XPS experiment, we cannot quantify the local  $O_3$  pressure near the liquid surface but assume that it is higher than in the kinetic experiments. This leads to saturating surface concentrations of the intermediate. In the kinetic experiments, at such a high concentration, the bulk reaction is dominating the loss of  $O_3$ , even though the loss rate at the surface remains the same as at the lowest partial pressures of  $O_3$ . As already discussed in Gladich et al. [Gladich et al., 2020], the  $BrO^-$  product produced in the bulk or at the surface is not detected by XPS due to fast diffusional exchange in the liquid phase beyond the probe depth of XPS.

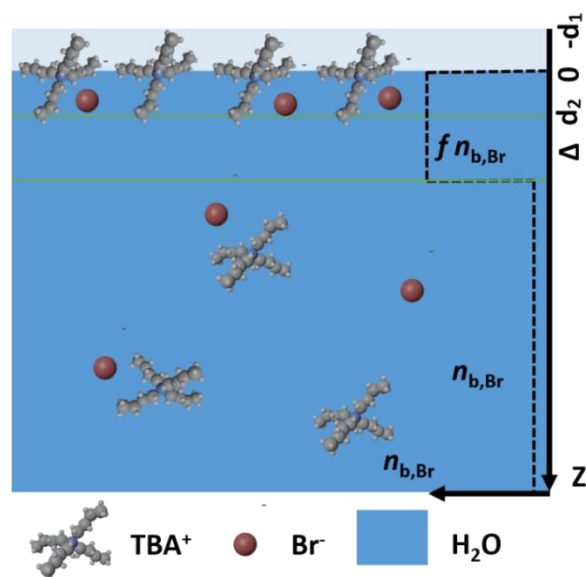


**Figure 3:** Scheme of the TBA covered interface used for the attenuation model. The reference level 0 for the depth scale ( $z$ ) denotes the position where the water density drops to zero and is put just above the N-group of TBA, such that the aliphatic carbons of three of the butyl chains reside at  $-d_1 < z < 0$  (on the vacuum side). The aliphatic carbons of the fourth chain are within  $z < d_2$ . The layer  $0 < z < \Delta$  is representing the layer in which the concentration of bromide is deviating from its bulk value,  $n_{b,Br}$ , by the factor  $f$ . Red, blue, dark and light grey spheres denote bromide, nitrogen, carbon and hydrogen atoms, respectively.

In an attempt to link the enhanced reactivity more quantitatively to the local interfacial concentration of bromide, we developed an attenuation model to account for the attenuation of photoelectrons by the ‘layer’ formed by the aliphatic carbon chains of the TBA surfactant that are residing at the interface (Figure 3). This model is then constrained by the available photoemission data. The attenuation model used in the present work follows the one developed by Lee et al. [Lee et al., 2019]. Its setup, depicted in Figure 3, assumes that the interfacial region contains the TBA, the concentration of which is constrained by surface tension measurements. In more detail, we assume that the cationic N and its surrounding C atoms reside on the bulk side of the interface, three of the remaining aliphatic chains above it, within a layer of thickness  $d_1$ , and one aliphatic chain pointing towards the bulk, extending to a depth  $d_2$ , inspired by molecular dynamics simulations presented by Winter et al. [Winter et al., 2005] for TBA iodide. We further consider a region of thickness  $\Delta$  within which the bromide concentration differs from that in the bulk aqueous phase, as in Lee et al. [M-T Lee et al., 2019]. Its thickness  $\Delta$  is independent of whether TBA is present or not. The details of

the attenuation model and the derivation of the equations describing the photoemission signals are provided in the Supporting Materials (section VI.). Since the structure of the bromide ozonide intermediate at the TBA covered interface is not clear and its coverage on the surface remains small, we refrain from applying the model in any way to the Br 3d photoemission intensities of the intermediate.

We first used the C 1s photoemission data shown in Figure S4 to constrain the thickness,  $d_1$ , of the top layer ( $-d_1 < z < 0$ ), which is the basis for the attenuation of all photoemission signals originating from the bulk. As shown in Figure 4a, the aliphatic group C 1s photoemission intensity for the TBA-Br solutions measured at 660 eV photon energy as a function of the concentration from 0.01 M to 0.2 M (see individual spectra in Supporting Materials, section IV, Figure S4) essentially tracks the evolution of the surface excess as derived from surface tension data (Supporting Materials, section VII, Figures S6 and S7) [Mata *et al.*, 2004].

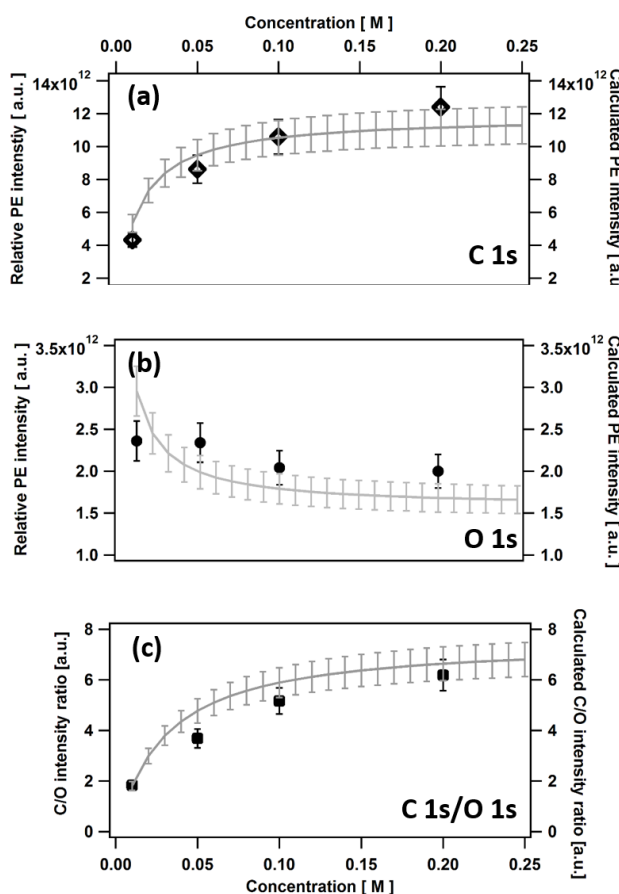


**Figure 4:** a) Normalized methyl carbon C 1s and b) liquid water O 1s photoemission intensity as a function of TBA-Br concentration for four different TBA-Br concentrations, measured at a photon energy of 660 eV and 900 eV, respectively; c) Normalized C/O intensity ratio as a function of TBA-Br concentration from the data in (a) and (b). Normalization is described in the text. Symbols present the experimental data, and the lines are the calculated quantities returned by the attenuation model described in the text.

Meanwhile, the correlation between C 1s photoemission intensity and the surface excess has been demonstrated for many surface-active organic species [Lee *et al.*, 2015; Lee *et al.*, 2016; Lee *et al.*, 2019; Pruyne *et al.*, 2014; Toribio *et al.*, 2018; Walz *et al.*, 2016]. The surface

excess formed the basis for the retrieval of the effective thickness of the layer formed by the aliphatic carbons from the calculated C 1s signal fitted to the data (Equation S6). The purpose was to replace detailed electron scattering calculations by assuming a homogeneous layer consisting of liquid butane, for which we could approximate the inelastic mean free path by that of liquid water (see Supporting Materials, section VII). In Figure 4b, we show the concomitant decrease of the condensed phase O 1s signal of H<sub>2</sub>O in agreement with the attenuation of photoelectrons by the increasing effective thickness of the aliphatic carbon layer (Equation S7). The ratio of the two signals is shown in Figure 4c, exhibiting the typical feature for surfactant behavior [Ammann *et al.*, 2018; Lee *et al.*, 2016]. Note that the calculated lines were only scaled with a factor that accounts for the detection efficiency. For the ratio in Figure 4c, this provides the calibration factor for the C 1s to O 1s photoemission intensity ratio,  $A/B$ , in Equation S10. The calculated effective layer thickness,  $d_1$ , as a function of the TBA bulk concentration, led to good agreement with the data. This thickness was then used for the quantitative analysis of the bromine signals further below. Apart from providing surface composition data, the ratio of photoemission intensities contributed by the aliphatic carbons to that by the amine coupled carbons contain information about the orientation of the surfactants [Lee *et al.*, 2016; Ottosson *et al.*, 2011; Prisle *et al.*, 2012]. For simple monocarboxylic acids, the head group is solvated while the aliphatic chains are residing above the surface. Therefore, photoelectrons from the aliphatic carbons are less attenuated than those from the head group carbon, leading to enhanced photoemission signal intensity ratios. However, in the case of TBA, this effect is relatively weak (Figure S5), because only one of the butyl chains is pointing upwards, while two are lying flat on the surface and one is pointing into the solution [Winter *et al.*, 2004] as schematically depicted in Figure 3. In the bulk phase, complete hydration of TBA with around 20 water molecules as well as counter-ions between the hydrocarbon arms of TBA was derived from molecular dynamics simulations [Bhowmik *et al.*, 2014]. No aggregation was apparent. At the surface, our results of the C/O intensity ratio indicate that at least part of the aliphatic carbon chains is not hydrated. This might be part of the driving force for residing at the surface. In addition, the large polarizability and size of TBA ions also contribute to their surface propensity [Winter *et al.*, 2004].

Figure 5 shows the photoemission spectra of the Br 3d (a), O 1s (b), C 1s (c), N 1s (d) and Cl 2p (e) core level regions for 0.1 M TBA-Br (red), 0.1 M TBA-Br/0.55 M NaCl (dark-blue), 0.1 M TBA-Br/0.1 M NaBr (pink), and 0.1 M TBA-Br/0.1 M NaBr/ 0.55 M NaCl (light-blue) aqueous solutions. We used photon energies of 229 eV for Br 3d, 696 eV for O1s (2<sup>nd</sup> order light component of the 348 eV photon energy adjusted at the monochromator), 448 eV for C 1s and 560 eV for N 1s to obtain the same kinetic energy of around 155 eV. Thus, Figure 5 was obtained at smaller kinetic energy than those in Figure 1 to achieve higher surface sensitivity. We measured the [Br·OOO]<sup>-</sup> intermediate at a kinetic energy of 370 eV to have a better signal-to-noise ratio for quantitative analysis and comparison with our previous work [Artiglia *et al.*, 2017]. The shape of O 1s and Br 3d have already been discussed above in relation to Figure 1. The lower kinetic energy leads to a higher ratio of gas phase to condensed phase water signal for the O 1s level. The C 1s (Figure 5c) exhibits, as also seen in Figure S4, two features

representing aliphatic chain carbon ( $-C_3H_7$ ) and the ammonium coupled carbon ( $-CH_2-N$ ) at a binding energy of 290.6 and 291.9 eV, respectively. The N 1s spectrum (Figure 5d) shows a single peak at a binding energy of 408.0 eV.

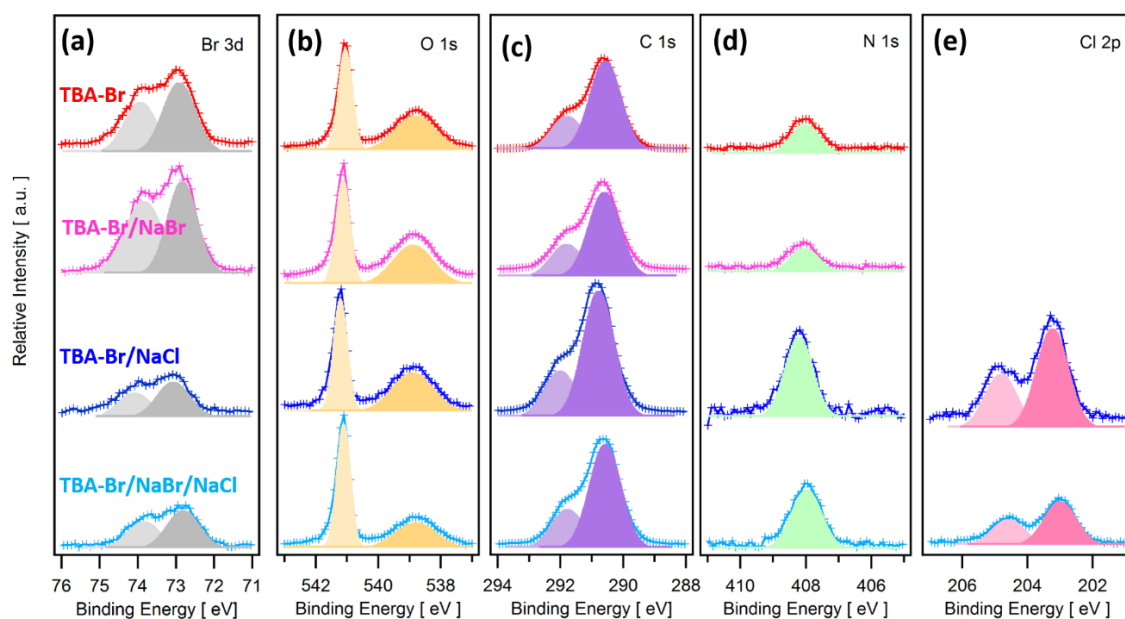


**Figure 5:** a) Br 3d, b) O 1s, c) C 1s, d) N 1s and e) Cl 2p photoemission spectra of aqueous solutions taken at a kinetic energy of 155 eV for 0.1 M TBA-Br (red), 0.1 M TBA-Br/0.55 M NaCl (dark-blue), 0.1 M TBA-Br/0.1 M NaBr (pink), and 0.1 M TBA-Br/0.1 M NaBr/ 0.55 M NaCl (light-blue), normalized to number of sweeps. Lines with symbols represent the measured data, and the shaded areas represent the fitted contributions of the corresponding core levels.

The first step towards the quantification of the surface composition is to consider signal intensity ratios, since then several uncertainty factors, such as transmission function of the analyzer or a variable jet position are canceling out. Table 1 summarizes the ratios of Br 3d, C 1s, N 1s, and Cl 2p intensity to that of O 1s. Each signal intensity has also been normalized to the total photoionization cross-section and photon flux. Since for the O 1s measurement we used 2<sup>nd</sup> order light, for which we have not quantified the photon flux precisely, these ratios are not absolute elemental ratios, but should be considered relative with respect to the different solutions. For the C 1s to O 1s signal intensity ratio, we note that based on the calibration factor obtained from fitting the TBA concentration dependent data (Figure 4), we can use the TBA-Br solution with its known surface excess to derive the TBA surface excess of the other solutions, as C 1s signal intensity ratios scale linearly with the surface excess for different solutions [Lee *et al.*, 2016; Lee *et al.*, 2019; Toribio *et al.*, 2018].

Qualitatively, and in extension to the data presented in Figure 1, the Br spectra in Figure 5 and Br/O ratios presented in the first column of Table 1 show the dramatic enhancement of the Br signal in the presence of TBA, as well as a partial suppression of this enhancement by 0.5 M NaCl. In addition, salting out of bromide to the surface by NaCl is apparent in the absence of TBA. Furthermore, the C 1s and N 1s data in Figure 5 and Table 1 indicate salting out of TBA in the presence of NaCl, meaning that more TBA is pushed to the interface in the presence of NaCl. These features will be discussed one by one below.

For a quantitative interpretation of the Br data and its link with the reactivity discussed above, we have used the observed Br/O signal intensity ratios to obtain the interfacial concentration of bromide,  $n_{\text{Br},\Delta}$ , within the layer of thickness  $\Delta$  (see the conceptual model of the interface, Figure 3). This is described by the factor,  $f$ , representing the enhancement ( $f > 1$ ) or depletion ( $f < 1$ ) in comparison to the bromide concentration in the bulk,  $n_{\text{Br},b}$  (Figure 3),  $n_{\text{Br},\Delta} = f n_{\text{Br},b}$ . The results are listed in Table 1 both in terms of  $n_{\text{Br},\Delta}$  in units of M and as effective surface coverage,  $n_{\text{Br},\Delta}\Delta$ , in units of molecule  $\text{cm}^{-2}$ . For the pure NaBr solution, we have used the same approach as in Lee et al. [Lee et al., 2019], to link the Br/O signal intensity ratio to the surface excess (Supporting Materials, section VI, Equations S11 and S14). Note that the choice of  $\Delta = 1$  nm is somewhat arbitrary. But this depth seems reasonable to represent the interfacial region in view of a number of molecular dynamics simulations on such systems [Gladich et al., 2020; Sobyra et al., 2019; Winter et al., 2005; Winter et al., 2004]. We note that all other surface concentrations discussed below are depending on this choice, leading to systematic uncertainty.  $f_0 = 0.5$  (for pure 0.1 M NaBr) is obtained from the surface excess of  $-3 \times 10^{12}$  molecules per  $\text{cm}^{-2}$  (Equation S11) that is consistent with surface tension data at 0.1 M concentration [Shah et al., 2013]. This means that within this surface layer, the average concentration of bromide is about 50% of its bulk value, thus 0.05 M, or an effective surface concentration of  $3 \times 10^{12}$  ions  $\text{cm}^{-2}$  (see Table 1). The depleted character at the surface of halide solutions is thus in agreement with surface tension data, but also other liquid jet photoemission studies and the most recent molecular dynamics simulations with revised force fields [Gladich et al., 2020; Olivieri et al., 2018; Ottosson et al., 2009].

**Table 1:** Ratios of normalized photoemission signal intensity of Br 3d, C 1s, N 1s and Cl 2p to that of O 1s of liquid H<sub>2</sub>O, calculated interfacial concentrations of bromide, their driving parameters as well as the first order loss rate coefficient of the intermediate,  $k_s$ .

Solution	Br/O	-CH <sub>2</sub> - N/O	-C <sub>3</sub> H <sub>7</sub> /O	N/O	Cl/O	$\Gamma_{\text{TBA}}$ [10 <sup>13</sup> cm <sup>-2</sup> ]	f	a	$n_{\text{Br},\Delta}$ , [M]	$n_{\text{Br},\Delta}\Delta$ [10 <sup>13</sup> cm <sup>-2</sup> ]	$k_s$ [10 <sup>-3</sup> s <sup>-1</sup> ]
0.1 M NaBr	0.06						0.5		0.05	0.30	4.5
0.1 M TBA-Br	0.75	1.24	4.03	0.18		29.6	9.9	17.0	0.99	5.96	0.43
0.1 M TBA-Br/0.1 M NaBr	0.95	1.06	3.54	0.14		28.0 <sup>a</sup>	15.8	27.8	1.60	9.63	
0.1 M NaBr/0.55 M NaCl	0.24				0.13		3.0		0.30	1.81	0.38
0.1 M TBA-Br/0.55 M NaCl	0.34	1.43	5.4	0.45	0.34	33.2 <sup>a</sup>	4.3	0.42	0.43	2.59	0.94
0.1 M TBA-Br/0.1 M NaBr/0.55 M NaCl	0.56	1.98	6.4	0.53	0.25	35.4 <sup>a</sup>	9.0	1.9	0.90	5.42	

<sup>a</sup> calculated based on calibration of C/O signal intensity ratio with the TBA-Br solution

<sup>b</sup> The error associated with the individual photoemission signal intensities is estimated at around  $\pm 10\%$ , which considers uncertainties due to the variability of the liquid-jet XPS experiment, the solution preparation, spectral fitting. Propagation leads to around 15% for elemental ratios and around 20% for the concentrations given. This does not include systematic errors related to the choice of the value for  $\Delta$  or other inherent assumptions of the attenuation model.

In the presence of TBA, the deviation of  $f$  from  $f_0$  is described as a linear function of the surface coverage of TBA, with the parameter  $a$  describing the maximum enhancement at

saturating coverage (SI, Equation S13). The parameter  $f$  was obtained from Equation S13 and using the calibration factor for the Br/O signal intensity ratio determined from the pure NaBr solution (Supporting material, Equation S15). Using  $f$ , we obtained the interfacial bromide concentration, which is enhanced by a factor of 20 in comparison to the pure NaBr solution. This takes into account the attenuation by TBA on the surface, which leads nearly to a doubling of the relative enhancement in comparison to that apparent from the Br 3d signal. This enhancement is likely due to electrostatic interactions between bromide and the positively charged TBA, including the formation of ion pairs. Such interactions have been found earlier for other surfactant systems [Öhrwall *et al.*, 2015] and specifically also for solutions containing TBA iodide [Bergersen *et al.*, 2007; Eschen *et al.*, 1995; Winter *et al.*, 2005; Winter *et al.*, 2004; Woods *et al.*, 2019]. Using He backscattering, Zhao *et al.* [Zhao *et al.*, 2020] determined that bromide is distributed within a width of around one nanometer at the interface for tetrahexylammonium (THA) bromide in glycerol as solvent. Note that in this work, the information depth is about one nm, but this depth is compatible with our choice of  $\Delta$  used to calculate local concentrations. The TBA surface coverage given in the table for TBA-Br is the same as that used for the fits in Figure 4 and is based on surface tension measurements at 0.1 M [Mata *et al.*, 2004]. In turn, the effective surface coverage of bromide is a factor of 5 lower, meaning that not all TBA ions have formed pairs with bromide. Bhowmik *et al.* [Bhowmik *et al.*, 2014] suggested that in solutions with higher bulk concentrations, bromide resides in the spaces between the butyl chains in fully hydrated form. Therefore, even if at the interface part of these chains are avoiding the aqueous phase, there would be sufficient room for equimolar amounts of bromide to approach the cations. Also, based on the C/O and Br/O ratios and the concentrations derived, the substantial amounts of water [Walz *et al.*, 2015; Walz *et al.*, 2016] (in terms of mole fraction) at the interface should not be a limiting factor for bromide approaching the interfacial region. The question remains whether OH<sup>-</sup> is competing with bromide or whether neutral TBAOH (TBA hydroxide) is stabilized at the interface. In the presence of additional 0.1 M NaBr, thus doubling the amount of bromide in the bulk, the interfacial bromide concentration increases by 60%, thus less than a factor of two. This non-linear response to additional bromide is also consistent with the presence of such competing processes. Note that in the calculation of the surface concentrations from recorded XPS intensities, the contribution by the increasing bulk concentration is taken into account (Supporting Materials, Equation S12), although it remains very small due to the predominant contribution of bromide at the interface. The surface excess of TBA, calculated by linear scaling based on the C/O ratios and using the 0.1 M TBA-Br solution as reference, did not change significantly in presence of additional 0.1 M NaBr added to TBA-Br (The calculated value is actually below that of TBA-Br but is considered remaining the within the error bounds of the 0.1 M TBA-Br solution).

When 0.55 M NaCl (representing roughly ocean water chloride concentration) is present together with 0.1 M NaBr, but in the absence of TBA, the interfacial concentration of Br<sup>-</sup> calculated from the Br/O photoemission intensity ratio is 0.30 M, which is a factor of 6 higher than in the case of the pure NaBr solution. This apparent salting out of bromide, or, in other



words, enhanced Br/Cl ratio at the interface due to the higher polarizability of bromide versus that of chloride, has been reported and discussed before [Ghosal *et al.*, 2008]. Exploring it further was not the scope of the present study.

In the presence of both NaCl and TBA bromide, several effects come together. Apart from the higher surface propensity of bromide in the presence of chloride, TBA experiences salting out, too, and chloride may compete with bromide for ion-pairing with TBA at the interface. Taking the calibration for the aliphatic C 1s to water O 1s photoemission ratio for the TBA-Br solution, the 20% increase of the C/O ratio leads to a surface excess of  $3.3 \times 10^{14} \text{ cm}^{-2}$  of TBA in the presence of 0.55 M NaCl, thus an increase by about 10% compared to the 0.1 M TBA-Br solution. Salting effects of organics in the presence of inorganic electrolytes, with salting out being the more common case, is a well described phenomenon, but predictive tools remain poorly constrained [Endo *et al.*, 2012; Toivola *et al.*, 2017]. Salting out has also been substantiated by XPS for butanol in the presence of iodide [Krisch *et al.*, 2007] or by scattering for THA bromide in the presence of 0.3 m NaBr [Zhao *et al.*, 2020]. In the latter case, though in glycerol, a widening of the depth profile of THA has been observed, possibly beyond the thickness of a monolayer. In the present work, the photoemission signals of the carbons directly attached at the amine nitrogen changed in accord with the aliphatic carbons, meaning that no substantial change in average orientation is apparent. On the other hand, the N 1s to O 1s signal intensity ratio changed by more than a factor of two. It could indicate that the amine group of a fraction of the TBA ions has moved towards the vacuum side of the interface, which would also point towards a more complex structure than the simple ideal monolayer assumed in our attenuation model. More detailed kinetic energy dependent XPS experiments would be required to explore this further. The analysis of the Br/O ratios and the estimation of the interfacial bromide concentration within  $0 < z < \Delta$  would not be affected by such a potentially thicker overlayer at  $z < 0$ , as Br and O photoemission signal would experience the same degree of attenuation.

While the amount of TBA at the surface increases in the presence of chloride, a three-fold decrease of the Br/O signal intensity ratio was observed, corresponding to a decrease of the interfacial concentration within  $0 < z < \Delta$  by about 60% in comparison to that of the 0.1 M TBA-Br solution in the absence of NaCl. The decrease in the bromide concentration can be rationalized by the competition between  $\text{Cl}^-$  and  $\text{Br}^-$  for ion-pairing with TBA. The association constant of TBA with  $\text{Br}^-$  is about one order of magnitude higher than that with  $\text{Cl}^-$  [Sawada *et al.*, 2001]. This explains why in spite of a factor of five excess of  $\text{Cl}^-$  still 40% of the  $\text{Br}^-$  concentration determined for the case of 0.1 M TBA-Br remains at the interface. A similar difference in association constants for  $\text{Br}^-$  and  $\text{Cl}^-$  exists with  $\text{NH}_4^+$  [Tomar *et al.*, 2007]. For alkylammonium cations, the association constants decrease with anion size and polarizability, e.g., for the pairs of TBA-I and TBA- $\text{ClO}_4$  [Moberg *et al.*, 1991] or for TBA-I and TBA-Br [Mbuna *et al.*, 2004]. For the latter pair, Winter *et al.* [Winter *et al.*, 2005] found only a small decrease of the iodine photoemission signal when adding NaBr to TBA-I, comparable to our observations. When looking at the chlorine signal in our experiments, the Cl/O ratio (see Table

1) increased by nearly a factor of 3 from the 0.1 M NaBr / 0.55 M NaCl solution to that with 0.1 M TBA-Br / 0.55 M NaCl. In turn, when adding another 0.1 M NaBr, the Cl/O ratio again decreases by about 1/3 due to the more competitive association of Br<sup>-</sup> with TBA. For the latter solution, the interfacial Br<sup>-</sup> concentration reaches nearly 60% (0.9 M) of the corresponding solution without NaCl (1.6 M).

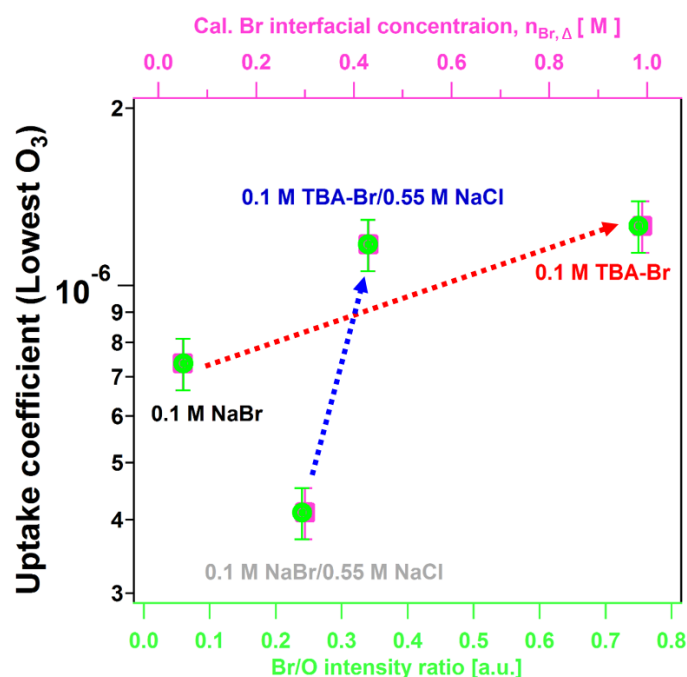


**Figure 6:** Uptake coefficient of O<sub>3</sub> at 36 ppb compared with measured Br<sup>-</sup>/O intensity ratio (lower x-axis, green) and calculated Br<sup>-</sup> interfacial concentration (upper x-axis, pink) for four different aqueous solutions.

In Figure 2b, we have observed a clear correlation between the uptake coefficient of O<sub>3</sub> with the photoemission signal from the bromide ozonide intermediate. With the estimated interfacial bromide concentrations, we can assess the relationship between the uptake coefficient at 36 ppb (where it is dominated by the surface reaction) and the interfacial bromide concentration (Figure 6). In the absence of NaCl, the uptake coefficient, thus the overall turnover of O<sub>3</sub> at the surface, increases by about 60%. This is paralleled by a 20-fold increase of the interfacial bromide concentration (red dotted arrow in Figure 6). In turn, only a 3-fold increase of the intermediate signal (Figure 2b) was observed. Even if taking into account a similar ratio between signal and concentration as for bromide, the steady state concentration of the intermediate increases by much less than that of bromide itself, but still considerably more than the uptake coefficient. Therefore, limitations seem to be at work that prevent interfacial bromide from being more efficiently reacted in the presence of TBA. This could be related to limitations imposed by the high density of alkyl chains at the interface. However, a previous study has shown that even strongly ordered monolayers of fatty acids have permeabilities sufficiently large to allow uptake coefficients of O<sub>3</sub> two orders of magnitude larger than in the present work [Rouvière and Ammann, 2010]. Therefore, it is more likely that the stability of TBA-Br ion pairs lowers the reactivity with O<sub>3</sub> to form the bromide ozonide intermediate. In addition, based on the first-order rate coefficients of the intermediate,  $k_s$  (last column of Table 1), which were retrieved from the fits to the kinetic

data, the presence of TBA affects the life-time of the intermediate by about one order of magnitude when comparing 0.1 M NaBr and 0.1 M TBA-Br. In the presence of NaCl, but in the absence of TBA, in spite of the substantially increased interfacial bromide concentration, the uptake coefficient is 60% lower than for pure NaBr, which is more in line with the reduced abundance of the intermediate. Thus, even for this inorganic mixture, abundance of bromide and of the bromide ozonide intermediate is not in accord with each other, which justifies further work. In the presence of TBA and NaCl combined, the uptake coefficient of O<sub>3</sub> was nearly as high as in the absence of NaCl, even though the interfacial bromide concentration was almost 60% lower. This again indicates that the interfacial abundance of bromide is not the sole indicator for reactivity, but that the details of how O<sub>3</sub> may accommodate to the surface in the presence of TBA and the way the ozonide intermediate may be stabilized are important.

### 6.1.5 Conclusion

In this study, we measured the surface propensity of cationic tetrabutylammonium at the aqueous liquid-vapor interface by liquid micro-jet X-ray photoelectron spectroscopy and the effect of this surfactant on ozone uptake to aqueous bromide solutions. The positively charged nitrogen group in TBA, along with its surface activity, is leading to an enhanced interfacial concentration of bromide and the [Br·OOO]<sup>-</sup> intermediate due to electrostatic interactions. In parallel, in kinetic experiments for the same system, a strongly enhanced ozone loss rate in the presence of TBA on the surface of bromide solutions was observed. An attenuation model was developed to account for the attenuation of photoelectrons by the carbon-rich layer of the TBA surfactant. The more quantitative analysis demonstrates that TBA-Br increases the local density of bromide ions by a factor of 20 above that of a neat aqueous bromide solutions at the same bulk concentration. Similarly, mixing TBA-Br with NaCl at seawater concentration led to an interfacial bromide ion density enhanced by about 43% compared to the corresponding mixture of just NaBr and NaCl. Still, the reaction rates of O<sub>3</sub> with these solutions were not simply proportional to the interfacial bromide concentrations, as other effects, such as the different interfacial structure, or the stabilization of the reaction intermediate, are additional factors influencing reactivity.

Aliphatic amines and amino acids are essential positively charged surfactants at the sea surface microlayer (the topmost organic-rich layer), with an average concentration in the range of 50-1500 ng L<sup>-1</sup> [Ge *et al.*, 2011; Pinxteren *et al.*, 2020; Pinxteren *et al.*, 2012]. This work shows that they may exert strong effects on halogen activation processes and their presence should be considered when it comes to assessing the impact of halogen chemistry on the atmospheric oxidation capacity and the climate.

## 6.2 Supplementary information

### Section I. O 1s valence spectra

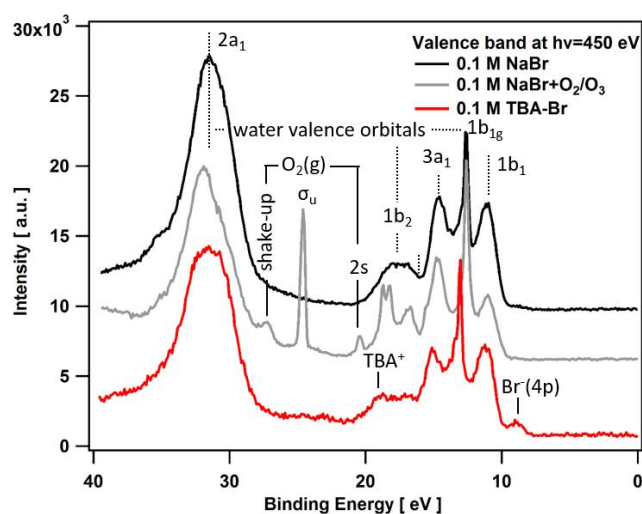


**Figure S1:** Valence spectra of three different solutions calibrated to the O1b<sub>1</sub> orbital of liquid water at 11.31 eV. [Avval *et al.*, 2019; Winter and Faubel, 2006; Winter *et al.*, 2004b]

### Section II. O 1s spectra of TBA-Br solutions in presence of O<sub>2</sub> and O<sub>3</sub>

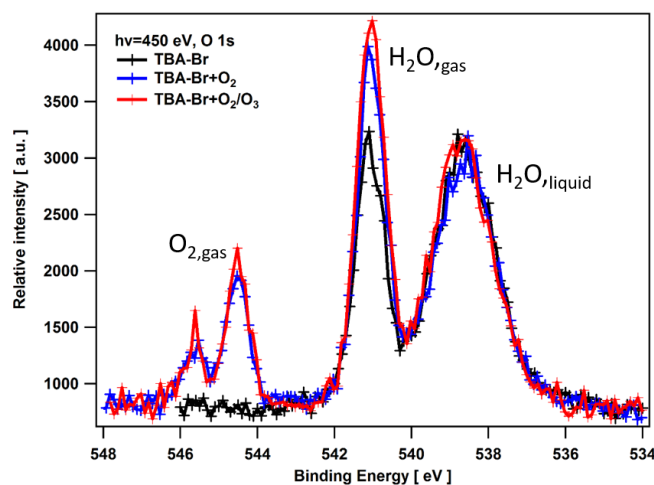


**Figure S2:** O 1s photoelectron spectra of aqueous solutions of 0.1 M TBA-Br, 0.1 M TBA-Br in presence of O<sub>2</sub>, and 0.1 M TBA-Br in presence of O<sub>2</sub>/O<sub>3</sub> at a photon energy of 450 eV, respectively.

### Section III. O 1s and Br 3d spectra of NaBr/NaCl solutions in presence of O<sub>2</sub> and O<sub>3</sub>

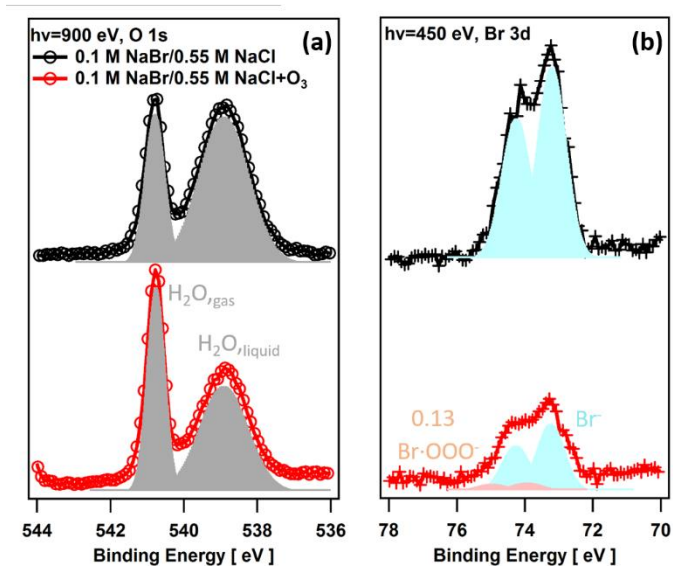


**Figure S3:** a) O 1s and b) Br 3d photoelectron spectra of aqueous solutions of 0.1 M NaBr/0.55 M NaCl and 0.1 M NaBr/0.55 M NaCl in the presence of O<sub>2</sub>/O<sub>3</sub> at a photon energy of 900 eV and 450 eV, respectively.

### Section IV. O 1s and C 1s spectra of TBA-Br solutions as a function of concentration

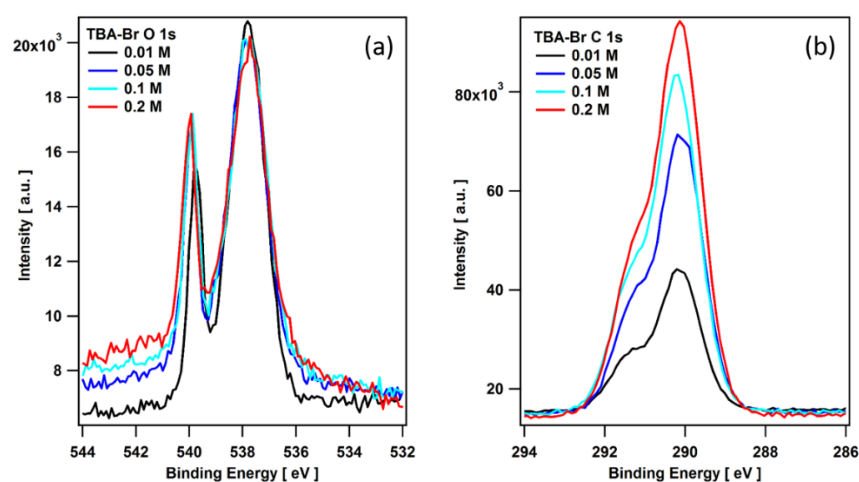


**Figure S4:** a) O 1s and b) C 1s photoemission spectra of aqueous TBA-Br solutions at concentrations ranging from 0.05 M to 0.2 M, excited by 900 eV and 660 eV, respectively, thus at a kinetic energy of 370 eV for both.

To study the relative surface concentration as a function of the bulk concentration, a series of O 1s and C 1s PE spectra of TBA-Br were recorded over a concentration range from 0.01 M to 0.2 M, shown in Figure S4(a) and (b), respectively. The PE intensities are given in arbitrary units, but the relative intensity scale is the same for both and can be used for comparison. In spite of the much larger density of O atoms, the O 1s signal intensity is lower than that of C 1s (cross-section in the same order of magnitude), because the O 1s electrons were excited by the second-order light at 900 eV photon energy, which has much smaller intensity than that at the primary photon energy of 450 eV used to excite C 1s for the same monochromator

settings. As discussed in the context of Figure 1 of the main text, in Figure S4a, the O 1s spectra display gas-phase water (sharp feature at higher binding energy) and liquid water (broad feature at lower binding energy) contributions. In Figure S4b, the C 1s spectra are composed of the contributions of 12 methyl carbons in the four butyl chains on the lower binding energy side and the four carbons bound to the amine on the higher binding energy side. As the spectra show, from black to red, the O 1s signal intensity from condensed phase water decreases (Figure S4a), when considering the increasing background, while that from gas-phase water stays the same. We also note the changing binding energy separation between the two contributions with increasing TBA concentration, as discussed in the main text. On the other hand, the C 1s signal intensity (Figure S4b) for both carbon species increases in parallel over the same TBA-Br concentration range. Clearly, the C1s PE intensity increases non-linearly with increasing concentration, which is explained by surface adsorption saturation of this amphiphilic compound. In turn, the decreasing condensed phase O 1s signal is attributed to the attenuation effect of TBA accumulating on the surface, which amounts to up to 20% of the O 1s signal for the most dilute solution. C1s and O1s intensities are analyzed quantitatively using the attenuation model.

## Section V. Orientation analysis for TBA-Br solutions

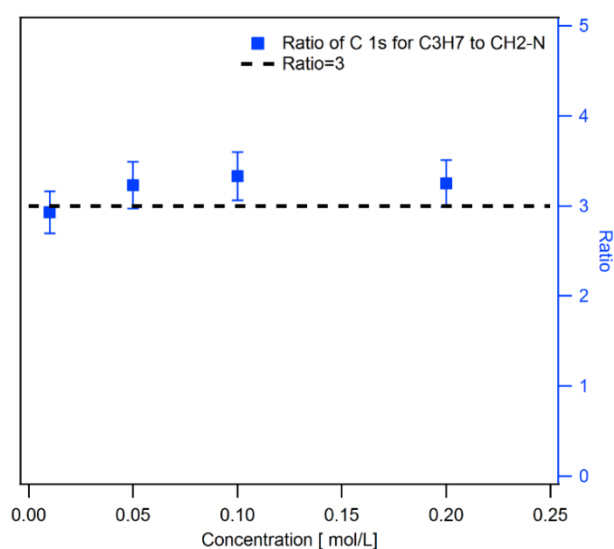


**Figure S5:** The ratio of C1s photoemission intensity of aliphatic carbon ( $-C_3H_7$ ) to that of amine coupled carbon ( $-CH_2-N$ , right-axis), at KE = 370 eV, as a function of TBA-Br concentration.

Figure S5 shows the ratio of C1s photoemission intensity of aliphatic carbon ( $-C_3H_7$ ) to that of amine coupled carbon ( $-CH_2-N$ , right-axis), at KE = 370 eV, as a function of TBA-Br concentration. This ratio tends to be just slightly above 3:1, the expected stoichiometric ratio, indicating a small net upward orientation of the butyl chains that leads to less attenuation of photoelectrons from aliphatic carbon than those from the amine coupled carbons. MD simulations by [Winter *et al.*, 2004] indicated that three butyl groups of  $TBA^+$  are found outside the surface and only one butyl group of  $TBA^+$  points into the liquid. The effect as apparent from our signal ratios remains weak, because two of these three chains are aligning

parallel to the interface, and the one pointing into the solution has an opposite orientation compared to that pointing out of the solution, though attenuation is stronger for the former. Single chain monocarboxylic acids have exhibited more pronounced effects on similar ratios due to more significant net upward orientation [Lee *et al.*, 2016; Ottosson *et al.*, 2011; Prisle *et al.*, 2012].

## Section VI. Calculation of photoemission signal intensity ratios based on the attenuation model

Since the number of carbon atoms per unit surface area varies with the bulk concentration of TBA, and since the actual density of carbon atoms above the surface is not well known to estimate the attenuation of electrons, we simplify the task by assuming the carbon atoms are assembled as in a liquid layer with the properties of liquid butane and that electron attenuation in that layer is equal to that in liquid water. The IMFP is around 1.1 nm and 2.1 nm for liquid butane at 155 eV and at 370 eV, respectively [Jablonski *et al.*, 2005], which is similar to that of liquid water (1.1 nm and 1.9 nm, respectively) [Shinotsuka *et al.*, 2017]. Choosing an entirely different density would require using a proper value for the IMFP, which is not known or would have to be obtained by scattering calculations. The number density (in atoms cm<sup>-3</sup>) of carbon atoms in liquid butane is:

$$n_{C,b,Butane} = \frac{4N_{Av}\rho_{Butane}}{M_{W,Butane}} \quad (S1)$$

$N_{Av}$  is the Avogadro constant, which is  $6.02 \times 10^{23}$  mol<sup>-1</sup>,  $\rho_{Butane}$  is the density of liquid butane, which is 600 g/L at 274 K, and  $M_{W,Butane}$  is the molecular weight of liquid butane, 58.12 g/mol.

The number density of carbon atoms above the interface (in atoms cm<sup>-3</sup>) is in turn related to the surface excess of TBA,  $\Gamma$ , and to the thickness of this layer,  $d_1$ , by:

$$n_{C,s} = 9 \frac{\Gamma}{d_1} \quad (S2)$$

As mentioned in the main text, each TBA contributes 9 carbon atoms into this layer, as one butyl chain is pointing into the liquid and the C atoms adjacent to the N are considered (and measured) separately. Equating  $n_{C,s} = n_{C,b,Butane}$  allows retrieving the thickness:

$$d_1 = \frac{9\Gamma M_{W,Butane}}{4N_{Av}\rho_{Butane}} \quad (S3)$$

For  $\Gamma$  of  $3.28 \times 10^{14}$  molecule cm<sup>-2</sup> for 0.5 mol/L TBA-Br (see below),  $d_1$  becomes 1.2 nm.

$\lambda_0$  is the inelastic mean free path for electrons in water [Shinotsuka *et al.*, 2017], while we use  $\lambda = 2/\pi i^* \lambda_0$  to account for the liquid jet measurement configuration [Winter and Faubel, 2006].  $\lambda_0$  is 1.8 nm at 370 eV kinetic energy, leading to  $\lambda = 1.15$  nm, while  $\lambda_0$  is 1.1 nm at 155 eV kinetic energy, leading to  $\lambda = 0.7$  nm.

The C1s photoemission signal intensity contributed by the aliphatic carbons contained within this layer is:

$$I_{C1s(CH2)_{\text{surface}}} = A \int_{-d_1}^0 n_{C,s} e^{-(z+d_1)/\lambda} dz = A n_{C,s} (-\lambda) (e^{-(z+d_1)/\lambda}) \Big|_{-d_1}^0 = A \lambda n_{C,s} (1 - e^{-d_1/\lambda}) = A \lambda \frac{9\Gamma}{d_1} (1 - e^{-d_1/\lambda}) \quad (S4)$$

$A$  denotes the factor accounting for photon flux, ionization cross-section and detection efficiency. Note that we have placed  $z = 0$  at the position, where the density of water drops to zero assumed to coincide with the position of the center (still hydrated) portion of the TBA ions. Therefore, no water is assumed to reside at  $z < 0$ . For small  $d_1$ , the expression in brackets simplifies to  $d_1/\lambda$ , so that the signal intensity simplifies to  $9A\Gamma$ .

The C1s signal from the carbons adjacent to the nitrogen (blue balls in Figure 3 of the main text) is obtained by assuming attenuation by the aliphatic overlayer, but assuming that they are residing in an infinitely thin 2D layer:

$$I_{C1s(CH2-N)_{\text{surface}}} = 4A\Gamma e^{-d_1/\lambda} \quad (S5)$$

For the C 1s signal from the aliphatic chain of TBA pointing into the solution, we assume that these three carbon atoms are homogeneously distributed within a layer of thickness  $d_2$  of 0.4 nm, by taking the length of the butyl chain as a reasonable constraint. The number density of carbon atoms for this layer is then three times the surface excess divided by  $d_2$ :

$$I_{C1sCH2_{\text{bottom chain}}} = A e^{-d_1/\lambda} \int_0^{d_2} \frac{3\Gamma}{d_2} e^{-(z)/\lambda} dz = A e^{-d_1/\lambda} \frac{3\Gamma}{d_2} (-\lambda) (e^{-(z)/\lambda}) \Big|_0^{d_2} = A \frac{3\Gamma}{d_2} \lambda (1 - e^{-d_2/\lambda}) e^{-d_1/\lambda} \quad (S6)$$

The photoemission signal contribution by all aliphatic carbons of TBA-Br in the bulk with a constant density  $n_{b,C}$  (C atoms  $\text{cm}^{-3}$ ), thus 12 times the number density of TBA molecules per  $\text{cm}^{-3}$ , is then obtained by integrating over the solution from  $z = 0$  onwards, and applying the constant attenuation factor by the aliphatic overlayer between  $-d_1$  and 0 :

$$I_{C1s(CH2)_{\text{bulk}}} = A e^{-d_1/\lambda} \int_0^{\infty} n_{b,C} e^{-(z)/\lambda} dz = A e^{-d_1/\lambda} n_{b,C} (-\lambda) (e^{-(z)/\lambda}) \Big|_0^{\infty} = A \lambda n_{b,C} e^{-d_1/\lambda} \quad (S7)$$

The overall C1s signal intensity contributed by aliphatic carbons is then given by:

$$I_{C1s} = I_{C1s(CH2)_{\text{surface}}} + I_{C1s(CH2)_{\text{bulk}}} + I_{C1s(CH2)_{\text{bottom chain}}} = 9A\Gamma + A e^{-d_1/\lambda} \lambda n_{b,C} + A e^{-d_1/\lambda} \frac{3\Gamma}{d_2} \lambda (1 - e^{-d_2/\lambda}) \quad (S8)$$

We calculate the photoemission signal contribution of O atoms, assumed to be homogeneously distributed over the bulk up to below the aliphatic carbon layer, which is not containing oxygen, completely analogously to C in the bulk:

$$I_{O1s, \text{bulk}} = B e^{-d_1/\lambda} \int_0^{\infty} n_{b,O} e^{-(z)/\lambda} dz = B n_{b,O} \lambda e^{-d_1/\lambda} \quad (S9)$$

The calculated C 1s to O 1s signal intensity ratio is then:

$$\frac{I_{C1s}}{I_{O1s, \text{bulk}}} = \frac{A}{B} \frac{9\Gamma + e^{-d_1/\lambda} \lambda n_{b,C} + e^{-d_1/\lambda} \frac{3\Gamma}{d_2} \lambda (1 - e^{-d_2/\lambda})}{n_{b,O} \lambda e^{-d_1/\lambda}} \quad (S10)$$



Fitting this equation to the measured data allows retrieving the calibration factor  $A/B = 0.685$ , which can then be used to calculate the unknown surface excess of TBA from the measured signals of the solutions containing additional NaBr or NaCl (values in Table 1 of the main text).

We introduced an additional layer of thickness  $\Delta$ , just below solution surface, starting at depth  $z = 0$ , within the aqueous solution. In the presence of TBA, this layer overlaps with the one containing the aliphatic portion of the butyl chain reaching down to  $d_2$ , but reaching deeper. In this layer, the Br atom density is set different from that of the bulk density by a factor,  $f$ , i.e.,  $fn_{b,Br}$ , while the density of bulk TBA is equal to that further away in the bulk.  $f$  is a function of the surface excess of TBA,  $\Gamma_{TBA}$ . In the simple terms of this model and in the absence of organic  $f = f_0$  is related to the surface excess of the bromide ions,  $\Gamma_{Br^-}$ , via:

$$\Gamma_{Br^-} = n_{b,Br}\Delta(f_0 - 1) \quad f_0 = \frac{\Gamma_{Br^-}}{n_{b,Br}\Delta} + 1 \quad (S11)$$

The Br photoemission signal intensity is then obtained from the following integration:

$$\begin{aligned} I_{Br} &= Ce^{-\frac{d_1}{\lambda}} \left[ \int_0^{\Delta} fn_{b,Br}e^{-(z)/\lambda} dz + e^{-\frac{\Delta}{\lambda}} \int_{\Delta}^{\infty} n_{b,Br}e^{-(z-\Delta)/\lambda} dz \right] = \\ I_{Br} &= Ce^{-\frac{d_1}{\lambda}} \left[ fn_{b,Br}\lambda - fn_{b,Br}\lambda e^{-\Delta/\lambda} + n_{b,Br}\lambda e^{-\frac{\Delta}{\lambda}} \right] \\ I_{Br} &= Ce^{-d_1/\lambda} n_{b,Br}\lambda [f + e^{-\Delta/\lambda}(1 - f)] \end{aligned} \quad (S12)$$

In the presence of TBA, we assumed that

$$f = f_0 \left( 1 + a \frac{\Gamma_{org}}{\Gamma_{org,max}} \right) \quad (S13)$$

We set  $\Gamma_{org,max}$  to  $3.3 \times 10^{14}$  molecule per  $\text{cm}^{-2}$  for TBA-Br (from the surface excess data already used to calculate the thickness of the aliphatic carbon layer).

Using equations (S9) and (S12), we can get the signal intensity ratio of Br 3d to O 1s as follows:

$$I_{Br^-, bulk}/I_{O1s, bulk} = \frac{C}{B} \frac{n_{b,Br}}{n_{b,O}} [f + e^{-\Delta/\lambda}(1 - f)] \quad (S14)$$

For pure NaBr solutions,  $f_0 = 0.5$  under the assumption that  $\Delta = 1$  nm, which leads to a surface excess of  $\sim -3 \times 10^{12}$  molecules per  $\text{cm}^{-2}$  for a 0.1 M NaBr solution, consistent with surface tension data [Shah *et al.*, 2013]. We apply this  $f_0$  value in equation (S14) to obtain the otherwise unknown factor  $D = \frac{C}{B}$ , the calibration factor for the quantification of the Br 3d to O 1s signal intensity ratio:

$$D = \frac{C}{B} = \frac{I_{Br^-} n_{b,O}}{I_{O1s} n_{b,Br} f_0 + e^{-\Delta/\lambda}(1 - f_0)} \quad (S15)$$

leading to  $D = 0.097$ .

We then used this value to calculate  $f$  from the measured Br 3d to O 1s signal ratios for the NaBr/NaCl, TBA-Br, TBA-Br/NaCl solutions, based on equation (S14):

For NaBr/NaCl solutions:

$$f_{NaBr/NaCl} = \left[ \frac{I_{Br-}}{D} - e^{-\Delta/\lambda} \right] / \left[ 1 - e^{-\Delta/\lambda} \right] = 2.946$$

For TBA-Br or TBA-Br/NaCl solutions:

$$f = \left[ \frac{I_{Br-}/I_{O1s}}{D} - e^{-\Delta/\lambda} \right] / \left[ 1 - e^{-\Delta/\lambda} \right] \quad (S16)$$

leading to:  $f_{TBA-Br} = 9.875$ ;  $f_{TBA-Br/NaCl} = 4.304$ ;

We used equation (S 13) to get the factor  $a$  describing the sensitivity to the surface coverage by TBA:

For TBA-Br:

$$a_{TBA-Br} = \frac{\Gamma_{org,max}}{\Gamma_{org}} \left( \frac{f_{TBA-Br}}{f_0} - 1 \right) \quad (S17)$$

For  $\Gamma_{org,max} = 3.3 \times 10^{14}$  and  $\Gamma_{org} = 3.0 \times 10^{14}$ , this leads to  $a_{TBA-Br} = 17.045$ .

Similarly, for TBA-Br/NaCl:

$$a_{TBA-Br/NaCl} = \frac{\Gamma_{org,max}}{\Gamma_{org}} \left( \frac{f_{TBA-Br/NaCl}}{f_{NaBr/NaCl}} - 1 \right) = 0.419$$

## Section VII. Surface excess of TBA-Br derived from surface tension measurements

Figure S6 shows the surface tension data of TBA-Br [Mata et al., 2004]. To determine the surface excess of TBA-Br at the interface the semi-empirical Meissner-Michaels equation was used to fit the surface tension data [Meissner and Michaels, 1949]:

$$\gamma = \gamma_0 \left[ 1 - b \ln \left( \frac{C_i}{a} + 1 \right) \right] \quad (S18)$$

where  $C_i$  is the concentration of TBA-Br based on mole fraction,  $\gamma_0$  is the surface tension without organics, and  $a$  and  $b$  are fitting parameters.

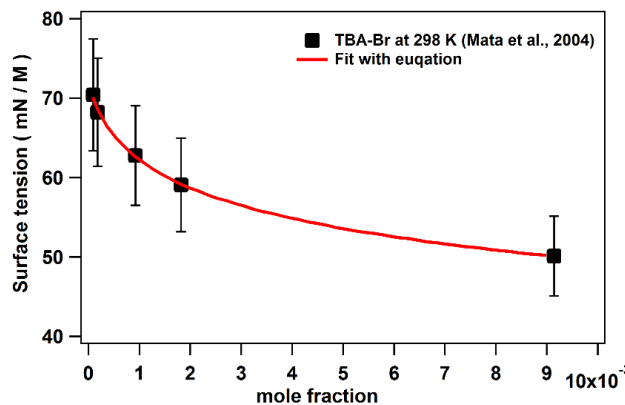


**Figure S6:** Measured surface tension [Mata et al., 2004] of aqueous TBA-Br solution as a function of TBA-Br mole fraction (symbols). The line displays the best fit of the Meissner-Michael equation to the data.  $a$  and  $b$  are fitting parameters,  $2.52 \times 10^{-4}$  and 0.193, respectively.

The thermodynamic description of surface tension is directly related to the surface excess,  $\Gamma_i$ , of a component  $i$  beyond a theoretical dividing plane (referred to as the Gibbs surface) placed parallel to the solution surface by the Gibbs equation [Casper, 1977]:

$$\Gamma_i = -\frac{X_i}{RT} \left( \frac{\partial \gamma}{\partial X_i} \right)_T \quad (\text{S19})$$

where  $X_i$  is the mole fraction of component  $i$ ,  $R$  is the universal gas constant and  $T$  is the temperature in Kelvin. Figure S7 shows the surface excess,  $\Gamma$  for TBA-Br solutions obtained using the Gibbs equation.

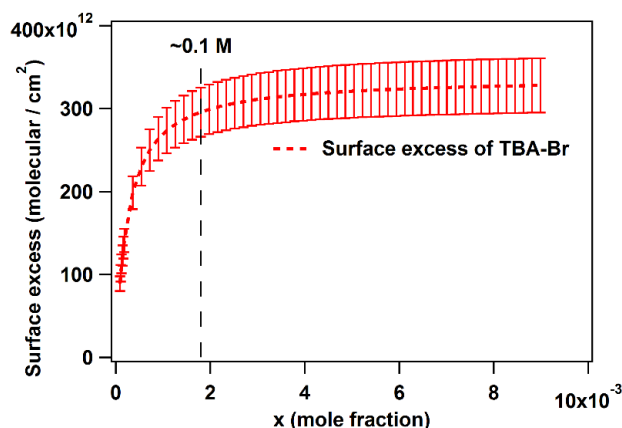


**Figure S7:** Surface excess of TBA-Br derived using the Gibbs equation and the experimental surface tension data [Mata *et al.*, 2004].

## Section VIII. Calculation of the uptake coefficient

To better understand the observed uptake coefficients, we use the parameterization of the uptake coefficients,  $\gamma$ , for uptake of  $O_3$  on aqueous bromide solutions used by Artiglia *et al.* [Artiglia *et al.*, 2017], which is based on the resistance model to represent the combination of surface and bulk processes contributing to uptake [Ammann *et al.*, 2013; Finlayson-Pitts and Pitts Jr, 1999].  $\gamma$  was calculated as direct addition of the bulk ( $\Gamma_b$ ) and surface ( $\Gamma_s$ ) limiting reaction contributions, since there was no indication that surface accommodation would limit uptake in this system [Berkemeier *et al.*, 2013; Lee *et al.*, 2015; Oldridge and Abbatt, 2011].

$$\gamma = \Gamma_s + \Gamma_b \quad (\text{S20})$$

Where

$$\Gamma_s = \frac{4k_s K_{Lang} N_{max}}{\omega_{O_3} (1 + K_{Lang} [O_3]_g)} \quad (\text{S21})$$

The reactive surface uptake calculated using equation (S21) represents a “Langmuir-Hinshelwood-type” surface reaction mechanism [Ammann *et al.*, 2013; Oldridge and Abbatt, 2011], where  $k_s$  is the apparent first-order rate coefficient of the adsorbed precursor to form the product  $BrO^-$ ,  $K_{Lang}$  is the Langmuir constant,  $N_{max}$  is the maximum surface coverage,  $\omega_{O_3}$  is the mean thermal velocity of ozone, which was  $34962 \text{ cm s}^{-1}$ . Artiglia *et al.* have recently shown that the Langmuir equilibrium constant,  $K_{lang}$ , and the maximum surface coverage,  $N_{max}$ , in equation (S 21) are linked to the equilibrium and maximum coverage of the reaction

intermediate [Br·OOO]<sup>-</sup> species, a bromide ozonide, at the surface, when describing the oxidation of bromide. Here, we used the same approach to get  $N_{\max}$  as Artiglia et al [Artiglia et al., 2017]. We got the [Br·OOO]<sup>-</sup>/Br<sup>-</sup> concentration ratio from the XPS data, and based on the attenuation model, we got the true surface Br<sup>-</sup> concentration from the measured Br 3d to O 1s photoemission intensity ratio. Then, we assumed that  $N_{\max}$  is equal to the [Br·OOO]<sup>-</sup> intermediate concentration, because the O<sub>3</sub> concentration in the XPS experiment was such that its surface coverage was indeed  $N_{\max}$ , thus under saturating conditions with respect to O<sub>3</sub>. We got  $N_{\max}$  as  $4.5 \times 10^{11}$  molecules per cm<sup>2</sup> for 0.1 M NaBr,  $1.99 \times 10^{11}$  molecules per cm<sup>2</sup> for 0.1 M NaBr/0.55 M NaCl, and  $1.44 \times 10^{13}$  molecules per cm<sup>2</sup> for both 0.1 M TBA-Br and 0.1 M TBA-Br/0.55 M NaCl, respectively.

The apparent equilibrium partitioning coefficient  $K_{\text{lang}}$  represents a lumped parameter describing the equilibrium between gas-phase ozone and the surface concentration of the ozonide and was chosen to be the same as in Artiglia et al [Artiglia et al., 2017], i.e., at 277 K:  $K_{\text{lang}} = 6 \times 10^{-13} \exp(686/T) = 7.1 \times 10^{-12}$  cm<sup>3</sup> per molecule.

The removal of the surface species depends on  $k_s$ , the rate coefficient for the formation of BrO<sup>-</sup>. This was the only fitting parameter to adjust the parameterized uptake coefficient to the measurement, which led to very good fits. Then, based on the fits of equation S20 to the measured uptake coefficients,  $k_s$  was  $0.0045 \text{ s}^{-1}$  for 0.1 M NaBr,  $0.00038 \text{ s}^{-1}$  for 0.1 M NaBr/0.55 M NaCl,  $0.00043 \text{ s}^{-1}$  for 0.1 M TBA-Br, and  $0.00094 \text{ s}^{-1}$  for 0.1 M TBA-Br/0.55 M NaCl.

For the bulk contribution,

$$\Gamma_b = \frac{R_{\text{bulk}}}{R_{\text{collision}}} = \frac{4RTH}{\omega_{\text{O}_3}} \sqrt{D_{\text{liq}} k_b^1} \quad (\text{S22})$$

where  $R$  is the gas constant ( $0.08206 \text{ L atm K}^{-1} \text{ mol}^{-1}$ ),  $T$  is the temperature (which is 277 K in this study),  $H$  is the Henry's law constant ( $\text{M atm}^{-1}$ ),  $D_{\text{liq}}$  is the diffusivity of ozone in the liquid phase ( $\text{cm}^2 \text{ s}^{-1}$ ),  $\omega_{\text{O}_3}$  is the thermal velocity of the ozone molecules in the gas phase ( $\text{cm s}^{-1}$ ), and  $k_{\text{bI}03} = k_{\text{bII}} \cdot a_{\text{Br}^-, \text{b}}$  is the pseudo-first order reaction rate coefficient, the product of the second order reaction rate coefficient  $k_{\text{b,II}}$ ,  $51.82 \text{ L mol}^{-1} \text{ s}^{-1}$  in the solutions (pH = 7) and the Br<sup>-</sup> activity in the bulk,  $a_{\text{Br}^-}$ ,  $0.1 \text{ mol L}^{-1}$ . The bromide activity in the bulk is not significantly depleted during the experiment [Artiglia et al., 2017]. Equation S22 is valid as long as the reacto-diffusive length,  $l_{\text{rd, O}_3} = \sqrt{D_{\text{liq}}/k_{\text{bI}}}$ , is smaller than the thickness of the solution ( $d_{\text{solution}}$ ), which is the case for our experiments ( $l_{\text{rd}} \leq 10 \text{ }\mu\text{m}$ ;  $d_{\text{solution}} < 4 \text{ mm}$ ). In turn, mixing of bromide across the full depth of the solution by diffusion was granted, as  $l_{\text{rdBr}} = \sqrt{D_{\text{liq}}/k_{\text{bI}03}} = \sqrt{D_{\text{liq}}/(k_{\text{bII}03} H p_{\text{O}_3})} \gg 4 \text{ mm}$ , so that diffusion limitations by bromide can be excluded, which is different to a recent study with the much more reactive iodide [Schneider et al., 2020].

The diffusion coefficient of ozone in the aqueous solutions ( $D_{\text{liq}}$ ) was calculated using the Stokes-Einstein relation, for which the diffusivity is dependent on the viscosity of the solution (equation S 23) [Lee et al., 2015].

$$D_{liq} = \frac{k_B T}{6 \pi \eta r_{O_3}} \quad (S23)$$

Where  $k_B$  is the Boltzmann's constant,  $\eta$  is the dynamic viscosity of the solutions at 277 K,  $r_{O_3}$  is the radius of the  $O_3$  molecule.

We chose the viscosity at 25°C of pure water, which is 0.8903 mPa s, [Isono, 1984] as a reference, to estimate the viscosity of the other solutions based on the ratios at room temperature [Simion et al., 2015]. The viscosity of 0.1 M NaBr at 25 °C is 0.8903 mPa s [Isono, 1984], the viscosity of 0.55 M NaCl at 25 °C is 0.9367 mPa s [Isono, 1984], and the viscosity of 0.1 M TBA-Br at 25°C is 1.002 mPa s [Baluja and Alnayab, 2019]. For pure water, the viscosity at 5 °C is 1.8496 mPa s, thus the viscosity of 0.1 M NaBr at 5 °C is 1.8606 mPa s, the viscosity of 0.55 M NaCl at 5 °C is 1.9460 mPa s, and the viscosity of 0.1 M TBA-Br at 5 °C is 2.0816 mPa s. The latter value we also chose to estimate the viscosity of the 0.1 M TBA-Br/0.55 M NaCl.

The solubility of ozone in the solution depends on the temperature, on the pH, and on composition of the solution. Studies have shown that salts tend to decrease or increase the solubility of ozone ("salting-out" or "salting-in") in solution [Biń, 2006; Weisenberger and Schumpe, 1996]. To account for this salting effect, the Henry's law constant ( $H$ ; mol L<sup>-1</sup> atm<sup>-1</sup>) or the solubility of ozone in the solution was calculated using the Setschenow relationship [Biń, 2006; Setschenow, 1889]:

$$\log\left(\frac{H_0}{H_{soln}}\right) = K C_s = \sum(h_i + h_G) C_i \quad (S 24)$$

$H_{soln}$  is the Henry's law constant of ozone in the solution of interest,  $H_0$  is the Henry's law constant of ozone in pure water, for which a value of 0.021 mol L<sup>-1</sup> atm<sup>-1</sup> [Rischbieter et al., 2000] was used at 5°C;  $K$  is the Sechenov coefficient;  $C_i$  is the concentration of ion,  $i$ , (in mol/L),  $h_i$  is the ion factor,  $h_G$  is the gas coefficient) [Rischbieter et al., 2000; Weisenberger and Schumpe, 1996].

Thus,  $h_{Na^+}=0.1143$ ,  $h_{Br^-}=0.0269$ ,  $h_{Cl^-}=0.0318$  Since  $h_{TBA^+}$  is not known to our knowledge, we choose  $h_{NH_4^+}=0.0556$  to replace it.

$$0.1 \text{ M NaBr: } H_{soln} = 0.021 * 10^{-(0.1*(0.1143-0.034)+0.1*(0.0269-0.034))} = 0.0206 \text{ mol L}^{-1} \text{ atm}^{-1};$$

0.1 M NaBr/0.55 M NaCl:

$$H_{soln} = 0.021 * 10^{-(0.65*(0.1143-0.034)+0.1*(0.0269-0.034)+0.55*(0.0318-0.034))} = 0.0187 \text{ mol L}^{-1} \text{ atm}^{-1};$$

$$0.1 \text{ M TBABr: } H_{soln} = 0.021 * 10^{-(0.1*(0.0556-0.034)+0.1*(0.0269-0.034))} = 0.0209 \text{ mol L}^{-1} \text{ atm}^{-1};$$

0.1 M TBABr/0.55 M NaCl:

$$H_{soln} = 0.021 * 10^{-(0.55*(0.1143-0.034)+0.1*(0.0556-0.034)+0.1*(0.0269-0.034)+0.55*(0.0318-0.034))} = 0.0190 \text{ mol L}^{-1} \text{ atm}^{-1}.$$

---

## Bibliography

---

- Abbatt, J. P. D., J. L. Thomas, K. Abrahamsson, C. Boxe, A. Granfors, A. E. Jones, M. D. King, A. Saiz-Lopez, P. B. Shepson, J. Sodeau, D. W. Toohey, C. Toubin, R. von Glasow, S. N. Wren and X. Yang (2012). "Halogen activation via interactions with environmental ice and snow in the polar lower troposphere and other regions." *Atmos. Chem. Phys.* 12(14): 6237-6271.
- Abbatt, J. P. D. and G. C. G. Waschewsky (1998). "Heterogeneous Interactions of HOBr, HNO<sub>3</sub>, O<sub>3</sub>, and NO<sub>2</sub> with Deliquescent NaCl Aerosols at Room Temperature." *The Journal of Physical Chemistry A* 102(21): 3719-3725.
- Alpert, P. A., R. Ciuraru, S. Rossignol, M. Passananti, L. Tinel, S. Perrier, Y. Dupart, S. S. Steimer, M. Ammann, D. J. Donaldson and C. George (2017). "Fatty Acid Surfactant Photochemistry Results in New Particle Formation." *Scientific Reports* 7(1): 12693.
- Ammann, M., L. Artiglia and T. Bartels-Rausch (2018). Chapter 6 - X-Ray Excited Electron Spectroscopy to Study Gas-Liquid Interfaces of Atmospheric Relevance. *Physical Chemistry of Gas-Liquid Interfaces*. J. A. Faust and J. E. House, Elsevier: 135-166.
- Ammann, M., R. A. Cox, J. N. Crowley, M. E. Jenkin, A. Mellouki, M. J. Rossi, J. Troe and T. J. Wallington (2013). "Evaluated kinetic and photochemical data for atmospheric chemistry: Volume VI – heterogeneous reactions with liquid substrates." *Atmos. Chem. Phys.* 13(16): 8045-8228.
- Artiglia, L., J. Edebeli, F. Orlando, S. Chen, M.-T. Lee, P. Corral Arroyo, A. Gilgen, T. Bartels-Rausch, A. Kleibert, M. Vazdar, M. Andres Carignano, J. S. Francisco, P. B. Shepson, I. Gladich and M. Ammann (2017). "A surface-stabilized ozonide triggers bromide oxidation at the aqueous solution-vapour interface." *Nature Communications* 8(1): 700.
- Avval, T. G., S. Chatterjee, G. T. Hodges, S. Bahr, P. Dietrich, M. Meyer, A. Thißen and M. R. Linford (2019). "Oxygen gas, O<sub>2</sub>(g), by near-ambient pressure XPS." *Surface Science Spectra* 26(1): 014021.
- Baluja, S. and E. A. M. Alnayab (2019). "Volumetric behaviour of tetra-n-butyl ammonium bromide in various solvents at different temperatures." *Revista Colombiana de Ciencias Químico-Farmacéuticas* 48(3).
- Bergersen, H., R. R. T. Marinho, W. Pokapanich, A. Lindblad, O. Björneholm, L. J. Sæthre and G. Öhrwall (2007). "A photoelectron spectroscopic study of aqueous tetrabutylammonium iodide." *Journal of Physics: Condensed Matter* 19(32): 326101.
- Berkemeier, T., A. J. Huisman, M. Ammann, M. Shiraiwa, T. Koop and U. Pöschl (2013). "Kinetic regimes and limiting cases of gas uptake and heterogeneous reactions in atmospheric aerosols and clouds: a general classification scheme." *Atmospheric Chemistry and Physics* 13(14).
- Bhowmik, D., N. Malikova, G. Méridet, O. Bernard, J. Teixeira and P. Turq (2014). "Aqueous solutions of tetraalkylammonium halides: ion hydration, dynamics and ion-ion interactions in light of steric effects." *Physical Chemistry Chemical Physics* 16(26): 13447-13457.
- Biń, A. K. (2006). "Ozone solubility in liquids." *Ozone: science & engineering* 28(2): 67-75.
- Brown, M. A., A. B. Redondo, I. Jordan, N. Duyckaerts, M.-T. Lee, M. Ammann, F. Nolting, A. Kleibert, T. Huthwelker, J.-P. Mächler, M. Birrer, J. Honegger, R. Wetter, H. J. Wörner and J. A. v. Bokhoven (2013). "A new endstation at the Swiss Light Source for ultraviolet photoelectron spectroscopy, X-ray photoelectron spectroscopy, and X-ray absorption spectroscopy measurements of liquid solutions." *Review of Scientific Instruments* 84(7): 073904.
- Carpenter, L. J., S. M. MacDonald, M. D. Shaw, R. Kumar, R. W. Saunders, R. Parthipan, J. Wilson and J. M. C. Plane (2013). "Atmospheric iodine levels influenced by sea surface emissions of inorganic iodine." *Nature Geoscience* 6(2): 108-111.
- Casper, J. M. (1977). "Physical chemistry of surfaces (3rd Ed.), Arthur W. Adamson, Wiley-Interscience, New York, 1976, 698 pp. \$24.95." *Journal of Polymer Science: Polymer Letters Edition* 15(10): 632-633.

- Ciuraru, R., L. Fine, M. van Pinxteren, B. D'Anna, H. Herrmann and C. George (2015). "Photosensitized production of functionalized and unsaturated organic compounds at the air-sea interface." *Scientific Reports* 5(1): 12741.
- Clifford, D. and D. J. Donaldson (2007). "Direct Experimental Evidence for a Heterogeneous Reaction of Ozone with Bromide at the Air–Aqueous Interface." *The Journal of Physical Chemistry A* 111(39): 9809-9814.
- Cochran, R. E., O. S. Ryder, V. H. Grassian and K. A. Prather (2017). "Sea Spray Aerosol: The Chemical Link between the Oceans, Atmosphere, and Climate." *Accounts of Chemical Research* 50(3): 599-604.
- Donaldson, D. J. and D. Anderson (1999). "Does molecular HNO<sub>3</sub> adsorb onto sulfuric acid droplet surfaces?" *Geophysical Research Letters* 26(24): 3625-3628.
- Edebeli, J., M. Ammann and T. Bartels-Rausch (2019). "Microphysics of the aqueous bulk counters the water activity driven rate acceleration of bromide oxidation by ozone from 289–245 K." *Environmental Science: Processes & Impacts* 21(1): 63-73.
- Endo, S., A. Pfennigsdorff and K.-U. Goss (2012). "Salting-Out Effect in Aqueous NaCl Solutions: Trends with Size and Polarity of Solute Molecules." *Environmental Science & Technology* 46(3): 1496-1503.
- Eschen, F., M. Heyerhoff, H. Morgner and J. Vogt (1995). "The concentration-depth profile at the surface of a solution of tetrabutylammonium iodide in formamide, based on angle-resolved photoelectron spectroscopy." *Journal of Physics: Condensed Matter* 7(10): 1961-1978.
- Finlayson-Pitts, B. J. and J. N. Pitts Jr (1999). *Chemistry of the upper and lower atmosphere: theory, experiments, and applications*, Elsevier.
- Flechsig, U., F. Nolting, A. F. Rodríguez, J. Krempasky, C. Quitmann, T. Schmidt, S. Spielmann and D. Zimoch (2010). "Performance Measurements at the SLS SIM Beamline." *AIP Conference Proceedings* 1234: 319-322.
- Flechsig, U., F. Nolting, A. F. Rodríguez, J. Krempaský, C. Quitmann, T. Schmidt, S. Spielmann and D. Zimoch (2010). "Performance measurements at the SLS SIM beamline." *AIP Conference Proceedings* 1234(1): 319-322.
- Ge, X., A. S. Wexler and S. L. Clegg (2011). "Atmospheric amines – Part I. A review." *Atmospheric Environment* 45(3): 524-546.
- Ghosal, S., M. A. Brown, H. Bluhm, M. J. Krisch, M. Salmeron, P. Jungwirth and J. C. Hemminger (2008). "Ion Partitioning at the Liquid/Vapor Interface of a Multicomponent Alkali Halide Solution: A Model for Aqueous Sea Salt Aerosols." *The Journal of Physical Chemistry A* 112(48): 12378-12384.
- Gladich, I., S. Chen, M. Vazdar, A. Boucly, H. Yang, M. Ammann and L. Artiglia (2020). "Surface Propensity of Aqueous Atmospheric Bromine at the Liquid–Gas Interface." *The Journal of Physical Chemistry Letters* 11(9): 3422-3429.
- Hunt, S. W., M. Roeselová, W. Wang, L. M. Wingen, E. M. Knipping, D. J. Tobias, D. Dabdub and B. J. Finlayson-Pitts (2004). "Formation of Molecular Bromine from the Reaction of Ozone with Deliquesced NaBr Aerosol: Evidence for Interface Chemistry." *The Journal of Physical Chemistry A* 108(52): 11559-11572.
- Isono, T. (1984). "Density, viscosity, and electrolytic conductivity of concentrated aqueous electrolyte solutions at several temperatures. Alkaline-earth chlorides, lanthanum chloride, sodium chloride, sodium nitrate, sodium bromide, potassium nitrate, potassium bromide, and cadmium nitrate." *Journal of Chemical & Engineering Data* 29(1): 45-52.
- Jablonski, A., F. Salvat and C. J. Powell (2005). "Evaluation of elastic-scattering cross sections for electrons and positrons over a wide energy range." *Surface and Interface Analysis* 37(12): 1115-1123.
- Jung, Y., E. Hong, M. Kwon and J.-W. Kang (2017). "A kinetic study of ozone decay and bromine formation in saltwater ozonation: Effect of O<sub>3</sub> dose, salinity, pH, and temperature." *Chemical Engineering Journal* 312(Supplement C): 30-38.
- Karashima, S. and T. Suzuki (2019). "Charge-Transfer-to-Solvent Reaction in a Hydrophobic Tetrabutylammonium Iodide Molecular Layer in Aqueous Solution." *The Journal of Physical Chemistry B* 123(17): 3769-3775.
- Koenig, T. K., S. Baidar, P. Campuzano-Jost, C. A. Cuevas, B. Dix, R. P. Fernandez, H. Guo, S. R. Hall, D. Kinnison, B. A. Nault, K. Ullmann, J. L. Jimenez, A. Saiz-Lopez and R. Volkamer (2020). "Quantitative detection of iodine in the stratosphere." *Proceedings of the National Academy of Sciences* 117(4): 1860-1866.
- Krisch, M. J., R. D'Auria, M. A. Brown, D. J. Tobias, C. Hemminger, M. Ammann, D. E. Starr and H. Bluhm (2007). "The Effect of an Organic Surfactant on the Liquid–Vapor Interface of an Electrolyte Solution." *The Journal of Physical Chemistry C* 111(36): 13497-13509.
- Lee, M.-T., M. A. Brown, S. Kato, A. Kleibert, A. Türlér and M. Ammann (2015). "Competition between Organics and Bromide at the Aqueous Solution–Air Interface as Seen from Ozone Uptake Kinetics and X-ray Photoelectron Spectroscopy." *The Journal of Physical Chemistry A* 119(19): 4600-4608.
- Lee, M.-T., M. A. Brown, S. Kato, A. Kleibert, A. Türlér and M. Ammann (2015). "Competition between organics and bromide at the aqueous solution–air interface as seen from ozone uptake kinetics and X-ray photoelectron spectroscopy." *The Journal of Physical Chemistry A* 119(19): 4600-4608.

- Lee, M.-T., F. Orlando, L. Artiglia, S. Chen and M. Ammann (2016). "Chemical Composition and Properties of the Liquid–Vapor Interface of Aqueous C1 to C4 Monofunctional Acid and Alcohol Solutions." *The Journal of Physical Chemistry A* 120(49): 9749-9758.
- Lee, M.-T., F. Orlando, M. Khabiri, M. Roeselová, M. A. Brown and M. Ammann (2019). "The opposing effect of butanol and butyric acid on the abundance of bromide and iodide at the aqueous solution–air interface." *Physical Chemistry Chemical Physics* 21(16): 8418-8427.
- Liu, Q., L. M. Schurter, C. E. Muller, S. Aloisio, J. S. Francisco and D. W. Margerum (2001). "Kinetics and Mechanisms of Aqueous Ozone Reactions with Bromide, Sulfite, Hydrogen Sulfite, Iodide, and Nitrite Ions." *Inorganic Chemistry* 40(17): 4436-4442.
- Mata, J., D. Varade, G. Ghosh and P. Bahadur (2004). "Effect of tetrabutylammonium bromide on the micelles of sodium dodecyl sulfate." *Colloids and Surfaces A: Physicochemical and Engineering Aspects* 245(1): 69-73.
- Mbuna, J., T. Takayanagi, M. Oshima and S. Motomizu (2004). "Evaluation of weak ion association between tetraalkylammonium ions and inorganic anions in aqueous solutions by capillary zone electrophoresis." *Journal of Chromatography A* 1022(1): 191-200.
- Meissner, H. P. and A. S. Michaels (1949). "Surface Tensions of Pure Liquids and Liquid Mixtures." *Industrial & Engineering Chemistry* 41(12): 2782-2787.
- Moberg, R., F. Boekman, O. Bohman and H. O. G. Siegbahn (1991). "ESCA studies of phase-transfer catalysts in solution: ion pairing and surface activity." *Journal of the American Chemical Society* 113(10): 3663-3667.
- Moreno, C. and M. T. Baeza-Romero (2019). "A kinetic model for ozone uptake by solutions and aqueous particles containing I<sup>-</sup> and Br<sup>-</sup>, including seawater and sea-salt aerosol." *Physical Chemistry Chemical Physics* 21(36): 19835-19856.
- O'Dowd, C. D., M. C. Facchini, F. Cavalli, D. Ceburnis, M. Mircea, S. Decesari, S. Fuzzi, Y. J. Yoon and J.-P. Putaud (2004). "Biogenically driven organic contribution to marine aerosol." *Nature* 431(7009): 676-680.
- Öhrwall, G., N. L. Prisle, N. Ottosson, J. Werner, V. Ekholm, M.-M. Walz and O. Björneholm (2015). "Acid–Base Speciation of Carboxylate Ions in the Surface Region of Aqueous Solutions in the Presence of Ammonium and Aminium Ions." *The Journal of Physical Chemistry B* 119(10): 4033-4040.
- Ohtani, N., T. Ohta, Y. Hosoda and T. Yamashita (2004). "Phase Behavior and Phase-Transfer Catalysis of Tetrabutylammonium Salts. Interface-Mediated Catalysis." *Langmuir* 20(2): 409-415.
- Oldridge, N. W. and J. P. D. Abbatt (2011). "Formation of Gas-Phase Bromine from Interaction of Ozone with Frozen and Liquid NaCl/NaBr Solutions: Quantitative Separation of Surficial Chemistry from Bulk-Phase Reaction." *The Journal of Physical Chemistry A* 115(12): 2590-2598.
- Olivieri, G., K. M. Parry, R. D'Auria, D. J. Tobias and M. A. Brown (2018). "Specific Anion Effects on Na<sup>+</sup> Adsorption at the Aqueous Solution–Air Interface: MD Simulations, SESSA Calculations, and Photoelectron Spectroscopy Experiments." *The Journal of Physical Chemistry B* 122(2): 910-918.
- Ottosson, N., M. Faubel, S. E. Bradforth, P. Jungwirth and B. Winter (2010). "Photoelectron spectroscopy of liquid water and aqueous solution: Electron effective attenuation lengths and emission-angle anisotropy." *Journal of Electron Spectroscopy and Related Phenomena* 177(2–3): 60-70.
- Ottosson, N., R. Vácha, E. F. Aziz, W. Pokapanich, W. Eberhardt, S. Svensson, G. Öhrwall, P. Jungwirth, O. Björneholm and B. Winter (2009). "Large variations in the propensity of aqueous oxychlorine anions for the solution/vapor interface." *The Journal of chemical physics* 131(12): 124706.
- Ottosson, N., E. Wernersson, J. Soderstrom, W. Pokapanich, S. Kaufmann, S. Svensson, I. Persson, G. Öhrwall and O. Björneholm (2011). "The protonation state of small carboxylic acids at the water surface from photoelectron spectroscopy." *Physical Chemistry Chemical Physics* 13(26): 12261-12267.
- Ottosson, N., E. Wernersson, J. Söderström, W. Pokapanich, S. Kaufmann, S. Svensson, I. Persson, G. Öhrwall and O. Björneholm (2011). "The protonation state of small carboxylic acids at the water surface from photoelectron spectroscopy." *Physical Chemistry Chemical Physics* 13(26): 12261-12267.
- Oum, K. W., M. J. Lakin and B. J. Finlayson-Pitts (1998). "Bromine activation in the troposphere by the dark reaction of O<sub>3</sub> with seawater ice." *Geophysical Research Letters* 25(21): 3923-3926.
- Prather, K. A., T. H. Bertram, V. H. Grassian, G. B. Deane, M. D. Stokes, P. J. DeMott, L. I. Aluwihare, B. P. Palenik, F. Azam, J. H. Seinfeld, R. C. Moffet, M. J. Molina, C. D. Cappa, F. M. Geiger, G. C. Roberts, L. M. Russell, A. P. Ault, J. Baltrusaitis, D. B. Collins, C. E. Corrigan, L. A. Cuadra-Rodriguez, C. J. Ebben, S. D. Forestieri, T. L. Guasco, S. P. Hersey, M. J. Kim, W. F. Lambert, R. L. Modini, W. Mui, B. E. Pedler, M. J. Ruppel, O. S. Ryder, N. G. Schoepp, R. C. Sullivan and D. Zhao (2013). "Bringing the ocean into the laboratory to probe the chemical complexity of sea spray aerosol." *Proceedings of the National Academy of Sciences* 110(19): 7550-7555.
- Prisle, N., N. Ottosson, G. Öhrwall, J. Söderström, M. D. Maso and O. Björneholm (2012). "Surface/bulk partitioning and acid/base speciation of aqueous decanoate: direct observations and atmospheric implications." *Atmospheric Chemistry and Physics* 12(24): 12227-12242.



- Pruyne, J. G., M.-T. Lee, C. Fábri, A. Beloqui Redondo, A. Kleibert, M. Ammann, M. A. Brown and M. J. Krisch (2014). "Liquid–Vapor Interface of Formic Acid Solutions in Salt Water: A Comparison of Macroscopic Surface Tension and Microscopic in Situ X-ray Photoelectron Spectroscopy Measurements." *The Journal of Physical Chemistry C* 118(50): 29350-29360.
- Rischbieter, E., H. Stein and A. Schumpe (2000). "Ozone solubilities in water and aqueous salt solutions." *Journal of Chemical & Engineering Data* 45(2): 338-340.
- Rouvière, A. and M. Ammann (2010). "The effect of fatty acid surfactants on the uptake of ozone to aqueous halogenide particles." *Atmos. Chem. Phys.* 10(23): 11489-11500.
- Sakamoto, Y., M. Goda and J. Hirokawa (2018). "Kinetics Study of Heterogeneous Bromine Release from the Reaction between Gaseous Ozone and Aqueous Bromide Solution." *The Journal of Physical Chemistry A*.
- Sawada, K., E. Takahashi, T. Horie and K. Satoh (2001). "Solvent Effects on Ion-Pair Distribution and Dimerization of Tetraalkylammonium Salts." *Monatshefte für Chemie / Chemical Monthly* 132(11): 1439-1450.
- Schneider, S. R., P. S. J. Lakey, M. Shiraiwa and J. P. D. Abbatt (2020). "Reactive Uptake of Ozone to Simulated Seawater: Evidence for Iodide Depletion." *The Journal of Physical Chemistry A* 124(47): 9844-9853.
- Setschenow, J. (1889). "Über die konstitution der salzlösungen auf grund ihres verhaltens zu kohlendäure." *Zeitschrift für Physikalische Chemie* 4(1): 117-125.
- Shah, A.-u.-H. A., K. Ali and S. Bilal (2013). "Surface tension, surface excess concentration, enthalpy and entropy of surface formation of aqueous salt solutions." *Colloids and Surfaces A: Physicochemical and Engineering Aspects* 417: 183-190.
- Shaloski, M. A., J. R. Gord, S. Staudt, S. L. Quinn, T. H. Bertram and G. M. Nathanson (2017). "Reactions of N<sub>2</sub>O<sub>5</sub> with Salty and Surfactant-Coated Glycerol: Interfacial Conversion of Br<sup>-</sup> to Br<sub>2</sub> Mediated by Alkylammonium Cations." *The Journal of Physical Chemistry A* 121(19): 3708-3719.
- Sherwen, T., M. J. Evans, L. J. Carpenter, J. A. Schmidt and L. J. Mickley (2017). "Halogen chemistry reduces tropospheric O<sub>3</sub> radiative forcing." *Atmos. Chem. Phys.* 17(2): 1557-1569.
- Shinotsuka, H., B. Da, S. Tanuma, H. Yoshikawa, C. J. Powell and D. R. Penn (2017). "Calculations of electron inelastic mean free paths. XI. Data for liquid water for energies from 50 eV to 30 keV." *Surface and Interface Analysis* 49(4): 238-252.
- Simion, A. I., C.-G. Grigoraş, A. Roşu and L. Gavrilă (2015). "Mathematical modelling of density and viscosity of nacl aqueous solutions." *Journal of Agroalimentary Processes and Technologies* 21(1): 41-52.
- Simpson, W. R., S. S. Brown, A. Saiz-Lopez, J. A. Thornton and R. v. Glasow (2015). "Tropospheric Halogen Chemistry: Sources, Cycling, and Impacts." *Chemical Reviews* 115(10): 4035-4062.
- Simpson, W. R., S. S. Brown, A. Saiz-Lopez, J. A. Thornton and R. von Glasow (2015). "Tropospheric Halogen Chemistry: Sources, Cycling, and Impacts." *Chemical Reviews* 115(10): 4035-4062.
- Simpson, W. R., R. von Glasow, K. Riedel, P. Anderson, P. Ariya, J. Bottenheim, J. Burrows, L. J. Carpenter, U. Frieß, M. E. Goodsite, D. Heard, M. Hutterli, H. W. Jacobi, L. Kaleschke, B. Neff, J. Plane, U. Platt, A. Richter, H. Roscoe, R. Sander, P. Shepson, J. Sodeau, A. Steffen, T. Wagner and E. Wolff (2007). "Halogens and their role in polar boundary-layer ozone depletion." *Atmos. Chem. Phys.* 7(16): 4375-4418.
- Sobyra, T. B., H. Pliszka, T. H. Bertram and G. M. Nathanson (2019). "Production of Br<sub>2</sub> from N<sub>2</sub>O<sub>5</sub> and Br<sup>-</sup> in Salty and Surfactant-Coated Water Microjets." *The Journal of Physical Chemistry A* 123(41): 8942-8953.
- Toivola, M., N. L. Prisle, J. Elm, E. M. Waxman, R. Volkamer and T. Kurtén (2017). "Can COSMOTerm Predict a Salting in Effect?" *The Journal of Physical Chemistry A* 121(33): 6288-6295.
- Tomar, P. A., R. R. Kolhapurkar, D. H. Dagade and K. J. Patil (2007). "Equilibrium Constant Studies for Complexation between Ammonium Ions and 18-Crown-6 in Aqueous Solutions at 298.15 K." *Journal of Solution Chemistry* 36(2): 193-209.
- Toribio, A. R., N. L. Prisle and A. S. Wexler (2018). "Statistical Mechanics of Multilayer Sorption: Surface Concentration Modeling and XPS Measurement." *The Journal of Physical Chemistry Letters* 9(6): 1461-1464.
- van Pinxteren, M., K. W. Fomba, N. Triesch, C. Stolle, O. Wurl, E. Bahlmann, X. Gong, J. Voigtländer, H. Wex, T. B. Robinson, S. Barthel, S. Zeppenfeld, E. H. Hoffmann, M. Roveretto, C. Li, B. Grosselin, V. Daële, F. Senf, D. van Pinxteren, M. Manzi, N. Zabalegui, S. Frka, B. Gašparović, R. Pereira, T. Li, L. Wen, J. Li, C. Zhu, H. Chen, J. Chen, B. Fiedler, W. von Tümpling, K. A. Read, S. Punjabi, A. C. Lewis, J. R. Hopkins, L. J. Carpenter, I. Peeken, T. Rixen, D. Schulz-Bull, M. E. Monge, A. Mellouki, C. George, F. Stratmann and H. Herrmann (2020). "Marine organic matter in the remote environment of the Cape Verde islands – an introduction and overview to the MarParCloud campaign." *Atmos. Chem. Phys.* 20(11): 6921-6951.
- van Pinxteren, M., C. Müller, Y. Iinuma, C. Stolle and H. Herrmann (2012). "Chemical Characterization of Dissolved Organic Compounds from Coastal Sea Surface Microlayers (Baltic Sea, Germany)." *Environmental Science & Technology* 46(19): 10455-10462.

- Walz, M. M., C. Caleman, J. Werner, V. Ekholm, D. Lundberg, N. L. Prisle, G. Ohrwall and O. Bjorneholm (2015). "Surface behavior of amphiphiles in aqueous solution: a comparison between different pentanol isomers." *Physical Chemistry Chemical Physics* 17(21): 14036-14044.
- Walz, M. M., J. Werner, V. Ekholm, N. L. Prisle, G. Ohrwall and O. Bjorneholm (2016). "Alcohols at the aqueous surface: chain length and isomer effects." *Physical Chemistry Chemical Physics* 18(9): 6648-6656.
- Wang, S., J. A. Schmidt, S. Baidar, S. Coburn, B. Dix, T. K. Koenig, E. Apel, D. Bowdalo, T. L. Campos, E. Eloranta, M. J. Evans, J. P. DiGangi, M. A. Zondlo, R.-S. Gao, J. A. Haggerty, S. R. Hall, R. S. Hornbrook, D. Jacob, B. Morley, B. Pierce, M. Reeves, P. Romashkin, A. ter Schure and R. Volkamer (2015). "Active and widespread halogen chemistry in the tropical and subtropical free troposphere." *Proceedings of the National Academy of Sciences* 112(30): 9281-9286.
- Watanabe, I., N. Takahashi and H. Tanida (1998). "Dehydration of iodide segregated by tetraalkylammonium at the air/solution interface studied by photoelectron emission spectroscopy." *Chemical Physics Letters* 287(5): 714-718.
- Weisenberger, S. and A. Schumpe (1996). "Estimation of gas solubilities in salt solutions at temperatures from 273 K to 363 K." *AIChE Journal* 42(1): 298-300.
- Weisenberger, S. and d. A. Schumpe (1996). "Estimation of gas solubilities in salt solutions at temperatures from 273 K to 363 K." *AIChE Journal* 42(1): 298-300.
- Winter, B. and M. Faubel (2006). "Photoemission from Liquid Aqueous Solutions." *Chemical Reviews* 106(4): 1176-1211.
- Winter, B., R. Weber, I. V. Hertel, M. Faubel, L. Vrbka and P. Jungwirth (2005). "Effect of bromide on the interfacial structure of aqueous tetrabutylammonium iodide: Photoelectron spectroscopy and molecular dynamics simulations." *Chemical Physics Letters* 410(4): 222-227.
- Winter, B., R. Weber, P. M. Schmidt, I. V. Hertel, M. Faubel, L. Vrbka and P. Jungwirth (2004). "Molecular Structure of Surface-Active Salt Solutions: Photoelectron Spectroscopy and Molecular Dynamics Simulations of Aqueous Tetrabutylammonium Iodide." *The Journal of Physical Chemistry B* 108(38): 14558-14564.
- Winter, B., R. Weber, W. Widdra, M. Dittmar, M. Faubel and I. V. Hertel (2004). "Full Valence Band Photoemission from Liquid Water Using EUV Synchrotron Radiation." *The Journal of Physical Chemistry A* 108(14): 2625-2632.
- Woods, E., C. A. Konyas and S. R. Rossi (2019). "Photoemission of Iodide from Aqueous Aerosol Particle Surfaces." *The Journal of Physical Chemistry A* 123(13): 2901-2907.
- Yeh, J. J. and I. Lindau (1985). "Atomic subshell photoionization cross sections and asymmetry parameters:  $1 \leq Z \leq 103$ ." *Atomic Data and Nuclear Data Tables* 32(1): 1-155.
- Zhao, X., G. M. Nathanson and G. G. Andersson (2020). "Experimental Depth Profiles of Surfactants, Ions, and Solvent at the Angstrom Scale: Studies of Cationic and Anionic Surfactants and their Salting Out." *The Journal of Physical Chemistry B*.

---

# Summary and Outlook

---

### 7.1 Summary

This thesis provides a detailed insight into halogen activation under simulated atmospheric conditions and provides a sound basis for an improved representation of halogen chemistry in atmospheric models.

The affinity of halide ions for the liquid-gas interface of aqueous solutions, which may influence their reactivity with gaseous species, has been debated. We determined the solvation environment of different bromine species at the liquid-gas interface by performing measurements with liquid jet XPS at variable photoelectron kinetic energy and thus probe depth. Our results show that bromide does not display a net surface preference, in good agreement with in situ XPS performed with solutions containing iodide ions. Parallel to that, chloride and fluoride are more strongly depleted than bromide, as expected from their smaller size, which agrees with recent theory, classical surface tension measurements and recent spectroscopic experiments, suggesting the lightest halide ions being most depleted from the surface. Similar to bromide, also hypobromite and bromate do not display propensity for the surface. Hypobromous acid, a key species in the multiphase cycling of bromine, is the only species showing substantial surface propensity as proven by the binding energy shift compared to the conjugate base and by the kinetic energy dependent measurements, which suggests a more critical role of the interface for this species in multiphase bromine chemistry than thought before.

In the aqueous bulk, oxidation of bromide by ozone involves a  $[\text{Br}\bullet\text{OOO}^-]$  complex as intermediate. The formation of HOBr through the bulk aqueous phase route is rather inefficient, and oxidation at the aqueous solution-air interface may dominate in many environments. The kinetic results related to the oxidation of bromide indicate surface enhancement of the reaction. The XPS results provide clear spectroscopic evidence of the bromide ozonide intermediate, the  $[\text{Br}\bullet\text{OOO}^-]$  pre-complex, which prefers the interface, and is likely at the origin of surface-enhanced kinetics. We further studied the formation of the intermediate at low pH, indicating a much lower surface concentration under acidic conditions possibly due to faster decay of the intermediate via release of molecular oxygen, which agrees with the larger overall ozone uptake coefficients. The surface concentration of the  $[\text{Br}\bullet\text{OOO}^-]$  intermediate increased almost linearly with the bromide concentration; the trend towards a smaller  $[\text{Br}\bullet\text{OOO}^-]$  to bromide ratio at high concentration could be a sign of saturation driven by a maximum possible coverage. The  $[\text{Br}\bullet\text{OOO}^-]$  intermediate concentration at the interface turned out to be tightly correlated with the uptake coefficient of ozone over the same bromide concentration range. This work clearly shows the preference of the intermediate for the liquid-gas interface, and sheds light on mechanistical and structural aspects of the reaction. The results provide evidence for a stronger contribution of the surface oxidation of bromide than previously thought, which will require re-assessment of the impacts on the global ozone budget and mercury deposition. In turn, the formation of ozonides on surfaces may be a widespread phenomenon and a key step of critical oxidation processes relevant not only for atmospheric chemistry but also for the effects of atmospheric particles on human health.

In another study, we used liquid jet XPS to assess the impact of a monofunctional surfactant with a positive headgroup (hexylammonium) and a negative headgroup (propylsulfate) on the abundance of bromide and sodium ions at the interface within the probe depth. The spectroscopic data were analysed with the support of an attenuation model to obtain quantitative information about the enhancement or depletion of cations and anions at the interface. The positively charged nitrogen group (even only a few percent at the liquid-vapor interface) in hexylamine, along with its surface activity, leads to an enhanced interfacial concentration of bromide, while the negatively charged sulfate group in propylsulfate has only a small effect on the interfacial concentration of bromide. In turn, sodium cations showed a corresponding enhancement in the presence of propylsulfate and only minor changes in the presence of hexylamine. In the presence of additional sodium chloride, salting effects and competition for ion-pairing with the ionic surfactant in combination determine the abundance of bromide anions and sodium cations. In the presence of soluble surface-active organics, the charge of the headgroup has a strong impact on the abundance of inorganic ions at the liquid-vapor interface. Thus, to some degree, this conceptual picture allows us to more generally predict how ionic surfactants are affecting the interfacial

abundance of the prominent halide,  $\text{SO}_4^{2-}$ , and  $\text{NO}_3^-$  anions and  $\text{NH}_4^+$  and other cations as a function of pH. However, other effects could complicate this picture, such as the stability of ion-pairs and molecular interactions among the surfactants.

Moreover, we measured the surface propensity of cationic tetrabutylammonium (TBA) at the aqueous liquid-vapor interface by liquid jet XPS and the effect of this surfactant on ozone uptake to aqueous bromide solutions. The positively charged nitrogen group in TBA, along with its surface activity, leads to an enhanced interfacial concentration of bromide and the  $[\text{Br}\cdot\text{OO}]^-$  intermediate due to electrostatic interactions as discussed for the simpler hexylammonium before. In parallel, in kinetic experiments for the same system, a strongly enhanced ozone loss rate in the presence of TBA on the surface of bromide solutions was observed. A similar model as above was used to account for the attenuation of photoelectrons by the carbon-rich layer of the TBA surfactant. The more quantitative analysis demonstrates that TBA increases the local density of bromide ions by a factor of 20 above that of a neat aqueous bromide solution at the same bulk concentration. Similarly, mixing TBA-Br with NaCl at seawater concentration leads to an interfacial bromide ion density enhanced by about 43% compared to the corresponding mixture of just NaBr and NaCl. Still, the reaction rates of  $\text{O}_3$  with these solutions were not simply proportional to the interfacial bromide concentrations, as other effects, such as the different interfacial structure, or the stabilization of the reaction intermediate are additional factors influencing reactivity. Aliphatic amines and amino acids are important positively charged surfactants associated with the sea surface microlayer (the topmost organic-rich layer), with an average concentration in the range of 50-1500 ng L<sup>-1</sup>. This work shows that they may exert strong effects on halogen activation processes and their presence should be considered when it comes to assessing the impact of halogen chemistry on the atmospheric oxidation capacity and the climate.

The overall aim of this PhD work has been to obtain molecular level knowledge of halide solution–vapor interfaces, which could be used for better understanding the fundamental marine atmospheric chemistry and quantitative atmospheric chemical models, and to support future assessments of halogen chemistry on atmospheric oxidation capacity and climate.

## 7.2 Outlook

The depth profile information of bromide-related solutions is always an exciting topic, and we met the challenge during our liquid jet XPS experiment. In the future, we could have a more detailed look into the normalization parameters to better characterize the depth profile information of the solutions, as we had to accept quite large uncertainties for absolute

elemental ratios. A clear understanding of the interfaces with molecular-level detail will remain an important topic in atmospheric chemistry.

On the one hand, we can improve the kinetics experiments by connecting the flow tube experiment setup to a mass spectrometer to look at the gas-phase products. This may give way to better understanding the relation between uptake coefficient,  $[\text{Br}\cdot\text{OOO}]^-$  intermediate, and the released HOBr and other products at neutral and acidic conditions of aqueous solutions.

Further, the HOBr formed from the oxidation of bromide by ozone may be recycled by the hydrogen peroxide ( $\text{H}_2\text{O}_2$ ) via halogen peroxides ( $\text{BrOO}^-$ ), which decompose rapidly to  $\text{O}_2$  and  $\text{Br}^-$ . Therefore, the ubiquitously present  $\text{H}_2\text{O}_2$  could limit the extent of bromide oxidation. A  $\text{H}_2\text{O}_2$  gas source and the  $\text{H}_2\text{O}_2$  detector available in the group could be combined with a kinetics experiment to study the potential of  $\text{H}_2\text{O}_2$  for recycling  $\text{OBr}^-$  back to  $\text{Br}^-$ .

As we discussed before, the surface concentration of the  $[\text{Br}\cdot\text{OOO}]^-$  intermediate increased almost linearly with the bromide concentration, and only a tiny fraction of hexylamine is actually protonated, leading to an enhanced interfacial concentration of bromide. Further experiment with liquid jet XPS and kinetics experiment in parallel for bromide concentration dependence in the presence of positively charged surfactants is necessary to set up a sound system to understand better the molecular-level detail in the chemistry of halide solutions.

Collaboration with the theoretical community could also be generally exploited further, for example with Ivan Gladich or Céline Toubin: simulation of bromide related aqueous solutions also in the presence of surface-active organic compounds using MD simulations. Such collaboration will drive a broader assessment of our experimental results. Contacts with the corresponding partner institutions and research groups are established. As we show in this thesis, in the presence of additional sodium chloride, salting effects and competition for ion-pairing with the ionic surfactants in combination determine the abundance of bromide anions and sodium cations. In the presence of soluble surface-active organics, the charge of the headgroup has a substantial impact on the abundance of inorganic ions at the liquid-vapor interface. Céline Toubin is now working on the hexylamine / propylsulfate system with MD simulations, and the first results also support our conclusion related to hexylamine / propylsulfate chapter. These calculations may be a good starting point to understand other effects, such as ion-pairing and molecular interactions among the surfactants.

In addition, a photoelectron attenuation model with a carbon-layer to represent the aliphatic surfactant chains was developed to retrieve the interfacial concentration of bromide and sodium in the presence of the different surfactants from the liquid jet XPS experiments. This model can be applied to further experiments addressing other halide or alkaline cations, or even other inorganic group ions, such as  $\text{SO}_4^{2-}$ ,  $\text{NO}_3^-$ ,  $\text{NH}_4^+$  that exist in atmospheric particles.

With liquid-jet XPS, we provided unambiguous spectroscopic evidence for the bromide ozonide intermediate, the  $[\text{Br}\bullet\text{OOO}^-]$  pre-complex, which has a preference for the liquid-vapor interface. The  $[\text{Br}\bullet\text{OOO}^-]$  intermediate concentration at the interface turned out to be tightly correlated with the uptake coefficient of ozone over the same bromide concentration range. The important conclusions from this part of the thesis project have already motivated some recent halogen modelling studies to emphasize the surface contribution to the oxidation of bromide [Koenig et al., 2017; Fernandez et al., 2019; Herrmann et al., 2019; Zhu et al., 2019; Herrmann et al., 2021]. More and more studies distinguish the surface contribution and bulk contribution of the halogen reactions when they design experiments [Moreno and Baeza-Romero, 2019].

Future experiments are also suggested that use a combination of liquid-jet XPS and molecular beam scattering, where the molecular beam of reactants hit a liquid jet [Shaloski et al., 2017] and scattered reactant and product molecules are detected with a time-of-flight mass spectrometer. On the one hand, XPS gives direct information about the spatial distribution of various atoms relative to the interface. On the other hand, molecular beam scattering provides information about the depth profile with higher resolution. Together, these experiments may provide molecular-level structural information with unprecedented detail about these highly complex and ubiquitous interfaces, which will furthermore unravel the much sought-after details on the depth profile information of mixed aqueous solutions comprised of both salts and organics relevant for marine aerosol or ocean surface water.

Besides, the surface propensity of bromide and other relevant elements show some strange phenomena when the solutions representative for seawater conditions contain an excess of sodium chloride. In the depth profiling experiments, where photoemission intensity ratios are measured as a function of the electron kinetic energy (see chapter 3), the relative intensity ratio increases, or decreases, or remains constant for solutes with concentrations at the surface being depleted, enhanced or neutral, respectively. In the presence of NaCl, the intensity ratio of bromide to oxygen or other relevant elements showed unexpected jumps at both low energy and high kinetic energies. Further studies with sodium chloride are necessary to better understand the impact of an excess of chloride on the affinity of the other halide ions for the surface. In addition, the different aspects that determine the influence of chloride on the oxidation of the other halides by ozone or other oxidants remain uncertain.

The multiphase reaction of  $\text{O}_3$  with  $\text{Br}^-$  has been of significant interest in this thesis. In addition, we could develop the attenuation model to characterize the solid knowledge of the surface propensities of bromide solutions in the presence of surface-active organic compounds with pH, temperature, or concentration dependence, based on XPS experiments. Such an attenuation model may provide a better understanding in terms of more chemical

## Chapter 7 Summary and Outlook

---

details and may thus also further our knowledge of the role of organics in the chemistry of halide solutions relevant for marine aerosol or ocean surface water.

On the other hand, reactions of  $O_3$  with a wide range of organic compounds are also of essential importance for a wide range of other environmentally relevant systems. Future studies of oxidation of iodine by ozone using liquid jet XPS and kinetic experiments are proposed. Especially the relation between the uptake coefficient and the  $[I\cdot OOO]^-$  intermediate in the oxidation of iodide by ozone could be the next step.



## Bibliography

---

- Fernandez, R.P., Carmona-Balea, A., Cuevas, C.A., Barrera, J.A., Kinnison, D.E., Lamarque, J.F., Blaszcak-Boxe, C., Kim, K., Choi, W., Hay, T. and Blechschmidt, A.M., 2019. Modeling the sources and chemistry of polar tropospheric halogens (Cl, Br, and I) using the CAM-Chem global chemistry-climate model. *Journal of Advances in Modeling Earth Systems*, 11(7), pp.2259-2289.
- Herrmann, M., Cao, L., Sihler, H., Platt, U. and Gutheil, E., 2019. On the contribution of chemical oscillations to ozone depletion events in the polar spring. *Atmospheric Chemistry and Physics*, 19(15), pp.10161-10190.
- Herrmann, M., Sihler, H., Frieß, U., Wagner, T., Platt, U. and Gutheil, E., 2021. Time-dependent 3D simulations of tropospheric ozone depletion events in the Arctic spring using the Weather Research and Forecasting model coupled with Chemistry (WRF-Chem). *Atmospheric Chemistry and Physics*, 21(10), pp.7611-7638.
- Koenig, T.K., Volkamer, R., Baidar, S., Dix, B., Wang, S., Anderson, D.C., Salawitch, R.J., Wales, P.A., Cuevas, C.A., Fernandez, R.P. and Saiz-Lopez, A., 2017. BrO and inferred Br y profiles over the western Pacific: relevance of inorganic bromine sources and a Br y minimum in the aged tropical tropopause layer. *Atmospheric Chemistry and Physics*, 17(24), pp.15245-15270.
- Moreno, C. and Baeza-Romero, M.T., 2019. A kinetic model for ozone uptake by solutions and aqueous particles containing I<sup>-</sup> and Br<sup>-</sup>, including seawater and sea-salt aerosol. *Physical Chemistry Chemical Physics*, 21(36), pp.19835-19856.
- Shaloski, M.A., Gord, J.R., Staudt, S., Quinn, S.L., Bertram, T.H. and Nathanson, G.M., 2017. Reactions of N<sub>2</sub>O<sub>5</sub> with Salty and Surfactant-Coated Glycerol: Interfacial Conversion of Br<sup>-</sup> to Br<sub>2</sub> Mediated by Alkylammonium Cations. *The Journal of Physical Chemistry A*, 121(19), pp.3708-3719.
- Zhu, L., Jacob, D.J., Eastham, S.D., Sulprizio, M.P., Wang, X., Sherwen, T., Evans, M.J., Chen, Q., Alexander, B., Koenig, T.K. and Volkamer, R., 2019. Effect of sea salt aerosol on tropospheric bromine chemistry. *Atmospheric Chemistry and Physics*, 19(9), pp.6497-6507.

---

## Acknowledgements

---

This thesis could not be conducted without contributions from a lot of people, both in scientific input and friendly support. Thanks to every single one of you. A non-exhaustive list of these people and or groups of people is presented below:

- I am grateful to Prof. Markus Ammann for offering me the opportunity to work on this project in the Surface Chemistry group and for being my supervisor and my doctor father, furthermore for helpful discussions about data analyses, manuscript guidance, comments and corrections, and for the scientific input. He is willing to share with me his tremendous knowledge on both science and life, and never bothers explaining to me again and again with great patience. Whenever I struggled with challenging situations, his encouragement and optimism always made me feel confident in my research and feel all hard work was worthwhile. I am sincerely thankful and am lucky to have such an excellent supervisor.
- I am grateful to Prof. Thomas Peter for accepting to act as the thesis co-examiner for reviewing this work. I learned a lot from him in the stratospheric chemistry lecture. His critical comments and advice on my PhD projects are pretty appreciated. Furthermore, I enjoyed the time we spent in the group retreat. It was great fun.
- I am grateful to Prof. Olle Bjoernehalm for acting as the thesis co-examiner for reviewing this work.
- I am grateful to Prof. Kristopher McNeill for accepting to act as the chairman of the thesis committee.
- I am grateful to the Swiss National Science Foundation (grant no 169176), for giving me this chance to join such a great project.
- I am grateful to Dr. Luca Artiglia for being such a great tutor. I appreciate all he taught me about Liquid-jet XPS. I enjoyed the shifts for the LJ-XPS at SLS. Thank you for your patience in guiding me in preparing and handling the experiment during beamtime and our fruitful cooperation.
- I am grateful to Dr. Thorsten Bartels-Rausch for lab-safety training, for helping a lot in the beginning, and for laughing and joking.
- I am grateful to Prof. Margit Schwikowski-Gigar for establishing an excellent mood within the lab, where it is a pleasure to work.

## Acknowledgements

---

- I am grateful to Andrés Laso and Mario Birrer for solving my technical issues, for exchanging ideas on how to improve my experimental setup and solve lab issues. It was always fun to work with you.
- I am grateful to Sabina Brütsch–Suter for allowing me to use the mill-Q water in her lab.
- I am grateful to Armin Kleibert, the beamline scientist at SIM, who helped me at the SIM beamline.
- I am grateful to Dr. Thomas Huthwelker, the beamline scientist at Phoenix, who helped me at the Phoenix beamline and the free usage of mill-Q water.
- Here I would like to give special thanks to my office mate (OFLA/102), Dr. Fabrizio Orlando, for helping me a lot in the beginning, who I enjoyed talking to and taught me how to fit XPS peaks, and become a great team-member when doing beamtime at SIM and Phoniex. I thank you for not only the scientific insight discussions but also the laugh and joke. Here I would like to give special thanks to Dr. Xiangrui Kong, with whom I have spent a lot of fun times, both academic and non-academic discussion. Thank you for giving me lots of help, laughing and joking during daily life, giving me a lot of encouragement and always having time for scientific discussion. He is a scientist role model to me, as I learned a lot from him. I am grateful to Dr. Huanyu Yang, Dr. Anthony Boucly, Jérôme Philippe Gabathuler, Yanisha Manoharan, Dr. Antoine Roger Roose, Dr. Astrid Waldner for being great office mates. With different research backgrounds, we always had interesting discussions. Sharing different opinions on science and life with you made my PhD time relieved.
- I am grateful to the Surface Chemistry group members to Dr. Jacinta Edebeli, who guided me to set up the flow tube experiment. I want to thank Dr. Peter Aaron Alpert, Dr. Pablo, Corral Arroyo for being great groupmates, for the nice working atmosphere, especially the scientific idea exchange and the weekend party and activities.
- I am grateful to LUC members for the friendly working atmosphere. We spent lots of fun together at seminars, coffee time, ice cream afternoon, Christmas party, lab retreat, hiking et al. together. Especially Dr. Ling Fang, Dr. Sven Avak, Dr. Anna Dal Farra, Dr. Anja Eichler, Dr. Theo Manuel Jenk, for a lovely time in EGU and talking in daily life.
- I am grateful to the Atmospheric Chemistry group for the group retreat we share with lots of fun and exchanging scientific ideas and enjoyable life in Gemmi and Ftan. Especially Dr. Jing Duo, whom I have spent a lot of fun times with, both academic and non-academic discussions.
- I am grateful to Doris Bühler at the Paul Scherrer Institute and Forney Petra and Eva Choffat at the Institute of Atmosphere and Climate, ETH Zurich for helping me deal with all the administrative things during my PhD life.

## Acknowledgements

---

- I am grateful to Dr. Roth Manfred for giving me much encouragement for my PhD study from the beginning.
- My deepest gratitude goes to my family and friends who have always supported me. No matter what decisions I make up, they always support me unconditionally. Wherever I go, I know they are always there for me. Thank you for everything! My Daughter, Ruisi Wang, who was born in March 2019, and my son Ruixian Wang, who was born in August 2021, have been wonderful children. Thanks for giving me power by sharing my daily life or just by smiling at me or only by watching videos/photos of you.

I am grateful to my parents, Mr. Houhuai Chen and Mrs. Donglian Zeng, for their best love in the world, the encouragement and support and motivation to keep taking that next step.

I am grateful to my younger brother, Mr. Degui Chen and my sister-in-law, Mrs. Yulong Cheng, for their love and encouragement, for covering my backing by taking care of my parents that allowed me to study abroad.

I am grateful to my parents-in-law, Mr. Aitao Wang and Mrs. Dingxiang Xie, for their encouragement, support and love. Especially, I am grateful to my-mother-in law for traveling abroad even during the Covid situation, taking care of my family and me with encouragement, support and love during my maternity-recovery period, and covering my backing by taking care of Ruisi and Ruixian.

I am grateful to my husband, Dr. Xing Wang. It would be an endless list of what you did for me. I only want to tell you that I love you!

**It is a precious journey in my life!**

## Curriculum Vitae

**Name** : Shuzhen Chen

**Gender** : Female

**Date of Birth** : 16<sup>th</sup> April 1990

**Telephone** : +41 78 898 8760

**E-mail** : [shuzhen.chen@psi.ch](mailto:shuzhen.chen@psi.ch)

**Address:** Fellerstrasse 50 F2, 3027, Bern, Switzerland

### **TECHNICAL SKILLS AND COMPETENCIES**

- Sound knowledge of **X-ray photoelectron spectroscopy method** combined with liquid microjet setup within synchrotron radiation light source.
- Experience with **high-vacuum** techniques, large **instrument maintenance** and lab-based flow tube method with gas dosing system.
- Knowledge background in atmospheric chemistry, **surface chemistry, physical chemistry, and electrochemistry**.
- Strong analytical skills with MS Office and good knowledge with Igor pro, Origin, **Python** and LabVIEW.
- Participate in several projects with solid experience, and rapid familiarization with new topics. **Experience with beam-time proposal application** and annual report preparation.
- Creative, team-minded, excellent communication and teamwork with 2-6 people.

### **ACADEMIC EXPERIENCE AND SKILL**

**PhD Studies** supervised by Prof. Markus Ammann

04/2016-04/2022 Multiphase kinetics and chemistry at halide solution – air interfaces

- Investigated the surface propensity of bromide and its oxidation products hypobromite and bromate, and of organic surfactants with differently charged headgroups, both individually and in combination with bromide using synchrotron-based liquid-jet X-ray photoelectron spectroscopy (XPS) methods at Swiss Light Source (SLS).
- Build up liquid-jet XPS measurements that provide direct experimental evidence for the bromide ozonide and focus on the surface propensity of bromide ozonide at low pH and as a function of bromide concentration and compared the corresponding interfacial density of bromide ozonide with the ozone uptake coefficient.
- Examined the difference between a monofunctional surfactant with a positive headgroup (hexylammonium) and a negative headgroup (propylsulfate) on the abundance of bromide and sodium

## Curriculum Vitae

---

ions at the liquid-vapor interface, and a photoelectron attenuation model is used to retrieve the interfacial concentration of bromide and sodium in the presence of the different surfactants.

- Presented the impact of tetrabutylammonium on the abundance of bromide and the bromide ozonide at the aqueous solution – air interface and compares the spectroscopic information with the results of ozone uptake kinetic experiments performed in parallel. In addition, a model is developed to account for the attenuation of photoelectrons by the carbon-rich layer established by the tetrabutylammonium surfactant.

**Undergraduate and Graduate Studies** supervised by Prof. Hongtao Liu

09/2013-03/2016 Exfoliation, assembly and electrochemical properties of Fe-based layered materials

- Fabricated the hybridize grown flower-like Ni-Fe layered double hydroxide and carbon black nanoparticles for high-rate alkaline cathode material.
- Synthesized the superlattice Ni-Fe hydrotalcite nanosheets and graphene composites for oxygen evolution reaction.

09/2012-06/2013 Preparation and property contrast of reduced graphene oxide papers

- Prepared the reduced graphene oxide papers by improved Hummers method and investigated its properties by **XRD, Raman, FR-IR, TGA, SEM and TEM**.
- Designed the aqueous graphene dispersions and high-quality graphene flakes for supercapacitor.

### **SELECTED CONFERENCES and WORKSHOPS**

12/2019 6<sup>th</sup> Annual APXPS workshop, Lund, Sweden, **talk**.

04/2019 General Assembly 2019 of the European Geosciences Union (EGU), Vienna, Austria, Poster.

11/2018 Third Sino-European School on Atmospheric Chemistry (SESAC3), Shanghai, China, Poster.

08/2018 256<sup>th</sup> ACS National Meeting & Exposition, Boston, Massachusetts, USA, **talk**.

02/2018 34<sup>rd</sup> Annual Meeting of the Swiss Working Group for Surface and Interface Science, Fribourg, Switzerland, **talk**.

04/2017 General Assembly 2017 of the European Geosciences Union (EGU), Vienna, Austria, PICO presentation.

09/2016 XPS ANALYSIS: from measurements to scientific answers, Roscoff, France, Poster.

### **INTERNSHIPS**

08/2012–09/2012 Internship in Sinopec Changling Branch Company, Yueyang, China.

# Curriculum Vitae

---

## TEACHING

09/2018–12/2018 Teaching assistant at ETH Zurich for atmospheric chemistry.

## LANGUAGE SKILLS

Native language: Chinese

Proficiency: English (professional usage)

Beginner level: Basic German

## SELECTED PUBLICATIONS & PATENTS

- Ivan Gladich, **Shuzhen Chen**, *et al.* "The Liquid–Gas Interface of Iron Aqueous Solutions and Fenton Reagents". *The Journal of Physical Chemistry Letters*, 2022, 13, 2994–3001.
- **Shuzhen Chen**, *et al.* "Impact of tetrabutylammonium on the oxidation of bromide by ozone at the liquid-vapor interface", *ACS Earth Space Chem.* 2021, 5, 11, 3008–3021.
- Ivan Gladich, **Shuzhen Chen**, *et al.* "Surface propensity of aqueous atmospheric bromine at the liquid–gas Interface". *The Journal of Physical Chemistry Letters*, 2020, 11, 9, 3422–3429.
- Fabrizio Orlando, Luca Artiglia, Huanyu Yang, Xiangrui kong, Kanak Roy, Astrid Waldner, **Shuzhen Chen**, *et al.* "Disordered adsorbed water layers on TiO<sub>2</sub> nanoparticles under subsaturated humidity conditions at 235 K". *The Journal of Physical Chemistry Letters*, 2019, 10, 23, 7433–7438.
- Luca Artiglia, Jacinta Edebeli, Fabrizio Orlando, **Shuzhen Chen**, *et al.* "A surface-stabilized ozonide triggers bromide oxidation at the aqueous solution-vapor interface". *Nature Communication*, 2017, 700, 1–8.
- Ming-Tao Lee, Fabrizio Orlando, Luca Artiglia, **Shuzhen Chen**, *et al.* "Chemical composition and properties of the liquid–vapor interface of aqueous C1 to C4 monofunctional acid and alcohol solutions". *The Journal of Physical Chemistry A*, 2016, 120(49), 9749–9758.
- **Shuzhen Chen**, *et al.* "A high-rate cathode material hybridized by in-site grown Ni-Fe LDH and carbon black nanoparticles". *Journal of Materials Chemistry A*, 2016, 4, 4877–4881.
- Hongtao Liu, **Shuzhen Chen**, *et al.* "Preparation methods of iron base non-noble metal catalyst for oxygen evolution reaction", 2015, Patents No: CN201510577234[P]
- Min Mao, **Shuzhen Chen**, *et al.* "Facile and economical mass production of graphene dispersions and flakes", *Journal of Materials Chemistry A*, 2014, 2, 4132–4135.
- Min Mao, Mengmeng Wang, Junyan Hu, Gang Lei, **Shuzhen Chen**, *et al.* "Simultaneous electrochemical synthesis of few-layer graphene flakes on both electrodes in protic ionic liquids", *Chemical Communications*, 2013, 49, 5301–5013.